Preparation, Characterization and Performance of Poly(vinyl alcohol) based Membranes for Pervaporation Dehydration of Alcohols

By

Md Nasim Hyder

A thesis
presented to the University of Waterloo
in fulfillment of the
thesis requirement for the degree of

Doctor of Philosophy
in
Chemical Engineering

Waterloo, Ontario, Canada, 2008

AUTHOR'S DECLARATION

I hereby declare that I am the sole author of this thesis. This is a true copy of the thesis, including any required final revisions, as accepted by my examiners.

I understand that my thesis may be made electronically available to the public.

Abstract

Pervaporation (PV), a non-porous membrane separation process, is gaining considerable attention for solvent separation in a variety of industries ranging from chemical to food and pharmaceutical to petrochemicals. The most successful application has been the dehydration of organic liquids, for which hydrophilic membranes are used. However, during pervaporation, excessive affinity of water towards hydrophilic membranes leads to undesirable swelling (water absorption) of the membrane matrix. To control swelling, often hydrophilic membranes are crosslinked to modify physicochemical (surface and bulk) properties. Since the transport of species in pervaporation is governed by sorption (affected by surface and bulk properties) and diffusion (affected by bulk properties), it is essential to study the effect of crosslinking on the surface and bulk physicochemical properties and their effects on separation performance.

This thesis focuses on the effect of crosslinking on the physicochemical properties (e.g., crystallinity, hydrophilicity, surface roughness) of hydrophilic polymeric membranes and their dehydration performance alcohol-water mixtures. Poly(vinyl alcohol), PVA was used as the base polymer to prepare membranes with various morphologies such as homogeneous, blended (with Chitosan, CS) and composite (with poly(sulfone), PSf) structures. Before applying the crosslinked membranes for the PV dehydration of alcohols, the physicochemical characterization were carried out using Attenuated Total Reflection-Fourier Transform Infrared Spectroscopy (ATR-FTIR), X-Ray Diffraction (XRD), Differential Scanning Calorimetry (DSC), Scanning Electron Microscopy (SEM), Atomic Force Microscopy (AFM), tensile testing, contact angle and swelling experiments.

The crosslinked membranes showed an increase in surface hydrophobicity from the contact angle measurements as compared to the uncrosslinked membranes. AFM surface topography showed that the membrane surfaces have nodular structures and are rough at the nanometer scale and affected by the crosslinking conditions such as concentration and reaction time. Surface hydrophobicity and roughness was found to increase with increasing degree of crosslinking. DSC measurements showed an increase in melting temperature of the polymer membranes after crosslinking. For the PV dehydration of ethanol, a decrease in flux and an increase in selectivity were observed with increase in the degree of crosslinking.

Effects of membrane thickness (of PVA layer) for crosslinked PVA-PSf composite membranes were studied on PV dehydration of ethanol. Total flux and selectivity were statistically analyzed as a function of the membrane thickness. In general, the outcome agrees with the solution-diffusion (S-D) theory: the total flux was found to be significantly affected by the PVA layer thickness, while the selectivity remains nearly unaffected. Using the S-D theory, the mass transfer resistance of the selective layers was calculated and found to increase with thickness. The relatively small change observed for selectivity has been related to the crosslinking of the PVA layer that increases the surface hydrophobicity of the membrane.

Chitosan-Poly(vinyl alcohol), or CS-PVA, blended membranes were prepared by varying the blending ratio to control membrane crystallinity and its effect on the PV dehydration of ethylene glycol. The blended membranes were crosslinked interfacially with trimesoyl chloride (TMC)/hexane. The crystallinity of the membrane was found to decrease with increasing CS wt% in the blend. Although the crosslinked CS-PVA blend membranes showed improved mechanical strength, they became less flexible as detected in tensile testing. The resulting crosslinked CS-PVA blended membranes showed high flux and selectivity simultaneously, for 70-80wt% CS in the blend. The effect of feed flow-rate was studied to find the presence of concentration polarization for 90wt% EG in feed mixture as well. The crosslinked blend membrane with 75wt% CS showed a highest total flux of 0.46 $kg/m^2/h$ and highest selectivity of 663 when operating at $70^{O}C$ with 90wt% EG in the feed mixture.

Effects of crosslinking concentration and reaction time of trimesoyl chloride (TMC) were studied on poly(vinyl alcohol)-poly(sulfone) or PVA-PSf composite membranes. Results showed a consistent trend of changes in the physicochemical properties: the degree of crosslinking, crystallinity, surface roughness, hydrophilicity and swelling degree all decrease with increasing crosslinking agent (TMC) concentration and reaction time. The crosslinked membrane performance was assessed with PV dehydration of ethylene glycol-water mixtures at a range of concentrations (30 to 90wt% EG). The total flux of permeation was found to decrease, while the selectivity to increase, with increasing TMC concentration and reaction time. The decrease in flux was most prominent at low EG concentrations in the feed mixtures.

A central composite rotatable design (CCRD) of response surface methodology was used to analyze PV dehydration performance of crosslinked poly(vinyl alcohol) (PVA)

membranes. Regression models were developed for the flux and selectivity as a function of operating conditions such as, temperature, feed alcohol concentration, and flow-rate. Dehydration experiments were performed on two different alcohol-water systems: isopropanol-water (IPA-water) and ethanol-water (Et-water) mixtures around the azeotrope concentrations. Judged by the lack-of-fit criterion, the analysis of variance (ANOVA) showed the regression model to be adequate. The predicted flux and selectivity from the regression models were presented in 3-D surface plots over the whole ranges of operating variables. For both alcohol-water systems, quadratic effect of temperature and feed alcohol concentration showed significant ($p < 0.0001$) influence on the flux and selectivity. A strong interaction effect of temperature and concentration was observed on the selectivity for the Et-water system. For the dehydration of azeotropic IPA-water mixture (87.5wt% IPA), the optimized dehydration variables were found to be 50.5^{O}C and 93.7 L/hr for temperature and flow-rate, respectively. On the other hand for azeotropic Et-water mixture (95.5wt% Et), the optimized temperature and flow-rate were found to be 57^{O}C and 89.2 L/hr, respectively. Compared with experiments performed at optimized temperature and feed flow-rate, the predicted flux and selectivity of the azeotropic mixtures showed errors to be within 3-6 %.

Keywords: Pervaporation, Membrane, Poly(vinyl alcohol), Chitosan, Poly(sulfone), Crosslinking, Blending, Ethanol, Isopropanol, Ethylene Glycol, Atomic Force Microscopy, X-Ray Diffraction, Contact Angle, Central Composite Rotatable Design.

Acknowledgements

I would like to express my gratitude to my supervisors, Professor Pu Chen and R.Y.M. Huang for their guidance and support throughout my research. Many of our lengthy and intellectually stimulating discussions with Professor Chen have encouraged me in both formulating fresh research ideas as well as in solving existing problems.

I would like to thank the examination committee members for their comments and suggestions.

I am thankful to all the members of the Nano-Bio Interfacial Engineering Lab and the Membrane Research Lab for their helpful discussions that widened my academic horizons. I would also like to take this opportunity to thank all my friends for creating a warm and caring community at Waterloo during the last 4 years. I would like to thank Dr. S. Xiao, Dr. R. Du, Dr. N. McManus, Dr. J. Forrest and Dr. T. Leung for their help in membrane preparation and characterization experiments. I appreciate the help of the staffs in the Department of Chemical Engineering during my PhD studies.

This research was financially supported by the Natural Sciences and Engineering Research Council (NSERC) of Canada, Ontario Graduate Scholarship (OGS), President's Graduate Scholarship (PGS), Faculty of Engineering Graduate Scholarship, Department of Chemical Engineering awards during my Ph.D. studies.

I would like to thank my family for their caring love and support. I wish to express the deepest gratitude to my parents for instilling in me the values of patience and perseverance. I owe my loving thanks to my son as well. And last but not the least, my deepest appreciation goes to my wife, Zakia Sultana, for her endless encouragement, love and support.

To My Family

Table of Contents

CHAPTER 5

Chitosan-Poly(vinyl alcohol) blend membranes for Pervaporation Dehydration of Ethylene Glycol

CHAPTER 6

Composite Poly(vinyl alcohol)-Poly(sulfone) Membranes crosslinked by Trimesoyl Chloride: Characterization and Dehydration of Ethylene Glycol

CHAPTER 7

Pervaporation Dehydration of Alcohol-Water Mixtures: Optimization of Operating Conditions for Permeate Flux and Selectivity by Central Composite Rotatable Design

CHAPTER 8

General conclusions, contributions and recommendations

List of Figures

List of Tables

NOMENCLATURE

A	effective area of membrane
a_i, a_j	activity of components i and j in mixture
C	concentration
c_i	concentration of component i in mixture
D_i	Fickian diffusion coefficient
D_{ii}	self diffusion coefficient of component i
D_{ij}	binary diffusion of i in j at infinite dilution of i
E_{pi}	energy of activation of component i
J_i	flux of component i
l	membrane thickness
L_i, L_{ij}	phenomenological constants
M_w	molecular weight of species i
P	pressure
P_f , P_p	feed pressure at inlet, permeate pressure
p_i, p_j	partial permeate pressure of species i and j
$P_{i,p}$, $P_{j,p}$	partial pressure of components i and j on permeate side
$P_{i,sat}$, $P_{j,sat}$	partial saturation pressure of components i and j on feed side
R	universal gas constant
R_i	resistance of membrane
S	solubility coefficient
S_{ji}	semi-empirical constant for diffusion coefficient model
T	absolute temperature
t	permeation time
T_g	glass transition temperature
T_m	melting temperature
u_{ij}	energy of interaction between species i and j
W	Weight
W_D	the initial weight of the dry membrane
w_i, w_j	weight fraction of species i and j in mixture
W_p	permeate mass collected over a period of time

Ws	the weight of the swollen membrane at sorption equilibrium
x_i, x_j	feed mole/weight fraction of species *i* and *j*
y_i, y_j	permeate mole/weight fraction of species *i* and *j*
Z	coordination number
Δp	transmembrane pressure difference

Greek Letters

θ_a	advancing contact angle
θ_r	receding contact angle
θ_{ap}	apparent contact angle
γ_{lv}	surface tension of a liquid
γ_{sl}	interfacial tension between a solid and a liquid
γ_{sv}	interfacial tension between a solid and a gas
δ_S δ_p	Solubility parameter of solvent and polymer
ϕ_i	volume fraction of component *i*
α_{ij}	membrane selectivity of species *i* over *j*
μ_i	Chemical potential of component *i*
τ_{ij}	binary interaction parameters for UNIQUAC theory
χ_{12}, χ_{1p}, χ_{2p}	interaction parameters in Flory-Huggins theory

Subscripts/ Superscripts

ap	apparent
(c)	crosslink
f	feed
g	gas
l	liquid
m	membrane
m	membrane/mixing
p	permeate/polymer
s	surface

sat	saturation
T	thermodynamic
t	total
v	vapor
w	water

ACRONYMS

PDMS	Poly(dimethylsiloxane)
PPCSD	Pseudo-Phase Change Solution Diffusion
PV	Pervaporation
PVA	Poly(vinyl Alcohol)
CS	Chitosan
PSf	Poly(sulfone)
PVP	Poly(vinyl pyrrolidone)
Et	Ethanol
EG	Ethylene Glycol
IPA	Isopropanol
TMC	Trimesoyl chloride
VLE	Vapor Liquid Equilibrium
VOC	Volatile Organic Compounds
GA or ga	Glutaraldehyde
fresh or uc	Un-crosslinked Membranes
PVAc	Poly(vinyl acetate)
UNIQUAC	UNIversal QUasichemical Activity Coefficient
S-D	Solution Diffusion theory
Et-water	Ethanol-water binary mixture
IPA-water	Isopropanol-water binary mixture
EG-water	Ethylene Glycol-water binary mixture

CHAPTER 1

Introduction

1.1 Overview

Pervaporation, a membrane separation process, is gaining considerable attention in a variety of industries ranging from chemical to food and pharmaceutical to petrochemical for the separation of solvents [Wynn, 2001]. Traditionally, distillation and liquid-liquid extraction have been widely used for solvent separations. However, distillation is an energy intensive process and the technique fails in the case of azeotropes i.e. mixtures wherein the relative volatility of the compounds is same. Liquid-liquid extraction suffers from the major drawback of enhanced downstream processing due to the presence of an additional solvent. The main advantages of membrane based separation are continuous operation, flexibility associated with the combination with other separation techniques, and the possibility of operation at low or moderate temperatures. Furthermore, the energy requirement of a membrane separation process is comparatively lower than that of the conventional technologies, such as distillation and membrane process scale-up is relatively easier to perform [Smitha *et al.*, 2004]. However, membrane separation is not an ideal technology, and like other separation techniques it has some disadvantages as well e.g., low fluxes, fouling and noncompatibility of membranes with some solvents/chemicals [Baker, 2004]. The various types of the membrane separation processes are gas permeation, pervaporation, dialysis, reverse osmosis, ultrafiltration and microfiltration. These processes serve in the daily aspects of our life from the desalination of brackish water/seawater to concentration of fruit juices, from waste water treatment to recovery of helium from natural gas and from dehydration of alcohols to dialysis of artificial kidneys. Of the above mentioned technologies, pervaporation is the only process which can be used for solvent separations over a wide range of concentrations.

In pervaporation, the components of a liquid mixture selectively permeate through a membrane under the influence of a chemical potential gradient. As shown in Fig. 1.1, on one side of the membrane is a liquid feed and on the other side is the gaseous permeate. Unlike any other membrane separation process, in pervaporation, there is phase change of

he liquid permeates on the feed side to the gaseous permeates on the other side of the membrane. During pervaporation, the chemical potential gradient can be created by several

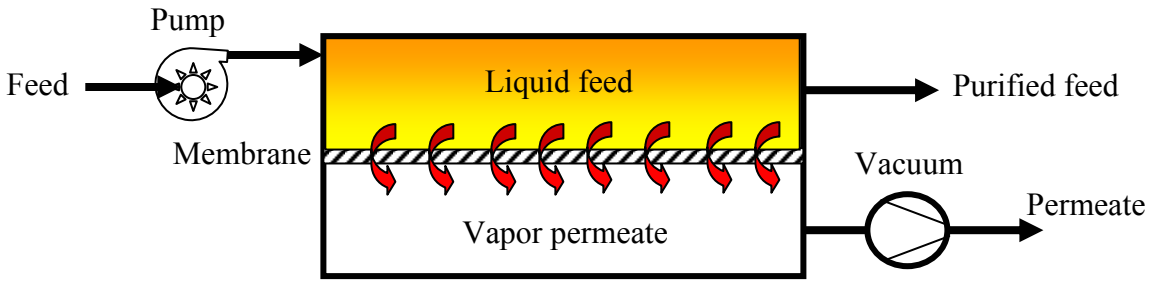

Figure 1.1: Schematic representation of a pervaporation process.

means such as creating a vacuum on the permeate side or the use of a sweep gas. The permeate product is usually collected by condensation over a very cold surface. Pervaporation finds many applications in the fields of dehydration of organic liquids, water treatment and organic-organic separations. The most successful application has been the dehydration of organic liquids. Currently, about one hundred commercial pervaporation units are operating worldwide, most of them dehydrating solvents, such as ethanol and isopropanol. Significant research continues for the dehydration of butanol, acetone, ethyl acetate, ethylene glycol and methylene chloride [Huang, 1991, Smitha *et al.*, 2004].

Although the pervaporation process was first conceived in the laboratory about 80 years ago [Kober, 1917], the process was first systematically studied in the laboratory in the 1960s [Binning *et al.*, 1961; Aptel *et al.*, 1974]. It was not until 1982, that the first commercial application of pervaporation was started by a German company GFT, GmbH (now Sulzer Chemtech) used it for the dehydration of ethanol. The major obstacle in diversifying pervaporation applications was the lack of availability of solvent resistant materials that can operate at high temperatures. Until recently, pervaporation was mainly used to study dehydration of ethanol [Lelkes *et al.*, 2000; Rautenbach *et al.*, 1988; Sanders *et al.*, 1988] and removal of aqueous organics/VOC's [Hickey *et al.*, 1994; Ji *et al.*, 1994; Karlsson *et al.*, 1993; Vane *et al.*, 2001] from dilute solutions. Over the years, the major emphasis being on new polymeric materials [Masuda *et al.*,1990; Xie *et al.*, 1993; Wei *et al.*, 1995], modeling of component transport through dense polymers [Brun, *et al.*, 1985; Mulder *et al.*, 1985; Kataoka *et al.*, 1991] and process design of commercial membrane modules [Wijmans *et al.*, 1996; Merz *et al.*, 1995].

Like any other membrane separation techniques, during pervaporation, the permeation rate varies from one component to another and is related to the molecular shape, size and chemical nature of permeates. The nature of the membrane, e.g., its hydrophilicity or hydrophobicity or affinity for a certain permeating component, also affects the separation performance. Finally, the interaction of one permeant with another along with the membrane has a very strong influence on the separation.

The choice of a particular membrane material is dictated by the types of application such as dehydration of alcohol and filtration of waste products in pharmaceutical industries, and the operating conditions such as temperature, concentration and flow-rate. In the PV dehydration of alcohols, a hydrophilic membrane such as poly(vinyl alcohol) is preferred due to its strong affinity to water. The strong affinity of membrane to water can provide a high selectivity, but sometimes excessive affinity results in swelling (absorption of water inside the membrane) of the membrane matrix [Huang, 1991]. Therefore, crosslinking is always done to control the extent of swelling in hydrophilic membranes used for dehydration. Crosslinking incorporates virtual bonds between polymer chains and reduce the flexibility [Baker, 2004]. In membrane separation, research has been done on different crosslinking agents/methods for membranes and their corresponding separation behavior. Although, crosslinking can modify physicochemical (surface and bulk) properties of a membrane, little research effort has been given to in this aspect. The effect of crosslinking on surface and bulk physicochemical properties and on permeation behavior remains mostly unexplored [Guo *et al.*, 2007]. In pervaporation, the membrane surface, in contact with the feed solution, determines the kind of mixtures or solution to be separated. The transport of permeates in a membrane is governed by the diffusion and to some extent by sorption (adsorption/absorption) processes; the adsorption of solvents on the membrane surface followed by absorption and then diffusion of the solvent molecules inside the membrane matrix. The adsorption process depends on the surface properties, e.g., surface hydrophilicity (or hydrophobicity) and roughness of the polymer material. The diffusion process is affected by membrane bulk properties such as thickness, crystallinity and free volume. Therefore, systematic characterization of the physiochemical properties of crosslinked membranes is crucial to develop robust membranes with better performance to operate for PV dehydration high temperatures.

1.2 Purpose of the study

1.2.1 Physicochemical properties of membrane

Since crosslinking affects the physicochemical properties of a membrane, the sorption and diffusion process could be affected by membrane surface (e.g., hydrophilicity, roughness), and bulk properties (e.g., thickness, crystallinity, mechanical strength) as well. Therefore, it is crucial to characterize the physicochemical properties of a crosslinked membrane to achieve improved separation performance. A list of characterization techniques such as Attenuated Total Reflection-Fourier Transform Infrared Spectroscopy (ATR-FTIR), X-ray Diffraction (XRD), Differential Scanning Calorimetry (DSC), Scanning Electron Microscopy (SEM), Atomic Force Microscopy (AFM), tensile testing, contact angle and swelling measurements will be used to determine the physicochemical properties of the membrane before and after crosslinking. These properties will be correlated to the membrane flux and selectivity to better understand the factor-effect relationship in pervaporation.

As for hydrophilic membranes, polyvinyl alcohol (PVA) will be used as the base polymer to develop various membrane structures, such as homogeneous, blended (with chitosan) and composite (with poly(sulfone) as the porous supporting layer) membranes. The hydrophilic membranes will be crosslinked to prevent excessive swelling during the PV dehydration. Since the crosslinking could modify the surface and bulk properties of a polymeric membrane, it would be interesting to study how these properties affect the separation performances.

1.2.2 Dehydration of organics

Organics such as ethanol, isopropanol, ethylene glycol etc… are commonly used as fuel, disinfectant, antifreeze in the petrochemical, electronic, aviation and food industry. 95.5 wt% Ethanol and 87.5 wt% isopropanol form azeotrope mixtures with water that cannot be separated by conventional distillation. Also, the separation of ethylene glycol-rich water mixture requires energy intensive distillation.

Pervaporation, being a less energy intensive and green separation process, could be an ideal candidate for the purification of the organics from water. Therefore, this thesis will focus on the PV dehydration of organics using hydrophilic polymer membrane.

1.2.3 Optimization

In pervaporation, the flux and selectivity are affected by operating conditions such as temperature, feed alcohol concentration and flow-rate. A statistical design of experiment would be used to optimize the separation variables for maximum flux and selectivity. A 2^{nd} order regression model will be developed to predict the flux and selectivity. The predicted results of the statistical model can be compared to the experimental data to identify the contributions of each operating conditions. This study can be extended to find optimum dehydration temperature and flow-rate to separate the alcohol-water azeotropic mixtures.

1.3 Research Objectives

The goal of this research is to study the effect crosslinking on the physicochemical properties and on pervaporation performance. To achieve this goal, poly(vinyl alcohol) based membranes were selected to prepare various crosslinked membranes such as homogeneous, blended and composite structures and study their pervaporation dehydration behavior of flux and selectivity for different binary alcohol mixtures. The specific objectives of this thesis are listed in the following:

1. Study the effect of crosslinking on the physicochemical properties of poly(vinyl alcohol) membranes; these properties will be measured using a variety of physicochemical tools, including atomic force microscopy, FTIR, X-ray spectroscopy calorimetry and contact angle. The outcome will provide essential information for understanding the sorption and diffusion of permeating components;
2. Correlate the membrane physicochemical properties to the permeation behavior;
3. Investigate the effect of crosslinking agent concentration and reaction time on membrane performance for dehydration of alcohols.
4. Study and optimize the effect of operating conditions on the pervaporation performance using a statistical design of experiment approach.

1.4 Structure of the thesis

This thesis will include the studies of various hydrophilic membranes, their characterization techniques and use for PV dehydration of organics. In Fig. 1.2, the structure of the thesis is illustrated that summarizes the aspect of this study. The first part will include the characterization and separation performance of PVA membrane and second part will focus on

the optimization of PV process variables. Although literature is abundant for the pervaporation dehydration studies of alcohol-water mixtures through PVA membranes [Yeom and Lee, 1996; Fleming and Slater, 1992; Nugay *et al*., 2002; Wynn 2003], membrane physicochemical properties effect have not been thoroughly investigated [Guo et al., 2007]. Also, PVA membranes have been used commercially for the dehydration of alcohol and other organics [Jonquieres *et al.*, 2000; Wynn, 2003] and therefore were a natural choice for this study.

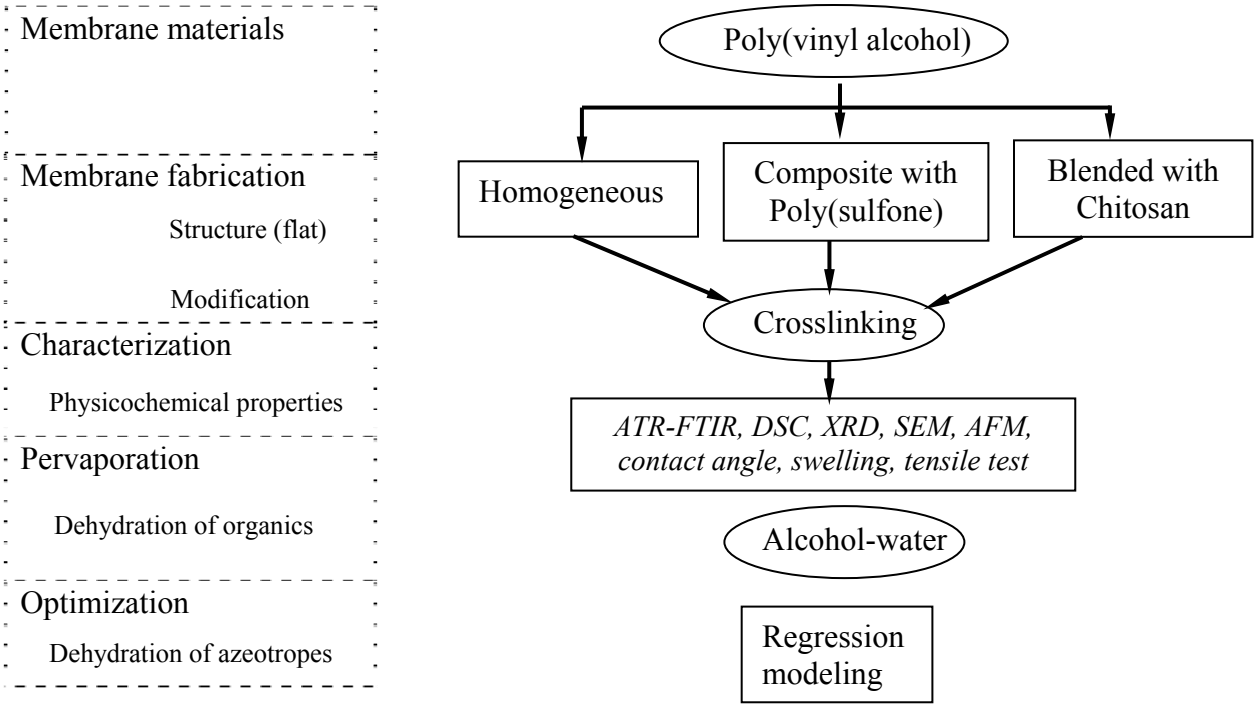

Figure 1.2: Structure of the research

This thesis consists of eight chapters. The scope of each chapter is listed as follows:

Chapter 1 gives an overview of the thesis, including a brief introduction to pervaporation process and its history, the factors affecting pervaporation, the membrane materials and their potential modifications to improve separation performance. The objectives and the scope of the thesis are also given in this chapter.

Chapter 2 reviews some aspects of the pervaporation processes, different types of membrane materials and physiochemical properties, membrane modification techniques, factors affecting pervaporation and their potential optimization to improve separation

performance. The physiochemical properties of membrane materials and their possible effect on pervaporation process are also presented in this chapter.

Chapter 3 presents a study on the effect of crosslinking on the physicochemical properties and PV dehydration performance of ethanol for poly(vinyl alcohol) membranes. Of particular interest are the surface properties like roughness and hydrophilicity and their relation to flux and selectivity of the crosslinked membranes.

Chapter 4 studies the effect of PVA layer thickness of crosslinked poly(vinyl alcohol)–poly(sulfone) composite membranes for the PV dehydration of ethanol. The PVA layer thickness was systematically varied to study the effect on flux and selectivity with relation to crosslinking of the membrane.

Chapter 5 reports the study on chitosan-poly(vinyl alcohol) blend membranes for pervaporation dehydration of ethylene glycol-water mixtures. This study demonstrates how blending can be used to control crystallinity in dense membrane to obtain high flux and selectivity. The effect of the blending (with chitosan) and crosslinking on hydrophilic poly(vinyl alcohol) membranes were presented and discussed in this chapter along with the effect of feed flow-rate on concentration polarization that can affect flux and selectivity.

Chapter 6 investigates the crosslinking effect on the composite poly(vinyl alcohol)-poly(sulfone), PVA-PSf membranes for the dehydration of ethylene glycol-water mixtures. This study focussed on the effect of crosslinking solution concentration and reaction time and their effect on flux and selectivity.

Chapter 7 presents a study on the optimization of operating conditions on flux and selectivity by Central Composite Rotatable Design (CCRD) for the PV dehydration of alcohols near azeotropic composition. Two systems were studied e.g., isopropanol-water and ethanol-water to find the optimum operating conditions of temperature, feed alcohol concentration and flow-rate.

Chapter 8 presents the conclusions of the studies conducted in the thesis, the original contributions of this research and recommendations for future work.

The experimental setup, physical properties of the polymers/solvents, concentration polarization, diffusivity correlation and error analysis are presented in appendix *A to E*.

CHAPTER 2

Background and literature review

This chapter briefly describes membrane separation processes with focus on pervaporation, factors affecting the pervaporation process and transport mechanisms in pervaporation. This chapter also describes the physicochemical properties of polymeric membranes and their characterization techniques.

2.1 Membrane separation

A membrane can be defined as a semi-permeable (active or passive) barrier which, under a certain driving force, allows preferential passage of one or more species (molecules, particles or gas) of a gaseous and/or liquid mixture or solution [Baker, 2004]. The stream passing through the membrane is called permeate while the stream rejected by the membrane is called retentate. The key parameters in the operation of a membrane are the flux, associated with the mass transfer across the membrane and the selectivity which refers to the ability to separate one or more species of a mixture. As a general rule, membranes with high flux usually show low selectivity, and the opposite.

The driving force across the membrane for the separation of a particular species can be pressure gradient (ΔP), partial pressure gradient (Δp), concentration gradient (ΔC), temperature gradient (ΔT), electric- potential gradient (ΔE) etc. Depending on the driving force and the physical dimension of the separated species, membrane processes can be classified as: reverse osmosis (RO), ultrafiltration (UF), nanofiltration (NF), microfiltration (MF), electro-dialysis (ED), Gas Separation, Pervaporation (PV), and Vapor Permeation (VP) (cf. Table 1). Since 1970s, the membrane market has been dominated by polymeric membranes where the application ranges from desalination of sea and brackish water, separation of azeotropic and close-boiling point mixtures, gas separation, food and beverage processing and hemodialysis.

Of the above mentioned technologies, pervaporation can be used for solvent separations over a wide range of concentrations irrespective of the presence of azeotropes. In pervaporation, generally the minor component in the feed is permeated through the membrane decreasing the membrane area requirement. And since only a part of the feed is vaporized in

the process, pervaporation is less energy intensive compared to distillation or vapor permeation.

Table 2.1: Membrane separation process [Baker, 2004]

Process	Driving Force	Separated size	Application
Microfiltration (MF)	ΔP (10-500 kPa)	0.1-10 μm	Sterilization of liquids
nanofiltration (NF)	ΔP (0.1-1 MPa)	5-10 nm	Separation of salts and microsolutes from solutions
Ultrafiltration (UF)	ΔP (0.1-1 MPa)	1-5 nm	Separation of macromolecular solutions
Reverse osmosis (RO)	ΔP (2-10 MPa)	< 5 nm	Separation of salts from seawater
Dialysis	ΔC	< 5 nm	Separation of salts and microsolutes from solutions
Electro-dialysis (ED)	ΔE	< 5 nm	Desalinization of ionic solutions
Gas Separation	Partial Pressure difference	< 1 nm	Separation of inorganic/ organic gases
Pervaporation (PV)	Partial Pressure difference	< 1 nm	Separation of azeotropic mixtures
Vapor Permeation (VP)	Partial Pressure difference	< 1 nm	Separation of azeotropic mixtures

2.1.1 Mass transport in membranes

The mass transfer mechanism in a membrane indicates how a set of molecules of one or several species are transported along the pores of a membrane layer. The mass transfer across a membrane depends on the pressure and temperature as well as on the pore size of the membrane and on the properties of the permeating molecules. Figure 2.1 summarizes mechanisms that can take place in a polymeric membrane.

a. Viscous flux: The mechanism is based on non-selective laminar mass transfer along the pores of the membrane due to the pressures gradient across the membrane. The transport happens in the membrane with a pore size greater than the mean-free path (λ) of the permeating molecules, defined by the *Kinetic Theory of Gases*. For an ideal gas, the mean free path can be calculated with the following relation

$$\lambda = \frac{1}{\sqrt{2\pi d_m^2}} \frac{RT}{PN_A} \tag{2.1}$$

where, d_m is the kinetic diameter of the molecules [m] and N_A is the Avogadro Number (6.023 x 10^{23} mol^{-1}).

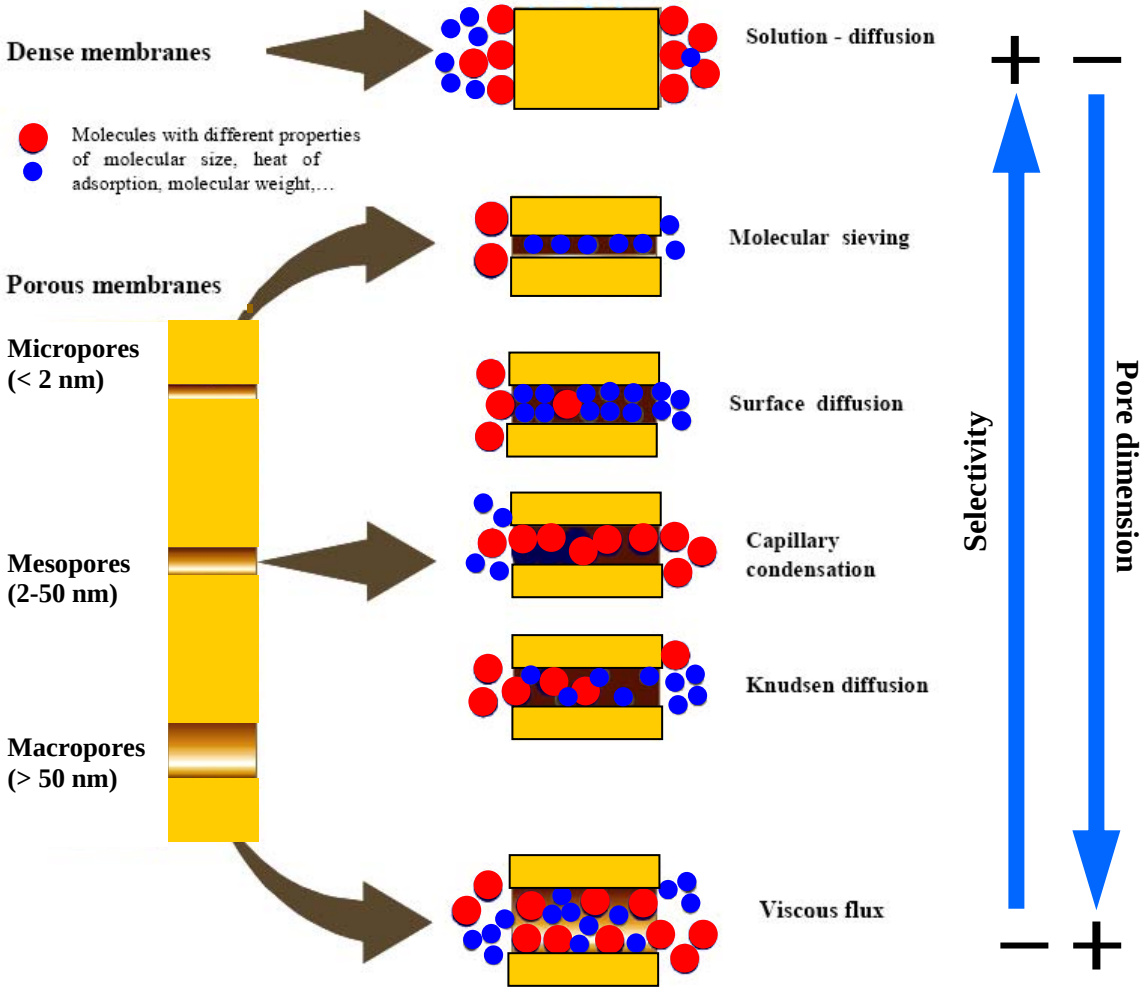

Figure 2.1: Schematic representation of mass transfer in a membrane [Hsieh, 1996]

b. Knudsen diffusion: In this case, the pore size of the membrane is lower than the mean free path of the permeating molecules. As a result, the frequency of collisions with the pore walls is higher than that of intermolecular collisions. The selectivity is usually low, except for permeating molecules with very different molecular weights.

c. Surface diffusion: When a permeate species adsorbed onto the porous membrane by jumping from one adsorption site to another across the membrane. If the adsorption

dominates, surface diffusion becomes deterred, while if it is too weak, adsorption does not contribute much to the overall mass transfer.

d. Capillary condensation: This mechanism occurs in the separation of gaseous mixtures with condensable vapors. This can be predicted by Kelvin Eq (2.2), one or more vapor species of a mixture can be condensed in the pores of the membrane if they are small enough, although the saturation pressure of the vapor is not reached:

$$\ln\left(P_V / P^O\right) = -\frac{4\sigma\overline{V}}{d_P RT} \tag{2.2}$$

where, P_V and P^O are, respectively, the vapor pressure of a drop of size d_p [m] and the saturation vapor pressure [Pa]; s is the surface tension [$N.m^{-1}$] and $\overline{V}$ is the liquid molar volume [$m^3.mol^{-1}$].

e. Molecular sieve: It occurs when the mean pore size of the membrane is very small and it can discriminate between two or more species depending on their molecular size. The membrane acts as a sieve that only lets the permeation of species with a molecular size lower than that of the pore.

f. Solution-diffusion: This is the common mechanism for a dense membrane applied to pervaporation and it does not usually take place in porous membranes. The permeating species adsorb onto the surface of the membrane (they are regarded as sorption), diffuse to the permeate surface and finally desorb. Transport through the membrane depends on feed components, membrane material and operating conditions. The pressure change from feed to permeate side of the membrane has a negligible effect on mass transfer [Olsson *et al.*, 2002]. Permeation rate is independent of the feed pressure of the membrane because of the large concentration gradient [Huang, 1991]. However, liquid permeation follows Fick's first law of diffusion, where the steady-state rate is inversely proportional to membrane thickness [Binning *et al.*, 1961]. Details about this mass transport mechanism will be described at the end of this chapter.

2.1.2 Process definition

Pervaporation is a non-porous membrane separation process, which is used for selective separation of solvents based on selective sorption and diffusion of one of the components through the membrane. The diffusing species undergo a phase change from liquid to vapor as they diffuse through the membrane. The membrane in pervaporation, acts as a barrier between the feed in the liquid phase and the permeate in the vapor phase. The driving force responsible for transport across the membrane is a chemical potential/activity gradient across the membrane which is generated by preheating the feed and vaporizing the permeate. The gas phase on the permeate side is created by either applying a vacuum or using an inert strip gas. The transport process in pervaporation through a polymer membrane can be visualized to occur by the following series of steps [Mulder and Smolders, 1986; Kataoka *et al.*., 1991]:

1) Transport of the species from the bulk liquid phase to the feed-membrane interface.
2) Preferential sorption of the species at the feed-membrane interface.
3) Diffusion of the species through the membrane.
4) Desorption and evaporation of the species at the membrane-permeate interface.

Step 1 depends on the velocity of the feed across the membrane surface. Generally, the separation modules are designed such that a high cross-flow velocity is almost always maintained across the membrane as a result of which the mass transfer resistance of the first step is negligible. However, the first step becomes critical when the species to be transported across the membrane are present in very small proportions in the feed and the selective sorption of the membrane for the same species is very high. An appropriate example of such a situation would be the removal of volatile organic compounds (VOC's) from aqueous solutions by hydrophobic membrane in pervaporation [Athayde *et al.*, 1997]. Step 4 is a very rapid process when pressures on the permeates side are low. However, as the permeate pressures approach the partial vapor pressure of the permeating species, the permeate flux does become dependent on the rate of vaporization [Frenesson *et al.*, 1986]. Steps 2 and 3 mentioned above are generic to all pervaporation processes. The sorption process in step 2 includes the adsorption of a selective component on the membrane surface and then the selective component is absorbed within the polymer network [Oasada and Nakagawa, 1992]. In step 3, the diffusion of the component takes place through the membrane due to a chemical potential gradient (concentration or partial pressure gradient). The adsorption of components

is affected by the surface properties e.g., surface hydrophilicity, surface roughness etc. of the membrane materials whereas the diffusion of components is affected by the polymer network e.g., density, crosslinking etc.

The sorption of components in the polymer membrane can be thought of a reverse process of making a polymer solution [Heintz *et al.*., 1994]. Generally, polymer molecules are long chains with a large number of segments, forming tightly folded coils which are entangled with each other. Both intra and intermolecular forces such as cohesive and attractive forces e.g., *dispersion*, *dipole-dipole interaction*, *induction*, and *hydrogen bonding* hold these polymer coils together. When a polymer material is added to a given solvent, attraction as well as dispersion forces begin acting between its segments, according to their polarity, chemical characteristics, and *solubility*.

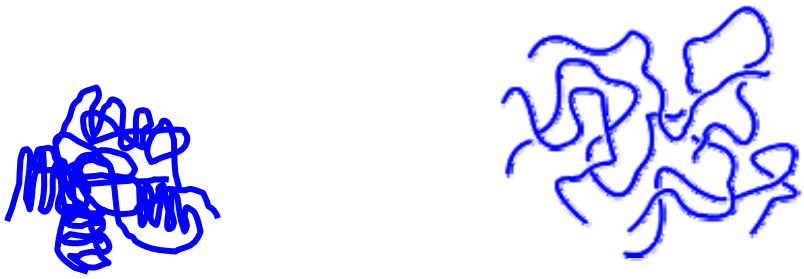

(a) polymer segments in the solid state (b) swollen polymer segments

Figure 2.2: Schematic representation of the swelling in for polymer

When the polymer-solvent interactions are higher due to excessive affinity between polymer and solvent molecules, the chain segments start to absorb selective species, increasing the volume of the polymer matrix, and loosening from their coiled shape as shown in Fig. 2.2. This phenomenon of the uncoiled solvated polymers is known as swelling. Hydrophilic polymeric membranes tend to swell easily for aqueous-organic mixtures separation and lose their stability quickly. To avoid this situation, polymeric membranes are modified using different processes e.g., crosslinking, blending etc. [Yeom and Lee, 1996; Nugay *et al.*, 2000].

For polymeric materials the "solvation-unfolding-swelling" process takes a long time. If the polymer-solvent interactions are still strong enough, the "solvation-unfolding-swelling" process will continue until *all* segments are solvated. Thus, the whole loosen coil will diffuse out of the swollen polymer, dispersing into the solution. But for a crystalline, hydrogen

bonded or crosslinked polymeric membrane, the polymer-polymer interactions are strong and the process stops at a swollen polymer membrane network as a result. The swollen polymer network is flexible for the transport of both the selective and non-selective components of mixtures. This results in the increase in total flux of the separation process. However, the selectivity of the separation process decreases due to the transport of non-selective components on the permeate side.

2.1.3 Separation parameters

A difference in chemical potential (due to partial pressure or activity) between feed and permeate side of the membrane is the driving force in pervaporation [Lipnizki *et al.*, 1999]. Feed components have different sorption and diffusion rates through the membrane, which govern selectivity and permeation rate [Qariouh *et al.*, 1999; Villaluenga and Tabe-Mohammadi, 2000].

In pervaporation process, separation performances are generally characterized by, total flux of the permeating components and the selectivity of the membrane for one component as compared to another. The total flux (J) through the membrane is defined as the total mass flow of all the permeating components through the membrane per unit area per unit time. The flux for each individual component can also be defined as:

$$J = \frac{M}{A * t} \tag{2.3}$$

where J is the total flux [$M/L^2 t$], M is the permeate mass collected, [M], A is Membrane surface area [L^2], and t is the time period of collected mass, [t].

The selectivity of the membrane can be expressed in terms of a separation factor, α_{ij} which is defined as:

$$\alpha_{ij} = \frac{y_i / y_j}{x_i / x_j} \tag{2.4}$$

where, y is the mass fraction of components i and j in the permeate and x is the mass fraction of components i and j in the feed mixture. Here, i is the preferential permeating component and j is the non-preferential permeating component.

For comparing the separation performance, it is quite common to express the component flux (J_i) in terms of membrane permeance (Q_i) of the membrane using the

following eq. [Baker, 2004]

$$J_i = Q_i\left(x_i\gamma_i p_i^o - y_i p_i^p\right) \tag{2.5}$$

where, x_i is the feed liquid molar fraction, γ_i: activity coefficient, p_i^o is the vapor pressure of component i, y_i is the molar fraction at permeate and p_i^p is the pressure at permeate side of component i. Membrane permeance is also known as permeability normalized by membrane thickness.

2.2 Factors affecting separation performance

Specific characteristics of the feed components, the membrane, and process operating parameters influence overall PV performance. Separation performance in pervaporation depends not only on the operating conditions e.g., concentration, temperature, flow-rate etc but also on the properties of the membrane materials e.g., crystallinity, degree of crosslinking, hydrophobicity etc… [Binning *et al.*, 1961; Cabasso, 1981; Miranda and Campos, 1999; Villaluenga and Tabe-Mohammadi, 2000; Guo *et al.*, 2007; Yoshida and Cohen, 2003; Smitha *et al.*, 2004].

2.2.1 Effects of operating conditions

The major operating factors that affect the flux and selectivity are temperature, feed concentration, flow-rate and partial pressure difference [Smitha *et al.,* 2004].

2.2.1.1 Feed concentration

Feed concentration is one of the most important factors affecting a pervaporation process. In theory, PV can be used to separate any liquid mixture in all concentration ranges [Johnson and Thomas, 1999]. However, it is primarily used for removing or recovering the minor component in organic/organic azeotropic, close-boiling point, or isomeric mixtures [Mulder *et al.*, 1985; Blume *et al.*, 1990]. The chemical potential gradient across the membrane is the driving force for a pervaporation process. It affects the sorption process at the liquid-membrane interface and the concentration dependent diffusion transport of the permeate [Shieh, 1996]. Generally high concentration of preferential components across the membrane promotes swelling. This results in the increase of void volume in polymer network [Villaluenga and Tabe-Mohammadi, 2000]. Therefore, it facilitates both components, low and high affinity to the membrane, penetrate through the membrane which leads to the higher total permeate flux.

2.2.1.2 Feed temperature

Feed temperature has a great influence on the pervaporation process. The solubility and diffusivity of the permeant in the membrane depends upon the temperature. Molecular-level interactions between membranes and diffusing species are expressed via a permeability constant used in the Arrhenius relationship:

$$Q = A_0 \exp\left(-\frac{E_p}{RT}\right) \tag{2.6}$$

where, A_o is the permeability constant [M/L^{2}t], E_p is the activation energy [ML^2/t^2,mole], R is the gas constant [ML^2 /t^2 K..mole] and T is the absolute temperature [K].

Generally, the permeation rate increases with the feed temperature. The increase in feed temperature stimulates the thermal mobility of the polymer chains in the matrix and the permeant molecules. Other explanations include the increase in diffusivity with temperature [Huang and Lin, 1968; Acharya *et al.*, 1988; Huang and Rhim, 1990; Cussler, 1997; Villaluenga and Tabe-Mohammadi, 2000; Bird *et al.*, 2002]. The rise of molecular diffusivities results in the increase of the permeation rate. Also, there is a phase change from liquid to vapor in the pervaporation process. With an increase in temperature, more energy is supplied to the permeants that can vaporize more easily. This results in a gas transport which is larger than the liquid transport inside the membrane. Consequently the mass transport across the membrane increases [Cussler, 1997; Baker, 2004].

2.2.1.3 Feed flow-rate

During PV separation, on the feed side, a concentration gradient is created due to a boundary layer on the membrane surface. Within this boundary layer the concentration of the permeating component decreases. This phenomenon is called concentration polarization [Bhattacharya and Hwang, 1997; Smitha *et al.*, 2004; Feng and Huang, 1996]. As a result the concentration of the components that are retained will increase within the boundary layer. Concentration polarization causes components that are enriched in the permeate to be depleted in the boundary layer, and components that are depleted in the permeate to be enriched in the boundary layer. Thus, concentration polarization works against the separation achieved by the membrane, reducing flux and selectivity. To reduce concentration polarization, it is necessary to increase the flow-rate and modify the design of the membrane cells (baffles) to reduce the formation of boundary layers. At higher feed velocity, the flow

inside the cell becomes turbulent on the feed side that reduces concentration polarization [Wijmans *et al.*, 1996].

2.2.1.4 Permeate pressure

Permeate pressure on the down-stream side of the membrane can affect the pervaporation process due to evaporation of species. At permeate pressure close to the vapor pressure of the selective species, can strongly influences the pervaporation characteristics [Dutta and Sikdar, 1991; Smitha *et al.*, 2004]. Generally in pervaporation, the feed pressure is kept atmospheric and as such the downstream pressure contributes for the difference in partial pressure. Lower downstream pressure results in an increase in the driving force in addition to the feed concentration and thereby increase in the permeation flux [Neel, 1991].

2.2.2 Membrane materials

In pervaporation, a variety of membrane materials have been developed to cater mainly two types of industrial liquid separations: organic-water and organic-organic separations. This section gives a brief overview of the various types of membrane materials developed and studied for both aqueous-organic and organic-organic separations. Some common examples of such separations are dehydration of alcohols, removal of water from esterification reactions, etc. The polymeric materials can be broadly classified into three categories: glassy polymers, rubbery or elastomeric polymers and ionic polymers. In general, the glassy and ionic polymers are more suited for making water-selective membranes for dehydration whereas the elastomeric polymers can be used for removal of organic compounds from aqueous streams. The structures of some of these polymers are shown in Fig 2.3.

(a) Poly(vinyl alcohol) or (PVA) (b) Poly(dimethylsiloxane) or (PDMS)

Figure 2.3: Repeating units of polymeric membranes

A polymer with higher affinity for one feed component gives greater selectivity. However, if the affinity is too high, the membrane is excessively swollen by the component, loses its integrity and therefore its selectivity. Consequently, it is important to suppress or control the degree of swelling by crosslinking or other methods [Villaluenga and Tabe-

Mohammadi, 2000]. The membranes used in pervaporation processes are classified according to the nature of the separation being performed. *Hydrophilic membranes* are used to remove water from organic solutions. These types of membranes are typically made of polymers with glass transition temperatures above room temperatures. Poly(vinyl alcohol) is an example of a hydrophilic membrane material. *Hydrophobic membranes* are used to recover organics from solutions. These membranes are typically made up of elastomer materials (polymers with glass transition temperatures below room temperature). The rubbery structure of these polymers make them ideal for allowing the organic to pass through. Examples include poly(dimethyl siloxane) or PDMS and poly(octylmethyl siloxane) or POMS [Wynn, 2003].

Selecting membrane materials for PV is often done by trial and error. This is time consuming and the best membrane may not be found due to the limited number of membranes tested. A more rational method would match the physico-chemical properties of the membrane material with the components of the liquid to be separated. This is done simplistically for common PV applications such as organic liquid dehydration or waste-water treatment by choosing hydrophilic or hydrophobic membranes. Generally, it is more economical in terms of energy to preferentially transport the component with the smallest weight fraction across the membrane. Koops and Smolders (1991) recommend that potential membrane materials be identified by: (1) literature search, (2) properties of the mixture, and (3) chemical and thermal stability of the polymer.

2.2.2.1 Hydrophilic polymers

For water selective membranes, the most important factor responsible for the separation is the specific interaction between water and the polymer. Polymers containing specific groups/active centers e.g., hydroxyl or amide groups are capable of strong interactions with water. Membranes prepared from these polymers generally display high selectivity in pervaporation. Semenova *et al.* (1997) have broadly classified the polymer-water interactions into two categories; i) hydrogen bonding interactions and ii) ion-dipole interactions.

Category 1. Hydrogen bonding interactions

The hydrogen bonding interactions are possible in polymers containing hydroxyl groups, such as in poly(vinyl alcohol), polymers containing amide/imide groups such as polyamides, polymers containing carboxylic groups (cellulose acetate, CA; polyvinyl acetate,

PVAc; etc.) and ether groups, all of which are capable of forming strong hydrogen-bond with water. It should be noted that in most cases, the polymer backbone (or certain segments) is usually hydrophobic while the pendant groups are hydrophilic. It is necessary to maintain an appropriate hydrophilicity-hydrophobicity balance to achieve the necessary separation properties. The techniques for controlling this balance have been discussed by Huang (1991). Some of these techniques include cross-linking, grafting, blending, copolymerization and incorporation of filler materials in the membranes [Uragami *et al.*, 1994; Yeom and Lee, 1996].

Category 2. Ion-Dipole interactions

These interactions are mainly present in polymers containing fixed charged ionic groups, which can strongly interact with water. Some examples of such materials are polymers containing partially quarternized ammonium basics, various ion-exchange membranes (Nafion) and polyelectrolyte complexes (chitosan, cellulose sulfate, etc.).

2.2.2.2 Hydrophobic polymers

The primary factor responsible for the separation efficacy of an organophilic membrane is the hydrophobicity of the polymer. A hydrophobic polymer generally has a strong affinity for organic solvents (such as trichloroethylene, toluene, ethyl acetate and others) resulting in a considerably high sorption of the permeates and hence good separations. For most aqueous-organic separations, the organic molecule is generally bigger than the water molecule. This results in lower membrane selectivity due to lower diffusion of the organic molecules. Thus, it is necessary that the organophilic membrane material should exhibit very high sorption selectivity in order to compensate for the low diffusion selectivity. Poly(dimethylsiloxane) (PDMS) exhibits very high sorption selectivity for apolar organic solvents and therefore it has been commercially used in the manufacture of organophilic pervaporation membrane modules. Bruschke (1991) of GFT has mentioned that PDMS provides the best combination of properties with respect to flux, selectivity and stability for removal of most organics.

2.2.3 Effect of permeant size

The first two steps of the permeation process involve dissolution of molecules into the polymer membrane, then diffusion of these molecules through the membrane. Differences in

either solubility or diffusivity give preferential permeation. Solubility depends primarily on differences in the chemical nature of the permeating species whereas diffusivity is determined largely by the size and shape of these molecules and the degree the diffusing species aggregate within the polymer [Huang and Lin, 1968]. In summary the following three general trends were observed by Huang and Lin (1968): for binary permeation of two components of a homologous series, the lower molecular weight species permeates preferentially, molecules with a smaller diameter will permeate faster than their bulkier counterpart and shape and size effects predominate for chemically similar molecules. However, molecules with large differences in chemical nature are affected more by parameters such as solubility, than shape and size. Binning *et al.* (1961) used several pure hydrocarbons to study the effect of size, shape and chemical nature on permeation through a PV membrane. The flux of a homologous series of normal paraffins through a polymer film under the standard conditions decreased with the number of carbon atoms. Johnson and Thomas (1999) attributed this phenomenon to decreased diffusivity with increased penetrant size. Thus even if solubility increases, the decrease in diffusivity reduces overall flux.

2.2.4 Membrane thickness

Permeation rate is inversely proportional to membrane thickness but selectivity is said to be independent of thickness. Binning *et al.* (1961) established a linear inverse relationship between flux and film thickness (0.8 - 1.9 mm), yet selectivity of the *n*-heptane / iso-octane mixture (50 vol%) remained unchanged at all four membrane thicknesses. For film thicknesses that could be produced in 1961, Binning *et al.* (1961) felt that PV could still retain selectivity and rapid permeation rates even when operating with very thin films (800 nm). Synthetic polymer membranes can be as thin as 0.1-35 μm [Smitha *et al.*, 2004]. In the last two decades, researchers have studied the effect of homogeneous membrane thickness on separation performance for different binary mixtures [Koops et al., 1994; Nijhuis et al., 1991]; the flux was found to be inversely proportional to the membrane thickness but the selectivity remains nearly unaffected.

2.2.5 Membrane swelling

Swelling behavior gives an idea about the sorption behavior of components in the membrane matrix. In pervaporation, excessive affinity of a permeating species for the selective

polymeric membrane can result in swelling of the membrane matrix [Ruckenstein and Sun, 1995]. Swelling will change both flux and selectivity [Smitha *et al.*, 2004], and the degree of membrane swelling must be suppressed or controlled [Villaluenga and Tabe-Mohammadi, 2000], because swelling decreases membrane selectivity, and causes loss of membrane integrity [Feng and Huang, 1997]. A trade-off between sorption and swelling is needed. For preferential permeation to occur, there must be a high degree of chemical affinity between one component and the membrane. However, if affinity is too great, the membrane will swell and lose integrity. [Villaluenga and Tabe-Mohammadi, 2000].

2.2.6 Crystallinity

Polymeric membranes can exist in a crystalline or amorphous state. However, because of their size and complexity they are often semi-crystalline, i.e. the polymer having both amorphous and crystalline regions (see Fig. 2.4). Any chain disorder or misalignment will result in an amorphous region. Six factors favor a polymer with a high percent crystallinity: a regular and symmetrical linear chain, a low degree of polymerization, strong intermolecular forces, small and regular pendant groups, a slow rate of cooling, and oriented molecules. For example, PVA molecules consisting of symmetrical and linear chain with strong hydrogen bonding display high crystallinity.

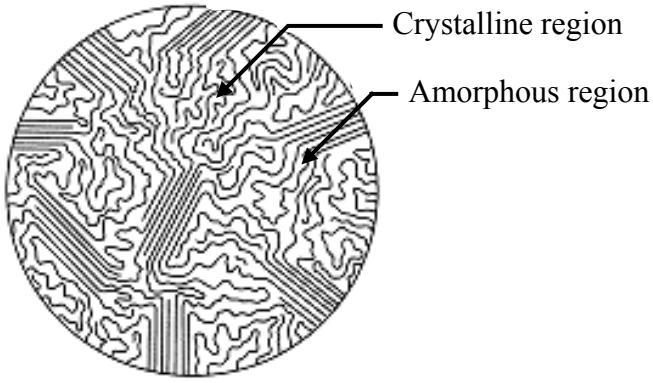

Figure 2.4: A *semi-crystalline* polymer showing regions of *crystalline* and amorphous regions [Gref *et al.*, 1993].

Highly crystalline polymers do not dissolve easily in many solvents, primarily due to a lack of flexible groups, which prevent a high degree of swelling. The crystallites act as physical cross-links keeping the polymer tightly packed. Because dissolution generally occurs in the amorphous part of the polymer, the degree of crystallinity has a large influence on the

dissolution of the feed into the membrane. Highly crystalline polymers have lower permeability than amorphous polymers [Gref *et al.*, 1993].

2.2.7 Free volume

The free volume of a polymer is the sum of the many small spaces between the polymer chains in the amorphous, noncrystalline materials. Because the polymer chains do not pack perfectly due to their side groups, some unoccupied space—free volume—exists between the polymer chains. The free volume of a polymer can be determined by measuring the polymer's specific volume, then calculating the occupied volume of the groups that form the polymer. Free-volumes in the amorphous polymeric membranes are tiny spaces between polymer chains caused by thermal motion of the polymer molecules [Baker, 2004]. These volume elements appear and disappear on about the same timescale as the motions of the permeants traversing the membrane. The larger the individual free volume elements (pores), the more likely they are to be present long enough to produce pore-flow characteristics in the membrane. Reverse osmosis, pervaporation and polymeric gas separation membranes have a dense polymer layer with no visible pores, in which the separation occurs. These membranes show different transport rates for molecules as small as 2–5 Å in diameter [Plate and Yampol'skii, 1994]. The fluxes of permeants through these membranes are also much lower than through the micro-porous membranes.

2.3 Membrane formation

Although research effort in synthesizing polymer membranes for different applications has existed for about half a century, major developments in preparing membrane materials were made only recently as a result of advances in synthetic polymer technology [Lipnizki *et al.*, 1999]. The phase inversion technique for forming membranes was initially explored by Sourirajan *et al.*, (1961), Mulder *et al.* (1983). Subsequently, researchers obtained greater permeabilities by reducing the thickness of the effective separation layer [Yeom *et al.*, 1996; Ray *et al.*, 1998; Smitha *et al.*, 2004]. Synthetic polymers have better thermal and mechanical properties than the natural polymers, with good flux and selectivity.

2.4 Membrane morphology

The proper choice of a membrane should he determined by the specific application objective: particulate or dissolved solids removal, hardness reduction or ultra pure water production,

removal of specific solvents etc… Work on membrane separations began in the early 1960s, using membrane materials such as dense metals, zeolites, polymers, ceramics and biological materials. Of these, polymers are the most widely used material [Smitha *et al.*, 2004]. Generally, in pervaporation, the membrane always has a selective layer through which the permeate transport occurs. Several different polymer membrane structures are commonly used today, including porous, dense and asymmetric membranes. Selecting a good membrane requires a sound knowledge of membrane structures. The following section explains the types of membranes commonly used in pervaporation.

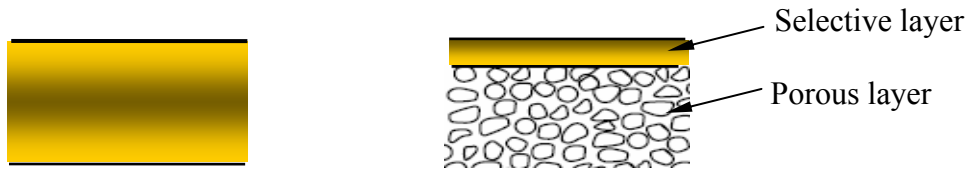

(a) dense membrane (b) composite membrane

Figure 2.5: Schematic morphologies of pervaporation membranes

2.4.1 Dense membranes

Homogeneous (dense) membranes are single phase structure free of discrete, well-defined pores or voids as shown in Fig 2.5 (a). The whole dense structure acts as the selective layer through which component molecules are transported due to pressure, concentration or electrical potential gradient. The membranes effectiveness depends on the polymer properties and the species to be separated and their interaction with the membrane [Chan *et al.*, 1999; Fan *et al.*, 2003]. Dense homogeneous membranes are not suitable for industrial applications because of their low permeation rate.

2.4.2 Composite membrane

These membranes consist of a dense selective layer, a porous support and a non-woven fabric. Like the asymmetric membranes, the selectivity depends on the top layer as shown in Fig 2.3(b). However the material used for the porous layer and the thin top layer are of different materials. Non-woven fabric is used for enhancing the mechanical strength of the membrane [Shieh and Huang, 1997; Schwarz *et al.*., 2003]. This kind of membrane is widely used in the industry.

For industrial applications and research purposes, polymeric membranes are casted into three types of modules: *Plate and frame*, *Spiral wound* and *Tubular*, *Capillary or Hollow fibre*. The plate and spiral-wound modules are most commonly used in pervaporation [Wynn, 2003]. Plate modules are generally used for the dehydration of organic-water solution and spiral wound modules are used for separating small amounts of organics from water.

2.5 Modifications of the polymeric membrane

Ideally, a membrane should give both a high flux and a high selectivity. However, an increase in flux is usually accompanied by a decrease in selectivity. Therefore, membrane performance has to be adjusted to achieve optimum performance for a given separation [Johnson and Thomas, 1999]. Membrane modification techniques such as, cross-linking, blending, grafting, and copolymerization can all affect polymers separation characteristics and membrane stability.

2.5.1 *Crosslinking*

In membrane technology, there are two reasons to crosslink a polymer. The first reason is to make the polymer insoluble in the feed mixture and the second reason is to decrease the degree of swelling of a polymer in order to achieve good selectivity. Crosslinking can be executed in different ways e.g., chemical reaction, irradiation, heat treatment, etc [Bitter, 1984; Uragami, 1994; Yeom and Lee, 1996; Krasemann *et al*., 2001]. However, excessive crosslinking may render the polymer membrane brittle with a loss in the dimensional stability for a particular application.

2.5.2 *Grafting*

Grafting is a polymer modification technique where oligomeric chains are attached as side chain branches irregularly onto the polymer main chain. This can be done by chemical reaction or by irradiation. If the molecules to be grafted contain a functional group that is able to react with a functional group of the polymer, grafting by chemical reaction can occur. Grafting by irradiation is a versatile technique for the modification of insoluble polymer films. Aptel *et al.*, (1974) have performed a lot of research on grafting films by irradiation.

2.5.3 *Blending*

A mixture of two polymers which are not covalently bonded is called a polymer blend. Polymer blending creates new polymeric materials that combine the properties of two homopolymers. The composition of the blend affects the physical, mechanical and permeation properties of the resultant polymer [Johnson and Thomas, 1999]. In principle, blending is an ideal technique for creating desired hydrophilicity or hydrophobicity to separate a particular mixture using membrane. The optimum-blending ratio can be determined by mixing the hydrophilic polymer with a hydrophobic one at various compositions and measuring the permeability and selectivity [Rhim *et al.*, 2002].

2.5.4 *Copolymerization*

Copolymerization can be applied for the same reason as the blends are used, but unlike in blends, the two polymers are covalently bonded which increases the mechanical stability of the membrane [Chiang and Lin, 2002]. Besides grafted copolymers, block and random copolymers can be formed by this technique.

2.6 Characterization of polymeric membrane

In pervaporation, the membrane surface in contact with the feed solution controls the sorption of permeates. For example, hydrophilic poly(vinyl alcohol), PVA membrane is used for the dehydration of alcohol. However, water has excessive affinity for PVA membrane and this leads to swelling instantaneously [Yeom and Lee, 1996]. The adsorption of solvents on the surface of the membrane and absorption of solvents inside the membrane is responsible for the swelling process. On the other hand, the diffusion process is affected by bulk properties of the membrane such as crystallinity, thickness, free volume etc… Therefore, the physicochemical bulk and surface characterization of polymeric membrane is important to understand and control the separation performance. The material and surface analytical techniques include a variety of physical, chemical, material, and mechanical characterizations. They can provide information that will allow one to select the materials and control the surface and bulk structure modification of the membrane, best suited for a particular application.

In the last two decades, techniques such as attenuated total reflectance IR spectrometry [Belfer *et al.*,1998], scanning [Pusch and Walch 1982; Cabasso,1981] and transmission

[Uemura and Inoue, 1984] electron microscopy, and X-ray photoelectron spectroscopy [Koo *et al.*, 1986], atomic force microscopy [Dietz *et al.,* 1992; Bessières *et al.*., 1996; Bowen and Doneva, 2000] have occasionally been used to characterize the surfaces of nanofiltration, ultrafiltration and reverse osmosis membranes. Other non-surface science techniques have been used to characterize the molecular structure of membrane materials, but these studies have only been applied to thick homogeneous films [Pusch and Walch 1982; Higuchi and Iijima, 1985; Scherer and Bailey, 1983]. A few researchers [Rosa, and de Pinho, 1997; Zhang and Hallstrom, 1990] used contact angle measurement to characterize the membrane surfaces used in nanofiltration and ultrafiltration separation. There have been relatively very few publications [Zeng *et al.*, 1997; Lee *et al.*, 1998] which have described the chemical composition and physical structure (layer thickness, morphology, composition gradients, etc.) of pervaporation membranes. Oftentimes, researchers observed the change in degree of crosslinking and describe the separation performance accordingly [Yeom and Lee, 1996]. However, none of the studies ever tried to study surface and bulk properties of the membrane and try to correlate these properties to the flux and selectivity. Therefore a good understanding of the polymer surface characteristics and its effect on pervaporation separation is necessary. In the following sections, some of the membrane surface characteristics are described briefly.

2.6.1 Surface characterization

Membranes in an aqueous environment have an attractive or repulsive response to water. The material composition of the membrane, its surface chemistry and structures determine the interaction with solvent mixtures [Andrade, 1985; Franken *et al.*, 1987]. Surface features such as roughness can affect the sorption process and thereby separation performance. The surface chemistry allows the membrane to be wetted forming a water film or coating on the surface. Hydrophilic materials have the ability to form "hydrogen-bonds" with water and favors dehydration of organics separation. On the other hand, hydrophobic materials have little or no tendency to adsorb water and water tends to "bead" on their surfaces. The surface properties are briefly explained in the following sections.

2.6.1.1 Surface roughness

Roughness includes the finest (shortest wavelength) irregularities of a surface. Roughness generally results from a particular production/fabrication process or material condition. The surface roughness and the roughness factor are obtained from images collected in an atomic force microscopic experiment. The statistics of surface roughness were derived from ASME B46.1 ("Surface Texture: Surface Roughness, Waviness and Lay") available from the American Society of Mechanical Engineers. The definition of

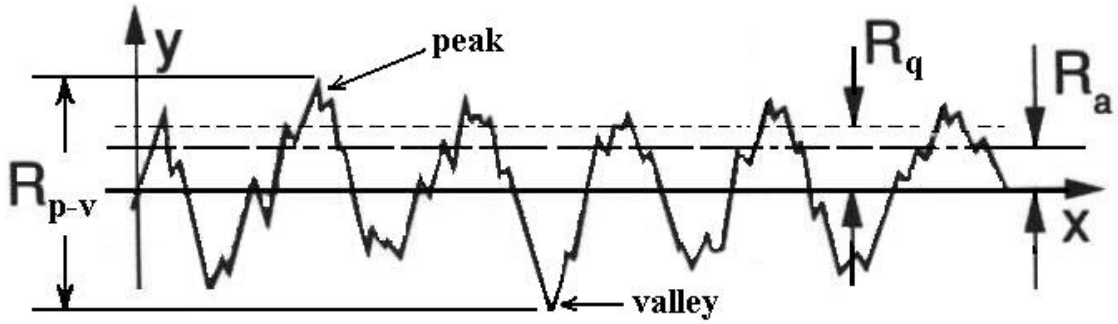

Figure 2.6: Schematic representation of a rough surface.

surface roughness used in this study, R_a, is the arithmetic average of the absolute values of the surface height deviations measured from the mean plane as shown in Fig 2.6

$$R_a = \frac{1}{L}\int_0^L |y(x)|\, dx \qquad (2.7)$$

where, L is the length of the profile, and *y(x)* is the roughness profile. The root mean square (RMS) roughness is defined as

$$R_q = \sqrt{\frac{1}{L}\int_0^L [y(x)]^2\, dx} \qquad (2.8)$$

Another parameter, the total maximum roughness, $R_{p\text{-}v}$, is the sum of the vertical distance from the deepest valley to the highest peak. And expressed as

$$R_{p-v} = |\max y(x)| + |\min y(x)|, \quad \text{for} \quad 0 < x < L \qquad (2.9)$$

2.6.3.2 Wettability

Wettability by water quantitatively indicates the hydrophobicity/hydrophilicity of a surface. It is difficult to obtain the physicochemical properties of a solid surface at the angstrom level.

One of the most sensitive ways known for obtaining true surface information is the contact angle based on Young's equation [Li and Neumann, 1996].

$$\gamma_{lv} \cos\theta_Y = \gamma_{sv} - \gamma_{sl} \tag{2.10}$$

where θ_Y is the Young contact angle (also known as the intrinsic contact angle symbolized by θ_e), and γ_{lv}, γ_{sv} and γ_{sl} are the interfacial tensions of the liquid-vapor, solid-vapor and solid-liquid, respectively as shown in Fig 2.7. The Young equation indicates that θ_Y is a unique function of the interfacial tensions, γ_{sv}, γ_{sl}, and γ_{lv}.

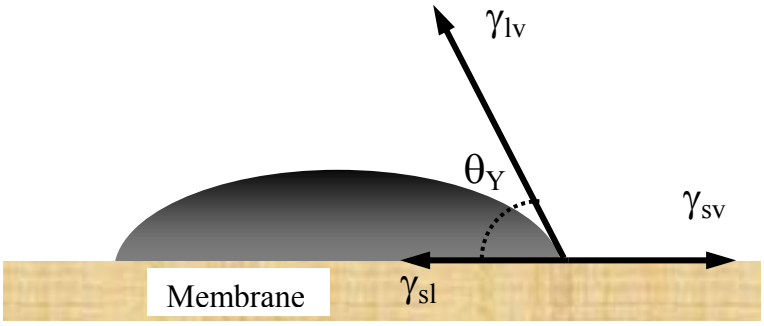

Figure 2.7: Schematic of a sessile drop on a surface

Contact angle is a common measure of the hydrophilicity/hydrophobicity of a surface. Generally the higher the contact angle with probe liquid, the less wettable the polymer. This kind of solid surface is also known as hydrophobic material. On the other hand hydrophilic materials tend to wet the surface. If water is used as the probe liquid, this can also give insight into how hydrophobic/hydrophilic is the polymeric membrane under investigation. It is commonly accepted that for a rough-heterogeneous surface having one continuous and one discontinuous phase, the advancing angle tends to represent the low-wettability phase and the retreating angle the high-wettability phase. Therefore, it is necessary to obtain both the advancing and the receding angle from contact angle measurements. Obviously this is a dynamic process but it is still possible to obtain the equilibrium contact angles [Long *et al.*, 2002].

It is interesting to note that the equilibrium contact angle (θ_Y) was developed for a smooth surface. However, on a rough surface, the contact angle measured by a probe liquid is called apparent contact angle (θ_{ap}), in which case Young's eq. (2.10) is modified to

$$\frac{\gamma_{lv}\cos\theta_{ap}}{\omega} = \gamma_{sv} - \gamma_{sl} \tag{2.11}$$

where ω is the surface roughness factor (defined as the ration of actual surface area to the geometrically projected area of a rough surface) and θ_{ap} is also known as Wenzel contact angle [Wenzel, 1936].

2.6.2 Bulk characterization

Diffusion of permeant is affected by membrane bulk properties such as crystallinity, melting point, degree of crosslinking, mechanical strength, thermal stability etc…. Over the last two decades, researchers have routinely characterized membranes with x-ray spectroscopy, differential calorimetry, tensile strength tester, thermo gravimetric analysis [Baker, 2004].

2.7 Transport mechanism in dense membrane

For scale-up of the pervaporation process, it is necessary to understand the transport mechanism of pervaporation membranes. A fundamental understanding of the driving force, sorption and diffusion processes in dense membranes is imperative for this purpose. Thus any modeling effort would have to encompass as many of the important factors as possible.

2.7.1 Sorption

Knowledge of sorption of all the permeants through the membrane material is essential to understand the pervaporation behavior. The sorption depends on the material-solvent interactions, degree of cross-linking, feed composition and temperature. Ideal sorption can be expected when the interactions between the penetrating components are weak and the concentration of non selective components in the feed, does not affect the sorption of the selective component. Over the years researchers have used ideal sorption for pervaporation modeling [Lee, 1975; Wijmans and Baker, 1993; Shieh and Huang, 1998], neglecting the interaction of liquids with polymeric materials. The following two models consider species interaction to predict the sorption of multicomponent liquid mixtures.

2.7.1.1 Flory-Huggins Theory

Flory-Huggins theory [Flory, 1953] based on free energy of mixing can explain the sorption behavior of multi-component mixtures in polymers. The activity of a species in the polymer can be expressed as a function of the volume fraction of the species, the molar volumes of the

components and the Flory-Huggins interaction parameters. The Flory-Huggins theory takes into account both enthalpic and entropic effects into the free energy of mixing (ΔG_m). For a three component system (two solvents and a polymer), the free energy of mixing is given by the following equation.

$$\Delta G_m = RT\left(x_1 \ln \phi_1 + x_2 \ln \phi_2 + \chi_{12} x_1 \phi_2 + \chi_{1p} x_1 \phi_p + \chi_{2p} x_2 \phi_p\right) \qquad (2.12)$$

where x and ϕ are the mole fraction and volume fractions respectively and χ's are the adjustable parameters. Subscripts 1, 2 and p denote solvents 1, 2 and the polymer respectively. The Flory-Huggins theory has been very successful in predicting the sorption of organic apolar solvents in rubbery polymers. Some typical examples are chloroform-PDMS, benzene-PDMS and carbon tetrachloride-PDMS systems. However, poor agreement between theoretical and experimental results is observed in the case of associated or polar solvents.

2.7.1.2 UNIQUAC/UNIFAC theory

The group contribution models such as UNIQUAC (UNIversal QUasi-Chemical theory) and UNIFAC (UNIQUAC Functional-Group Activity Coefficients) are used to correlate and predict liquid-vapor and liquid-liquid equilibria, i.e., solution properties such as activity coefficients, partition coefficient, Henry's law constant [Abrams and Prausnitz, 1975; Grant and Higuchi, 1989; Yalkowsky and Banerjee, 1992]. The UNIFAC theory combines the concept that a liquid mixture is composed of a solution of functional groups with an extension of the UNIQUAC theory of liquid mixtures [Fredenslund *et al.*., 1975; Gmehling, 1986]. The UNIFAC model showed good agreement for a variety of solvent-polymer systems (dilute concentrations of polymer) when considered with free volume correction [Oishi and Prausnitz; 1978]. UNIQUAC theory states that the activity of component i (a_i) in a system is the sum of a combinatorial part (a_i^C) mainly due to differences in molecular size and shape and a residual part (a_i^R) reflecting energetic interactions. According to the UNIQUAC theory, the activity of component i in a multi-component liquid mixture containing n species, can then be expressed as [Heintz and Stephan; 1992, 1994]:

$$\begin{aligned} \ln a_i\left(x_1,.....x_i,.....x_n\right) = \ln \phi_i + \frac{Z}{2} q_i \ln\left(\frac{\theta_i}{\phi_i}\right) + l_i - \sum_{j=1}^{n} \phi_j \frac{r_i}{r_j} l_j \\ - q_i^* \ln \sum_{j=1}^{n} \theta_j^* \tau_{ji} + q_i^* - q_i^* \sum_{j=1}^{n} \frac{\theta_j^* \tau_{ij}}{\sum_{k=1}^{n} \theta_k^* \tau_{kj}} \end{aligned} \qquad (2.13)$$

where,

$$\phi_i = \frac{r_i x_i}{\sum_{j=1}^{n} r_j x_j} \tag{2.14}$$

$$\theta_i = \frac{q_i x_i}{\sum_{j=1}^{n} q_j x_j} = \frac{\frac{q_i}{r_i}\phi_i}{\sum_{j=1}^{n} \frac{q_j}{r_j}\phi_j} \tag{2.15}$$

$$l_i = \frac{Z}{2}(r_i - q_i) - (r_i - 1) \tag{2.16}$$

$$\theta_i^* = \frac{q_i^* x_i}{\sum_{j=1}^{n} q_j^* x_j} = \frac{\frac{q_i^*}{r_i}\phi_i}{\sum_{j=1}^{n} \frac{q_j^*}{r_j}\phi_j} \tag{2.17}$$

In Eq. (2.13) to (2.17), θ and θ* are the surface fractions of the various components in the mixture, r, q, q* and l are parameters related to the size and shape of the molecule, Z is the coordination number. τ_{ij} and τ_{ji} are binary interaction parameters describing the intermolecular interactions between the various components. These parameters are generally obtained by fitting the VLE data of the liquid mixture to the above equation. For polymeric systems, it is easier to express a_i as a function of the volume fractions ϕ_i in the system. The main reason for this is the fact that the mole fraction of the polymer is generally very small compared to the solvent species, due to its high molecular weight. For polymeric systems (m refers to the polymer), Eq (2.16) takes the form

$$\begin{aligned} \ln a_i(\phi_1,.....\phi_i,.....\phi_n,\phi_m) = \ln\phi_i + \frac{Z}{2} q_i \ln\left(\frac{\theta_i}{\phi_i}\right) + l_i - \sum_{j=1}^{n} \phi_j \frac{r_i}{r_j} l_j \\ - r_i\phi_m\left(\frac{Z}{2}\left(1 - \frac{q_m}{r_m}\right) - 1\right) - q_i^* \ln\sum_{j=1}^{n} \theta_j^* \tau_{ji} + q_i^* - q_i^* \sum_{j=1}^{n} \frac{\theta_j^* \tau_{ij}}{\sum_{k=1}^{n} \theta_k^* \tau_{kj}} \end{aligned} \tag{2.18}$$

The solvent-membrane parameter τ_{im} in Eq. (2.18), is generally estimated by fitting Eq. (2.18) to the pure component vapor sorption data. The last two terms in Eq. (2.13) and (2.18) (terms containing q* and θ*) have been specifically added to take into account the hydrogen bonding present in the system. The inclusion of these terms aids the prediction of sorption isotherms for highly associating non-ideal systems. In fact due to the presence of the modified surface

parameters (q^* and θ^*), Eq. (2.123 and (2.18) represent UNIQUAC-HB (UNIQUAC-Hydrogen Bonding) model [Anderson and Prausnitz, 1978; Prausnitz *et al.*, 1986]. Heintz and Stephan (1994) successfully modeled the sorption of alcohols from aqueous-organic mixtures using the above theory in PVA membranes. The only drawback of the UNIQUAC model is that it requires knowledge of the pure component vapor sorption isotherm and the VLE data for the liquid mixtures to generate the values of the binary interaction parameters. Often times such data is hard to find in literature making the applicability of this model difficult.

2.7.1.3 Hansen Solubility Parameters

Solubility parameters proposed by Hansen (1969) are an ideal means of quantifying the affinity between a polymer membrane and any given solute, and hence predict the selective permeation through the membrane. Hansen solubility parameters (HSP) have significant potential for identifying novel membrane materials for PV fractionation [Feng and Huang, 1997], based on the concept that preferential sorption is the prerequisite to preferential permeation [Mulder *et al.*, 1985; Mulder and Smolders, 1986]. Hansen solubility parameters are able to quantify the relationship between the polymer and solvent/solute. In the last two decades, researchers have shown that HSP have great potential for selecting pervaporation membrane materials [Mulder *et al.,* 1982; Cabasso, 1983; Lloyd and Meluch, 1985; Yamaguchi 1992; Jonquières *et al.,* 1996; Ray *et al.,* 1997; Wang *et al.,* 2001; Buckley-Smith and Fee, 2002; Mandal and Pangarkar, 2003; Pal *et al.,* 2005].

2.7.2 Diffusion

In pervaporation dense membranes, the diffusion of the various species can be the rate-controlling step. The diffusion process can be affected by the coupling effect of the diffusing components, the plasticizing effect of the diffusing components in polymeric materials and the dependence of the diffusion coefficient on the concentration of the diffusing species. Different models, both fundamental and semi-empirical, have been proposed to explain the diffusion of a permeant through polymeric membrane.

2.7.2.1 Free Volume theory

In polymeric membrane, solvent molecules diffuse through the voids and intermolecular spacing between the polymer chains termed as “free volume” of polymer. The diffusion coefficient of the permeant can be expressed as a function of the fractional free volume of the

polymer and two adjustable parameters, which are representative of the permeant-polymer interactions [Fujita *et al.*, 1960; Fujita, 1961; Kreituss and Frisch, 1981]. The thermodynamic diffusion coefficient (D_{iT}) of component i through a polymer film can be expressed as

$$D_{iT} = RTC_i \exp\left(\frac{E_i}{V_{fp}}\right) \tag{2.19}$$

where C_i and E_i are constants and V_{fp} is the free volume of the polymer. Yeom and Huang (1992a) obtained good agreement between calculated and experimental diffusivities for permeation of benzene, toluene, hexane and heptane through polyethylene films using Eq. (2.18). The "free volume" model however, has a couple of limitations. It cannot satisfactorily 9explain the diffusion of molecules through swollen membranes [Dutta and Sikdar, 1996]. Also, a lot of experimental data is required to determine the various parameters in the model. Due to these drawbacks, the semi-empirical correlations describing the diffusion of species through the polymer on a macro-level are more popular.

2.7.2.2 Semi-empirical Correlations

Semi-empirical diffusivity-concentration relations have been proposed by several researchers to model permeation through dense membranes. Lee *et al.*, (1975), Kataoka *et al.*, (1991) and Wijmans *et al.*, (1993) assumed a constant diffusivity to model diffusion in a dense membrane. However, the diffusion coefficient of the species through a polymer depends on the concentration of the permeating species [Huang. 1991]. An improved model was proposed by Greenlaw *et al.*, (1977). The diffusion coefficient was assumed to be a linear function of the concentration of the permeating species.

$$D_i = D_i^0\left[C_i + S_{ji}.C_j\right] \tag{2.20}$$

where S_{ji} is an empirical constant signifying the coupling or the interaction between the two components. An exponential dependence of diffusivity on concentration has been conventionally used to model pure component permeation through dense films [Aptel *et al.*, 1974].

$$D_i = D_i^0 \exp\left(\gamma_i C_i\right) \tag{2.21}$$

Based on Eq. (2.20), Suzuki and Onozato (1982) proposed a new model for multicomponent permeation through dense membranes. The parameter γ, in Eq. (2.21), takes into account the plasticizing effect of the species on the polymer matrix

$$D_i = D_i^0 \exp\left(\gamma_i C_i + \gamma_j C_j\right) \tag{2.22}$$

In Eq (2.22), the exponential parts of the expressions for D_i and D_j are the same. This equation has therefore been replaced by the more popular 'six-coefficient' model, which has been widely used to model complex, non-ideal ternary systems [Brun *et al.*, 1985; Jeon and Kim, 1992; Jonquieres *et al.*, 1996].

2.7.3 Pore Flow Model

Sourirajan *et al.* (1987) have proposed the pore-flow model [Sourirajan and Matsuura, 1985] for pervaporation membranes. According to the mechanism, feed liquid enters the membrane pores on the feed side. At a certain thickness (z_l) in the membrane, the liquid undergoes a phase change to the vapor phase. The vapor phase then traverses along the remaining length (z_v) of the pore and emerges on the permeate side. Figure 2.8 shows a schematic of the pervaporation process in a membrane pore. Thus the pervaporation process can be considered as a combination of liquid transport (reverse osmosis) and vapor transport (gas separation) in series. Based on the model, the total flux equation (Okada and Matsuura, 1991) appears as

$$J_i = \left[\frac{Q}{z}\left(P_f - P_{sat,mix}\right) + \frac{B_i}{z}\left(P_{i,sat}^2 - P_{i,p}^2\right) + \frac{B_j}{z}\left(P_{j,sat}^2 - P_{j,p}^2\right)\right]\left(y_i M_i + y_j M_j\right) \tag{2.23}$$

where Q, B_i, B_j are constants, z is the thickness of membrane, P_f is the feed pressure at pore inlet, $P_{i,p}$ is the partial pressure of component i on permeate side, $P_{i,sat}$ is the partial saturation pressure of component i on feed side, y_i is the permeate mole fraction of component i and M_i is the molecular weight of component i.

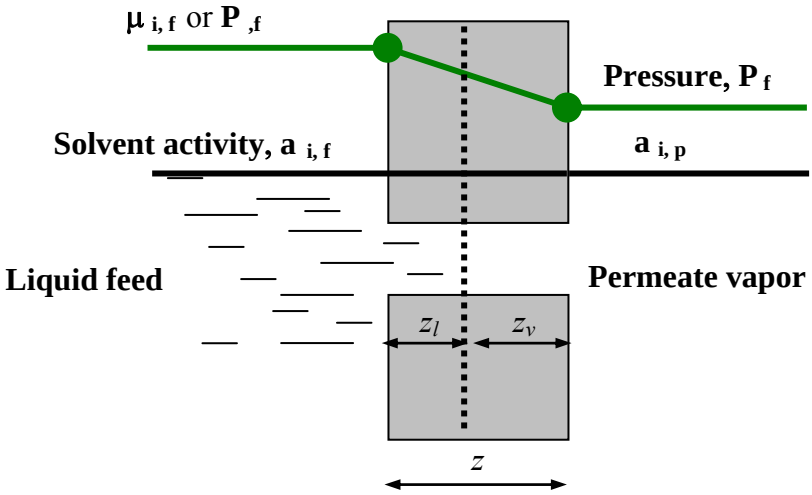

Figure 2.8: Schematic of Pervaporation Process in a Membrane Pore [Okada *et al.* 1991].

It is apparent from Eq (2.23) that the total flux according to the pore-flow model depends on the pressure gradient across the membrane. The ratio B_j/B_i decides the selectivity of the membrane for a particular component. Okada *et al.* (1991) have extended the above model to predict ethanol/water separation using silicone and PVA membranes. The authors observed that the pore flow model could explain the trends for the ethanol/water-silicone membrane system quite well. However, it failed to do so for the ethanol/water-PVA membrane system. The reason for this is the fact that the pore flow model fails to take into account membrane swelling and hence pore enlargement at high water concentrations.

2.7.4 Solution-Diffusion Model

The mass transport through a dense membrane is commonly described by the solution-diffusion model, which was first postulated by Graham in 1866. The chemical potential across the membrane can be expressed as a concentration gradient [Basu *et al*., 2004]. The solution-diffusion (S-D) model is the most widely accepted transport model for pervaporation separation [Mulder and Smolders, 1986; Kataoka *et al.*, 1991; Neel, 1991; Heintz *et al*., 1991; Fleming and Slater, 1992; Shieh, 1996]. The main assumption of the model is that a thermodynamic phase equilibrium exists at both sides of the membrane (feed and permeate side). The model also assumes that the pressure and temperature variation through the membrane is negligible. There is a step change in both the pressure and the temperature at the permeate interface. Figure 2.9 shows a schematic of the chemical potential/gradients existing in the pervaporation process according to the solution-diffusion model.

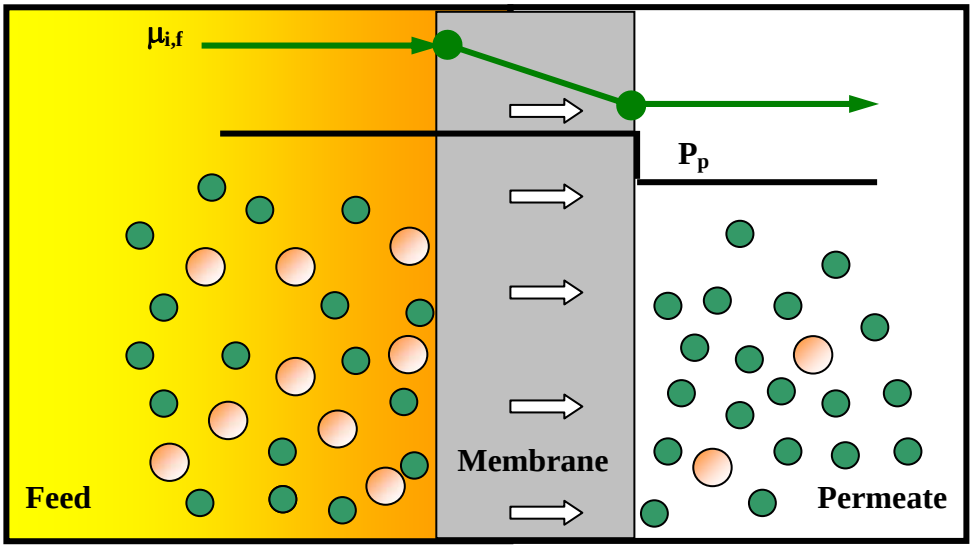

Figure 2.9: Pervaporation Membrane based on Solution-Diffusion Model

Since the pressure remains constant, no phase change is possible within the membrane. Kataoka *et al.* (1991) have assumed a linear pressure profile across the membrane thickness and simulated the effect of variables such as feed and permeate pressure on the pervaporation performance. Their simulation results showed that both reverse osmosis and pervaporation show identical flux and separation behavior at very high feed pressures (> 100 atm). Also, the simulations showed that a higher pervaporation flux and lower selectivity would be observed for a linear pressure profile as compared to a flat pressure profile. The S-D model requires knowledge about the sorption of the various species on the membrane and the diffusion through the membrane. Several researchers [Aptel *et al.*, 1974; Ghai *et al.*, 1987; Nguyen, 1987] have delved into such theoretical aspects of solution-diffusion model for liquid permeation through dense membranes. The simplest transport model equation based on the Fickian mechanism can be written as

$$J_i = -D_i \frac{dc_i}{dz} \tag{2.24}$$

where,

J_i = flux component of i ($M/L^2 t$)

D_i = diffusion coefficient of component i, (L^2/t)

c_i = concentration of component i (M/L^3)

z = transport distance, (L)

According to Eq (2.24), a trans-membrane concentration gradient is the driving force for the mass transport. The diffusion coefficient is a function of temperature. In this model, the sorption step represents the static process while diffusion is a dynamic process. The solution-diffusion model is mostly used for binary mixture separation. For multicomponent systems, flux coupling and thermodynamic interaction of the components are important [Fleming and Slater, 1992].

The permeability coefficient (P) is generally expressed as the product of the solubility coefficient (S) and diffusion coefficient (D):

$$P = S * D \tag{2.25}$$

In Eq. (2.25), the solubility coefficient, S, is a thermodynamic parameter [Stern, 1994], and it represents the sorption amount of permeant in the membrane under equilibrium. It is affected by the sorption of species in the membrane and the interaction between the permeant

species and polymer. The solubility of a solvent in a polymer may be quite large due to their high affinities [Huang, 1991].

The diffusion coefficient, *D*, is a kinetic parameter and reflects the mobility of the permeating species through a membrane. It depends on the geometrical shape of permeant molecules and the polymer property. For a given permeant molecule, the polymer properties (i.e., chemical structure, mobility of polymer segments, crystallinity, and degree of crosslinking) also influence the diffusivity [Baker, 2004].

CHAPTER 3

Correlation of Physicochemical Characteristics with Pervaporation Performance of Poly(vinyl alcohol) Membranes

3.1 Introduction

In industrial applications, such as food and pharmaceutical processes, membranes are frequently used for the separation of mixtures of liquids. Pervaporation is one of the membrane separation techniques; it is energy-efficient due to its low temperature and pressure operating conditions. In membrane pervaporation, the components of a liquid mixture selectively permeate through the membrane and evaporate on the other side of the membrane. The separation efficiency depends on the physicochemical properties of the membrane (hydrophobic or hydrophilic, chemical compatibility, mechanical strength, temperature resistance) and operation conditions (feed concentration and pressure gradient across the membrane). In PV separation, four basic steps are involved [Mulder *et al.*, 1985; Kataoka *et al.*, 1991]: Step 1 is the transport of the liquid to the membrane surface on the feed side, depending on the velocity of the feed liquid across the membrane surface. Step 2 is the sorption process, including adsorption of selective components on the membrane surface and subsequent absorption into the polymer membrane [Oasada and Nakagawa, 1992]. In step 3, diffusion of the selective components takes place through the membrane under a chemical potential gradient. The diffusion of the components is partly determined by the properties, e.g., density and crosslinked structure, of membrane material, often a polymer. Step 4 involves desorption and evaporation at the membrane surface on the permeate side, a rapid process with a low pressure on the permeate side. The adsorption of liquid components is affected by the membrane surface properties, such as wettability, roughness and heterogeneity. Depending on the particular design of pervaporation membrane operation, especially for relatively thin pervaporation membranes, adsorption and subsequent absorption may dominate the membrane performance, impacting the follow-up diffusion and evaporation. Higher sorption of selective solvents tends to give better separation results.

Portions of this work have been published in *J. Membr. Sci.*, 283 (2006) 281-290.

It is apparent that surface physicochemistry may play an important role in membrane separation, especially in the sorption step. Over the last two decades, many techniques have been used in characterizing the surface properties and their effects on membrane separation, including attenuated total reflectance IR spectroscopy [Belfer *et al*., 1998], scanning [Cabasso, 1981; Pusch and Walch, 1982] and transmission [Uemura and Inoue, 1984] electron microscopy, X-ray photoelectron spectroscopy [Gierke *et al*., 1981; Koo *et al*., 1986] and atomic force microscopy [Dietz *et al*., 1992; Bessières *et al*., 1996; Long *et al*., 2003]. Some researchers [Zhang and Hallstrom, 1990; Rosa and de Pinho, 1997] have used contact angle measurement for characterizing nanofiltration and ultrafiltration membranes in relation to membrane fouling. However, there have been relatively few publications [Zeng *et al*., 1997; Lee *et al*., 1998] that focus on the relationship between the physicochemical properties of the pervaporation membrane, such as chemical structure, surface morphology and pervaporation performance.

In this study, crosslinked poly(vinyl alcohol), PVA, membranes were characterized using a set of physicochemical techniques, including microscopy and contact angle measurement. The resulting properties were related to the pervaporation operation that separates water from an ethanol-water mixture. Pervaporation using PVA membranes were studied extensively [Yeom and Lee, 1996; Nugay *et al*., 2002; Rhim *et al*., 2002], but only a few research groups have studied [Rosa and de Pinho, 1997; Zeng *et al*., 1997; Lee *et al*., 1998] the surface properties of the membranes and their impact on the separation performance. To better design pervaporation membranes and optimize their separation processes, it is necessary to understand the membrane surface and its effect on pervaporation separation.

3.2 Experimental

3.2.1 Materials

Poly(vinyl alcohol), PVA, (99.7% hydrolyzed, MW 108,000, PDI 1.3) was purchased from Fisher Scientific, Canada. All other chemicals, including acetic acid (glacial, 99.7%), acetone (99%), glutaraldehyde (25% aqueous) and sulfuric acid (98%), were obtained from BDH, Toronto, Canada. Deionized water (18.4 MΩ cm) used for all the experiments was produced by a Millipore system. The chemicals and solvents were used as received.

3.2.2 Membrane preparation

Poly(vinyl alcohol) solutions were prepared by dissolving 5, 7 and 10 wt% of the polymer in deionized water at 90 ^{O}C for 1 hour, by stirring the solution until it was completely homogeneous. The solution was then cast onto a glass plate (Fig. A.4, Appendix A) and dried under ambient conditions (temperature 20^{O}C and humidity 70%) in fumehood for 24 hours. After that, the membrane film with the glass plate was dried in a vacuum oven (at 40 ^{O}C) for 3 h for the removal of traces of solvent. The membrane film was hydrophilic and absorbed water quickly, assuming a swollen film state. Swelling of the membrane film was not desirable since it would disrupt the membrane integrity and lower the separation efficiency. Thus, the membranes used in this study were further crosslinked thermally by heat treatment and/or with chemical agents. In the heat treatment, the membrane was thermally crosslinked by heating the film in a vacuum oven at 125^{O}C for 30 minutes. In the chemical treatment, on the other hand, the membrane film was chemically crosslinked in glutaraldehyde solutions [Yeom and Lee, 1996]. The chemical crosslinking solution consisted of 1 or 2.5 wt% glutaraldehyde (ga), 0.5 wt% sulfuric acid (H_2SO_4), 48 wt% acetone, and deionized water. Each dry PVA film was immersed in the prepared crosslinking solution for 30 minutes at room temperature (20^{O}C and humidity 70%). After the reaction, the membrane was taken out and washed several times with pure water and finally immersed in pure water for 6 hours at

Table 3.1: Abbreviations of fresh and cross-linked poly(vinyl alcohol) membranes

Conditions	Polymer Poly(vinyl alcohol) or PVA		
	5%	7%	10%
Not Crosslinked (fresh)	PVA1	PVA2	PVA3
Crosslinked (thermal): 125 ^{O}C	PVA4	PVA5	PVA6
Crosslinked (chemical): glutaraldehyde (ga)			
1%	PVA7	PVA8	PVA9
2.5%	PVA10	PVA11	PVA12

40^{O}C to eliminate residual H_2SO_4. The crosslinked membrane was then dried in a vacuum oven (at 40^{O}C) for 24 hours. The thickness of the crosslinked membrane was about 20-28 μm. The membranes prepared with different conditions are shown in Table 3.1 with their succinct

naming, e.g., PVA4 stands for the membrane prepared with 5 wt% poly(vinyl alcohol) and the crosslinked by heat treatment.

3.2.3 Characterization

To quantify the chemical composition of a membrane film before and after crosslinking, FTIR spectroscopy was employed. Infrared spectra of the fresh and crosslinked membranes of similar thickness (25 μm) were measured with a midrange (500-4000 cm^{-1}) Biorad Excalibur FTIR spectroscope (California, USA).

Differential scanning calorimetry (DSC) was used to quantify changes in polymer physical properties, e.g., crystallinity and melting point before and after crosslinking the membrane [Higuchi and Iijima, 1985]. DSC heat curves indicate what happened to polymers when they were heated, e.g., thermal transitions including melting and glass transitions. DSC curves were obtained from a DSC Q100 module (TA Instruments, Delaware, USA). The DSC scan rate was 10 ^{O}C/min, and approximately 2.5 mg of the polymers were used.

Tapping mode on a commercial AFM (Picoscan, Molecular Imaging, Tempe, AZ, USA) was used to determine topography and phase images of the polymer membrane surfaces. AFM tapping mode technique allows high resolution topographic imaging of sample surfaces that are easily damaged, such as the polymer membrane films. After image acquisition, the roughness of the membrane surface was determined by a built-in image processing toolbox in the AFM software.

Water contact angle is a common measure of hydrophobicity of a surface, which was adopted in the present work. Contact angle measurements using Sessile drop [Sharma *et al.*, 2004] was based on a setup shown in Fig. E.7 (Appendix E). All the membranes were thoroughly washed with deionized water and dried in a vacuum oven before using for contact angle experiment. A square sample of 30 mm^2 was cut from the membrane film, and placed in a sample chamber at 25^{O}C. The chamber was saturated with water during the experiment, in order to minimize water evaporation from the sessile drop. The membrane film was mounted on a glass slide, and a steel syringe system connected to a motor-driven programmable controller deposited the water drop on the membrane sample surface. An initial water drop with a diameter of around 5 mL was deposited to ensure that the drop was axisymmetric. Using the motor-driven syringe, water was pumped into the sessile drop from above, causing a steady increase in sessile drop volume. The advancing contact angle was obtained from a

sequence of images of the growing drop. The acquired images were analysed by an in-house image analysis software CAMADS [Xia and Chen, 2003]. Upon withdrawing the liquid from the sessile drop, the receding contact angle was obtained. The water pumping rate used was 2 μl per second. All the advancing and receding contact angle measurements were repeated three times and the results were averaged.

3.2.4 Pervaporation

The prepared membranes were tested for pervaporation separation on a setup shown in Fig. A.1 (Appendix A). Pervaporation experiments were conducted for dehydration of an ethanol-water (Et-water) mixture. The feed solution contained 10-70% ethanol. The feed pressure was at atmospheric pressure while the pressure on the permeate side was kept below 3 mbar using a vacuum pump (Leeson Electric Co., WI, USA). To achieve a 'pseudo-steady-state' at a given temperature, the experiment was run for two hours prior to collection of the permeate. To assess experimental errors, each experiment was repeated three times. The permeate vapor was collected in a cold trap (glass tube) immersed in liquid nitrogen for about 5-20 minutes. Once enough permeate was collected, the cold trap was removed. It was then heated to room temperature, and the permeate was weighed to determine to the flux. The feed solution temperature varied from 25 to 50^{O}C using a temperature controller (accuracy ± 2^{O}C). The total flux (J) and the selectivity (α) of the membrane were calculated using the Eqs (2.3) and (2.4), shown in Chapter 2 [Huang, 1991; Oasada and Nakagawa,1992; Cussler, 1997].

3.3 Results and discussion

3.3.1 Infrared spectroscopy

The IR spectra of the fresh and crosslinked membranes were plotted in Fig 3.1. The IR spectrum of the fresh PVA membrane shows the absorption peaks at ~ 3315 cm^{-1} for the -OH group. The hydroxyl groups in the poly(vinyl alcohol) react with the aldehyde groups during the crosslinking reaction. Typical products from the reaction between poly(vinyl alcohol) and glutaraldehyde are acetal groups or ether linkages in the polymer network [Huang, 1991; Yeom and Lee, 1996] shown in Fig. 3.2 for the crosslinked membranes.

From Fig. 3.1, for PVA6 and PVA12 crosslinked membranes, a decrease in absorbance was found at ~ 3315 cm^{-1} as compared to PVA3. Also, PVA6 and PVA12 shows increase in the absorbance peak at ~1097 cm^{-1} is likely due to –COC groups [Yeom and Lee,

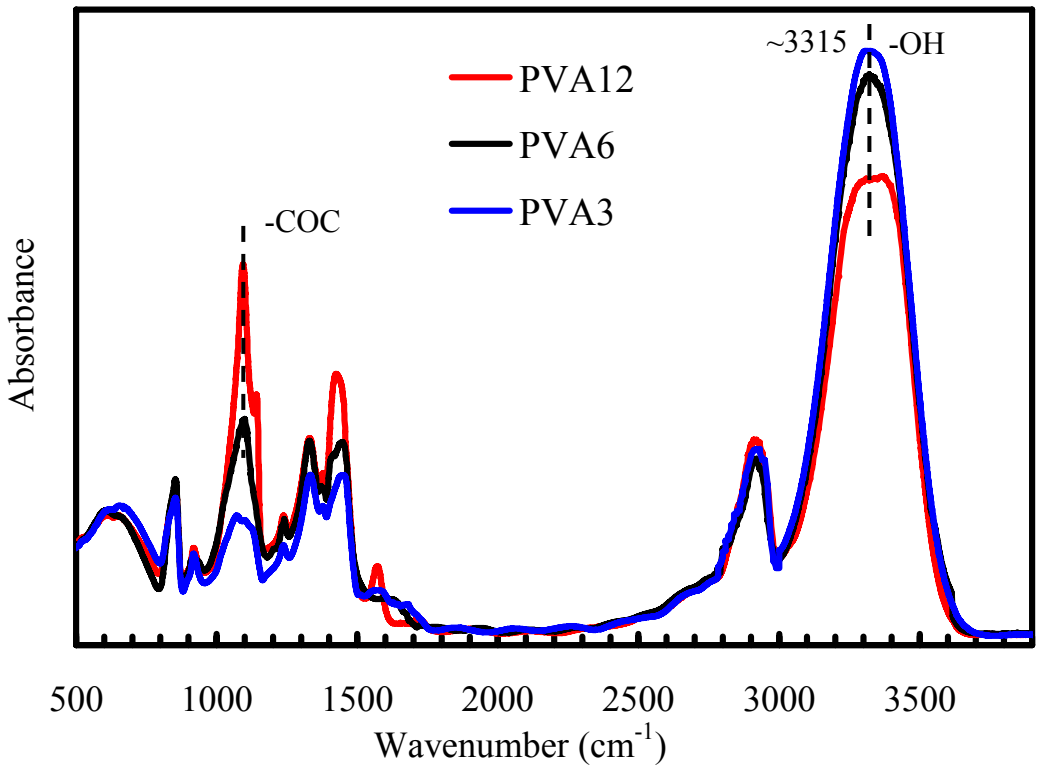

Figure 3.1: FTIR spectra of the 10 wt% PVA membranes at room temperature.

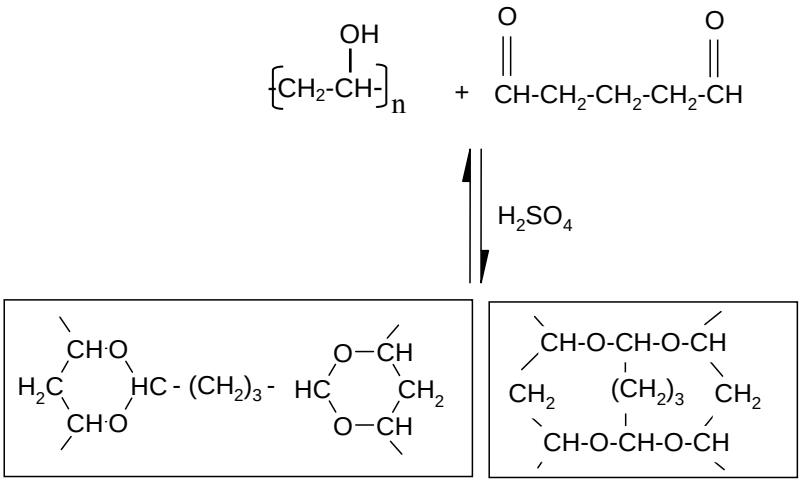

Acetal group Ether group product

Figure 3.2: Crosslinking reaction [Yeom and Lee, 1996].

1996, Stuart, 2004]. For the thermal crosslinking reaction, ether linkages are produced with the removal of water molecules (i.e., a chemical reaction), with only a moderate increase in absorbance peak at ~1097 cm^{-1} for PVA6 membrane. At higher polymer (PVA) concentrations, the membrane contains a large number of -OH groups, not all of which can react with aldehydes during the limited crosslinking time.

3.3.2 Differential scanning calorimetry

Poly(vinyl alcohol) is a semi-crystalline polymer [Nugay *et al*., 2002; Rhim *et al*., 2002] that changes its structure after the crosslinking reaction [Yeom and Lee, 1996]. The heating curve from a differential scanning calorimetry can detect changes in melting temperature (T_m) of the crosslinked membranes as compared to the fresh membrane. In the DSC curves of the PVA membranes shown in Fig. 3.3, a melting endothermic peak can be seen at 196^{O}C for the fresh PVA membrane, and the melting temperature shifted to 215 ^{O}C for PVA12.

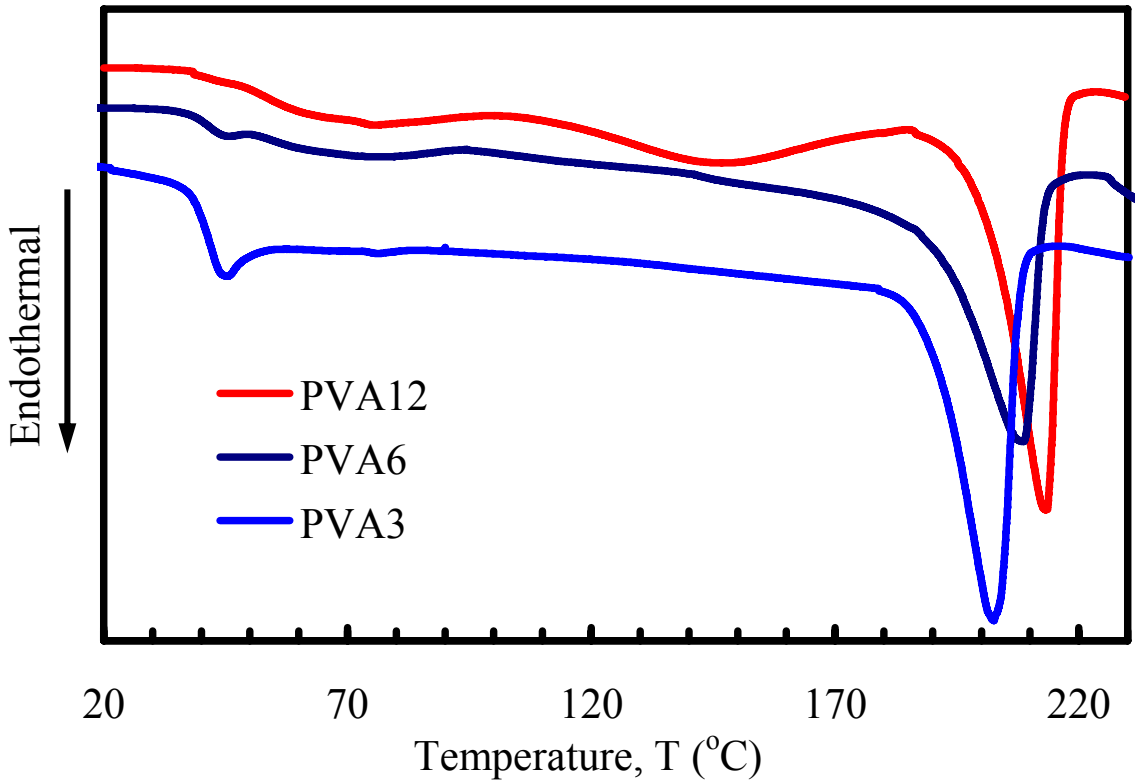

Figure 3.3: DSC heating curves of the 10 wt% PVA membranes cf. Table 3.2

From the DSC curves, the melting temperatures of all the membranes can be determined and the results are listed in Table 3.2. It can be seen that the melting temperature of the membrane increases after the crosslinking reaction.

3.3.3 Microscopy results

Figure 3.4 shows typical 3D AFM images of the membrane over an area of 6.4 × 6.4 μm^2. Table 3.2 shows the results of maximum peak-valley and root mean square (RMS) roughness obtained from AFM images; these values are frequently quoted in membrane surfaces studies [Bessières *et al*., 1996, Freger *et al*., 2002]. In the AFM image analysis, the

Table 3.2: Results of the PVA membranes from DSC and AFM experiments

Membranes	Melting temperature (^{O}C)	Maximum peak-valley, R_{p-v} (nm)	RMS roughness R_q (nm)
PVA1	196.1	27.5 ± 1.3	1.4 ± 0.1
PVA4	206.6	37.5 ± 1.8	2.3 ± 0.2
PVA7	209.1	23.3 ± 2.6	4.8 ± 0.2
PVA10	209.8	33.3 ± 3.2	4.1 ± 0.3
PVA2	194.2	24.5 ± 1.9	1.6 ± 0.1
PVA5	206.3	27.5 ± 2.4	2.1 ± 0.1
PVA8	201.2	35.3 ± 4.1	2.8 ± 0.2
PVA11	211.4	39.2 ± 1.7	3.6 ± 0.2
PVA3	198.1	33.2 ± 2.9	2.9 ± 0.2
PVA6	207.8	29.2 ± 3.7	3.7 ± 0.1
PVA9	209.2	49.2 ± 6.2	5.8 ± 0.3
PVA12	213.7	43.2 ± 5.7	6.6 ± 0.2

root mean square (RMS) roughness

$$R_q = \sqrt{\frac{\sum_{i=0}^{n}\sum_{j=0}^{n}\left(D_{ij} - h_m\right)^2}{n-1}} \tag{3.1}$$

where the average (mean) height is defined as $h_m = \left(\sum_{i=0}^{n}\sum_{j=0}^{n} D_{ij}\right)/n$, n being the total number of *image data points* and D_{ij} the height value of the i, j^{th} point on the image (Fig. 3.5); the maximum roughness, R_{p-v}, is the difference between the vertical distance from the deepest valley to the highest peak and expressed as

$$R_{p-v} = \left|\max D_{ij}\right| + \left|\min D_{ij}\right|, \tag{3.2}$$

The mean values and standard deviations reported in Table 3.2 were obtained from the image analysis tool built in the Picoscan AFM software. It may be seen from Table 3.2,

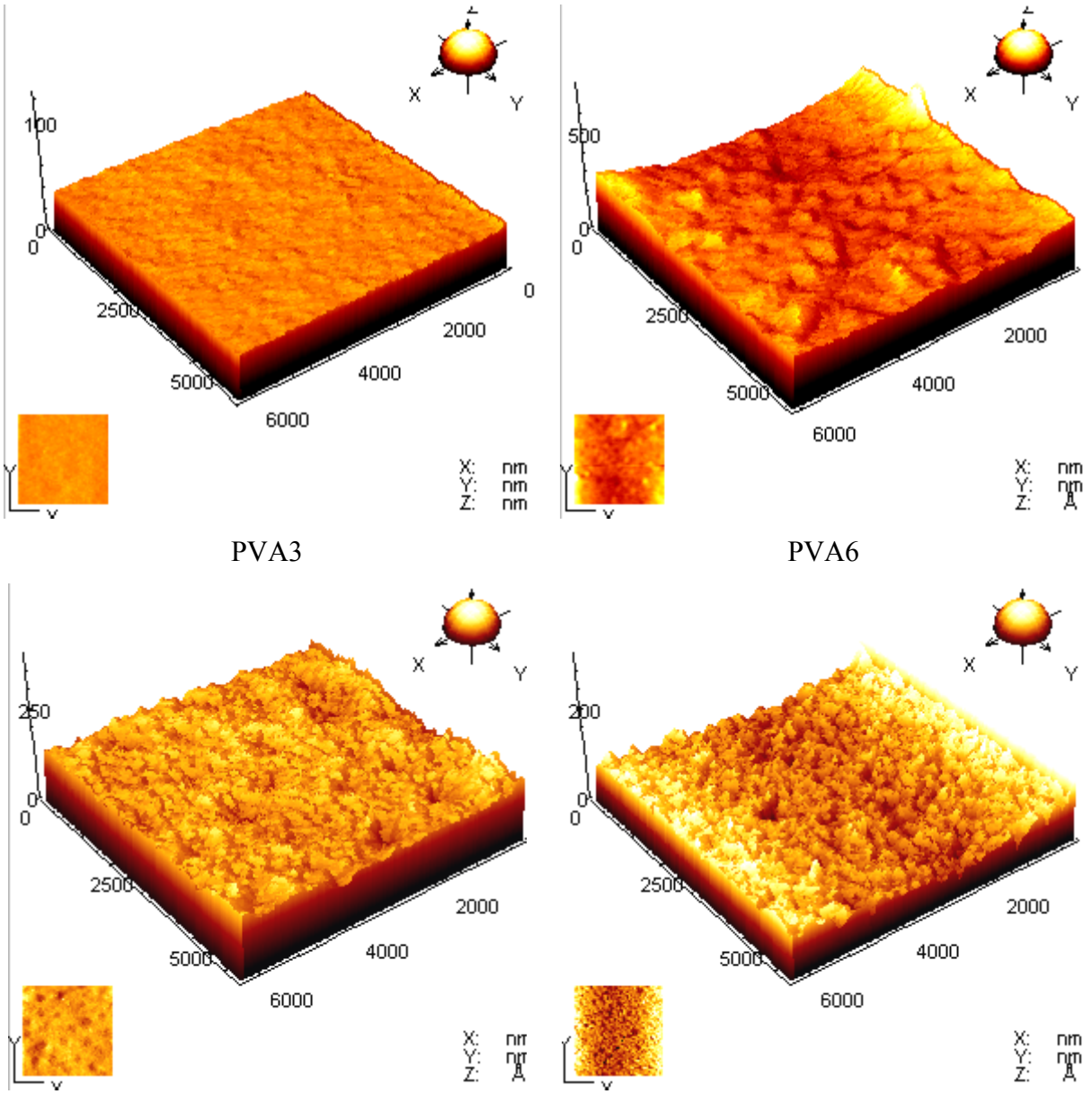

Figure 3.4: 3-D AFM topograph of the 10 wt% PVA membrane surfaces. Scanned area is 6.4 x 6.4 μm^2, and AFM used in tapping mode at 25 ^{0}C.

that the 10 % PVA membrane crosslinked with 2.5.wt% glutaraldehyde is the roughest and the fresh 5% PVA membrane is the smoothest. Also, the roughness of the crosslinked membranes is always higher than that of the fresh membrane at any polymer concentrations, e.g., PVA3 has RMS roughness of 2.9 nm whereas PVA12 has RMS roughness of 6.6 nm.

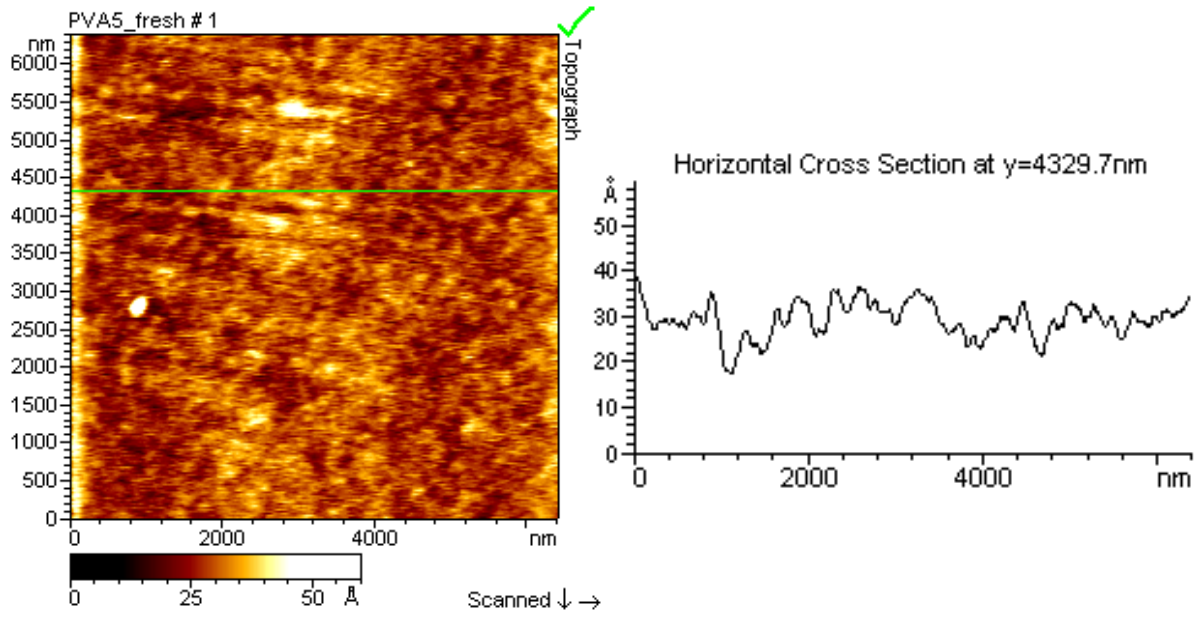

Figure 3.5 Topographic image of the 5 wt% PVA membrane surface. The vertical line scan on the image shows surface roughness of the membrane.

3.3.4 Contact angle results

The PVA membranes are hydrophilic in general. However, it was observed that the crosslinking reactions make the membranes less hydrophilic. The membrane surfaces are rough in nanometer scale, evident from the AFM results. In contact angle experiments, for rough and heterogeneous surfaces, the advancing contact angle, θ_a , receding contact angle, θ_r and contact angle hysteresis ($\theta_a - \theta_r$) are generally measured [Li, and Neumann, 1996; Extrand, 1998, 2003]. The advancing contact angle is used as an indication of the hydrophobicity of a surface [Zhang and Hallstrom, 1990; Rosa and de Pinho, 1997; Extrand 1998]. The results from our contact angle experiments are presented in Table 3.3. The contact angle measurements for the fresh membranes could not be done as they swelled quickly within a minute (30 s). For the nine crosslinked membranes, their advancing contact angle increases with increasing glutaraldehyde concentration, indicating that the sample treated with higher glutaraldehyde concentrations is more hydrophobic. In addition, chemical-crosslinked membranes are more hydrophobic than heat-treated ones, e.g., PVA12 showing an average advancing contact angle (θ_a) of 81.5^O whereas the heat treated counterpart showing $\theta_a \approx 74.1^O$.

Table 3.3: Results of contact angle experiments at 25 ^{0}C

Sample	Advancing contact angle, θa (^{O})	Receding contact angle, θr (^{O})	Hysteresis, θa–θr (^{O})
PVA4	70.7 ± 1.1	15.4 ± 1.3	54.3 ± 2.4
PVA7	74.0 ± 1.3	18.8 ± 1.6	57.2 ± 2.9
PVA10	76.2 ± 1.5	19.4 ± 1.1	57.8 ± 2.6
PVA5	72.0 ± 1.3	15.8 ± 1.1	56.3 ± 2.4
PVA8	76.8 ± 1.4	17.9 ± 0.9	60.1 ± 2.3
PVA11	78.4 ± 1.2	18.7 ± 1.2	60.9 ± 2.4
PVA6	74.1 ± 1.6	16.8 ± 0.6	57.3 ± 2.2
PVA9	80.1 ± 1.5	17.3 ± 0.8	62.6 ± 2.3
PVA12	81.5 ± 1.3	16.6 ± 0.8	64.8 ± 2.1

Note: Each value shown in table 3 is obtained via a statistical t-test analysis with a 95% confidence level, i.e., $\theta \pm (\sigma_{n-1} t_{95\%}/\sqrt{n})$. The number of samples, n, is the number of data points for the contact angle analyzed by the in-house CAMADS software, always greater than 8 (n >8).

Comparing the advancing contact angles of water on the PVA membranes shown in Table 3.3, one finds that the average advancing contact angle of PVA4 (70.7^O) is the smallest and PVA12 has the maximum value (81.5^O). This is due to the decrease in –OH group (cf. Fig. 3.1) and hence hydrophilicity of the PVA membrane after reacting with glutaraldehyde. For all the membrane samples, steady-state receding contact angles were found. Table 3.3 also shows the contact angle hysteresis of the PVA membranes crosslinked at different conditions. The membranes crosslinked with 2.5wt% glutaraldehyde shows the highest contact angle hysteresis, and the hysteresis increases as the PVA concentration in the membrane increases.

3.4 Separation Results

Separation experiments with fresh membranes could not be performed for the same reason that contact angle experiments could not be done; that is, the fresh membrane swells quickly, giving high flux but very low selectivity [Huang, 1991; Yeom and Lee, 1996, Nugay *et al*., 2002; Smitha *et al*., 2004]. All the nine crosslinked PVA membranes were tested for

pervaporation separation. In the following sections, the results for different feed concentrations and crosslinking conditions are presented.

3.4.1 Effect of ethanol feed concentration

Figure 3.6 shows the typical results of the total flux and selectivity of the three different membranes crosslinked chemically with the 1 wt% glutaraldehyde solution for different feed ethanol concentrations at 40 ^{0}C. It can be seen that the total flux increases as the feed ethanol

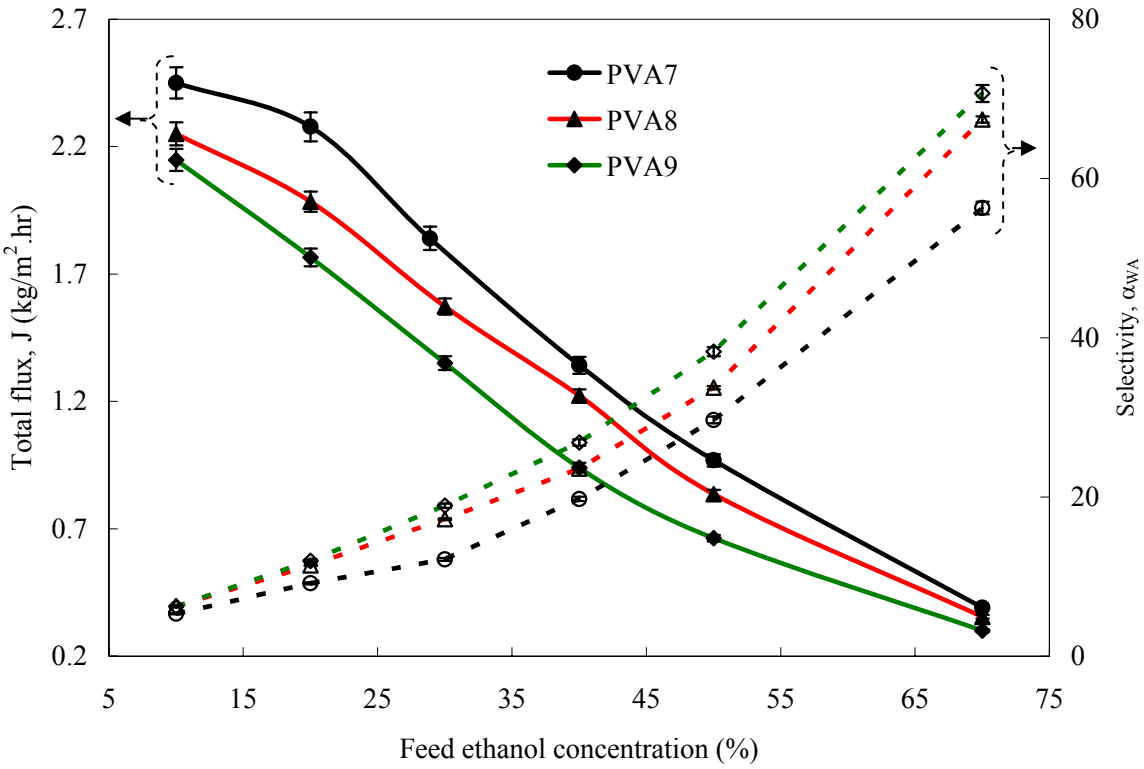

Figure 3.6: Total fluxes and selectivities of the PVA membranes (single layer with an average thickness of 22 μm) at 40^{O}C at different feed ethanol concentrations.

concentration decreases and the flux is higher for a lower polymer concentration. The total flux of the 5 wt% poly(vinyl alcohol) PVA7 membrane is also observed to increase from 0.39 kg/m^2/hr to 2.45 kg/m^2/hr as the feed ethanol concentration decreases from 70 wt% to 10 wt%. There can be two reasons for the observed increase in flux. As the ethanol concentration is decreased, the water portion is increased. As a result, water transport increases and hence the total flux is increased [Immelman *et al*., 1993; Uragami *et al*., 1994]. Also, at high water concentrations, the membrane is in swollen state, which further enhances water transport through the predominantly hydrophilic membranes. However, the selectivity is low in low

ethanol concentration. Swollen membrane makes the polymer network more flexible for ethanol molecules to transport to the permeate side and thereby lowering the selectivity. However, at high ethanol concentrations, the membrane swells less, and hence diffusion of water through the membrane is slightly hindered. Figure 3.6 also shows the selectivity of the membranes for ethanol-water separation. For the 70% ethanol-water solution, the 10 wt% PVA membrane crosslinked with 1 wt% glutaraldehyde gives the highest selectivity of 70.7, at 40^{O}C, but lowest total flux of 2.14 kg/m^2/hr.

3.4.2 Effect of feed temperature

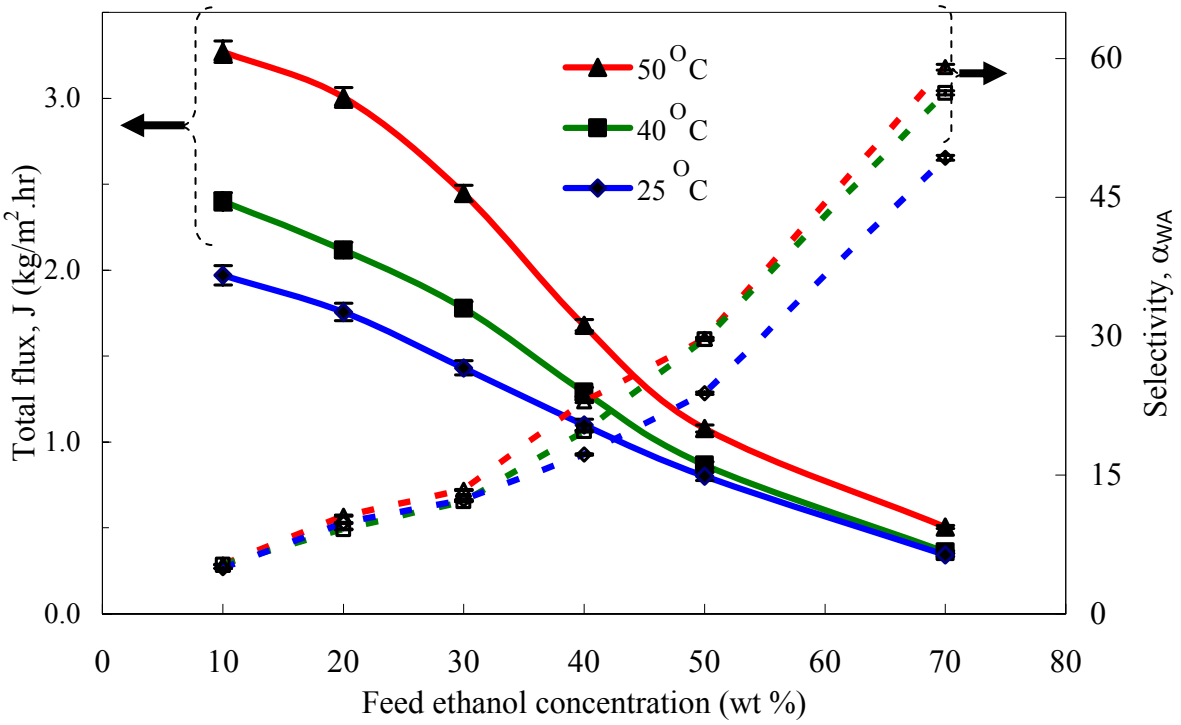

Figure 3.7: Total fluxes and selectivities of the PVA7 membranes at different temperatures.

In Fig. 3.7, the total flux increases as the temperature increases at all ethanol concentrations in the feed solution. At higher temperatures, the thermal energy drives the water molecules at a faster rate for sorption and diffusion through the membrane, e.g., for PVA7, the total flux being 1.97 kg/m^2/hr at 25^{O}C and 3.27 kg/m^2/hr at 50^{O}C, for the 10% feed ethanol-water solution. Figure 3.7 also shows the behavior of water selectivity with temperature change. For the 10% ethanol-water solution, the PVA7 membrane gives a selectivity of 59 at 60^{O}C compared to 49.3 at 25^{O}C. With an increase in temperature, more energy is supplied to the

transported solvent (water in the present case) that can vaporize more easily on the permeate side, likely resulting in an increase in both total flux and selectivity [Huang, 1991].

3.4.3 Effect of crosslinking reaction

The separation performance of the crosslinked membranes showed in Fig. 3.8 presents the effect of crosslinking conditions. The thermally crosslinked membrane, PVA4, shows somewhat a higher flux of 2.71 kg/m^2/hr than the chemically crosslinked membrane, PVA7 showing a total flux of 2.45 kg/m^2/hr, respectively, for a 10% ethanol-water solution.

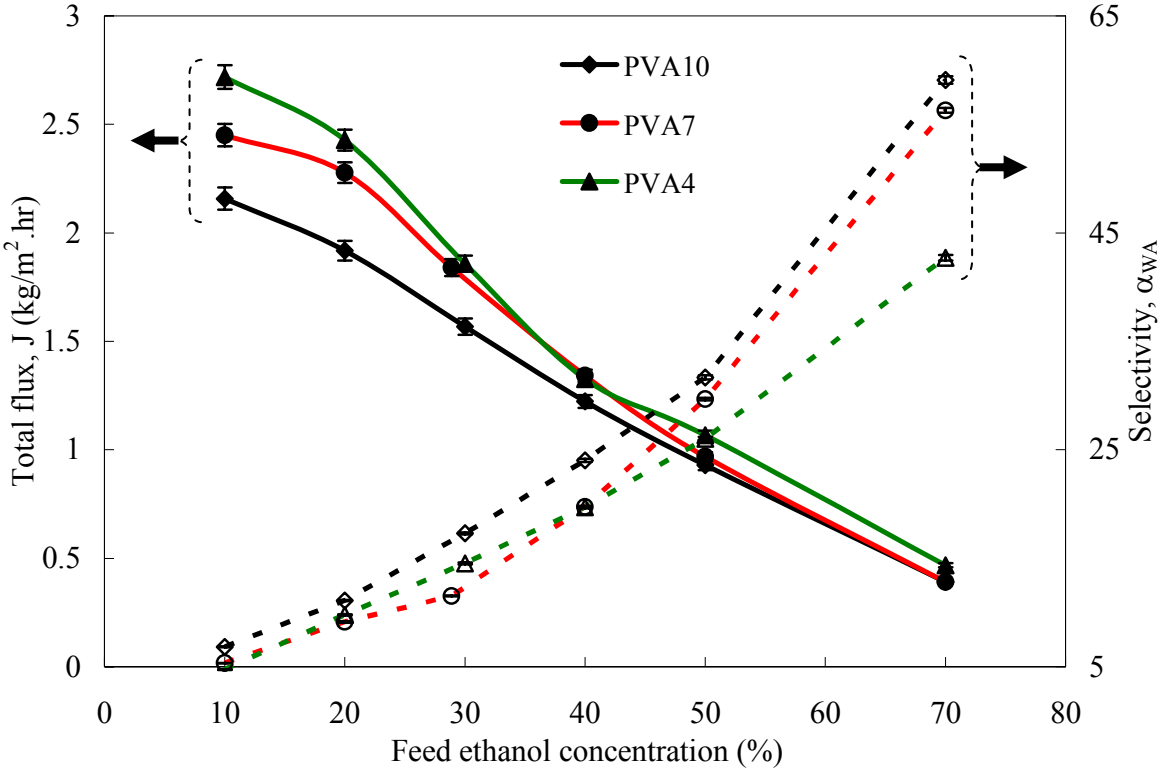

Figure 3.8: Total fluxes and selectivities of the PVA7 membranes for pervaporation separation under different crosslinking conditions at 40^{O}C.

However, the selectivities show the opposite trend; PVA10 shows a higher selectivity than PVA4 at all feed solution concentrations. For the chemically crosslinked membranes, e.g., membrane crosslinked with 2.5wt% glutaraldehyde, the crosslinking in the membrane film results in a rigid structure, see Table 3.2. This rigid structure of the polymer chains has less mobility and hinders the diffusion of liquid molecules [Yeom and Lee, 1996; Uragami *et al*., 1994]. Both the solubility and diffusivity of water in the membrane likely decline, resulting in a lower flux but higher selectivity.

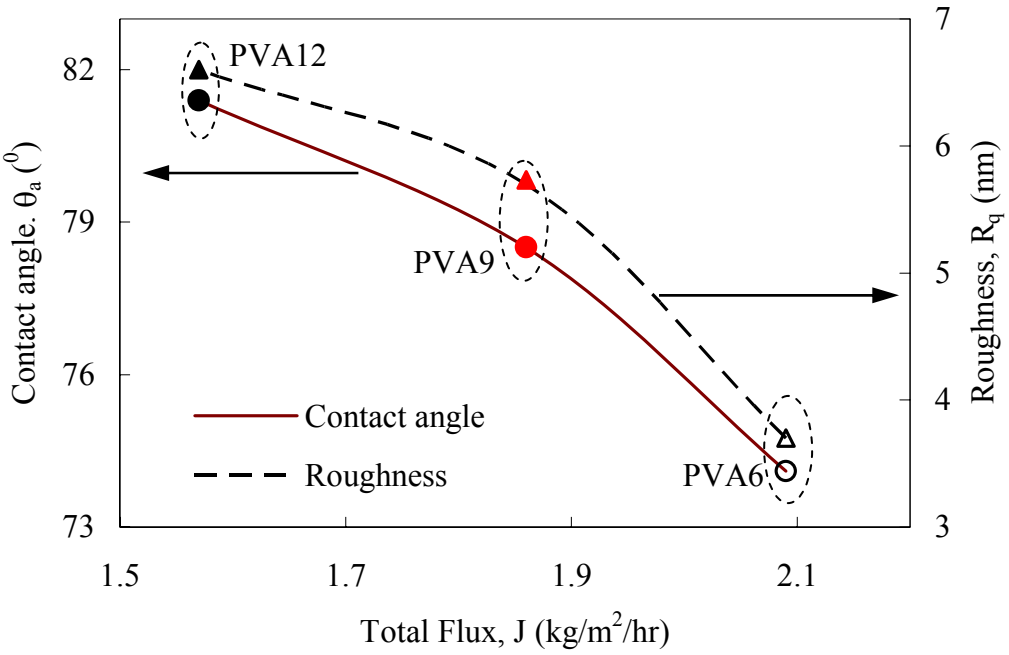

Figure 3.9: Correlation plot of advancing contact angle and surface roughness against flux for 10 wt% PVA crosslinked membranes. All experiments were performed at 25^{O}C.

This behavior can be further supported by a correlation plot shown in Fig. 3.9 for the crosslinked 10 wt% PVA membrane. PVA12 has the highest contact angle and roughness of 84.1^{O} and 6.6 nm, respectively, but gives the lowest total flux of 1.57 kg/m^2/hr with the 10wt% Et-water mixture. All nine crosslinked membranes are shown in Fig. 3.10 for the total flux and contact angle data. The thermally crosslinked membrane tends to be more hydrophilic, with a lower θ_a, than the chemically crosslinked membranes; for example, the 10 wt% PVA membrane crosslinked with heat treatment at 125^{O}C (PVA6) shows an advancing contact angle of 74.1^{O} (θ_a) and a total flux of 2.09 kg/m^2/hr, while the 10 wt% PVA membrane crosslinked with 2.5 wt% glutaraldehyde (PVA12) gives a higher advancing contact angle of 81.4^{O} (θ_a) but a lower flux of 1.57 kg/m^2/hr. In addition, from the FTIR spectra in Fig. 3.1, at 3315-3340 cm^{-1}, the peak value for –OH groups of PVA6 is higher than PVA12. The higher peak associated with the PVA6 membrane implies that it is more hydrophilic than PVA12. As a result of being more hydrophilic, the thermally crosslinked membrane has higher diffusion and hence higher total flux than the chemically crosslinked membranes. Fig. 3.11 represents the results of advancing contact angles and total fluxes (for a 10% ethanol-water mixture) with respect to polymer concentration in the membrane. At any PVA concentrations, all the heat crosslinked membranes have smaller advancing contact

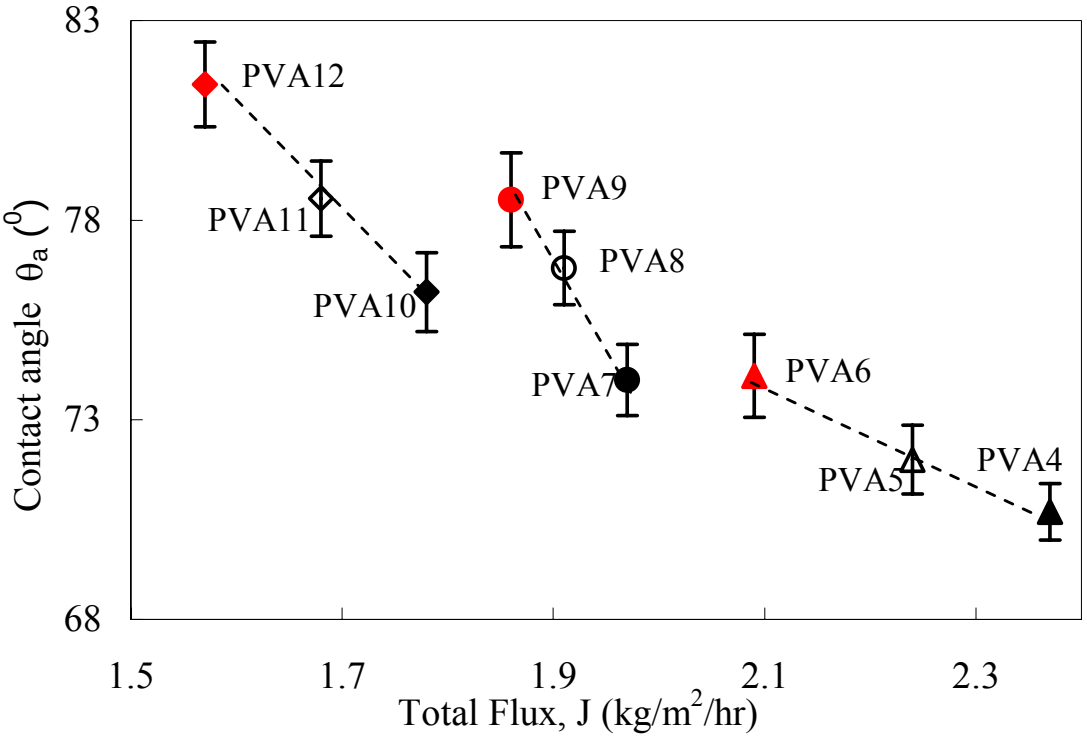

Figure 3.10: Correlation plot of advancing contact angle against total flux for different crosslinked membranes. Both experiments were performed at 25^{O}C.

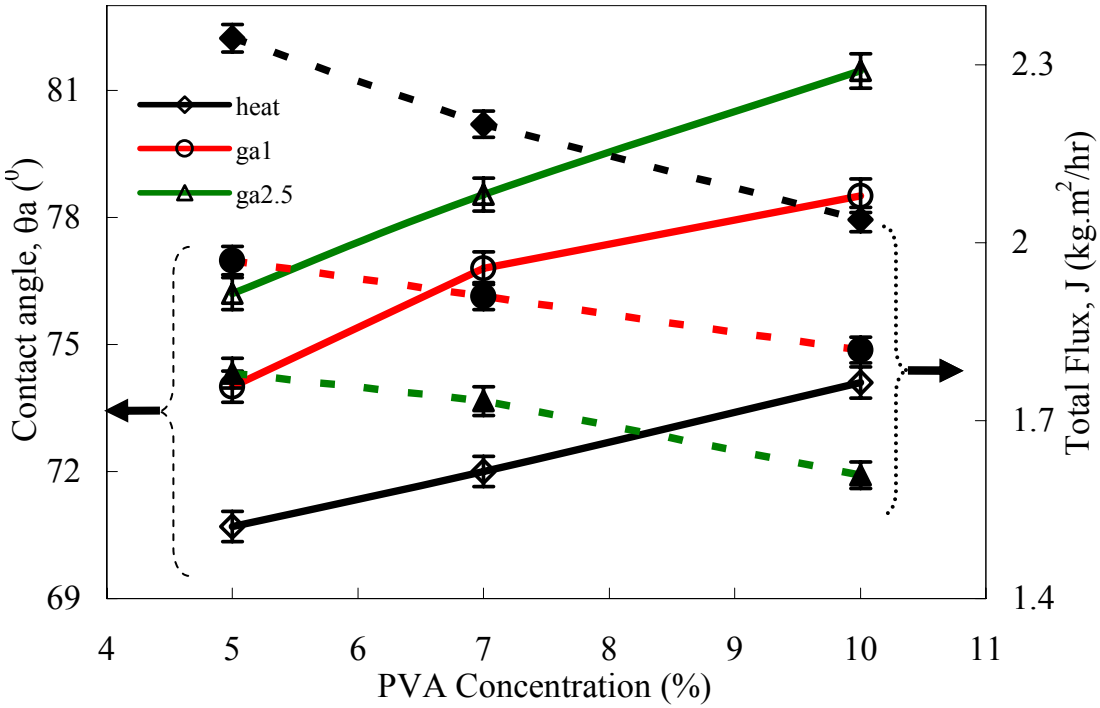

Figure 3.11: Correlation plot of advancing contact angle and total flux against PVA concentration. All experiments were performed at 25^{O}C.

angles (than chemically crosslinked membranes) but their total fluxes are higher. The heat crosslinked membrane may not have as rigid a structure as the chemically crosslinked membrane, and they are more hydrophilic.

Table 3.4 Comparison of results from different measurements

Membranes	Separation performance		AFM	Contact angle
	Maximum total flux, J ($kg/m^2/hr$)	Maximum selectivity, α_{WA}	RMS roughness R_q (nm)	Advacing θ_a (^{O})
PVA4	2.37	49.28	2.3 ± 0.2	70.7 ± 1.1
PVA5	2.24	55.89	2.1 ± 0.1	72.0 ± 1.3
PVA6	2.09	57.34	3.7 ± 0.1	74.1 ± 1.6
PVA7	1.97	53.27	4.8 ± 0.2	74.0 ± 1.3
PVA8	1.91	60.32	2.8 ± 0.2	76.8 ± 1.4
PVA9	1.86	64.38	5.8 ± 0.3	80.1 ± 1.5
PVA10	1.78	57.01	4.1 ± 0.3	76.2 ± 1.5
PVA11	1.68	64.18	3.6 ± 0.2	78.4 ± 1.2
PVA12	1.57	68.77	6.6 ± 0.2	81.5 ± 1.3

Note: All the experiments below were performed at 25^{O}C (± 2^{O}C). For the pervaporation separation experiment, the maximum fluxes were obtained with the 10wt% feed ethanol-water solution and the maximum selectivities were obtained with the 70wt% feed ethanol-water solution.

Table 3.4 represents a more detailed comparison of the results from different experiments, including FTIR, AFM, contact angle and separation experiments at 25^{O}C. The results are arranged in an ascending order for the membranes of maximum total fluxes. The PVA4 membrane shows the lowest surface roughness (2.3 nm), lowest contact angle hysteresis (54.3^O) and highest flux (2.37 $kg/m^2/hr$ for the 10% feed ethanol-water solution), but the lowest water to ethanol selectivity of (49.3 for 70wt% feed Et-water solution). On the other hand, PVA12 shows the highest surface roughness (6.6 nm), highest contact angle hysteresis (64.8^O) and lowest total flux (1.57 $kg/m^2/hr$ for 10wt% the feed ethanol-water solution), but the highest water to ethanol selectivity (68.8 for the 70 wt% feed ethanol-water solution). We believe that the trends observed between the membrane performance and its

physicochemical properties will be very useful in understanding pervaporation membranes and in their materials design for particular separation applications, whether it is for high temperature operations or more hydrophilic solvents.

3.5 Conclusions

A combination of Fourier spectroscopy, differential scanning calorimetry, atomic force microscopy and contact angle measurements is an effective way to find the physicochemical properties of polymeric membranes. FTIR measurements on the poly(vinyl alcohol) membranes showed that the hydroxyl groups of the polymer decreases with increasing concentration of glutaraldehyde in the crosslinked solution. The decrease of the hydroxyl groups was due to formation of acetal or ether linkage groups after the crosslinking reaction. The resulting membranes were less hydrophilic. DSC measurements showed an increase in melting temperature of the polymer membranes after crosslinking. Advancing and receding contact angles were suitable to measure the hydrophobicity of the polymer membranes because the surfaces are rough as found from AFM experiments. Topographic images from the AFM experiments showed that the membrane surfaces possess nanometer sized structures. The crosslinked membranes showed an increase in surface roughness when compared to the fresh membrane. The pervaporation experiments showed that the thermally crosslinked membrane gives a higher flux compared to the chemically crosslinked membrane. The thermally crosslinked membrane is more hydrophilic than the chemically crosslinked membranes, helping transporting water at a higher flux through the membrane. However, the selectivity of the thermally crosslinked membrane is lower as compared to the chemically crosslinked membranes. In general, less hydrophilic membranes, e.g., 10wt% PVA crosslinked with 2.5wt% glutaraldehyde (θ_a= 81.4^O and Rq =6.6 nm), give a lower flux but a higher selectivity in the separation experiment.

CHAPTER 4

Effect of Selective Layer Thickness on Pervaporation of Composite Poly(vinyl alcohol)-Poly(sulfone) Membranes

4.1 Introduction

In pervaporation, separation efficiency depends on the physicochemical properties of polymeric membrane, e.g., thickness, hydrophobicity, chemical compatibility, mechanical strength and temperature resistance, as well as on operating conditions, e.g., temperature and feed concentration gradient across the membrane [Binning *et al.*, 1961; Huang, 1991; Uragami *et al.*, 1994; Smitha *et al.*, 2004]. The flux through a homogeneous membrane is usually dominated by a diffusion process. Thicker membrane gives more permeation resistance, and thereby decreases the flux [Huang, 1991]. In the last two decades, researchers have studied the effect of homogeneous membrane thickness on separation performance for different binary mixtures [Brun *et al.*, 1974; Aptel *et al.*, 1974; Pusch and Walch, 1982; Yong *et al.*, 1990; Huang, 1991; Osada, 1992; Koops *et al.*, 1994; Nijhuis *et al.*, 1991; Qunhui *et al.*, 1995; Villaluenga *et al.*, 2005]; the flux was found to be inversely proportional to the membrane thickness but the selectivity remains nearly unaffected. Some researchers related the selectivity to the existence of micropores in the membrane matrix [Spitzen *et al.*, 1988] or the existence of a dry layer in the membrane near the permeate side [Koops *et al.*, 1994]. However, the very existence of micropores or dry permeate layers in the membrane is somewhat unclear. If the selectivity remains nearly unchanged with membrane thickness, the factors that are unaffected by the thickness must be sought, in order to explain such an observation.

In pervaporation separation, especially with thin membranes, adsorption of the feed solution and subsequent absorption may influence the membrane performance, further impacting the follow-up diffusion and evaporation [Huang 1991; Smitha *et al.*, 2004]. Surface properties, e.g., hydrophobicity and roughness, may become important as they govern the adsorption and consequent absorption of permeating components.

Portions of this work have been published in *J. Membr. Sci.*, 318 (2008) 387-396.

Thinner polymer membranes often lack mechanical stability, especially when vacuum is applied on the permeate side [Osada, 1992; Nijhuis *et al.*, 1991; Qunhui *et al.*, 1995; Villaluenga *et al.*, 2005]. To overcome this problem, when studying the thickness effect, researchers are increasingly using composite membranes, where a thin selective layer of interest is supported by a mechanically stable layer [Osada, 1992; Cabasso, 1981; Feng and Huang., 1996]. A porous polymer, e.g., poly(sulfone) (PSf), which itself is widely used in ultrafiltration and nanofiltration [Du *et al.*, 2004], can be used as a support layer for the composite membrane. Poly(vinyl alcohol) (PVA), a hydrophilic polymer, is often used in the pervaporation of water-alcohol mixtures, for its good chemical stability and low manufacturing cost [Huang, 1991; Yeaom and Lee, 1996]. However, because of its tendency to swell in aqueous solution, the PVA used has to be crosslinked before being in contact with the liquid. Researchers [Ohya *et al.*, 1992; Wu *et al.*, 1994; Lang *et al.*, 1996; Chen and Chen, 1996; Wei *et al.*, 2005] in the past have studied the separation performance of flux and selectivity of alcohol-water mixture through crosslinked PVA-PSf membrane for different preparation techniques, separation temperatures, crosslinking conditions etc. However, the effects of the selective layer thickness of the PVA-PSf composite membrane on separation performance of flux and selectivity have not been studied before. In this study, crosslinked PVA-PSf composite membranes of varying selective PVA layer thicknesses (4 to 52 μm) were prepared. The composite membranes were characterized using a number of physicochemical techniques, including contact angle measurement [Rosa and de Pinho, 1997, Li *et al.* 2007] for surface hydrophobicity, scanning electron and atomic force microscopes for micro/nanostructure and surface roughness [Dietz *et al.*, 1992]. Dehydration of ethanol-water (Et-water) mixtures was performed at room temperature using the prepared PVA-PSf composite membranes. The separation parameters, e.g., flux and selectivity from the pervaporation experiment, were related to the thickness of the selective PVA layer.

4.2 Theoretical Background

The mass transport in membrane pervaporation can be written in terms of the chemical potentials [Meulman *et al.*, 1999]

$$J_i = k_{ov,i}\left(\phi_{b,i} - \phi_{p,i}\right) = \frac{\left(\phi_{b,i} - \phi_{p,i}\right)}{R_{ov,i}} \qquad (4.1)$$

where $k_{ov,i}$ is the overall mass transfer coefficient of component i, $\phi_{b,i}$ and $\phi_{p,i}$ are the volume fractions of component i at the bulk (feed) and the permeate side, respectively, and $R_{ov,i}$ is the overall resistance to mass transfer of component i ($R_{ov,i}$=1/ $k_{ov,i}$) [Nijhuis *et al.*, 1991].

During the separation process, the mass transport resistance may come from the feed boundary layer and the membrane itself, neglecting any flow coupling effects of components (e.g., between membrane and solvents). The resistance-in-series model incorporated with the well known S-D model [Spitzen *et al.*, 1988; Smitha *et al.*, 2004] successfully describes the mass transport in membrane pervaporation. According to this model, the overall mass transport resistance can be written as [neglecting the resistance on the permeate side]

$$R_{ov,i} = R_{bl,i} + R_{m,i} \tag{4.2}$$

where $R_{bl,i}$ is the boundary layer resistance and $R_{m,i}$ is the resistance from the membrane for component i. The membrane mass transfer coefficient, $k_{m,i}$, can be found easily once the resistance is known ($k_{m,i}$ = 1/ $R_{m,i}$). On the feed side of the membrane cell, in a cross flow design, the resistance of the boundary layer is insignificant. Since the mass transport in the membrane is governed by the solution-diffusion (S-D) model, the membrane resistance per unit area can be written as [Villaluenga *et al.*, 2005]

$$R_{m,i} = L/\left(D_i S_i\right) \tag{4.3}$$

where L is the membrane thickness, D_i is the diffusivity and S_i is the solubility of component i in the membrane. It can be seen from Equation (4.3) that the mass transfer resistance is proportional to the membrane thickness. The mass transfer resistance can be obtained from the flux measurement at different feed concentrations.

4.3 Experimental

4.3.1 Materials

Poly(vinyl alcohol) (99.7%, MW~133,000, PDI~1.3) was purchased from Fisher Scientific (ON, Canada). Poly(sulfone) (P-1700) was obtained from Amoco Performance Products (OH, USA) and was dried at 50^{O}C in a vacuum oven for 24 hr before use. *N*, *N*-Dimethylacetamide (DMAc) was from Acros Organics (NJ, USA) and poly(vinylpyrrolidone) (PVP, K30, MW~40,000) from Fluka Chemika (Buchs Switzerland). All other chemicals, including acetic acid (glacial, 99.6%), acetone (99%), glutaraldehyde (25% aqueous) and sulfuric acid (98%), were obtained from BDH (Toronto, Canada). Deionized water (18.2 MΩ cm) used for all

experiments was produced by a Millipore Milli-Q system (MA, USA). All the solvents were used as received.

4.3.2 Membrane preparation

The PSf support (substrate) membrane was prepared using the phase inversion technique [Du *et al*., 2004]. The polysulfone porous substrate membrane was prepared through non-solvent induced phase separation method. A mixture of 14 g PSF and 6 g poly(vinylpyrrolidone) (PVP) were dissolved in 80 mL DMAc at 70^{O}C to form a homogeneous solution, which was then left at 50^{O}C for 24 h in order for air bubbles to be released. The clear polymer solution was cast onto a glass plate to form a thin layer of the polymer solution of 0.28 mm thickness, followed by immersion into non-solvent water at 21^{O}C to undergo coagulation, during which process phase separation of the polymer-solvent system took place, thereby forming an asymmetric microporous membrane. The dissolving of PVP in water can accelerate the initial separation of polymer and solvent to form large pores. The substrate membrane so formed was rinsed with running water for 24 h to wash away the PVP additive completely, and then it was immersed in a glycerol–water solution (volume ratio of 1:1) for 24 h before being dried at ambient conditions. The thickness of the dry PSf microporous membrane was 120 ± 10 μm, measured by a micrometer and later verified by SEM image analysis. The PVA-PSf composite membranes were prepared by coating a layer of PVA onto the PSf substrate. Before applying the coating, the PSf membrane was washed with deionized water for 24 hr to remove glycerol and then washed with ethanol several times. The PVA stock solution was prepared by dissolving 5wt% of the polymer in deionized water at 90^{O}C for 1 hr, stirring the solution until it was completely homogeneous. The solution was then deposited onto the PSf substrate with a retainer ring made of poly(vinyl chloride) (10mm high and 75mm in diameter) that was adhered on the surface of the PSf substrate [Du *et al.*, 2004]. The substrate was positioned horizontally, and the coating solution was allowed to contact the surface of the substrate membrane for a given period of time. Thickness of the selective PVA layer thickness was controlled by PVA solution concentration (2 to 5wt%) and coating time (3 to 10 mins). Afterwards the excess coating solution was removed, and the membrane was dried in a fumehood at 25^{O}C for 24 hours. The membrane was then dried in a vacuum oven (at 40^{O}C) for 3 hr for the removal of traces of the solvent. The PVA-PSf composite membranes were

further crosslinked with a glutaraldehyde solution [Yeom and Lee, 1996]. This crosslinking solution consisted of 2wt% glutaraldehyde (GA), 0.5wt% sulfuric acid (H_2SO_4), 48wt% acetone, and rest deionized water. The PVA side was crosslinked for 30 minutes at room temperature (25^OC) with the crosslinking solution. After the reaction, the membrane was taken out and washed several times with pure water and finally immersed in deionized water for 6 hours at 40^OC to eliminate residual H_2SO_4. The crosslinked membrane was then dried in a vacuum oven (at 40^OC) for 24 hours.

4.3.3 Characterization

Table 4.1 Membrane characterization results

Composite Membrane	PVA layer thickness, μm	Surface roughness Rq (nm)	Contact angle, θ_{ap} (^{O})	Degree of Swelling (SD) (g/g) x100	Swelling per unit thickness (SD/thickness)	Mass transfer resistance, R_m (s/m)
PVA52	52	8.5 ± 1.1	62.1 ± 1.4	72.5 ± 7.1	1.5 ± 0.6	14.2 x10^5
PVA38	38	6.8 ± 0.8	60.9 ± 1.5	69.3 ± 5.8	1.8 ± 0.5	10.8 x10^5
PVA23	23	6.2 ± 0.5	57.8 ± 1.2	64.1 ± 5.1	2.9 ± 0.5	7.55 x10^5
PVA11	11	4.7 ± 0.9	54.4 ± 1.1	51.2 ± 4.2	4.8 ± 0.7	5.87 x10^5
PVA4	4	4.2 ± 0.6	51.1 ± 1.6	48.7 ± 4.9	12.5 ± 0.9	3.98 x10^5

Note: PSf support film thickness is 120 ±10 μm. The membrane thickness was measured with a micrometer and SEM image analysis software. Picoscan AFM software was used to measure surface roughness. Swelling results presented here are for pure water only at 25^OC. Mass transfer resistances have average error of 8%.

A micrometer was used to determine the composite membrane thickness by measuring at least 10 different locations including the center. The thicknesses of the selective layers were determined from the cross-sectional SEM image analysis. To quantify the chemical composition of a membrane film before and after the crosslinking, Attenuated Total Reflectance (ATR)-FTIR spectroscopy was employed for the PVA-PSf membranes. Infrared spectra of the fresh and crosslinked membranes (of equal thickness) were obtained with a midrange (500-4000 cm^{-1}) Bruker Tensor 27 ATR-FTIR spectroscope (Milton, Canada).

The membrane structure and morphology were observed using a Scanning Electron Microscope (SEM) (LEO1530 FE-SEM, Zeiss/LEO, Oberkochen, Germany). The membrane samples were quenched and broken in liquid N_2 for cross-sectional imaging.

A commercial Atomic Force Microscope (AFM) (Picoscan, Molecular Imaging, Tempe, AZ, USA) was used to determine the topography of the composite membrane surfaces. After image acquisition, roughness of the membrane surface was determined by a program in the AFM image processing toolbox [Dietz *et al.*, 1992].

To determine the hydrophobicity of the composite membrane surfaces, apparent contact angle measurements were conducted with static water sessile drops [Rosa and de Pinho, 1997, Li *et al.* 2007]. All the contact angle measurements were repeated four times, and the results were averaged for each sample.

4.3.4 Swelling experiments

The crosslinked PVA-PSf membranes, of equal cross-sectional area (but different thicknesses), were weighed and immersed in different feed mixtures containing 0-90 wt% ethanol at $25^{O}C$ for 24 hr. Swollen membranes were blotted carefully with tissue paper to remove any surface solution, and the weight of the swollen membranes was measured by a mass balance [Sharma *et al.*, 2004]. The membranes were weighed several times to ensure constant weight and they have reached equilibrium swelling. The degree of swelling (DS) was calculated by

$$\text{Swelling degree (\%)} = \left(\frac{W_S - W_D}{W_D} \right) x\,100 \qquad (4.4)$$

where W_S is the mass of the swollen membrane (in g) and W_D is the mass of the dried membrane (in g).

4.3.5 Pervaporation

The separation experiment was conducted at room temperature on a lab scale pervaporation setup [Fig. A.1 in Appendix A] for the dehydration of Et-water mixtures. The feed solution was pumped at a flow rate of 2.3 L/min to the membrane cell. The feed solution contained 10 to 85wt% ethanol. The permeate composition was analyzed using a Hewlett Packard 5890 Series II gas chromatograph with Helium as the carrier gas with a flow rate of 20 ml/min. A

10 µl syringe was used to inject a fixed volume of liquid permeates. Each experiment was repeated four times under the same steady-state condition.

4.4 Results and discussion

The thickness of the PVA selective layer varied from 4 to 52 µm in the PVA-PSf composite membrane. Table 4.1 shows the data of the different membranes prepared for this study, and, for example, PVA4 is a crosslinked composite membrane with a selective PVA layer thickness of 4 µm.

4.4.1. Infrared spectroscopy: crosslinking

The IR spectra of the fresh and crosslinked membranes are shown in Figure 4.1. The PVA membrane films show absorption peaks at 3300-3400 cm^{-1} for the hydroxyl (-OH) groups. A decrease of the absorption peak intensity is observed for the crosslinked PVA membrane, indicating that the number of the hydroxyl group decreased after crosslinking. The absorbance peaks at 990-1050 cm^{-1} and at ~ 1097 increase corresponding to the acetal and ether groups

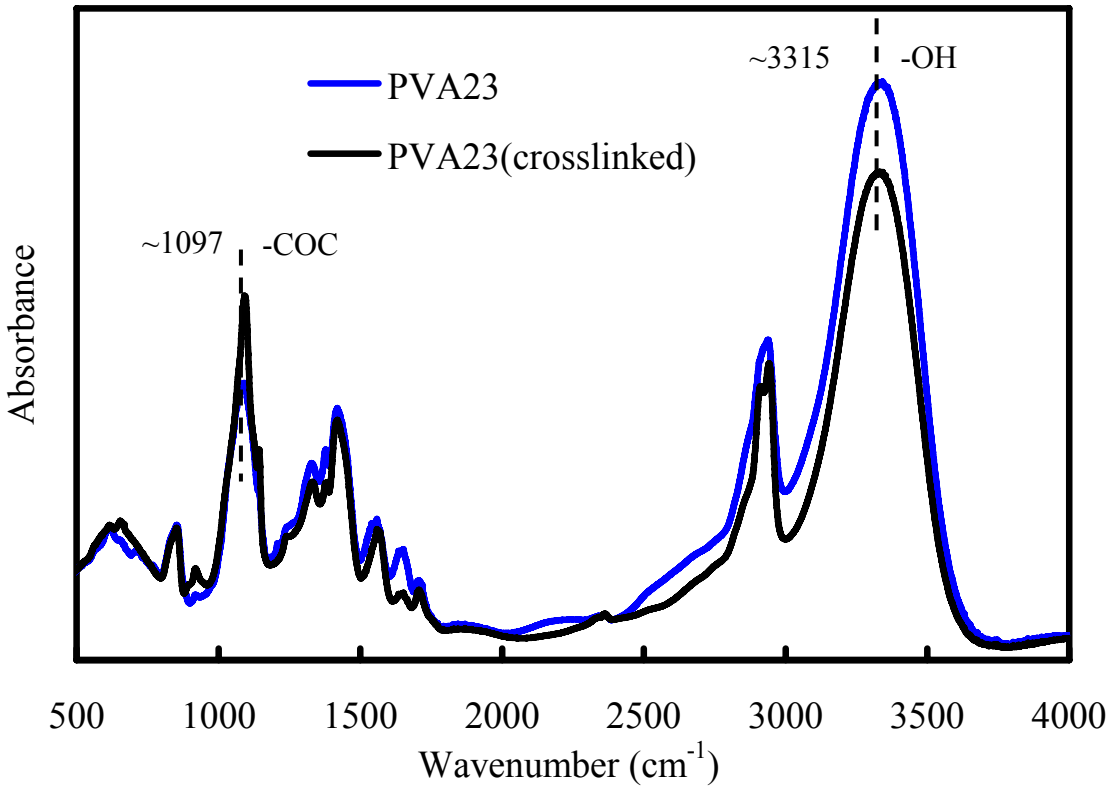

Figure 4.1: ATR-FTIR spectra of the PVA23 membranes before and after crosslinking.

in the PVA membrane [Yeom and Lee, 1996], reflecting a crosslinked PVA membrane.

4.4.2 Scanning electron microscopy: microstructure

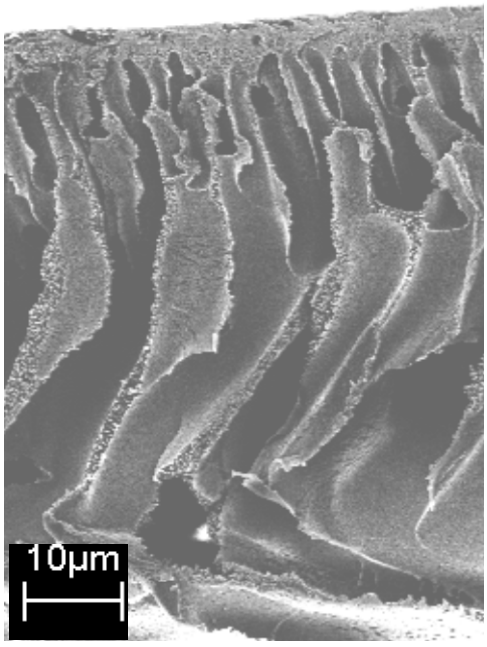

(a) PSf

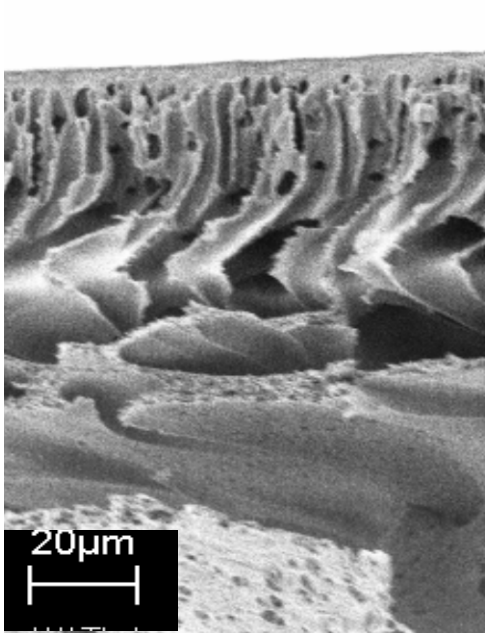

(b) PVA4

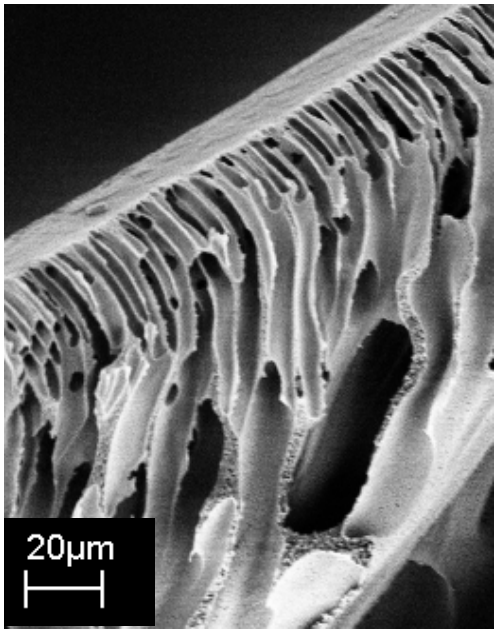

(c) PVA11

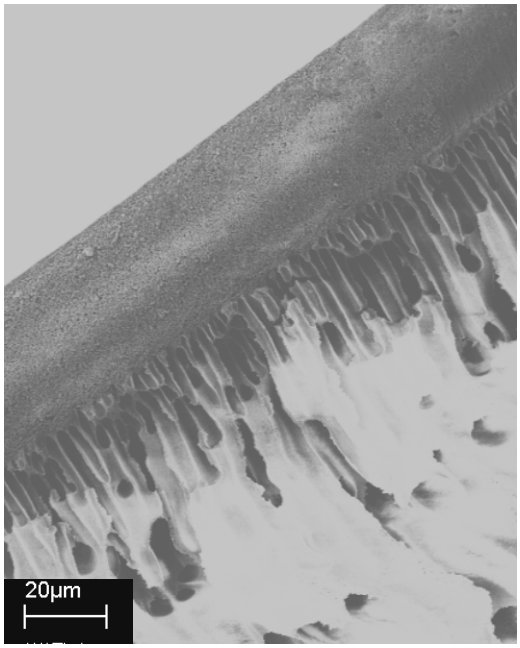

(d) PVA38

Figure 4.2: SEM micrographs of the membranes: (a) Poly(sulfone), (b) PVA4, (c) PVA11, (d) PVA38 µm, cf. Table 4.1.

Ideally the support layer for PVA should be porous to present little resistance to the permeate transport. The phase inversion process [Du *et al.*, 2004] created a porous polysulfone

structure. Figure 4.2 shows the cross sectional structure of the membrane. Figure 4.2(a) shows the structure of the porous support layer made of PSf only. From SEM image analysis, we found the PSf support contains pores on the surface of 3-10 microns in diameter. Therefore, it was expected that after coating, the PVA solution would invade the pores to some extent. However, it was not clear from cross-sectional SEM images although an interface is visible between PVA and PSf layers. The composite membrane surfaces were found to be free of any pores. Figure 4.3(b)-(d) shows the structure of the composite membranes with different selective PVA layers supported by the PSf substrate. The top PVA layers for all the composite membranes were found to be free of any large defects or cracks. In order to characterize the membrane surface property, we employed Atomic Force microscopy techniques.

4.4.3 Atomic force microscopy: surface roughness

Figure 4.3 shows the AFM images of the surface of the membrane over a scan area of 3 × 3 μm^2. Table 4.1 shows the root mean square (RMS) roughness, Rq obtained from the AFM image analysis [Dietz *et al.*, 1992]. The membrane surface is rough on a nanometer scale. The PSf substrate itself shows a surface roughness of 85 nm. From Table 4.1, the roughness slightly increases as the selective layer thickness increases, e.g., PVA4 showing a roughness of 4.2 nm and PVA52 showing a roughness of 8.5 nm. These rough surfaces will be in contact with the feed solution during the pervaporation process. The hydrophobicity of the rough PVA surface was quantified using contact angle measurement on these crosslinked membrane surfaces.

4.4.4 Contact angle measurement: surface hydrophobicity

Sessile drops of water were used to measure the apparent contact angle (θ_{ap}) to evaluate the hydrophobicity of the surface of the PVA layer [Li *et al.* 2007]. The fresh (non crosslinked) PVA-PSf composite membrane shows a static contact angle of 28.3^O. Crosslinking of PVA increases the contact angle, making it less hydrophilic. Results from the experiments of the crosslinked membrane surfaces are presented in Table 4.1. Thicker crosslinked membranes show higher contact angles and tend to be more hydrophobic, e.g., 51^O on the PVA4, and 62^O on the PVA52. The increased in hydrophobicity may be attributed to the increases in surface roughness of the crosslinked membrane (AFM results in Table 4.1). Recently, Li *et al.* (2007)

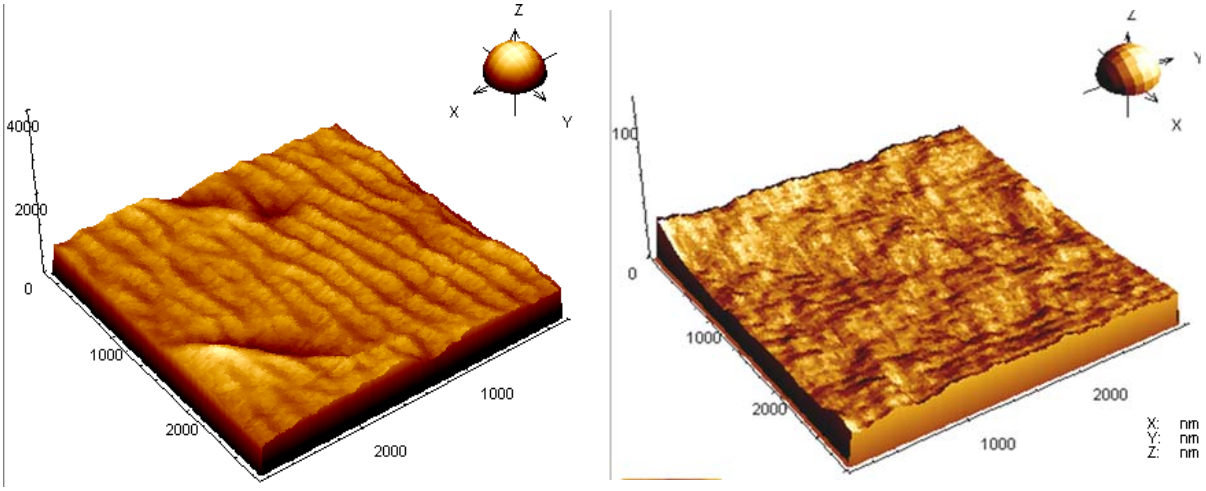

PSf PVA4

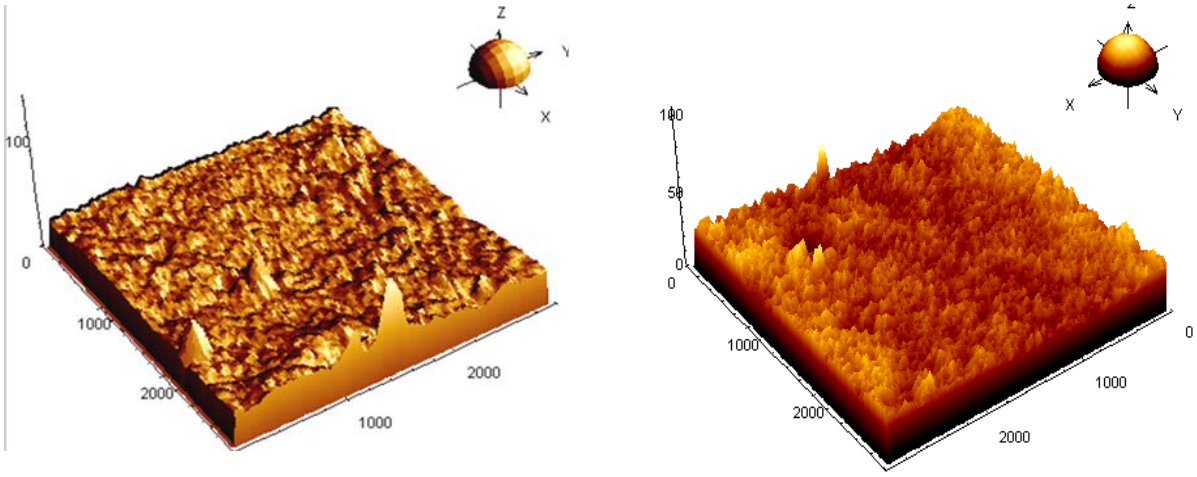

PVA11 PVA38

Figure 4.3: 3D AFM topographic images of the PVA membrane surfaces. Scanned area are 3 x 3 μm^2, and AFM was used in tapping mode at $25^{O}C$.

reported the static contact angle of crosslinked PVA membranes to be within 54^{O} – 65^{O} which agree well with our results.

4.7.5 Swelling characteristics

Swelling behavior gives an idea about the sorption behavior of components in the membrane matrix. Swelling results of the composite membranes by water mixtures (10-100 % water in Et-water mixtures) are shown in Figure 4.4. Results for the PSf support layer is not shown as retention of water occurs inside the porous structure rather than swelling. However, the swelling of PVA layers in the composite membrane were calculated by subtracting equivalent

weight of the wet PSf support layer. From Fig. 4.4, with increasing water concentration in the mixture, the degree of swelling increases. For glutaraldehyde crosslinked PVA membrane, Yeom and Lee (1996) found the swelling ratio to be within 1.07 to 1.37. In this study, we found the ratio to be within 0.12 to 0.79 depending on the thickness and water content in the feed mixture. Interestingly, thicker membranes show slightly higher swelling, and PVA52 gives the highest extent of swelling. Water absorbs inside the hydrophilic PVA selective layer and swells the compact crosslinked structure. Ideally, in the swollen membrane, the resistance to permeate diffusion decreases [Yeom and Lee, 1996; Smitha *et al.*, 2004] and a higher flux can be achieved. However, the flexible swollen membrane might also allow all components of the mixture to diffuse through easily, resulting in a poor selectivity. Higher swelling is an indication of a flexible membrane structure, possibly leading to a higher total flux. Since thicker membrane shows higher swelling, one may expect a higher total flux due to less resistance. But such a conclusion is based on the assumption that the length of the diffusion

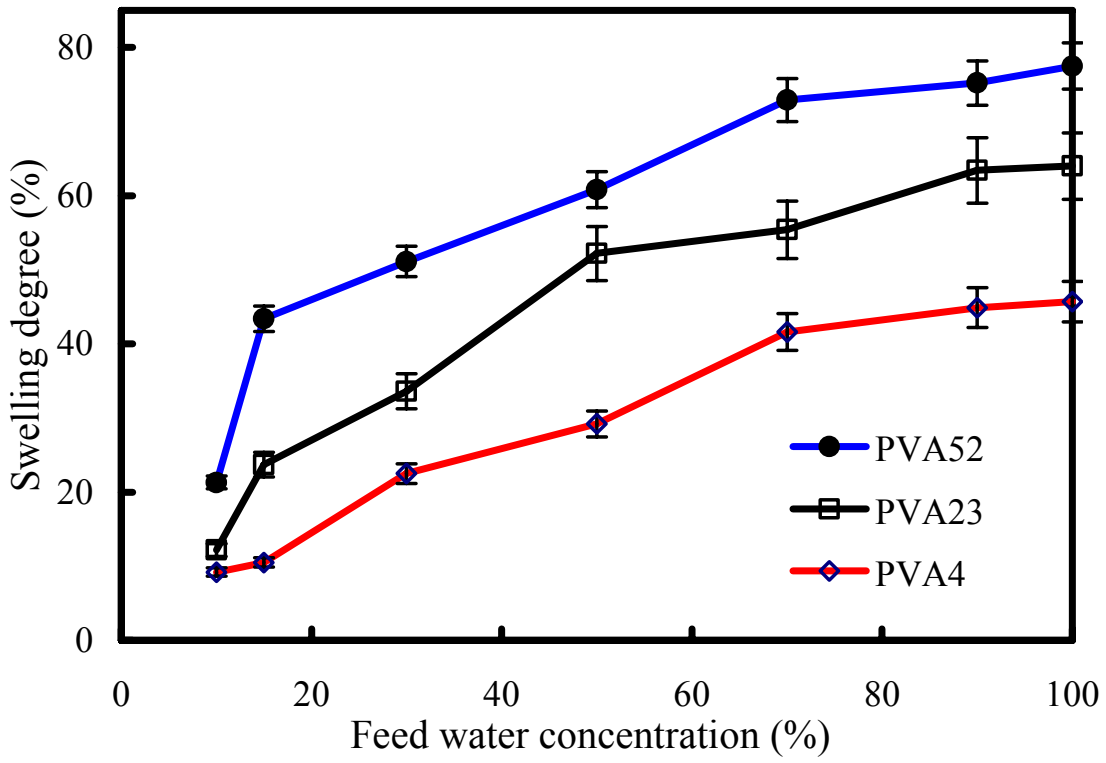

Figure 4.4: Swelling Degrees against feed water concentrations of Et-water mixtures

path within the membrane is unchanged, at least to a certain extent. It is known that the total flux is inversely proportional to the thickness, and therefore a thicker membrane can significantly reduce the total flux. As a result, the total flux is influenced by both membrane

swelling and thickness in two opposite ways. The introduction of the parameter, swelling per unit thickness, is to account for competition between the two factors. Such a parameter can be correlated with the measured flux data and explain the trend of the total flux with the membrane thickness. To compare the results for different thickness of the composite membrane, we have used a parameter called swelling per unit thickness (SD_T) of the PVA layer,

$$\text{Swelling degree per unit thickness, } SD_T = \frac{Swelling\ Degree}{Thickness_{PVA}} \tag{4.5}$$

The results for swelling degree and swelling degree per unit thickness of pure water are shown in Table 4.1. It can be seen that although PVA52 membrane shows the highest Swelling Degree of 73%, it has the lowest SD_T 1.5. Since the top PVA layers were crosslinked interfacially, it could be possible that the thicker membranes are not crosslinked completely throughout the entire structure. As a result, the swelling degree would vary greatly along the thickness, leading to an overall higher degree of swelling for a thicker membrane.

4.5 Separation behavior: flux and selectivity

4.5.1 Effect of feed concentration

Figure 4.5 shows the results of the total flux and selectivity of the PVA23 composite membrane (23 μm thick PVA layer) against the feed ethanol concentration at room temperature. The PVA layer is highly selective for water and therefore the total flux can be considered mainly the water flux. In Fig. 4.5, the total flux decreases while the selectivity increases with increasing feed ethanol concentration. At low ethanol feed concentrations (high water concentrations), the PVA layer is in swollen state (Fig.4.4), facilitating an increase in permeate transport and thereby a higher flux. The total flux through the composite membrane is observed to increase from 0.05 to 0.51 kg/m^2/hr as the feed ethanol concentration decreases from 85wt% to 10wt%. Although the composite membrane is crosslinked, at high water concentrations, it still swells to some extent, thereby enhancing the total flux. The selectivity decreases with decreasing ethanol concentration. The swollen PVA membrane at higher water concentrations allows ethanol molecules to transport to the permeate side more easily. As a control experiment, the results of a homogeneous (no porous PSf support) PVA membrane of a comparable thickness (23 μm) is shown in Fig. 4.5. The homogeneous membrane shows a

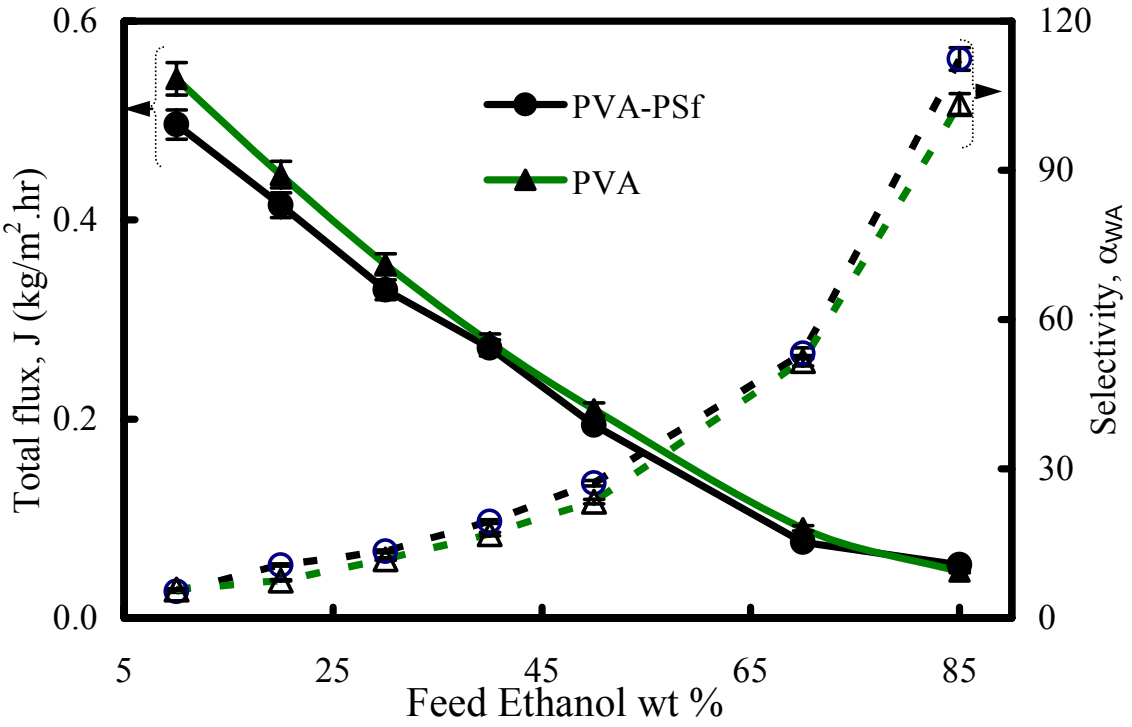

Figure 4.5: Total flux and selectivity of the composite PVA23 membrane at 25^{O}C with different feed ethanol concentrations. The homogeneous PVA membrane of a 23 μm thickness is shown for comparison.

Table 4.2 Comparison of separation performance with literature

Composite membrane (type)	Temp. (^{O}C)	Type of mixture & concentration	PVA layer thickness (μm)	J (kg/m^2.hr)	α	PSI (kg/m^2.hr)	Ref.
PVA-PSf (flat sheet)	70	Et-Water (94%)	2.5	0.039	180	6.98	Wu *et al.*[25]
PVA-PSf (hollow-fiber)	50	Et-Water (95%)	5	0.06	93	5.52	Wei *et al.*[23]
PVA-PSf (flat sheet)	70	Et-Water (85%)	4	0.096	77	7.29	present work*

PSI: pervaporation separation index = J * (1-α) [Huang, 1991]

*For separation performance comparison, dehydration of Et-water mixture through PVA4 was done at 70^{O}C

slightly higher total flux (0.57 kg/m^2/hr for the 10 wt% Et in feed mixture) and a negligible change in selectivity (5.8). Note that the total flux of the PSf support layer was determined to

be 130 kg/m^2/hr for 10wt% Et-water mixture. This high flux shows that the PSf substrate provides very little resistance to the permeate flow in the composite membranes and mainly provides mechanical support. For the thinnest membrane, PVA4, a comparison of the separation performance of the present study (for 85 wt% Et in feed mixture at 70^{O}C) with relevant literature is presented in Table 4.2. Although the membranes preparation techniques and separation conditions were different, the table shows an overall performance of total flux and selectivity of different membrane structures. It can be seen that the thinnest membrane from the present study, PVA4 has a comparable [Wu *et al.*, 1994; ,Wei *et al.*, 2005] separation index of 7.39 kg/m^2/hr.

4.5.2 Effect of membrane thickness

Figure 4.6 shows the total flux and selectivity against feed ethanol concentration for the composite membranes of different PVA layer thicknesses. Thinner membranes give higher fluxes. The increase in flux is more prominent at low ethanol concentrations. As for selectivity, no such distinct changes are observed. The percentage changes in total flux, ΔJ and selectivity, $\Delta\alpha$ were calculated using the equations shown below and results are summarized in Table 4.3, for two different feed solutions (10 and 85wt% Et in feed mixture). The percentage (%) change of flux and selectivity were calculated as follows:

$$\text{change in flux } \Delta J\ (\%) = \left(\frac{J - J_{52}}{J_{52}} \right) x\ 100 \tag{4.6}$$

$$\text{change in selectivity } \Delta\alpha(\%) = \left(\frac{\alpha - \alpha_{52}}{\alpha_{52}} \right) x\ 100 \tag{4.7}$$

where J_{52} and α_{52} are the reference flux and selectivity of the PVA52 composite membrane. At higher ethanol fractions, e.g., at 85wt% Et in feed mixture, the total flux is 0.081 kg/m^2/hr for PVA4 and 0.035 kg/m^2/hr for PVA52 (a 131% increase in flux when thickness

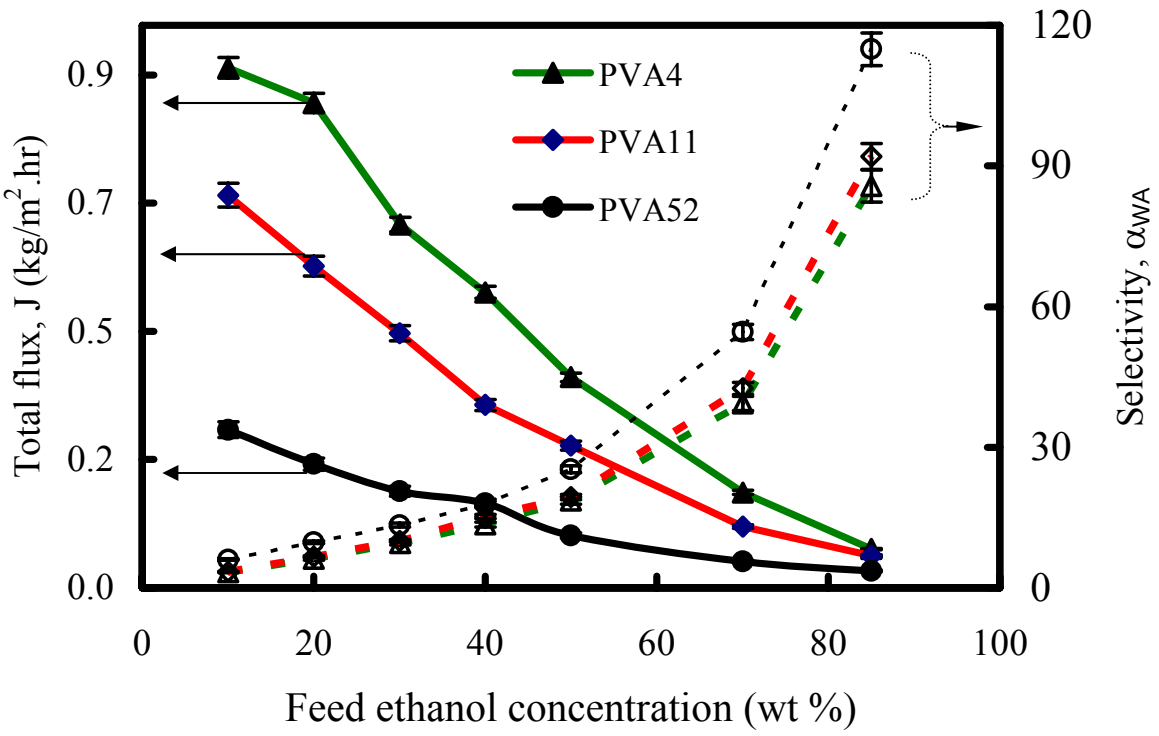

Figure 4.6: Total flux and selectivity against feed Et-water mixtures at 25^{O}C

is changed by 92%). On the other hand, the selectivity changes by merely 17% and 18% at most for the feed mixture of 10 and 85wt% Et-water, respectively.

Table 4.3 Dehydration performance of Et-water

Composite Membranes	Separation performance (10wt% Et-water solution)				Separation performance (85wt% Et-water solution)			
	J (kg/m^2/hr)	ΔJ (%)	α	Δα(%)	J (kg/m^2/hr)	ΔJ (%)	α	Δα(%)
PVA52	0.28	0	6.61	0	0.035	0	110.7	0
PVA38	0.36	30	6.55	1	0.042	17	105.2	8
PVA23	0.50	78	6.33	4	0.049	36	100.6	9
PVA11	0.70	149	5.94	10	0.055	55	97.3	12
PVA4	0.86	193	5.51	17	0.081	131	95.1	14

Note: The separation experiments above were performed at 25^{O}C. The changes in flux or selectivity were calculated with respect to the PVA52 composite membrane that has the highest selective PVA layer thickness of 52 μm, cf. Eq. (4.6) and (4.7). Average error in flux measurement is ± 3.8% and in selectivity is ± 7.5%

The total flux is significantly influenced by the PVA layer thickness. The change is more significant when the feed mixture has higher water content. The total flux of 10 and 40 wt% Et in feed mixture are presented in Fig. 4.7 as a function of the selective PVA layer thickness. The total flux at low ethanol concentration (10wt% Et-water decreases almost exponentially while at the high ethanol concentration (40 wt% Et-water), the flux decreases nearly linearly. The swollen membrane with its flexible structure provides rapid transport of permeates at the 10wt% feed ethanol concentration. The effect of surface property e.g., hydrophobicity on selectivity at different feed concentrations is shown in Fig. 4.8, where the selectivity is normalized by the feed ethanol concentrations. The selectivity was found to increase slightly with the membrane hydrophobicity. This increase is more pronounced at higher ethanol concentrations in the feed (lower water fractions in the feed). When the amount of water is less in the feed, the membrane is less swelled. This condition along with a longer diffusion distance gives an increased selectivity. However, asymmetric crosslinking could also affect the swelling degree and thereby diffusion resistance.

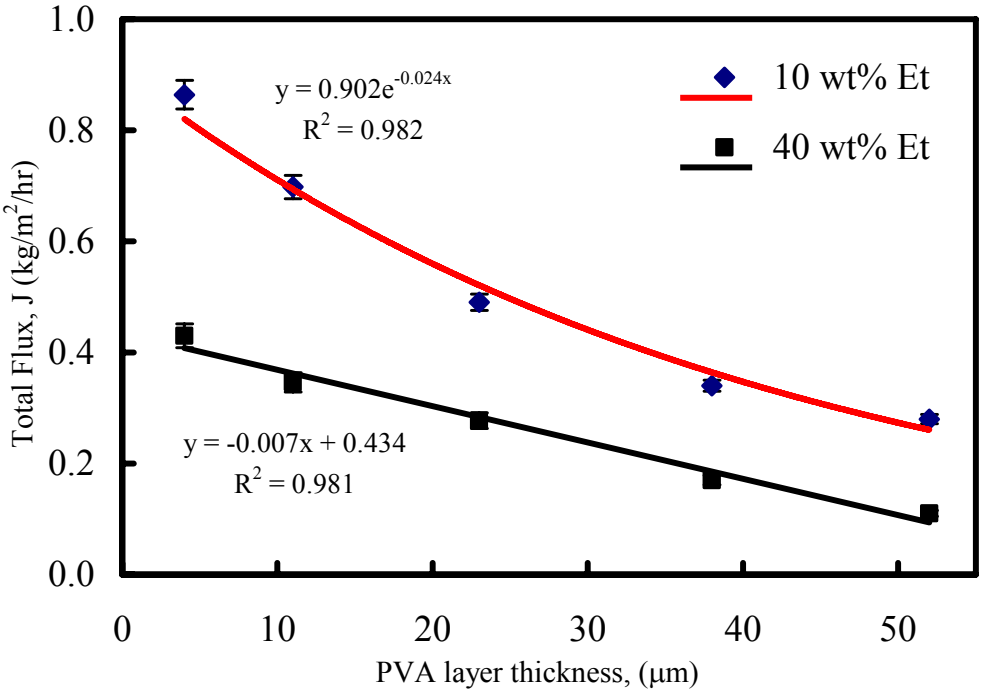

Figure 4.7: Total flux against PVA layer thickness for 10 and 40wt% Et in feed mixtures.

It is interesting to observe that even though PVA52, the thickest membrane is the most swollen one; it shows lowest flux and highest selectivity. Since a thicker membrane gives more resistance to permeate flow, the flux and selectivity are affected accordingly.

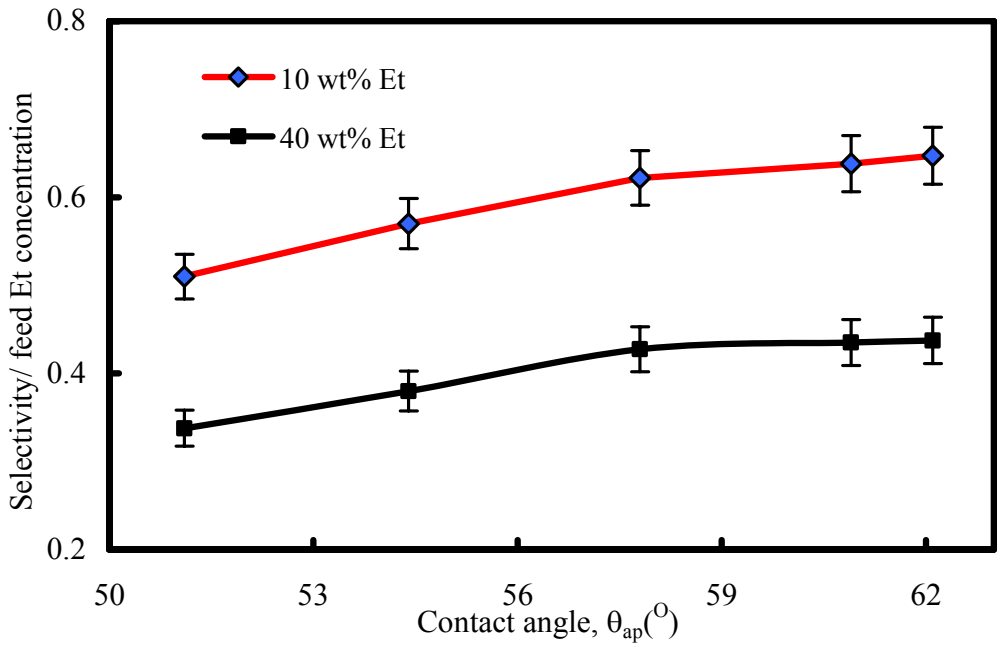

Figure 4.8: Selectivity/feed ethanol concentration against contact angle (hydrophilicity) for different feed mixtures.

Although PVA52 is the most swollen membrane; it has the lowest swelling per unit thickness (Table 4.1) and the higher resistance, which might have determined the flux and selectivity. Other factors, e.g., coupling effects between permeate and membrane, might play a role in determining flux and selectivity. Detailed mechanisms are still under study.

As stated before, in pervaporation dehydration, water is the preferential permeating component of the Et-water mixture through the hydrophilic PVA-PSf composite membrane. The water flux was calculated from the component composition by analyzing the permeate with a gas chromatograph. In Figure 4.9, the permeated water flux is plotted against the mass of water, (kg/m^3), in the feed mixture. The mass transfer resistance [Nijhuis *et al.*, 1991; Cussler, 1997, Bird *et al.*, 2002] calculated from the slope of the lines are summarized in Table 4.1. These results agree well with the well known S-D theory discussed in Section 4.2 and the membrane mass transfer resistances (R_m) increases linearly with the increase in thickness, Fig. 4.10. For composite poly(octanomer)-poly(sulfone) membrane (thickness 5 μm), Nijhuis *et al.*(1991) found the mass transfer resistance of to be 2.2×10^4 (s/m) for trichloroethylene permeation. In our study, for PVA4 membrane, the mass transfer resistance of water to be 3.98-14.2 $\times 10^5$ (s/m) for different thickness. A linear equation can be fitted to the data well ($R^2 = 0.9943$).

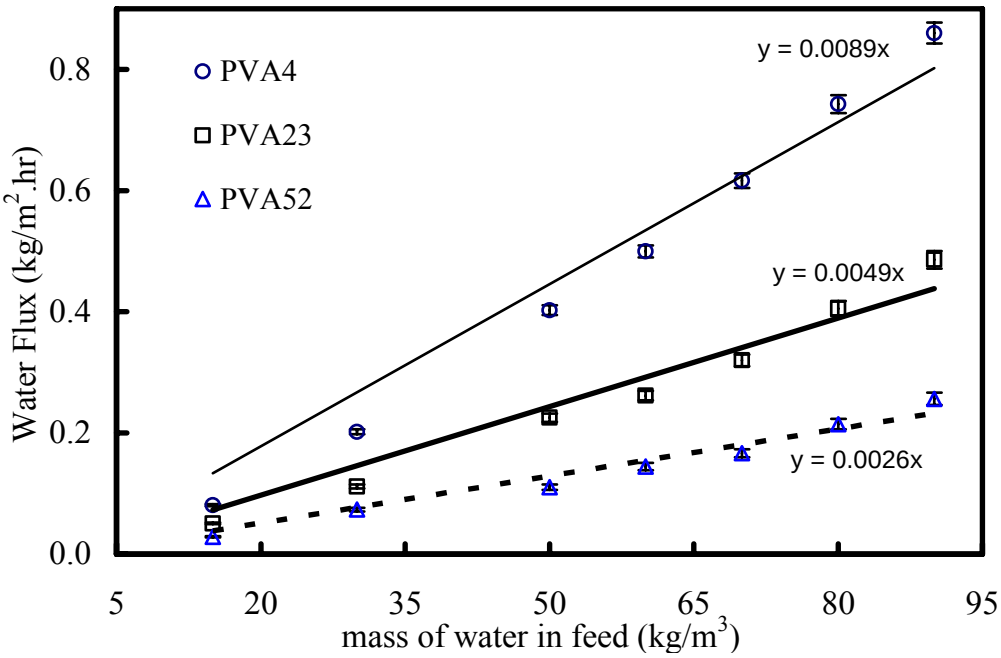

Figure 4.9: Water flux against mass of water in feed mixtures at 25 ^{0}C

However, it shows a finite mass transfer resistance of 3.2 x 10^5 (s/m) when the PVA layer thickness approaches zero. This resistance could be due to the feed boundary layer [Nijhuis *et al.*, 1991; Villaluenga *et al.*, 2005], resistance from the selective layer surface, the support layer or a combination of all three. However, in this experiment, the feed mixture was supplied in the membrane cell in a cross-flow manner that significantly decreases the resistance due to the feed boundary layer, and also the support layer gives very little resistance (at 2.45 x10^3 s/m) to the permeate flow. It could be possible that the membrane surface resistance plays a role here. The PVA surface layer becomes less hydrophilic after crosslinking reaction, which may give high resistance to the flow of permeate. Due to the interfacial crosslinking of PVA layer, with an increase in membrane thickness, the chances of the availability of polar groups increases, the flux decreases since diffusion of feed is retarded due to the increased resistance to mass transfer. On the feed side of the pervaporation experiment, upstream layer of the membrane is swollen and flexible due to sorption of feed liquid, thus allowing the unrestricted transport of feed components. However, the downstream layer is virtually unswollen due to continuous evaporation in the permeate side; therefore, this layer forms the restrictive barrier, which allows only the interacting and smaller molecules such as water to pass through. It is expected that the thickness of the unswollen layer would increase with an increase in the overall membrane thickness. As observed in this study,

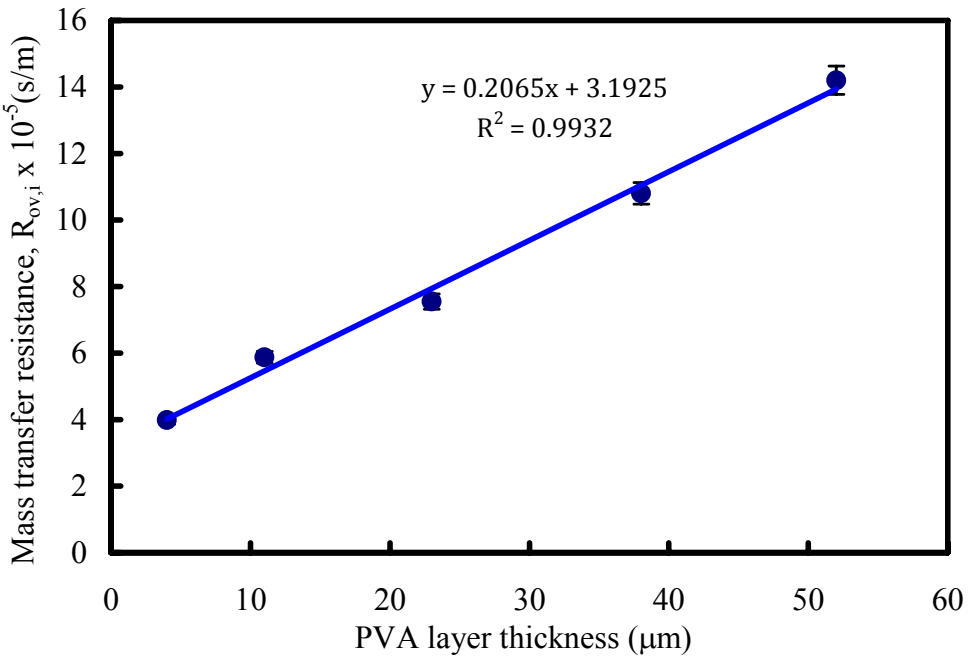

Figure 4.10: Mass transfer resistance against selective PVA layer thickness.

selectivity remains unchanged with thickness. The total flux and selectivity data at three different feed Et-water mixtures for the different PVA layer thicknesses were analyzed statistically using a one-factor ANOVA [Montgomery, 1991]. The factorial analysis can show if a factor, e.g., thickness, has any significant effect on the measured parameters, e.g., flux and selectivity, by calculating the variances of the experimental data. The data contain 4 replicates for each flux and selectivity measurement. In Table 4.4, the calculated F values for the flux and selectivity are given for different feed mixtures of Et-water. For comparison, the critical F value is obtained from the *F* table with 5% level of significance ($p = 0.05$). All the calculated F values (923.97, 97.86 and 42.26) for the flux are higher than the critical F (3.1), indicating that the flux is significantly affected by thickness.

On the other hand, the calculated F values (0.036, 2.41 and 2.96) for the selectivity are below the critical F (3.1), suggesting that a change in thickness does not affect the selectivity significantly (less than 20%). From the physicochemical characterization results in Table 4.1, the surface roughness and hydrophobicity of the membrane change to an extent (surface roughness changes from 4.2 nm to 8.3 nm and contact angle change from 51^{O} to 63^{O}). As indicated in the above mass transfer resistance analysis, the surface may also play a role when the membrane is thin. It is possible that the relatively small change in surface properties, e.g.,

Table 4.4 One-factor (i.e., thickness) ANOVA analysis for flux and selectivity

One way ANOVA for thickness	F values for Total Flux of different feed solutions			F values for Selectivity of different feed solutions			F Critical
	10wt% Et-water	40wt% Et-water	85wt% Et-water	10wt% Et-water	40wt% Et-water	85wt% Et-water	
$F_{calculated}$	923.97	97.86	42.26	0.036	2.41	2.96	3.1
Significance, *p*	<0.000001	<0.00001	<0.00001	0.99	0.095	0.056	0.05

Note: The F values shown here are from an ANOVA table that contains data of flux and selectivity for five different thicknesses. For each thickness, the flux and selectivity measurements were repeated four times.

surface roughness and hydrophobicity, may cause the small change in the selectivity. This can be further supported from the results shown in Fig. 4.8, where the selectivity changes moderately when the selective layer thickness is small, but becomes essentially constant when the thickness becomes sufficiently large. This last result is consistent with the S-D theory outlined in Section 4.2, where the composition (or concentration) ratio is independent of the selective layer thickness provided that the diffusivity and solubility coefficient remain unchanged.

The total flux shown in Fig. 4.7 was normalized with the driving force to calculate the permeance (Q) of the membrane using the following eq. [Huang, 1991],

$$J_i = Q_i\left(x_i\gamma_i p_i^o - y_i p_i^p\right) \tag{4.8}$$

where Ji is the flux of component *i,* x_i is the feed liquid molar fraction, γ_i: activity coefficient, p_i^o is the vapor pressure of component *i*, y_i is the molar fraction at permeate and p_i^p is the pressure at permeate side of component i. Fig. 4.11 shows the permeance plotted against reciprocal of thickness of the selective PVA layer that shows a straight line. The slope of the line indicates the permeability of the membrane and it increases at lower ethanol content in the feed, e.g., at 10 wt% Et in feed mixture the permeability is higher than the permeability at 40wt% Et. This behavior is expected since at low feed Et, membrane swells is more and gives less resistance to permeation.

Finally, the separation performance from this study were compared with the available literature [Nijhuis *et al.* 1991; Koops *et al.*, 1994] and presented in Table 4.5. Increase in flux and decrease in selectivity can be seen as the membranes thickness decreases irrespective of

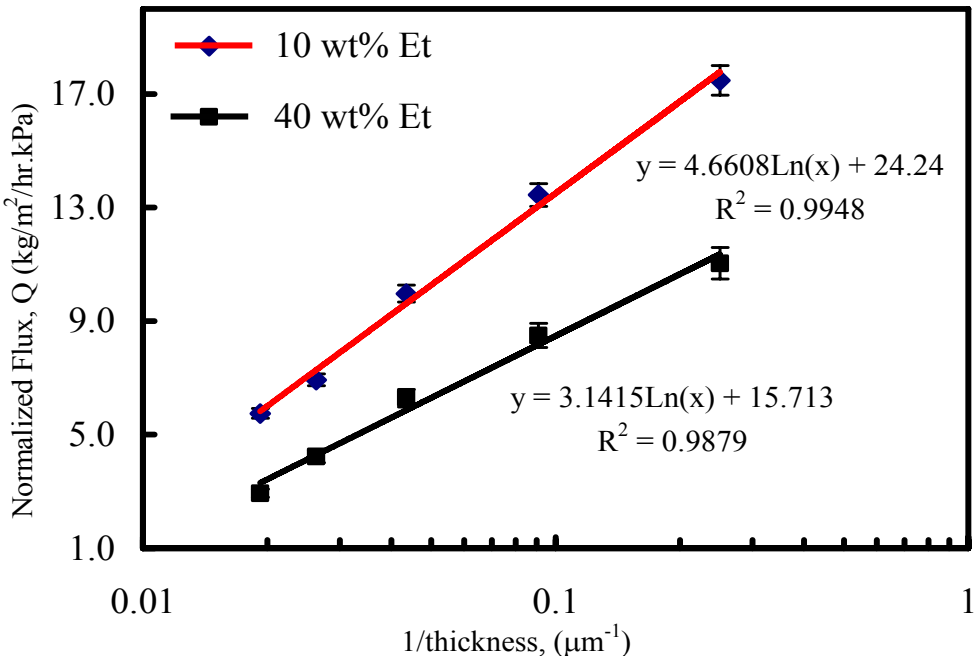

Figure 4.11: Permeance against reciprocal of thickness for 10 and 40wt% Et in mixtures.

different polymers, separation mixtures or temperatures. Results from Table 4.5 shows that the percentage change in selectivity is much less compared to the percentage change in flux. For homogeneous PVC membranes, with a decrease of thicknesses from 11 to 3 μm, Koops *et al.*(1994) found an increase of 371% in flux and a decrease of 50% in selectivity. They speculated the decrease in selectivity with respect to the crazes (cracks) in the membrane structure.On the other hand, Qunhui *et al.* (1995) found for homogeneous Chitosan membranes, with a decrease of thicknesses from 50 to 10 μm, the flux increased by 334% and selectivity decreased by 4%. They [Koops *et al.*, 1994] considered swelling effect to be the cause for the decrease in selectivity. From our study, we did not find any visible cracks in the membrane but results from Table 4.1 show that the swelling degree per unit thickness, SD_T of PVA4 membrane is about 10 times higher than that of PVA52. Also, in Table 4.2, results from contact angle experiments suggest a small change in hydrophobicity. Therefore, we believe that the change in selectivity can arise from several factors like hydrophobicity, swelling, degree of crosslinking etc… However the relative significance of the factors could not be determined in the present context of study.

Table 4.5 Comparison of dehydration performance for thickness from literature

Membrane (type)	Temp (^{O}C)	Type of mixture & concentration	PVA layer thickness (μm)	J (kg/m^2.hr)	α	Increase in flux (%)	Decrease in select. (%)	Ref.
PVA-PSf (flat sheet)	25	Et-water (85 wt% Et)	52	0.035	110.7	131	14	present work*
			4	0.081	95.1			
Chitosan (flat sheet)	25	Et-water (80 wt% Et)	50	0.183	7839	334	4	Qunhui *et al.* (1995)
			10	0.794	7543			
PVC (flat sheet)	80	Acetic acid-water (80 wt% AA)	11	0.034	481	347	50	Koops *et al.* (1994)
			3	0.152	237			

Note: The increase in flux and the decrease in selectivity were calculated with respect to the thicker membrane. PVC stands for poly(vinyl chloride).

4.9 Conclusions

PVA-PSf composite membranes were studied to determine the effect of selective layer thickness on the separation performance of Et-water mixtures. The thickness of the selective PVA layer was varied on the PSf support layer in the composite membrane. An increase in selective layer thickness markedly decreased the total flux and the water mass transfer coefficient. The decrease in flux is more prominent at low ethanol concentrations in the feed than at higher ethanol concentrations. Results agreed with the solution diffusion theory and the mass transfer resistance varies linearly with thickness. Analysis of the mass transfer resistance showed that the crosslinked membrane surface resistance is significant for thin membranes. Statistical analysis showed that the flux is significantly affected by the thickness of the PVA layer, but the selectivity is not. The selectivity was also shown to be affected by surface properties after crosslinking, especially when the membrane is thin. Physiochemical characterization for the composite membranes showed that the surface roughness and hydrophobicity change with PVA layer thickness. The flux was found to be affected more by thickness than by crosslinking and vice versa for the selectivity which is not affected by thickness.

CHAPTER 5

Chitosan-Poly(vinyl alcohol) blend membranes for Pervaporation Dehydration of Ethylene Glycol

5.1 Introduction

In pervaporation (PV) dehydration, extensive research efforts are given towards the development of membranes that yield both high permeability and selectivity [Huang, 1991; Oasada and Nakagawa, 1994]. For the dehydration of organic-water mixtures, hydrophilic polymers, such as poly(vinyl alcohol) (PVA), poly(vinyl chloride) (PVC) and chitosan (CS), have been used extensively to prepare the membranes [Huang, 1991; Chiang and Lin; 2002; Krumova *et al.*, 2000]. Very often membranes made from a single polymer suffer from the inherent drawback of trade-off between flux and selectivity [Shao and Huang, 2007; Smitha *et al.*, 2004]. For example, due to the hydrophilic nature of PVA, a low selectivity results when the PVA membranes experience excessive swelling, while having a higher flux [Finch, 1973; Krumova, 2000].

Over the years researchers have used many physical and chemical methods, such as crosslinking, grafting or blending, to modify polymer materials for membrane development in pervaporation [Chiang and Lin; 2002; Xiao *et al.*, 2006]. Of these methods, polymer blending proves to be an effective way to fabricate PV membranes with a number of desired properties [Yang *et al.*, 2004]. Successful blending can improve separation performance by altering polymer chain mobility through intermolecular interactions between polymers [Yang *et al.*, 2004; Rao *et al.*, 2007]. Chitosan, a natural polymer, with high hydrophilicity, good chemical resistance, biodegradability, and membrane-forming property, is commonly used to prepare hydrophilic blend membranes [Uragami and Takigawa, 1990; Lee, 1993; Ren and Jiang, 1998]. CS-PVA blend membranes have been reported to have good mechanical strength in addition to good membrane performance characteristics for biomedical applications and pervaporation separation [Lee *et al.*, 1992; Yang *et al.*, 2004; Ariyaskul *et al.*, 2006; Lu *et al.*, 2006]. Lu *et al.*(2006) found that the permeation flux was dramatically increased (while selectivity was increased only slightly) through blending CS with PVA for benzene/cyclohexane mixtures. The improved PV separation performance was reported by

different researchers over a wide range of CS compositions ranging from 10-80 wt% [Ariyaskul *et al.*, 2006; Lu *et al.*, 2006] in the blend. However, until recently separation results were not correlated to the physicochemical properties, such as crystallinity, melting points and hydrophilicity, of the blend membranes. There is much work in these detailed investigations to improve the membrane performance further by studying the effect of crystallinity on flux and selectivity.

Ethylene glycol (EG) is one of the major chemicals used in the polyester industry and as a non-volatile antifreezer in the aircraft industry. Purification and recycling of EG are often done with pervaporation dehydration [Feng and Huang, 1996]. However, there has been no study exploring the use of CS-PVA blend membranes for EG dehydration. This situation leads us to study of preparation of CS-PVA blend membranes for EG dehydration. In particular, we will investigate the effects of CS-PVA blending ratios and crosslinking with trimesoyl chloride (TMC). The CS-PVA blend membranes are prepared from PVA blended with varying amounts of CS using a solution casting method [Ariyaskul *et al.*, 2006]. The blend membranes were interfacially crosslinked with TMC. The physicochemical properties of the CS-PVA blend membrane samples were investigated by Attenuated Total Reflection-Fourier Transform Infrared Spectroscopy (ATR-FTIR), X-ray Diffraction (XRD), Differential Scanning Calorimetry (DSC), Scanning Electron Microscopy (SEM), Atomic Force Microscopy (AFM), tensile testing, contact angle and swelling measurements. The PV dehydration was performed on different ethylene glycol-water mixtures (in the feed) over 25 to 70^{O}C.

5.2 Experimental

5.2.1 Materials

Poly(vinyl alcohol) (99.7%, MW~133,000, PDI~1.3) was purchased from Fisher Scientific (ON, Canada). Chitosan flakes (Flonac-N, MW~100,000, 99% deacetylation degree) were obtained from Kyowa Technos (Chiba, Japan). Acetic acid (glacial, 99.6%), ethylene glycol (reagent, 99.5%) and sodium hydroxide (pellets, ACS reagent, ≥ 97.0 %) was purchased from Fisher Scientific (Ottawa, Canada). All other chemicals including hexane (ACS reagent, ≥98.5%, bp: 69^{O}C), trimesoyl chloride (TMC) (98%, mp: 34.5–36^{O}C, bp: 180^{O}C at 16 mmHg) were purchased from Sigma-Aldrich (Oakville, Canada). Deionized water

(18.2 MΩ cm) used for all experiments was produced by a Millipore Milli-Q system (MA, USA). All the solvents were used as received.

5.2.2 Membrane preparation

The polymer films were prepared by the solution casting method. The PVA solutions were prepared by dissolving 5wt% of the polymer in deionized water at 90^{O}C for 1 hr, stirring the solution until it was completely homogeneous. Chitosan solutions were prepared by dissolving chitosan in 1% aqueous acetic acid solution at room temperature with stirring. Both polymer solutions were filtered using sintered glass, degassed in a vacuum chamber and then carefully mixed at various weight ratios of CS to PVA, 25:75, 50:50, 70:30, 75:25, 80:20 (Table 5.1). The mixtures were stirred for 24 hrs to obtain homogeneous solutions.

The solutions were cast onto a horizontal glass plate with a retainer ring made of poly(vinyl chloride) (20 mm in height and 90 mm in diameter), which was adhered on the surface of the glass plate [Hyder *et al.*, 2008]. The cast solvents were then evaporated in a fumehood at 25^{O}C for 24 hours and the resulting membrane films were dried in a vacuum oven (at 40^{O}C) for 3 hr to remove traces of the solvents. The dried membranes were peeled off from the glass plates, and immersed into a sodium hydroxide aqueous solution (1 mol/L) for at least 24 h to neutralize trace of any acetic acid residues in the membranes. The membranes were then rinsed with deionized water several times. The obtained CS-PVA membranes were fully dried under ambient conditions and subsequently were kept in a desiccator ready for further treatments.

The air side of the CS-PVA blend membranes was crosslinked with a TMC/hexane [Xiao *et al.*, 2006] solution. 1 g TMC was dissolved in 200 ml hexane to obtain a 0.5 wt/v % TMC/hexane solution that was used for the crosslinking for 30 minutes. The crosslinked membranes were then washed several times with pure water and finally immersed in deionized water for 6 hours at 40^{O}C to eliminate residual solvents. The crosslinked membranes were dried in a vacuum oven (at 40^{O}C) overnight. The thicknesses of the CS-PVA blend membranes were measured by a micrometer screw gauge at five locations (center and four corners), and the mean thickness was calculated that ranged between 25-35 μm. Samples with air bubbles, nicks, tears or a mean thickness variation of greater than 5% were excluded. Table 5.1 shows the data of the different membranes prepared for this study. For example, CS-PVA1 is a crosslinked blend membrane with 75 wt% of PVA and 25 wt% of

CS in the blend. Uncrosslinked membranes will be referred to as (uc) and the crosslinked ones as (C).

5.2.3 Membrane Characterization

To quantify the chemical composition of a membrane film before and after the crosslinking, Attenuated Total Reflectance spectroscopy (ATR-FTIR) was employed. Samples of the membranes were dried, in vacuum at 85^{O}C overnight. Infrared spectra of the fresh and crosslinked membranes were obtained with a midrange (500-4000 cm^{-1}) Bruker Tensor 27 ATR-FTIR spectroscope (Milton, Canada). Measurements were repeated at least three times to ensure reproducibility.

A differential scanning calorimeter, DSC Q100 module (TA Instruments, Delaware, USA), was used to quantify the changes in polymer physical properties, e.g., the melting point before and after blending or crosslinking of the membranes. DSC thermographs were obtained from 0 to 350^{O}C at a heating rate of 10^{O}C/min where approximately 2.5 mg of the samples were used. The baseline corrections of the DSC thermographs were obtained by running an empty aluminum sample cell for all measurements.

The X-ray diffraction (XRD) patterns of the membrane samples were obtained with an Inel diffractometer (Paris, France) with monochromatized $CuK\alpha_1$ characteristic radiation (wavelength $\lambda = 0.154$ nm at 40 kV, 50 mA, and scan speed of 1^{O}/min, in a 2θ range of 5–40^{O}) at room temperature.

The blend film strength and strain were measured using an Instron 5548 (Instron Corporation, Norwood, MA, USA) micro tensile tester. All the thin film samples were cut to specificied dimensions and pulled/stretched until breakup. The tensile strength and strain were calculated from the elongated samples at breakup. All the measurements were performed at 25^{O}C.

The membrane structures were observed using a Scanning Electron Microscope (SEM) (LEO1530 FE-SEM, Zeiss/LEO, Oberkochen, Germany). The membrane samples were quenched and broken in liquid N_2 for cross-sectional imaging. All the samples were vacuum dried and gold coated before SEM imaging.

A commercial Atomic Force Microscope (AFM), Picoscan, (Molecular Imaging, Tempe, AZ, USA) was used to determine the topography of the blend membrane surfaces.

After image acquisition, surface roughness of the membrane was determined by the software in the AFM image processing toolbox.

To determine the hydrophilicity of the blend membranes, apparent contact angle measurements were conducted with static water sessile drops [Rosa and de Pinho, 1997] using the Axisymmetric Drop Shape Analysis Profile (ADSA-P) approach. All the contact angle measurements were repeated at least four times, and the results were averaged for each sample.

5.2.4 Swelling experiments

For swelling experiments, the crosslinked CS-PVA membranes were dried (at 40^{O}C under vacuum for 6 hr) and weighed. Different ethylene glycol-water (EG-water) mixtures, containing 10-100 wt% water, were used to immerse the samples for 48 hr at 25^{O}C. Constant weight experiments [Xiao *et al.*, 2006] were used to make sure that the swelled membranes had reached equilibrium. The swollen membranes were blotted carefully with tissue paper to remove any surface solution, and the weight of the swollen membranes was measured by a mass balance. The swelling degree was calculated using the following equation (5.1)

$$\text{Swelling degree } (\%) = \left(\frac{W_S - W_D}{W_D} \right) x\,100 \qquad (5.1)$$

where W_S is the mass of the swollen membrane (in g) and W_D is the mass of the dried membrane (in g).

5.2.5 Pervaporation

The separation experiment was conducted at room temperature on a lab scale pervaporation setup shown in Fig A.1 [Appendix A] for the dehydration of ethylene glycol-water mixtures. In the feed mixtures, EG (10 – 90 wt%) concentrations were varied. The total flux (J) and the selectivity (α) of the membrane were calculated from the collected permeate mass, using a spring balance and gas chromatograph [Feng and Huang, 1996; Ariyaskul *et al.*, 2006; Xiao *et al.*, 2006]. The permeate composition was analyzed using a Hewlett Packard 5890 Series II gas chromatograph with helium as the carrier gas with a flow rate of 20 ml/min. A 10 μl syringe was used to inject a fixed volume of liquid permeates. Each experiment was repeated four times under the same steady-state condition.

5.3 Results and discussion

The CS-PVA blend membranes were initially prepared from solution casting. At the step of crosslinking, the acyl chloride groups of TMC reacted with the hydroxyl (-OH) groups of PVA and the amino groups of CS to form poly(vinyl esters) and amide linkages between polymer chains. Hexane acted as the solvent for TMC and it facilitated TMC's diffusion in the CS-PVA structure. Initial separation performance of CS-PVA3 (C) (75 wt% CS, cf. Table 5.1) showed excellent flux and selectivity for the dehydration of EG-WATER mixtures. To improve the performance further with a change in polymer ratio of CS-PVA, we prepared two other blends CS-PVA4 (70 wt% CS) and CS-PVA5 (80wt% CS). The results of physicochemical characterization and separation performance of these blend membranes are listed in Table 5.1 and Table 5.2, and explained below.

Table 5.1 Physicochemical properties of the crosslinked (C) blend membranes

Membrane	Ratio of CS:PVA in blend (mass ratio)	Surface roughness Rq (nm)	Contact angle θ_{ap} (^{O})	Melting point (^{O}C)	Mechanical Properties at film breakup	
					Strength (MPa)	Strain (%)
*CS	100	48.5 ± 3.2	55.1 ± 2.4	335	65.1 ± 1.9	8.15 ± 0.9
*PVA	100	9.1 ± 1.1	58.9 ± 1.5	239	57.9 ± 2.1	11.2 ± 0.8
CS-PVA1	25:75	35.6 ± 2.5	55.8 ± 1.9	290	67.9 ± 2.8	11.5 ± 1.1
CS-PVA2	50:50	44.7 ± 0.9	60.4 ± 2.1	285	70.4 ± 2.5	10.1 ± 1.2
CS-PVA3	75:25	62.2 ± 3.6	68.1 ± 2.7	316	74.7 ± 2.1	8.3 ± 0.9
CS-PVA4	70:30	58.2 ± 2.8	65.2 ± 1.6	310	74.1 ± 2.3	8.5 ± 0.8
CS-PVA5	80:20	61.2 ± 3.1	68.9 ± 2.3	318	74.5± 2.7	8.2 ± 0.9

Note: Blended film thicknesses were 30 ± 5 μm. Picoscan® AFM software was used to calculate the root mean square surface roughness.

* Properties of homogeneous CS and PVA membranes data were measured as a control.

5.3.1 Infrared spectroscopy: TMC crosslinking

It is well known that crosslinking of the polymer chains restricts their mobility and reduces the swelling of the polymer matrix. A schematic of structures and reaction mechanisms of CS-PVA blend with the crosslinker, TMC/hexane solution, is shown in Fig. 5.1. The

hydroxyl group (-OH) of PVA and the amino group (-NH_2) of CS react with TMC to form benzoate esters. Crosslinking can also occur between TMC and hydroxyl (-OH) groups of CS, but the reaction is slower than that with the amino (-NH_2) groups [Xiao *et al.*, 2006].

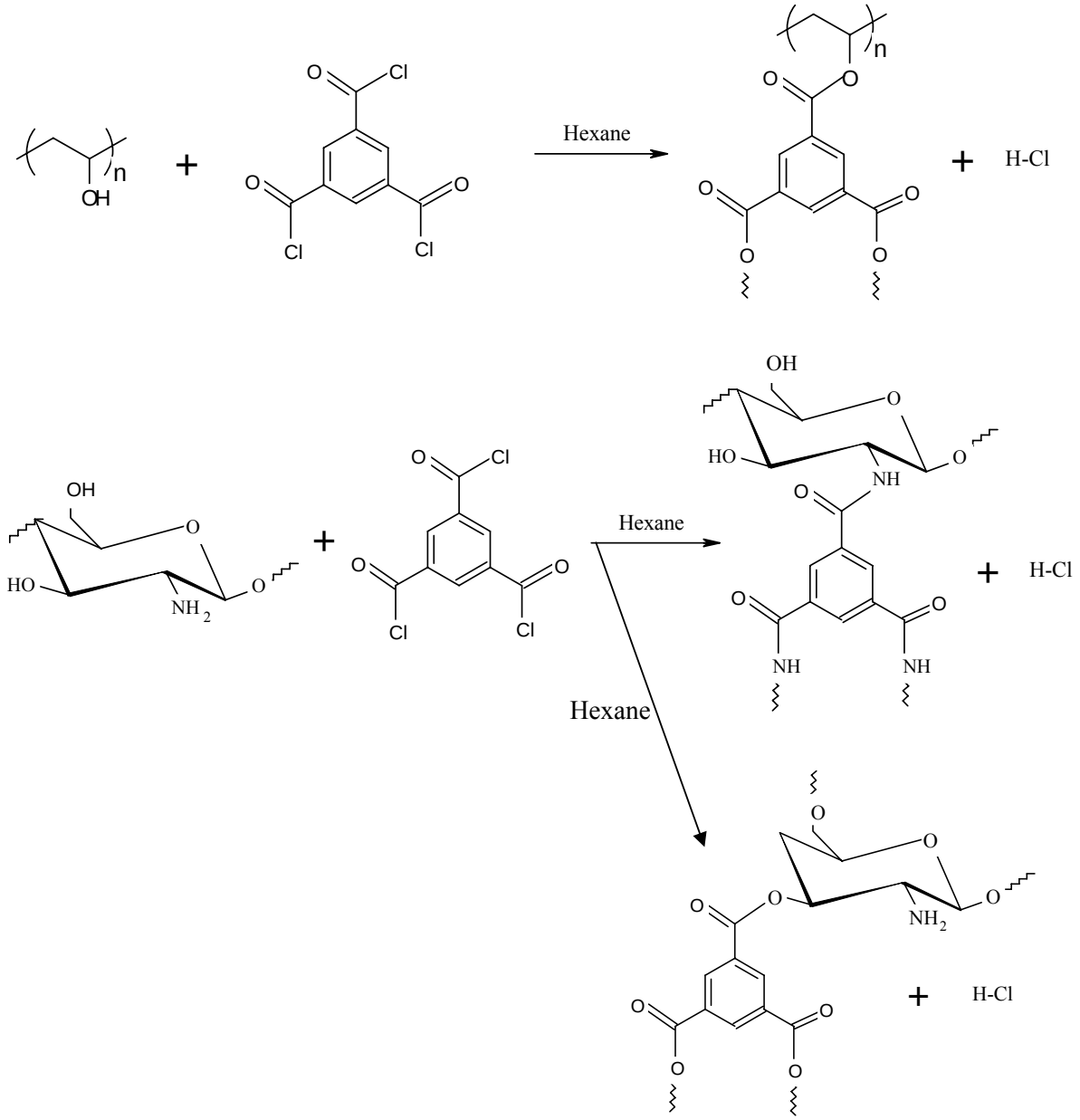

Figure 5.1: Crosslinking reaction with PVA and CS in TMC/hexane solution

In Fig. 5.2 (a), ATR-FTIR spectra of uncrosslinked CS-PVA blend membranes are shown. As controls, spectra of homogeneous CS and PVA membranes are also shown in Fig 5.2(a).

For the homogeneous PVA spectrum, the absorption peak at 3300 cm^{-1} relates to intermolecular hydrogen bonding and -OH stretch vibration [Smirnov, 1967].

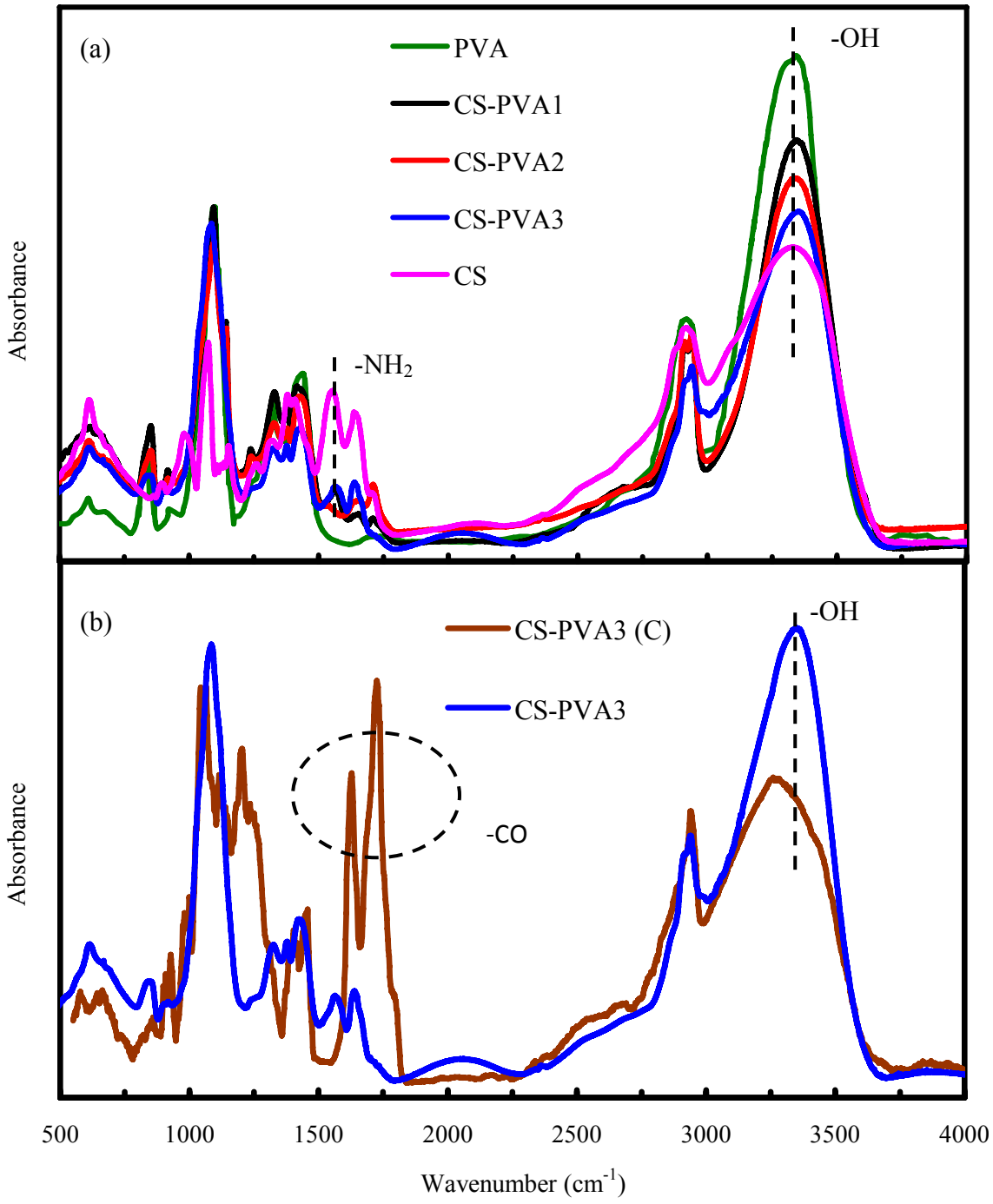

Figure 5.2: ATR-FTIR spectra of (a) uncrosslinked and (b) crosslinked CS-PVA3 blend membrane at 25 ^{O}C.

Absorption corresponding to asymmetrical stretching and symmetrical stretching vibration of $–CH_2$ occurs between 2898-2935 cm^{-1} [Hind *et al.*, 2001; Almeida *et al.*, 2002].

For the homogeneous CS spectrum, absorption shows a peak at 1560 cm^{-1} for $–NH_2$ and a broad peak at about 3200-3300 cm^{-1} for –OH stretch vibration. CS-PVA blend membranes show peaks that come from both CS and PVA, e.g., CS-PVA3 showing a major wide peak around ~ 3300 cm^{-1} corresponding to the –OH groups in CS and PVA and a small peak at 1560 cm^{-1} from the $–NH_2$ groups of CS [Yang *et al.*, 2004]. At lower CS (wt%) contents in the blend, weak absorption peaks around 1530-1620 cm^{-1} for the $–NH_2$ and –C=0 groups can be observed.

Figure 5.2(b) shows the spectra of TMC crosslinked and uncrosslinked CS-PVA3 blend membranes. The two show great differences at 3300 cm^{-1}, and in regions of 1500–1800 and 1200–1500 cm^{-1}. For CS-PVA3 (C), the -C-O absorption band of benzoate esters appears in the region of 1715–1730 cm^{-1}, where the peak at 1719 cm^{-1} can be identified to be -C-O in trimesoyl ester groups [Xiao *et al.*, 2006]. The crosslinked CSPVA3 (C), shows a decreased peak intensity at 3300 cm^{-1}, compared to the uncrosslinked sample. This indicates that the number of the hydroxyl groups decreased after crosslinking [Ahmad and Ooi, 2005; Xiao *et al.*, 2006].

5.3.2 Differential scanning calorimetry: thermal behavior

The change in the physical properties of the blend membranes can be observed in the glass-transition temperature (T_g) and melting point (T_m) [Gilman *et al.*, 1994; McNeil, 1997]. In Fig. 5.3 (a), differential scanning calorimetry (DSC) thermograms of uncrosslinked blend membranes are presented together with those of the component polymers, CS and PVA. The uncrosslinked blend membranes CS-PVA1, CS-PVA2, CS-PVA3, CS-PVA4 and CS-PVA5 show melting transitions (lowest peaks) at 298, 273, 298, 304 and 310^{O}C, respectively. An increase in the melting transition temperature from 298^{O}C to 310^{O}C with increasing CS content in the blend suggests good blend compatibility at these compositions (CS 70-80 wt%). In Fig. 5.3(b), the melting point is shown to increase to 316^{O}C after crosslinking CS-PVA3 (C) with TMC. Complete results of the blend membrane melting points are presented in Table 5.1. The glass transition (T_g) temperature could not be determined from the DSC thermograms of the crosslinked blended membranes and therefore not reported.

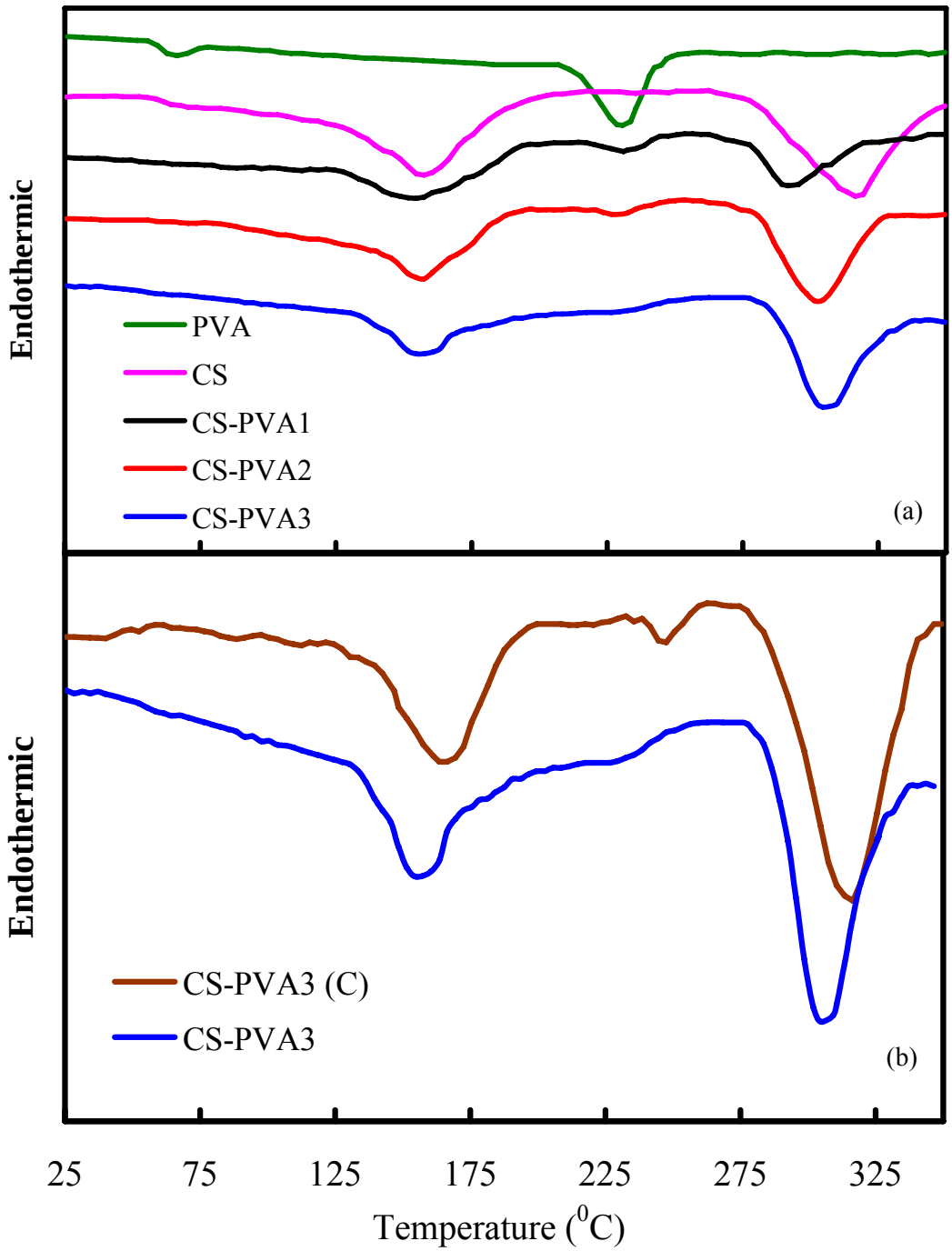

Figure 5.3: DSC thermograms of (a) uncrosslinked and (b) crosslinked CS-PVA3(C) blended membranes.

5.3.3 X-ray diffraction: crystallinity

If there were no or weak interaction between CS and PVA molecules in the blend membrane, each component would show its own crystallinity in the blend and X-ray diffraction (XRD) patterns would express a simple addition of patterns of CS and PVA, with the same ratio as

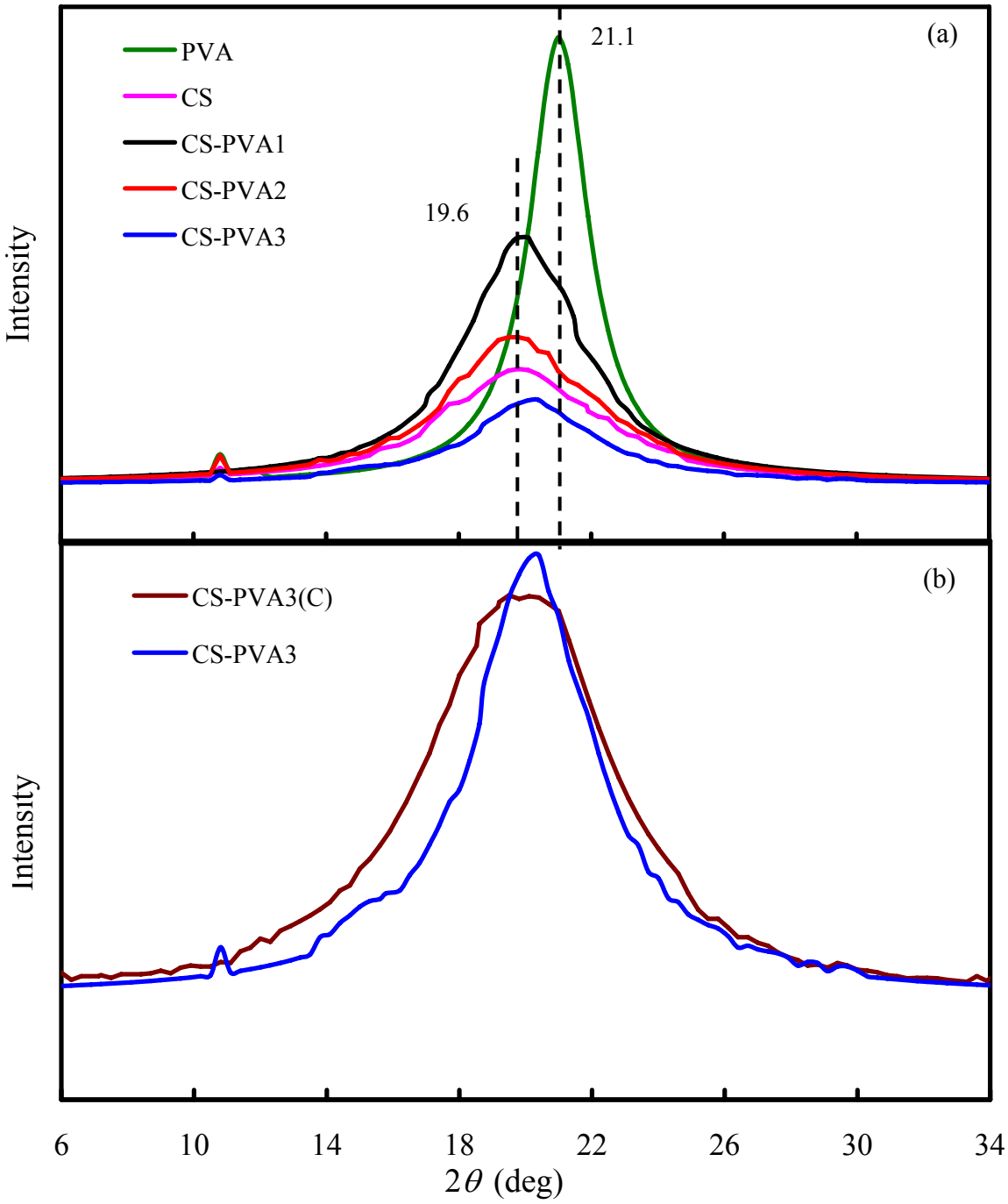

Figure 5.4: XRD spectra of (a) uncrosslinked and (b) crosslinked CSPVA3(C) blended membranes.

that for blending [Zhou *et al.*, 2008]. Figure 5.4(a) presents XRD patterns of uncrosslinked CS-PVA blend membranes along with component CS and PVA membranes. The diffraction scan of the CS sample shows only one peak at $2\theta = 19.6^{O}$. For the PVA sample, there are two peaks at $2\theta = 10.7^{O}$ and 21.1^{O} [Zhou *et al.*, 2008]. Compared to CS, PVA is more crystalline.

In the PVA membrane, the high crystallinity was mainly caused by the intramolecular hydrogen bonding [Lu *et al.*, 2006]. The peak at $2\theta = 10.7^{O}$ of PVA almost disappears in the blends with incorporation of CS at 70-80 wt%. This indicates that strong interaction occurred between CS and PVA in the blend membranes at 70-80 wt% of CS. From Fig. 5.4(a), compared to the CS or PVA membrane, blend membranes show a relatively obtuse and broad peak around 19.6^{O}, indicating a decrease in crystallinity of the blends. With an increase in CS content in the blends, the crystallinity peak decreases, since CS is less crystalline than PVA because of the presence of bulky acetyl structure. Figure 5.4(b) shows the x-ray spectra of CS-PVA3 blend before and after crosslinking. Since the CS molecules are bigger than the PVA molecules, the blending of PVA inside the CS network can make the structure less compact. This also resulted in the decrease in crystallinity after blending. After the crosslinking of CS-PVA blends with TMC, a small decrease and broadening of intensity peak occurs (in Fig. 5.4 (b)) due to the decrease in intramolecular hydrogen bonding in PVA and increase in intermolecular hydrogen bonding between CS and PVA.

5.3.4 Mechanical test: strength and strain

A successful blending should lead to intermolecular interaction between two component polymers, thereby improving mechanical strength of the blend. Mechanical testing gives an indication of the strength and elasticity of polymer films [Kim *et al.*, 1992; Biesheuvel and Verweij 1999]. In Table 5.1, the stress and strain at breakup of blend membrane samples are presented. From Fig 5, blending improves strength that increases with increasing CS content up to 75wt%, but the strain decreases correspondingly. CS-PVA3 shows a breakup strength of 69 MPa and strain of 11 (%), compared to 57 MPa and 9 (%) for CS and 49 MPa and 15 (%) for PVA. CS shows a less elongation-at-break than PVA, implying that an increase in CS content in the blend will decrease the flexibility of the films. Due to the interaction between -OH and $-NH_2$ groups of the two polymers, blending improves the mechanical strength of the film [Kim *et al.*, 1992]. Crosslinking the blend membrane with TMC shows a higher strength but lower strain at breaking. The increase in strength and decrease in strain at breakup for the blends suggest a good blending of the component polymers. From Table 5.1, after crosslinking, the strength of blend membranes increases from 67.9 MPa to 70.4 MPa and 74.7 MPa for 25, 50 and 75 wt% CS in blend, respectively.

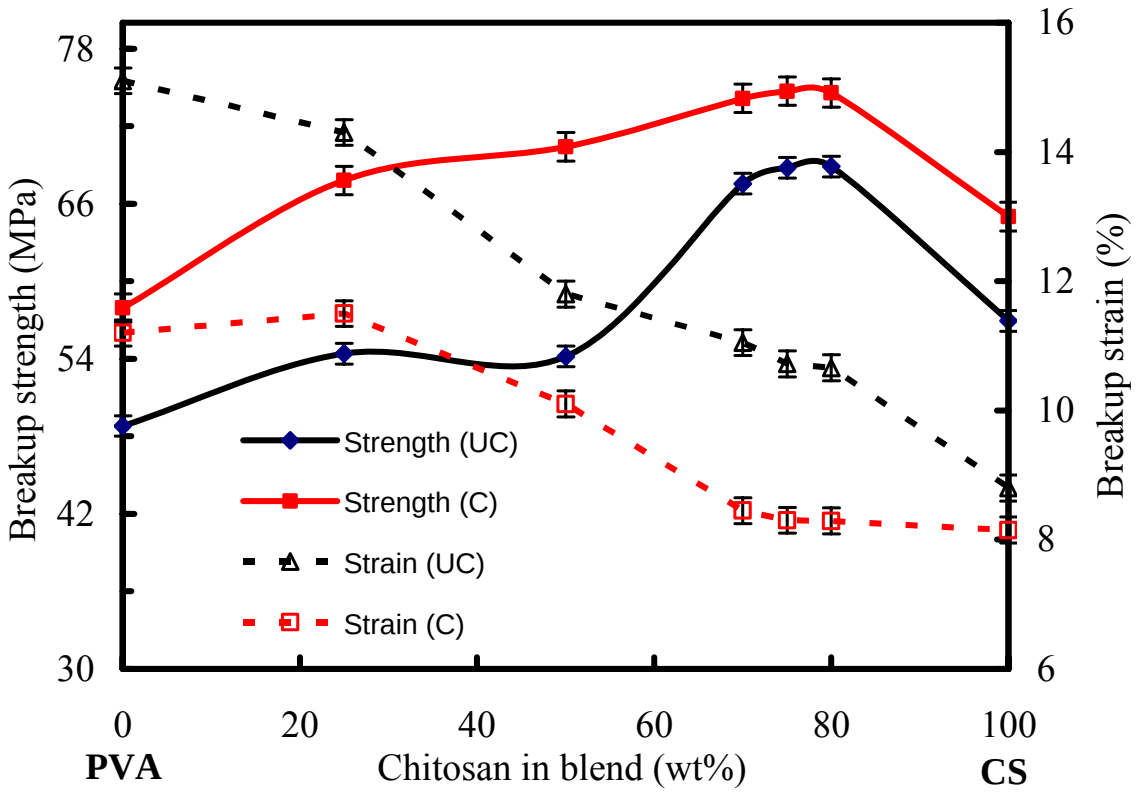

Figure 5.5: Tensile strength and strain at breakup against chitosan amount in blend membranes (wt%).

5.3.5 Microscopy: microstructure and surface roughness

In Fig. 5.6 (a), the cross sectional structure of CS-PVA1(C) blended membrane is shown. From SEM images, the blending of the two polymers, CS and PVA, appears to be uniform and homogeneous (free of any separating layers/interfaces) and free of large pores. In order to characterize the membrane surface properties, we employed Atomic Force Microscopy techniques.

In Fig. 5.6 (b) and (c), 3D AFM images of the surfaces of the crosslinked blend membranes are shown over an area of 6 × 6 μm^2. These 3D surface images show the blend membranes are rough on the nanometer scale. Table 5.1 shows the root-mean-square (RMS) roughness, Rq, obtained from the AFM image analysis [Dietz *et al.*, 1992; Bessières *et al.*, 1996]. Compared to PVA, CS surface is rougher, e.g., PVA shows a surface roughness of 9 nm, where it equals 48 nm for CS. From Table 5.1, the surface roughness was found to increase with CS content in the blend, e.g., CS-PVA1(C) showing a roughness of 36 nm while CSPVA3 (C) showing a roughness of 62 nm. Interestingly, the surface roughness

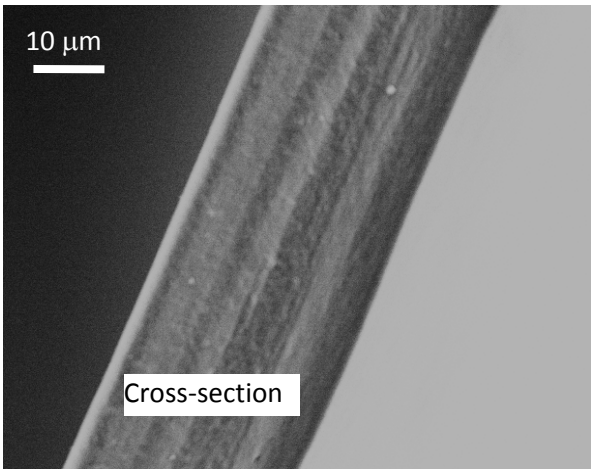

(a) CS-PVA1 (C)

SEM Cross-section

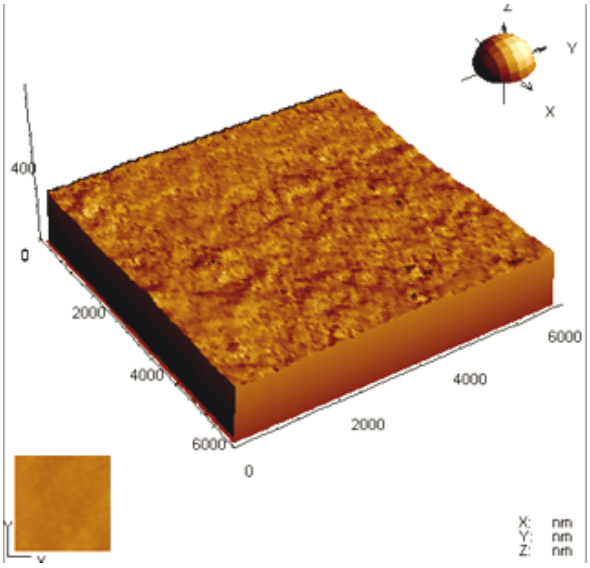

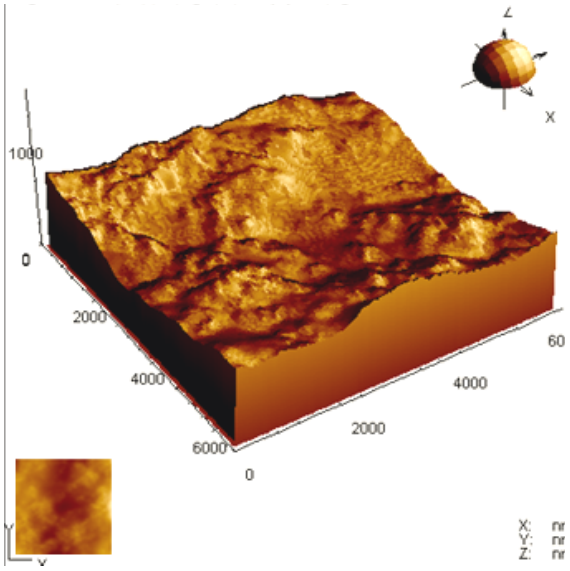

(b) CS-PVA1 (C)

(c) CS-PVA3 (C)

AFM topography of crosslinked

Figure 5.6: Microscopic images of the crosslinked blend membranes SEM cross-sections (a) CS-PVA1 (c), and AFM topography (b) CS-PVA1 (C) and (c) CS-PVA3 (C)

reaches a maximum and remains constant once the CS content is ~ 70wt% in the blend as can be seen in Table 5.1.

5.3.6 Contact angle measurement: surface hydrophobicity

Results from the contact angle experiments of the crosslinked membranes are presented in Table 5.1. Surface hydrophobicity of the blend membranes was quantified by the apparent

static contact angle (θ_{ap}) of a water sessile drop at 25^{O}C [Zhang and Hallstorm, 1990; Rosa and de Pinho, 1997]. An uncrosslinked CS-PVA3 blend membrane shows a contact angle of 24.3^{O}, but quickly absorbs water inside the membrane film. Crosslinking of the CS-PVA blend membrane increases the contact angle, making it less hydrophilic. The contact angle increases with CS content in the blend. A higher contact angle of 68^{O} was observed for CS-PVA3 (C), compared to 60^{O} for CS-PVA2 (C). The increase in the apparent contact angle may also be related to the increase in surface roughness (Table 5.1) [Chapter 2].

5.3.7 Swelling characteristics

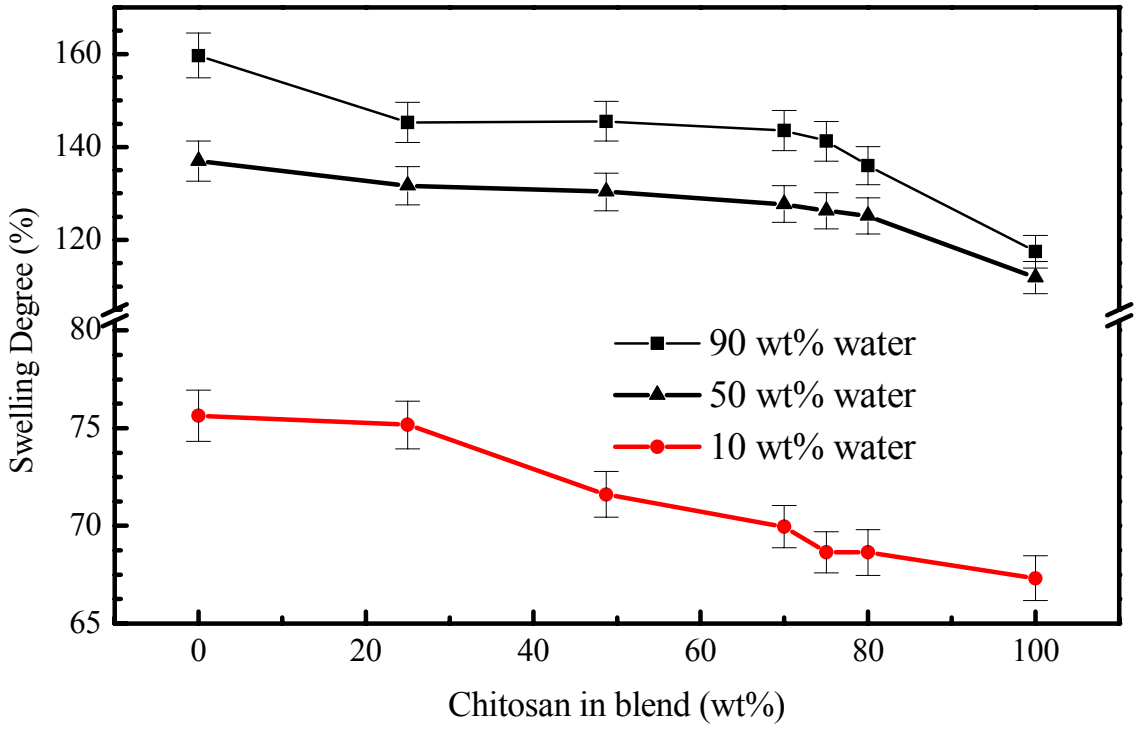

Figure 5.7: Swelling degree at different water concentrations of EG-water mixtures for crosslinked membranes against CS amount in blends (wt%).

Swelling behavior of the membrane depends on the structure and composition of the polymer membrane. In Fig. 5.7, the swelling degree is plotted against the CS content (wt%) in the crosslinked blend membrane for different feed mixtures (10-90wt% water in EG-water mixtures). From Fig 5.7, the SD increases with increasing amount of water over the whole composition scale. Also, the higher the CS (wt%), the lower the swelling. The blend membranes exhibited a higher swelling degree than the CS membrane, possibly as a result of many hydrophilic -OH groups of PVA. Higher swelling is an indication of a more flexible

membrane structure, possibly leading to a higher total flux [Uragami *et al.*, 1994; Xiao *et al.*, 2006; Ariyaskul *et al.*, 2006].

5.4 Dehydration performance: flux and selectivity

Dehydration experiments were performed with the TMC crosslinked CS-PVA blend membranes for different mixtures of ethylene glycol-water (EG-water) at different feed temperatures. As a control, separation results of crosslinked CS and PVA membranes were reported as well.

Table 5.2 Comparison of separation performance of the blended membranes

Membranes	Swelling Degree (SD) (g/g) x100	Separation performance			
		(10wt% water in feed)		(50wt% water in feed)	
		Total flux, J ($kg/m^2/hr$)	Selectivity, α	Total flux, J ($kg/m^2/hr$)	Selectivity, α
*CS	67.32 ± 1.14	0.09	575	0.41	24.8
*PVA	75.64 ± 1.31	0.12	354	0.40	28.4
CS-PVA1	75.17 ± 1.22	0.11	594	0.39	40.7
CS-PVA2	71.61 ± 1.16	0.12	659	0.43	41.8
CS-PVA3	68.64 ± 1.06	0.11	986	0.44	44.2
CS-PVA4	69.96 ± 1.09	0.13	807	0.46	42.1
CS-PVA5	68.64 ± 1.05	0.14	885	0.43	40.2

Note: The separation experiments were performed at 25^OC (± 2^OC). The average error in flux measurement is ± 3.8% and in selectivity is ± 7.5% . All the membranes were crosslinked with trimesoyl chloride (TMC). Swelling results presented here are for 50 wt% water in EG-water mixtures at 25^OC.

5.4.1 Effect of feed concentration

Figure 5.8 shows the total flux and selectivity of the blend membranes against the feed water concentration at 25^OC. Total flux increases while the selectivity decreases with increasing water concentration in the feed. As can be seen, with an increase in feed water concentration (around 20 wt%), selectivity decreased drastically with a small increase in flux. Although the blend membranes are crosslinked, at high water concentrations, swelling occurs to some

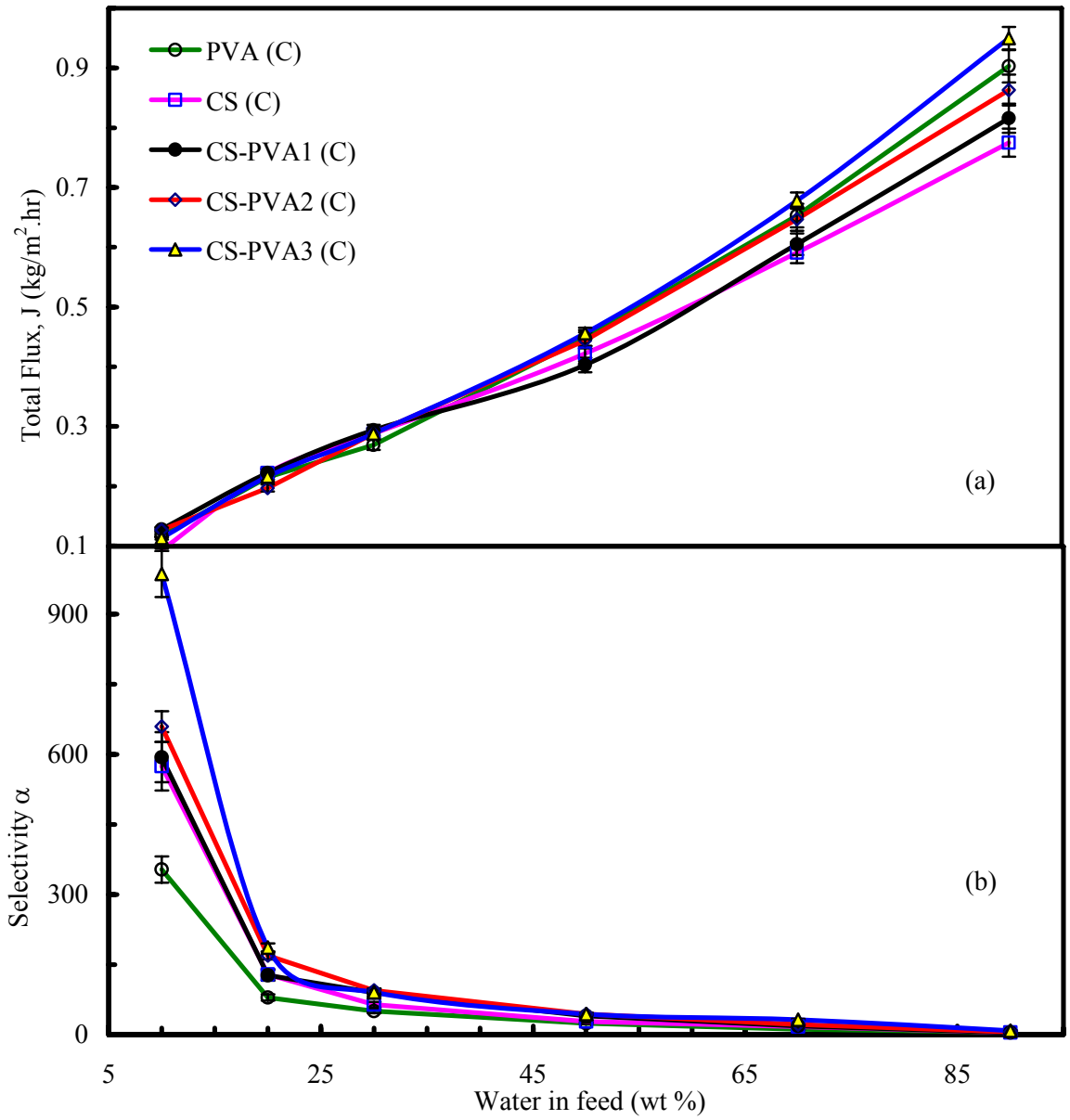

Figure 5.8: (a) Total flux and (b) selectivity of the crosslinked blend membranes at 25^{O}C for 10-90 wt% feed water mixtures. The data for homogeneous PVA and CS membranes are presented as a control.

extent, thereby enhancing total flux. At higher concentrations of water in the feed mixture, the membranes swelled to a greater extent, so that polymeric chains are more flexible to favor transport of a large number of water molecules, as well as some ethylene glycol molecules. Separation results for the blend membranes are presented in Table 5.2. It is interesting to note that the selectivity of the blend membrane is much higher than that of the

homogeneous membranes, highest selectivity of 986 for CS-PVA3 (C) membrane, compared to 354 for PVA and 575 for CS at 10wt% water in the feed EG-water mixture.

5.4.2 Effect of feed temperature

Table 5.3 Activation energies of water and EG for 10wt% feed water mixtures.

Membranes	Activation Energy (kJ/mol)		
	Water $E_{P,W}$	Ethylene Glycol, $E_{P,EG}$	$\Delta Ep = E_{P,W} - E_{P,EG}$
CS-PVA1	8.4	14.6	- 6.2
CS-PVA2	7.9	11.4	-3.5
CS-PVA3	6.3	5.5	0.8
CS-PVA4	7.7	9.1	-1.4
CS-PVA5	6	4.3	1.7

Note: The polymer ratio in the blend is 75:25, 70:30 and 80:20 for CS-PVA3, CS-PVA4 and CS-PVA5, respectively, see Table 5.1.

To investigate the effect of operating temperature on blend membrane performance, PV dehydration experiments were performed for 25^{O}C to 70^{O}C. As the temperature increases, polymer chain can move more freely and the free volume in the membrane increases. And at a high temperature, diffusing species would have greater kinetic energies, resulting in an increase in permeation. In Fig. 5.9 (a), the total flux and selectivity results are presented against temperature for CS-PVA3 (C). As temperature rises, the flux increases almost continuously (0.11 to 0.46 kg/m^2/h), and the selectivity decreases (986 to 663). Generally, temperature affects permeation on two aspects: one is the driving force, and the other the membrane permeance [Baker, 2004]. A semi-log plot of water permeance versus reciprocal of temperature (1/T) at various feed water concentrations has been shown in Fig. 9 (b) for CS-PVA3 (C). A logarithmic temperature dependence was observed. Researchers have reported Arrhenius behavior for the membrane permeance in the form [Huang, 1991],

$$Q_i = A_O \exp\left(-\frac{E_{pi}}{RT}\right) \tag{5.2}$$

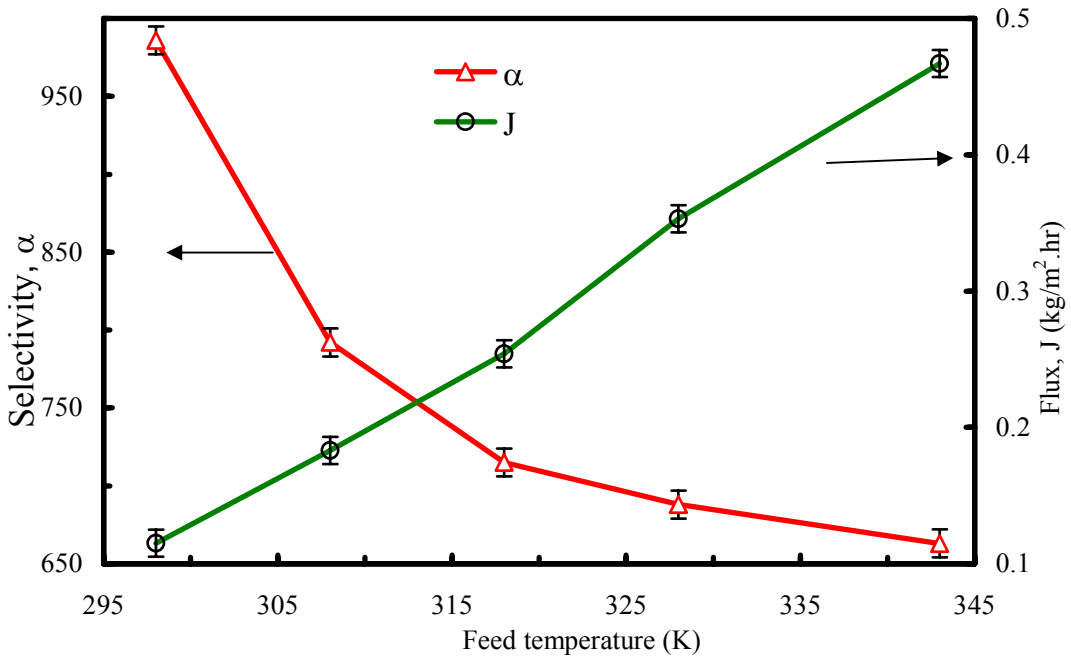

Figure 5.9: (a) Total flux and selectivity against feed temperature (K) for the CS-PVA3 (C) blend membrane at 10wt% water in the feed mixture.

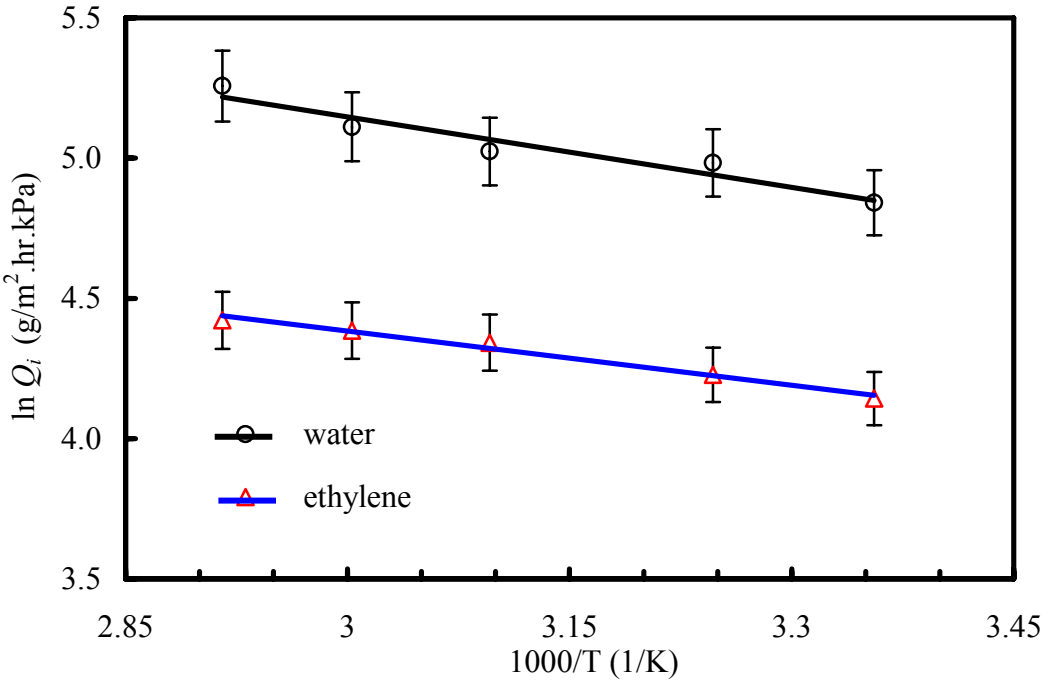

Figure 5.9: (b) Arrhenius plot of permeance against 1/T for water and EG.

where Q_i is the permeance of component i, A_O is a constant, Ep_i is the activation energy of permeating component i, and T is the absolute temperature. From Fig 5.9 (b), the activation energy for permeation through the polymer matrix was calculated from the slope of the best-fit lines and presented in Table 5.3. It can be seen from Fig. 5.9 (b) as temperature rises,

water and EG permeance, both increases. A higher slope (activation energy) usually implies that the diffusion of the water molecules is more restricted. An increase in temperature increases the saturated vapor pressure of the permeant, resulting in an increase in the driving force for mass transport through the membrane. As can bee seen in Table 5.3, the activation energy of permeation for EG ($E_{p,EG}$) tends to be higher than that of water ($E_{p,W}$), especially in the blend membranes with a lower CS content (25-70 wt%). Also, in Table 5.3, the difference between the activation energy (ΔE_P) of water and EG increases as CS (wt%) amount increases. As a result, the decrease of CS content in the membrane could reduce the permeability of water through the membrane.

5.4.3 Effect of feed flow-rate

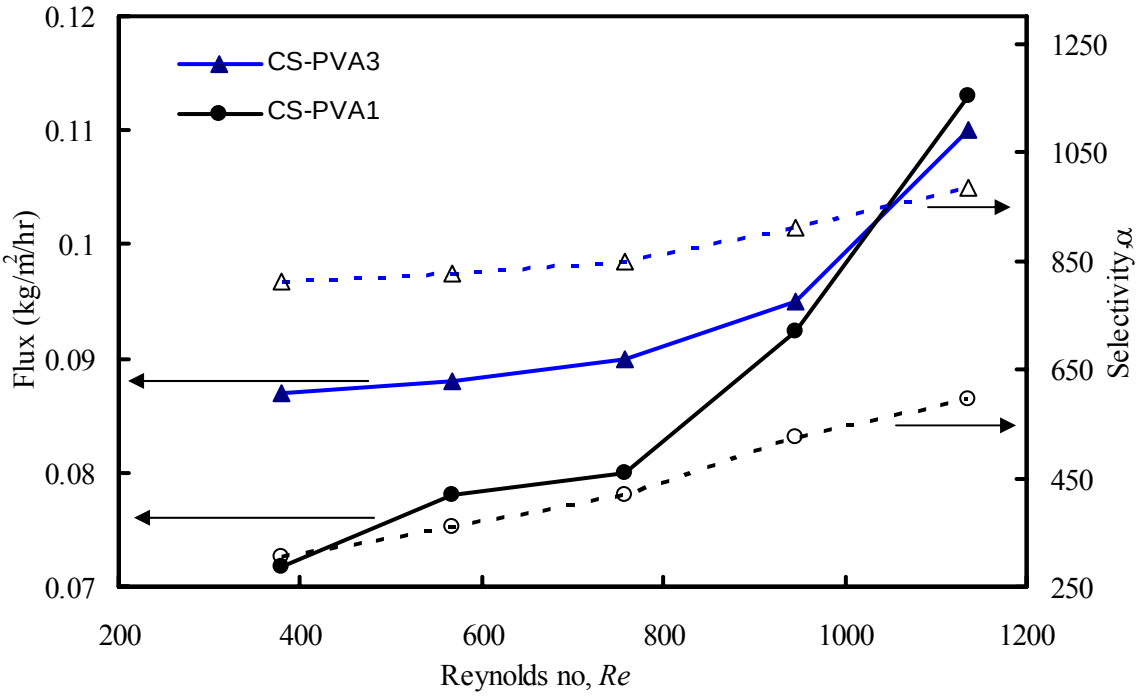

Figure 5.10: Effects of feed flow-rate (Reynolds number) on pervaporation performance of blended membranes for 10 wt.% water in feed at 25^{O}C (feed flow rate changing from 40 to 120 L/h) at 25^{O}C.

The effects of feed flow-rate on the pervaporation performance of 10 wt% water in the feed mixture for CS-PVA1 and CS-PVA3 membranes are shown in Fig. 5.10, against the Reynolds number [Appendix C]. It can be seen from Fig. 5.10, the permeation flux and the selectivity increases slightly with increasing feed flow-rate. At low Reynolds number (flow-rate), the viscous feed EG-water mixture would be prone to concentration polarization effect

that affects flux and selectivity [Feng and Huang, 1996]. The concentration polarization index (CPI) *X*s/*X*f was calculated according to Eq. (C-2) [Appendix C]. From Table 5.5, the lower CPI value of the CS-PVA1 membrane indicates that concentration polarization might have affected the permeation slightly compared to the CS-PVA3 membrane.

5.4 Effect of feed flow-rate on concentration polarization [Appendix C]

Membrane	Alcohol in mixtures (wt%)	Flow-rate (L/hr)	Parameters	
			Reynolds no, *Re*	X_s/X_f
CS-PVA1	Ethylene glycol 90 wt%	40	379	0.898
		80	757	0.927
		120	1135	0.945
CS-PVA3		40	379	0.937
		80	757	0.954
		120	1135	0.963

5.4.4 Effect of CS amount (wt%) in the blend

Comparing the separation results presented in Table 5.2, for 10wt% water in the feed mixture, CS-PVA3 (C) shows highest selectivity of 986 with a total flux of 0.11 kg/m^2/hr. Similar results of high flux and selectivity were observed for CS-PVA4 and CS-PVA5 membranes. In Fig. 5.11 (a) and (b), the total flux and selectivity are plotted against the chitosan amount (wt%) in the blend membrane at two different feed water concentrations. On the horizontal axis, at 0 wt% CS means the PVA membrane and at 100% CS means the CS membrane. In Fig 5.11 (a), with increasing CS, the total flux increases gradually (compared to PVA, CS- PVA1 and CS-PVA2 blend) reaching a maximum around 70-80 wt% CS. The highest total flux (0.96 kg/m^2/hr for 90% water in feed mixtures, Fig. 5.8 (a)) was obtained around 75 wt% CS at 25 ^{O}C. From Fig 5.11 (b), the blend membranes displayed higher selectivity over the whole range of CS (25 to 80wt%) than CS and PVA membranes. Selectivity reaches a maximum at ~75 wt% CS in the blend, as shown by the dotted lines in Fig 5.11. Since amount of CS in the CS-PVA blend affects crystallinity more than crosslinking, an optimum degree of amorphous/crystallinity is achieved around 70-80 wt% CS in the blend that gives high flux and selectivity simultaneously.

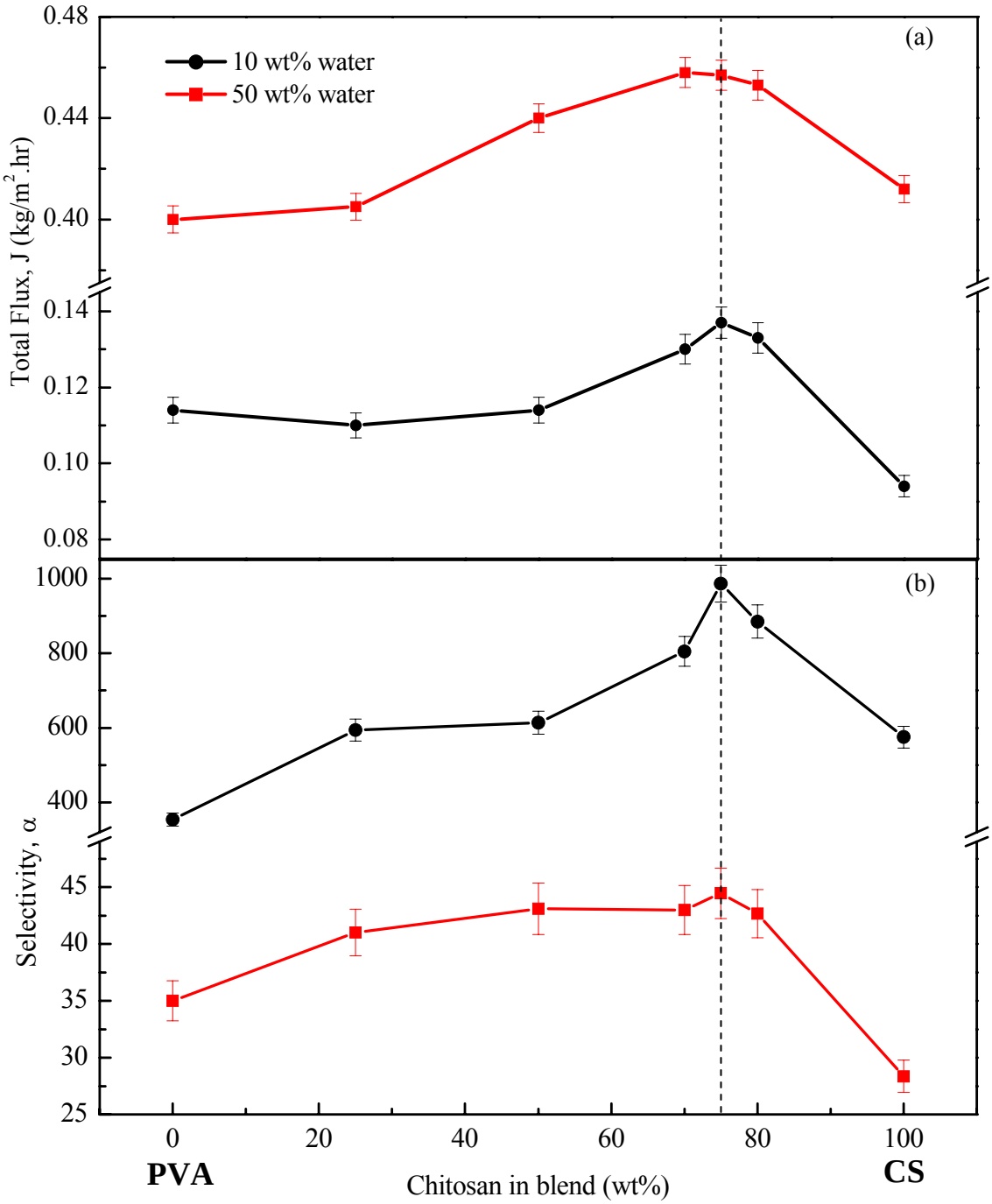

Figure 5.11: (a) Total flux and (b) selectivity against chitosan amount in the blend membranes (wt%) for two different feed water mixtures at 25^{O}C.

5.5 Comparison of results with literature

Table 5.5 Comparison of separation performance with the literature

Membranes (type)	Temp (^{O}C)	Type of mixture & (concentration of organics)	Film thickness (μm)	J (kg/m^2.hr)	α	References
PVA (Homogeneous)	70	EG-Water (80%)	15	0.21	933	Wu *et al.*(1994)
CS-PSf (Composite)	35	EG-Water (90%)	4	0.3	103	Feng and Huang (1996)
CS-PVA (Blend)	30	IPA-Water (90%)	40	0.13	17,991	Rao *et al.* (2007)
CS-PVA (Blend)	60	Et-Water (90%)	100	0.4	450	Lee *et al.* (1992)
CS-PVA (Blend)	60	IPA-Water (90%)	20	0.64	>10000	Ariyaskul *et al* (2006)
CS-PVA3 (Blend)	70	EG-Water (90%)	34	0.46	663	This study*

In Table 5.5, we have summarized previous studies relevant to this study for separation performance. All these polymeric membranes differ from each other in membrane preparation (casting, phase inversion), crosslinking solution, module type (flat or hollow fiber), separation temperature, type and concentration of feed mixtures. We could not find any literature that studied the exactly same blend membrane separation for EG-water mixtures. From Table 5.4, blend membranes showed better separation performance than component membranes at high temperatures. Rao *et al.* (2007) and Ariyaskul *et al.* (2006) have studied CS-PVA blend membranes for isopropanol-water dehydration and obtained excellent total flux and selectivity. For dehydration of EG-water mixtures researchers have been using crosslinked PVA or CS membranes, showing good flux but somewhat poor selectivity. In this study, we prepared a series of blend membranes with varying CS (25-80 wt%) and found the blend membranes containing 70-80 wt% CS give improved separation results. Compared with the literature in Table 5.5, the CS-PVA3 blend membrane shows

excellent total flux (0.46 kg/m^2/h) and selectivity (663) with a feed solution of 90wt% EG. Compared to the results of Wu *et al.* (1994) and Feng *et al.* (1996) using crosslinked CS and PVA membranes, the CS-PVA3 blend membrane shows a better flux (0.46 kg/m^2/hr) even with a relatively thicker membrane. It should be noted that, the separation performance for CS-PVA3 (C) decreases once the amount of water in the feed exceeds 20% as seen from Fig. 5.8.

5.6 Conclusions

Effects of CS content (wt%) on the separation performance of CS-PVA blend membranes were studied for ethylene glycol dehydration. The blend membranes were prepared with solution casting of PVA and different amounts of chitosan (25, 50, 70, 75, 80 wt%). Trimesoyl chloride was used to crosslink the blend membranes. Good blend compatibility was confirmed by DSC and XRD, whereas successful crosslinking was confirmed by ATR-FTIR. Tensile test results showed improved blend membrane strength at breakup. Contact angle results confirmed the decrease in hydrophilicity after crosslinking. Pervaporation dehydration results show high flux and selectivity of the blend membranes, especially when the chitosan amount is between 70-80 wt%. At 25 ^{O}C, for 10wt% EG in feed, the blend membrane containing 75wt% chitosan showed good permeation flux and improved selectivity at 0.11 kg/m^2/hr and 986, respectively. With increasing temperature, the total flux increased markedly without a significant drop in selectivity. However, the selectivity was found to decrease markedly when the feed water concentration was above 20wt%. The high CPI index of CS-PVA3 membrane suggests that membranes with higher surface roughness could help lower the concentration polarization on the feed side. Comparing the results with the literature, we believe CS-PVA blend membranes of 70-80 wt% CS would be an excellent candidate for high temperature industrial PV dehydration.

CHAPTER 6

Composite Poly(vinyl alcohol)-Poly(sulfone) Membranes crosslinked by Trimesoyl Chloride: Characterization and Dehydration of Ethylene Glycol

6.1 Introduction

Polymeric membrane pervaporation (PV) finds many applications in the fields of dehydration of organic mixtures, water treatment and organic-organic separation [Mulder *et al.*, 1985; Oasada and Nakagawa, 1992;]. The most successful pervaporation application is the dehydration of aqueous-organic mixtures. Significant research efforts are made on using different membrane materials for dehydration of isopropanol, acetone, tetrahydrofuran, ethylene glycol and methylene chloride [Binning *et al.*, 1965; Huang, 1991; Oasada and Nakagawa, 1992; Pusch and Walch, 1982; Smitha *et al.*, 2004].

The separation of ethylene glycol-water (EG-water) ranks among one of the most energy intensive distillation processes in the chemical industry [Hollis *et al.*, 2002]. Ethylene glycol is used as an antifreeze in the automobile and aviation industies, as a desiccant for natural gas production, and as a minor ingredient in the textile industry for the manufacture of polyester fibers and resins [Brown *et al.*, 1983; Feng and Huang, 1996]. However, due to the high toxicity of EG, it is important to separate and control the release of EG from waste streams as released to the environment [Brown *et al.*, 1983]. Considering the high cost of multi-stage evaporation and distillation, glycol enriched water mixtures are now dehydrated by pervaporation using polymeric membranes [Feng and Huang, 1996; Chen and Chen, 1996; Nam and Lee, 1999; Guo *et al.*, 2007].

Homogeneous membranes prepared with poly(vinyl alcohol) (PVA), poly(vinyl acetate) (PVAc) and chitosan are widely used for dehydration of organics [Brun *et al.*, 1974; Kang *et al.*, 1990; Uragami *et al.*, 1994; Nam and Lee, 1999]. PVA membranes give a good flux but a poor selectivity because of swelling. To enhance membrane performance, a variety of membrane modification techniques are employed such as crosslinking, blending and grafting chemical agents to the original polymer matrix [Pusch and Walch, 1982; Yong *et al.*,

1990; Nijhuis *et al.*, 1991; Huang and Rhim, 1993; Koops *et al.*, 1994; Qunhui *et al.*, 1995; Yu *et al.*, 2002; 13-20]. Among these chemical treatments of membranes, crosslinking has been used extensively to modify membrane's physicochemical properties, such as crystallinity, hydrophobicity, and mechanical strength [Huang and Rhim, 1993; Yu *et al.*, 2002; Guo *et al.*, 2007]. For hydrophilic PVA membranes, researchers have used different crosslinking agents such as maleic acid, sulfur-succinic acid and glutaraldehyde [Huang and Rhim, 1993; Rhim *et al.*, 1994]. Although these crosslinked membranes showed low swelling and high selectivity, the permeation flux was found to be limited due to higher diffusion resistance after crosslinking [Huang and Rhim, 1993].

Trimesoyl chloride (TMC), an aromatic compound having three acyl chloride groups, is extensively used in the preparation of nanofiltration and reverse-osmosis membranes because of its molecular structure that presents relatively large spacing between crosslinked polymer molecules and thereby low resistance to permeation [Ahmad and Ooi, 2005]. In PV dehydration of isopropanol-water mixtures, TMC crosslinked homogeneous PVA membranes had shown an acceptable, yet still low, flux and a high selectivity [Xiao *et al.*, 2006]: 0.11 $kg/m^2/hr$ and 390 at 60^OC, respectively, of 90 wt% isopropanol in the feed. Although TMC molecules contain three ester groups that show high polarity for water and may lead to an increase in permeation, the relatively low flux obtained could be due to the membrane thickness of 60 μm (thicker membranes giving higher diffusion resistance [Huang, 1991; Hyder *et al.*, 2008]. Therefore, to achieve a high flux, it would be interesting to use thin film PVA membranes and study the effect of crosslinking by TMC. To fabricate very thin selective layers, one may use composite membranes where a support layer is constructed to provide mechanical strength to the membrane [Du *et al.*, 2006]. To the best of our knowledge, no reports are available on poly(vinyl alcohol)-poly(sulfone), (PVA-PSf), composite membranes crosslinked with TMC in the application of dehydration of EG-water mixtures. Therefore, in this study, thin film PVA-PSf membranes were prepared and the PVA layer was crosslinked by a varying TMC concentration and reaction time. The degree of crosslinking reaction, crystallinity, surface roughness and hydrophobicity of the thin PVA layers were determined from *attenuated total reflection-Fourier transform infrared spectroscopy* (ATR-FTIR), *x-ray diffraction* (XRD), *scanning electron microscopy* (SEM), *atomic force microscopy* (AFM) and contact angle measurements. For each crosslinked

membrane, pervaporation dehydration of EG-water mixtures was conducted at 25^0C. The flux and selectivity of different membranes were analyzed as a function of TMC concentration and reaction time. The diffusion coefficients of water and ethylene glycol were calculated using a diffusivity correlation based on thermodynamics of irreversible process and universal quasi-activity theory [Appendix D]. Results were compared with the simple solution-diffusion mechanism (based on Fick's law of diffusion) to find the effect of membrane-permeant interaction on diffusion coefficient.

6.2. Experimental

6.2.1 Materials

Poly(vinyl alcohol) (99.7%, MW~133,000, PDI~1.3) was purchased from Fisher Scientific (ON, Canada). Poly(sulfone) (P-1700) was obtained from Amoco Performance Products (OH, USA) and was dried at 50^OC in a vacuum oven for 24 hr before use. *N*, *N*-Dimethylacetamide (DMAc) was from Acros Organics (NJ, USA), and poly(vinylpyrrolidone) (PVP, K30, MW~40,000) from Fluka Chemika (Buchs Switzerland). All other chemicals including hexane (ACS reagent, ≥98.5%, bp: 69^OC) and trimesoyl chloride (TMC) (98%, mp: 34.5–36^OC, bp: 180^OC at 16 mmHg) were purchased from Sigma-Aldrich (Oakville, Canada). Deionized water (18.2 MΩ cm) used for all experiments was produced by a Millipore Milli-Q system (MA, USA). All the solvents were used as received.

6.2.2 Membrane preparation

The fabrication procedure of PVA composite membrane has been described previously in Chapter 4 [Hyder *et al.*, 2008]. Briefly, the composite membrane was prepared by coating a layer of PVA onto a PSf porous substrate. The membrane was then dried in a vacuum oven (at 40 ^{O}C) for 3 hr. The crosslinking solutions at various concentrations were prepared by dissolving 0.05 to 0.7 wt% TMC in hexane. The crosslinking reaction time was varied from 10 to 90 minutes. The TMC concentration range (0.05 to 0.7 wt%) and reaction time (10 to 90 mins) were selected based on previous study by Xiao et al., (2006). The authors found that PVA membranes crosslinked with more than 1 wt% TMC and 60 mins gave low flux due to excessive crosslinking. Moreover, these membranes are thinner (5 ± 2 μm) than the

membrane studied in the literature (50-60 μm). The top PVA layers of the composite membranes were crosslinked interfacially by depositing different TMC/hexane solutions at 25^{O}C. After reaction over a specified time, the membranes were taken out and washed several times with deionized water and finally soaked in water for 6 hours at 40^{O}C to eliminate any residual hexane. The crosslinked membranes were then dried in a vacuum oven (at 40^{O}C) for 24 hours. Table 6.1 shows the data of the different membranes prepared for this study; for example, PVA1 is a composite membrane crosslinked with 0.05 wt% TMC for 60 minutes. The TMC concentration was varied from 0.05 to 0.7 wt% in hexane for PVA1 to PVA4 and each of them was crosslinked for 60 min. The crosslinking reaction time was varied from 10 to 90 min using 0.7 wt% TMC for PVA5 to PVA8. A micrometer screw gauge was used to determine the composite membrane thickness by measuring at least 10 different locations including the center of the membrane. The PVA layer thickness was about 5 ± 2 μm and the PSf support thickness was 120 ± 10 μm. Figure 6.1 (a) shows a scanning electron microscopy image of the cross section of a PVA1 membrane. As can be seen, the thin PVA layer is supported by a porous PSf structure. The top PVA layer does not contain any visible pores or cracks.

Table 6.1 Membrane characterization results

Composite Membrane	Crosslinking condition		Surface roughness Rq (nm)	Contact angle θ_{ap} (^{O})
	TMC density (wt%)	Reaction time (min)		
PVA1	0.05	60	18.1 ± 1.6	42.1 ± 1.8
PVA2	0.3	60	26.8 ± 1.8	44.9 ± 2.1
PVA3	0.5	60	30.2 ± 2.1	46.8 ± 1.7
PVA4	0.7	60	48.7 ± 2.9	51.4 ± 1.9
PVA5	0.7	10	32.1 ± 2.2	49.5 ± 1.4
PVA6	0.7	30	32.2 ± 1.8	51.7 ± 1.6
PVA7	0.7	75	34.2 ± 1.6	53.4 ± 1.1
PVA8	0.7	90	33.8 ± 1.9	50.2 ± 1.2

Note: The PSf support film thickness is 120 ± 10 μm. The membrane thickness was measured with a micrometer and SEM image analysis software. Picoscan AFM software was used to measure surface roughness.

6.2.3 Membrane Characterization

To characterize the chemical composition of a membrane film before and after the crosslinking, Attenuated Total Reflectance (ATR)-FTIR spectroscopy was employed. Infrared spectra of the fresh and crosslinked membranes were obtained with a midrange (500-4000 cm^{-1}) Bruker Tensor 27 ATR-FTIR spectroscope (Milton, Canada) at $25^{O}C$.

The membrane surface morphology was observed using a commercial Atomic Force Microscope (AFM) (Picoscan, Molecular Imaging, Tempe, AZ, USA) at room temperature. After image acquisition, root mean square (RMS) roughness of the membrane surface was determined by a program in the AFM image processing toolbox [Hyder *et al.*, 2006].

The X-ray diffraction (XRD) patterns of the membrane samples were obtained with an Inel diffractometer (Paris, France) with monochromatized $CuK\alpha_1$ characteristic radiation (wavelength $\lambda = 0.154$ nm at 40 kV, 50 mA, and scan speed of 1°/min, in a 2θ range of 5 – 40^{O}) at room temperature.

To determine the hydrophobicity of the composite membrane surfaces, contact angle measurements were conducted with static water sessile drops [Rosa and de Pinho, 1997]. All the contact angle measurements were repeated four times, and the results were averaged for each sample.

6.2.4 Swelling experiments

The crosslinked PVA membranes, of equal surface area, were weighed and immersed in different EG-water mixtures containing 50-90 wt% water at $25^{O}C$ for 24 hr. Constant weight experiments were used to make sure that the swelled membrane had reached equilibrium [Guo *et al.*, 2007]. Swollen membranes were blotted carefully with tissue paper to remove any surface solution, and the weight of the swollen membranes was measured by a mass balance. The swelling degree (*SD*) was calculated by

$$\text{Swelling degree (\%)} = \left(\frac{W_S - W_D}{W_D} \right) \text{x } 100 \qquad (6.1)$$

where W_S is the mass of the swollen membrane (in g) and W_D is the mass of the dried membrane (in g).

6.2.5 Pervaporation separation

The separation experiments were conducted on a lab scale pervaporation setup in Fig A.1 [Appendix A] for the dehydration of EG-water mixtures. The feed solution was pumped at a flow rate 1.95 L/min to the membrane cell. The feed solution contained 30 to 90 wt% ethylene glycol in EG-water mixtures. Each experiment was repeated four times under the same steady-state condition.

6.3 Results and discussion

Different composite membranes were prepared by a varying concentration of TMC and reaction time. A host of physicochemical methods were used for characterizing the resulting membranes prepared by varying the TMC concentration and reaction time. Detailed results on pervaporation performance of the membranes were obtained for dehydration of EG-water mixtures.

6.3.1 Atomic Force Microscopy: surface roughness

The crosslinked membrane surfaces (top of PVA layer) were characterized using Atomic Force microscopy techniques. Figures 6.1 (b) and (c) show the AFM images of the surfaces of PVA1 and PVA4 membranes over a scan area of 6×6 μm^2. Comparing these two images, the surface seems to be rougher with an increase in the crosslinking concentration of TMC. Table 6.1 shows the root mean square (RMS) roughness, R_q, obtained from the AFM image analysis [Dietz *et al.*, 1992]. The membrane surface is rough on a nanometre scale. The surface roughness increases with TMC concentration, e.g., PVA1 showing a RMS roughness of 18.1 nm and PVA4 of 48.7 nm. These membrane surfaces will be in contact with the feed solution during the pervaporation process. However, as can be seen from Table 6.1, the crosslinking reaction time did not affect the surface roughness as significantly.

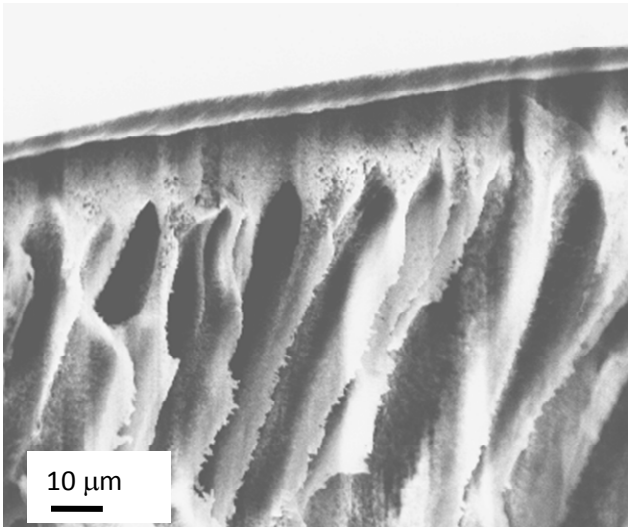

(a) PVA1

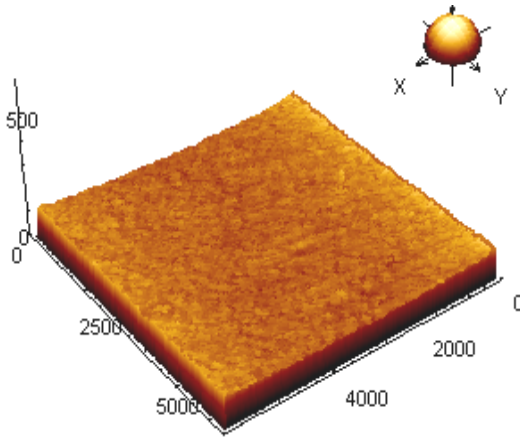

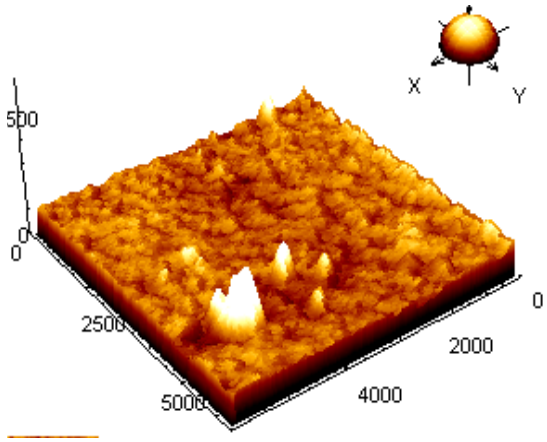

(b) PVA1 (c) PVA4

Figure 6.1: (a) SEM cross section of crosslinked PVA1 membrane (b) AFM surface scan of PVA1 and (c) PVA4 membranes, scanned area is 6 x 6 μm^2

6.3.2 Infrared spectroscopy: crosslinking

The crosslinking reaction between PVA and TMC is shown schematically in Fig. 5.2 (Ch. 5). The hydroxyl group of PVA will react with the acyl group of TMC to form an interchain structure. The IR spectra of the uncrosslinked and crosslinked composite membranes are shown in Fig. 6.2. The uncrosslinked PVA layer shows absorption peaks at 3300-3400 cm^{-1}

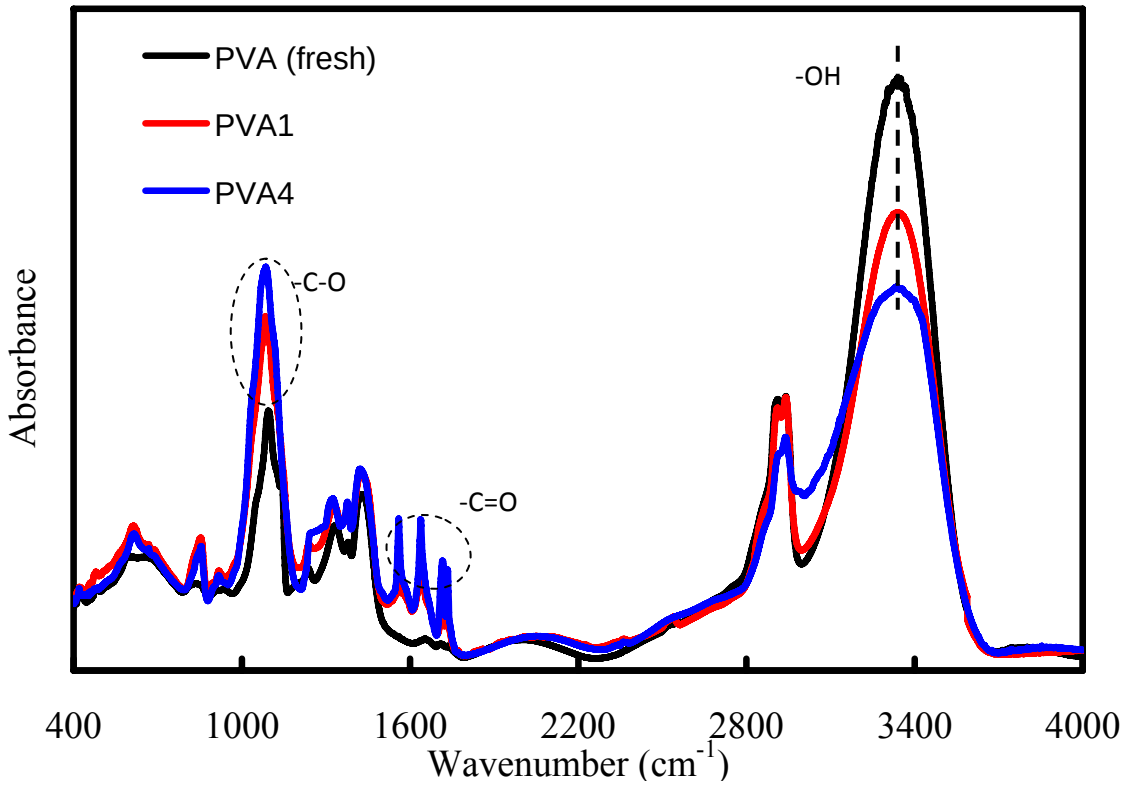

Figure 6.2: ATR-FTIR spectra of the PVA layers before and after crosslinking at 25^{O}C.

corresponding to the hydroxyl (-OH) groups of PVA. A decrease in absorption peak intensity is observed for the TMC crosslinked PVA layer, indicating that the number of hydroxyl groups decreased after crosslinking [Xiao *et al.*, 2006]. The uncrosslinked and crosslinked composite PVA membranes show great differences at 3300 cm^{-1}, and in the regions of 1500–1800 and 1200–1400 cm^{-1}. The –C-O absorption peaks can be seen around 1100 cm^{-1} and the –C=O absorption band of benzoate esters appears in the region of 1715–1730 cm^{-1} [Ahmad and Ooi, 2005; Xiao *et al.*, 2006].

6.3.3 X-ray diffraction: crystallinity

In Fig. 6.3, XRD patterns of the PVA layers of the composite membranes are shown before and after crosslinking. The diffraction scan of uncrosslinked PVA layer show a characteristic crystalline peak at $2\theta = 21.1^{O}$ [Zhou *et al.*, 2008]. It is known that pure PVA membranes maintain high crystallinity by intramolecular hydrogen bonding [Lu *et al.*, 2006]. Compared to that of the uncrosslinked PVA membrane, the peak intensity (at $2\theta = 21.1^{O}$) decreases of the membrane after crosslinking with TMC. It is clear that the uncrosslinked PVA membrane exhibits more crystallinity than the crosslinked one. The decrease and broadening in peak

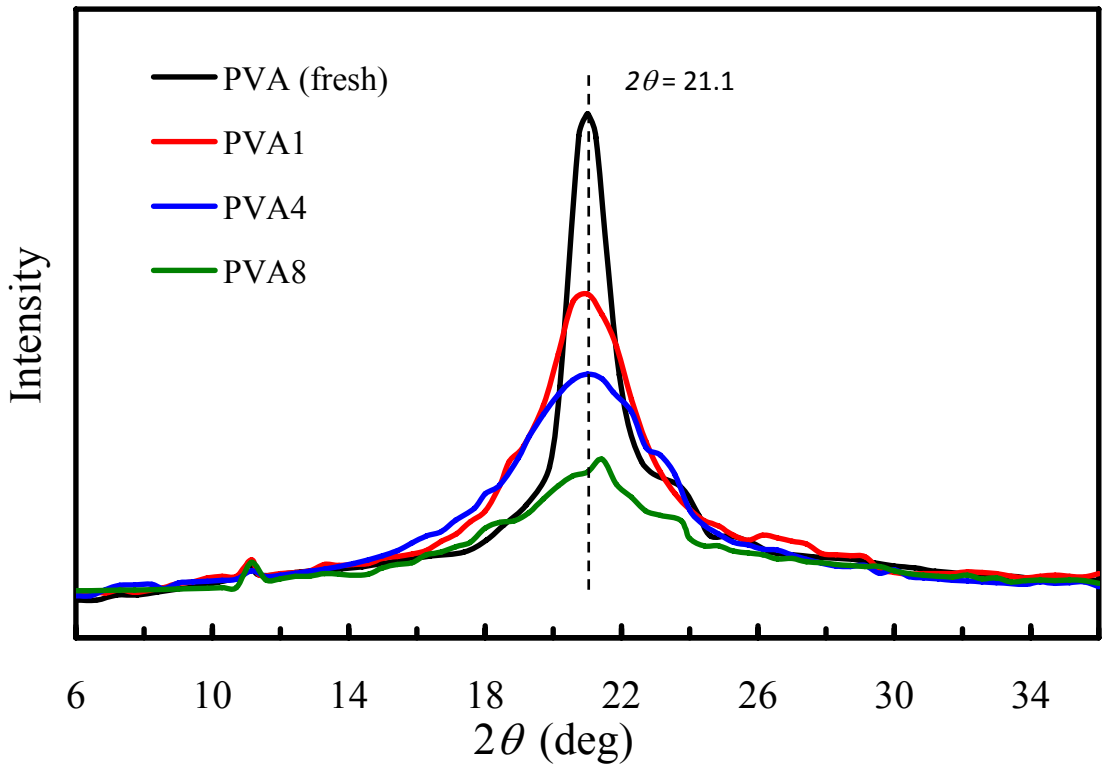

Figure 6.3: XRD spectra of PVA layers before and after crosslinking at 25^{O}C

intensity relates to an increase in TMC concentration during the crosslinking reaction, e.g., PVA1 showing a higher peak intensity than PVA4. An increase in TMC concentration competes and thus reduces the number of intramolecular hydrogen bonds, thereby decreasing membrane crystallinity. The crosslinking reaction time has an effect on crystallinity similar to the TMC concentration, where for example, PVA8 shows a lower peak intensity than PVA4.

6.3.4 Contact angle measurement: surface hydrophobicity

Crosslinking the PVA layer decreases the amount of hydroxyl groups on PVA molecules that can form strong hydrogen bonds with water, thereby affecting hydrophilicity. Sessile drops of water were used to measure the apparent static contact angle (θ_{ap}) on the membranes [Rosa and de Pinho, 1997; Li *et al.*, 2007]. The uncrosslinked PVA surface shows a static contact angle of 23.3^{O}. Crosslinking of PVA increases the contact angle, making it more hydrophobic. Results of the contact angles measured are presented in Table 6.1. An increasing trend in contact angle (from 42.1 to 51.8^{O}) was observed with increasing TMC concentration, from 0.05 to 0.7 wt%. However, the crosslinking reaction time (from 10 to 90 minutes) did not affect the contact angle significantly, varying only from 49.5 to 53.4^{O}. Li *et*

al. (2007) found the static contact angle of crosslinked PVA membranes to be within 53 to 65^{O}, which are less hydrophilic than the contact angles (41 to 54^{O}) found in this study.

6.3.5 Swelling characteristics

To determine the effect of crosslinking on water sorption in the PVA layer, the swelling degree was obtained and reported in Table 6.2. It was observed that the higher the concentration of TMC in the crosslinking solution, the lower the swelling degree. The swelling degree of two EG-water mixtures (50 and 90wt% EG in feed mixtures) against TMC concentration is shown in Figure 6.4(a). The swelling degree decreases with increasing TMC concentration initially and remains nearly constant beyond 0.5wt% TMC, indicating that crosslinking with high TMC concentrations in the PVA layer might lead to a more rigid and less water-expandable membrane structure. The swelling degree of the PVA layers in the composite membranes was calculated by subtracting the equivalent weight of the wet PSf support layer. Figure 6.4 (b) shows the swelling degree against crosslinking reaction time.

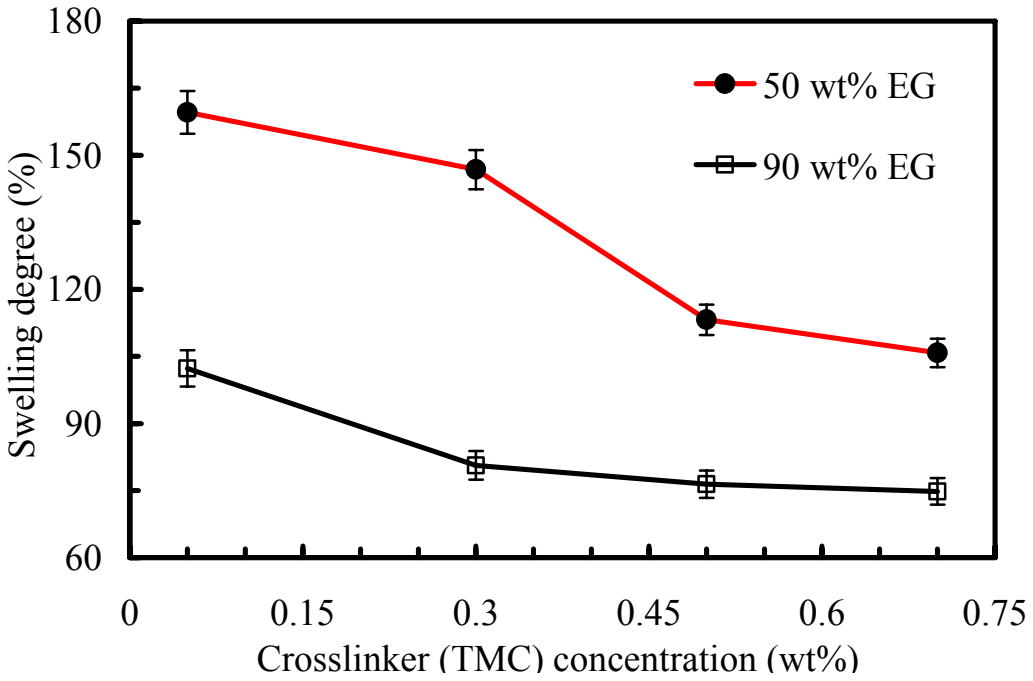

Figure 6.4 (a) Swelling Degrees against TMC concentration for different feed EG in mixtures at 25^{O}C for PVA1 to PVA4 membranes. Crosslinking reaction time was 60 min for all membranes.

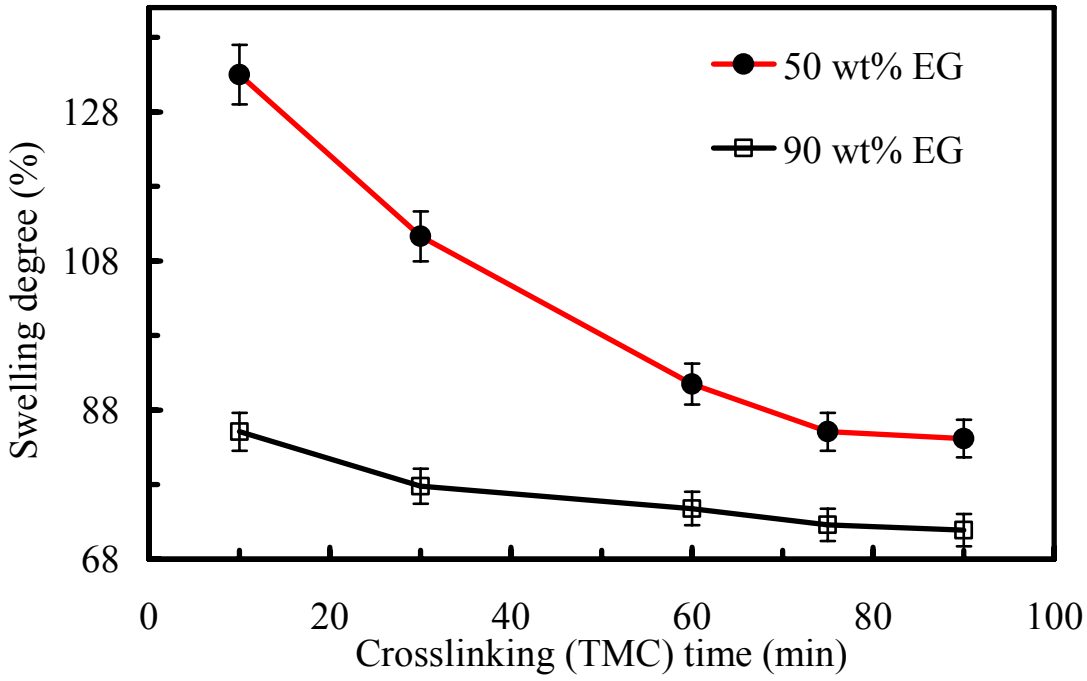

Figure 6.4(b): Swelling Degrees against TMC reaction time for different feed EG in mixtures at 25^{O}C for PVA4 to PVA8 membranes. TMC concentration was 0.7 wt% for all membranes.

The swelling degree reaches a plateau after a sufficiently long reaction time, ~75 min. This result suggests that an optimal crosslinking reaction time is ~75 min, and no improvement will be gained in controlling swelling with any longer reaction time. Compared to the results of glutaraldehyde crosslinked membranes reported in the literature [Guo *et al.*, 2007], the TMC crosslinked membranes showed a higher degree of swelling. This higher swelling degree in TMC crosslinked membranes could arise from the bigger molecular size of TMC than that of glutaraldehyde. After crosslinking, the benzoate ester groups of TMC could create a less compact structure than the ethyl ester groups of glutaraldehyde, leading to a higher swelling degree.

6.4 Pervaporation performance: flux and selectivity

6.4.1 Effect of feed concentrations

Figure 6.5 shows the results of the total flux and selectivity of the composite membranes against feed EG concentration (wt%) at 25^{O}C. The PVA layer is highly selective for water and therefore the total flux can be considered mainly the water flux [Huang and Rhim, 1993].

In Fig. 6.5, the total flux decreases, while the selectivity increases, with increasing feed EG concentration for the PVA1 and PVA4 membranes. At low EG concentrations in feed mixtures, the swelling degree is relatively high

Table 6.2 Diffusion coefficients of water and ethylene glycol at 25^{O}C

Composite Membranes	50 wt% EG in feed mixture			90 wt% EG in feed mixture		
	Swelling degree (%)	Diffusion coefficients		Swelling degree (%)	Diffusion coefficients	
		D_w x 10^8 (m^2/s)	D_{EG} x 10^9 (m^2/s)		D_w x 10^8 (m^2/s)	D_{EG} x 10^9 (m^2/s)
PVA1	159.6	20.13	3.95	102.3	47.67	0.60
PVA2	142.1	14.10	2.33	80.6	34.29	0.28
PVA3	113.3	12.36	1.67	76.4	33.12	0.32
PVA4	105.8	9.8	1.05	74.8	32.53	0.19
PVA5	133.2	20.05	4.66	85.1	46.18	0.76
PVA6	110.8	15.82	2.93	77.9	38.79	0.46
PVA7	91.5	7.63	0.79	72.6	26.56	0.16
PVA8	86.3	5.77	0.53	71.9	21.93	0.13

Note: The swelling measurements were performed at 25^{O}C (± 2^{O}C). Average error for swelling degree is ± 6.3%. Diffusion coefficient were calculated from simple S-D theory [Eq. (6.4)]

and such swollen membranes facilitate an increase in permeate transport, leading to a higher flux. However, the swollen membranes also allow EG molecules to transport across the membranes more easily, thereby potentially reducing the selectivity. As a control experiment, the total flux of the PSf support layer was determined to be 98.4 kg/m^2/hr for 30 wt% EG in the feed mixture. This high flux, at least two orders of magnitude higher than that of the composite membrane, shows that the PSf substrate provides very little resistant to the permeate flow and mainly provides mechanical support in the PVA-PSf composite membrane.

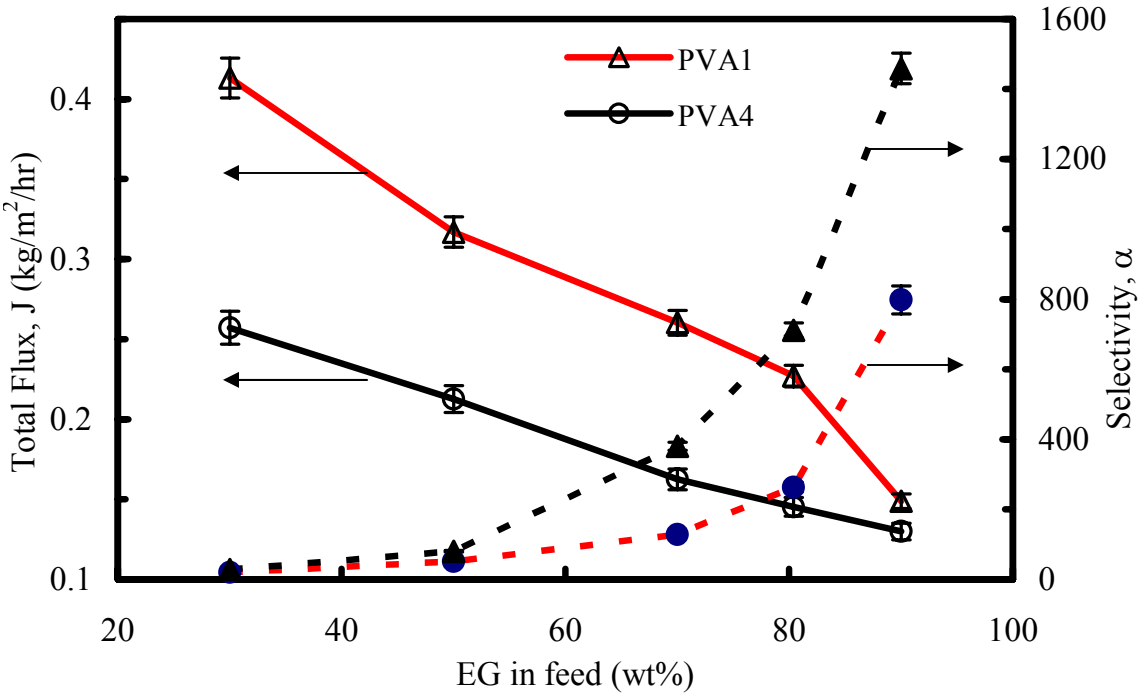

Figure 6.5: Total flux and selectivity against feed EG concentrations at 25^{O}C for PVA1 and PVA4 membranes.

6.4.2 Effect of feed temperature

The effect of operating temperature, ranging from 25 to 60^{O}C (298 to 333 K), on the pervaporation performance of the PVA4 membrane was studied and is shown in Fig. 6.6, for 90 wt% EG in the feed mixture. With an increase in temperature, the total flux increases but the selectivity decreases. At high temperatures, diffusing species have a greater kinetic energy, resulting in an increase in permeation rate. A semi-log plot of permeance (flux normalized by driving force) versus reciprocal of temperature (1/T) for water and ethylene glycol is shown in Fig. 6.6 (b). It should be pointed out that temperature affects permeation on two aspects: one is the driving force, and the other the membrane permeance. The temperature dependence of permeation flux can be expressed by the Arrhenius type relationship [Huang, 1991; Baker, 2004]:

$$Q_i = A_O \exp\left(-\frac{E_{pi}}{RT}\right) \tag{6.2}$$

where Q_i is the permeance of component i, A_O is a constant, Ep_i is the activation energy of permeating component i, and T is the absolute temperature. From Fig 6.6 (b), the activation energy for permeation through the crosslinked composite membrane was

calculated from the slope of the best-fit lines. The activation energy, $E_{p,}$ for water was estimated to be 7.4 kJ/mol, and for ethylene glycol, 1.2 kJ/mol. Permeating molecules with a

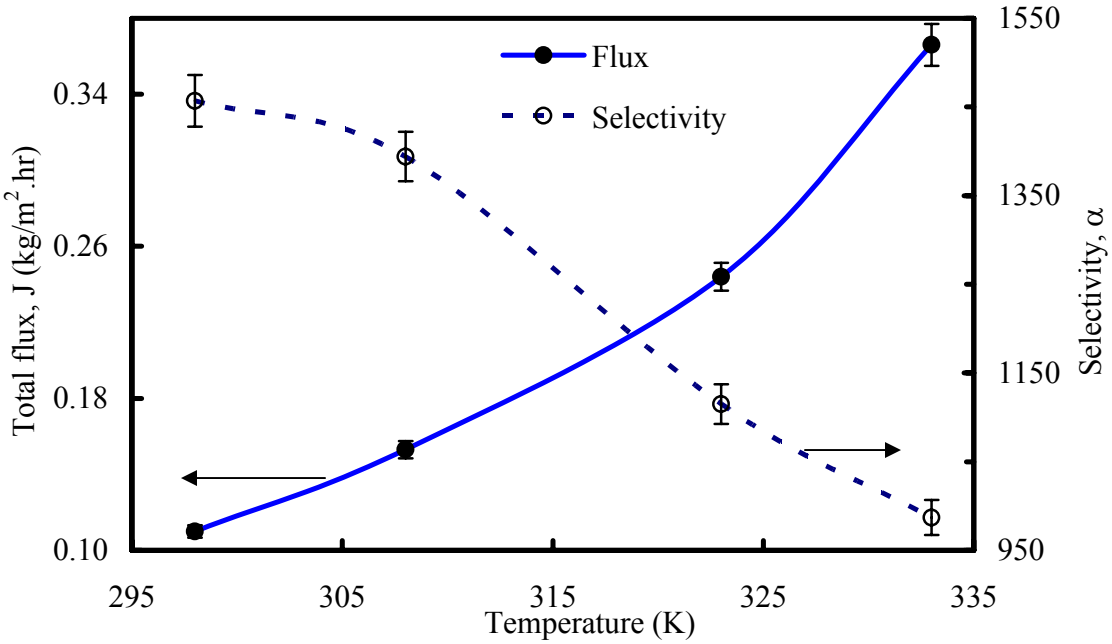

Figure 6.6 (a): Total flux and selectivity against feed temperature (K) for PVA4 composite membrane for 90wt% EG in feed mixtures.

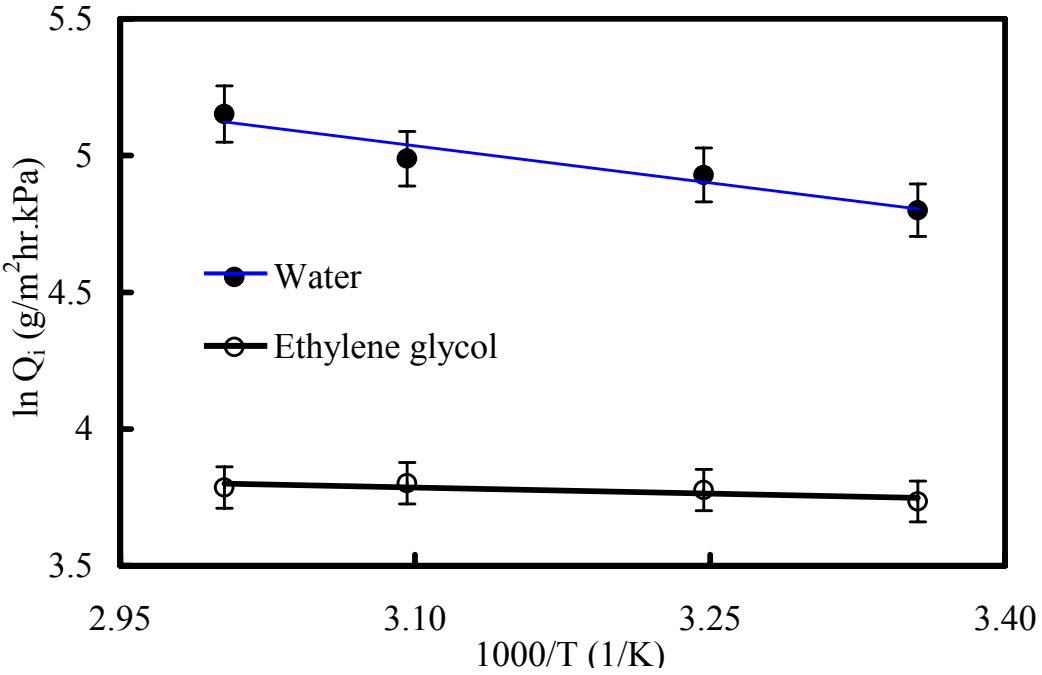

Figure 6.6 (b): Arrhenius plot of flux against 1/T for water and ethylene glycol.

higher activation energy show a stronger temperature dependence of the flux. Therefore the permeance of water tends to increase at high temperature. An increase in temperature increases the saturated vapor pressure of the permeant, resulting in an increase in the driving force for mass transport through the membrane.

The total flux and selectivity from the present study (for 90% EG in the feed mixture at 60^{O}C) were compared with other PVA composite membranes reported previously and presented in Table 6.3. Although the membrane preparation techniques (e.g., use of crosslinkers, supports and feed mixtures) and separation conditions were different, the dehydration performance of the PVA4 composite membrane prepared in this study shows a comparable, good flux and selectivity.

Table 6.3 Comparison of composite membrane separation performance with literature

Composite membrane (Crosslink agent)	Temp (^{O}C)	Type of mixture (alcohol wt%)	PVA layer thickness (μm)	J (kg/m^2.hr)	α	PSI (kg/m^2.hr)	References
PVA-PAN (MA)	60	Et-Water (80 wt%)	26	0.04	1320	52.8	Ohya *et al.* (1992)
PVA-PSf (MA)	50	Et-Water (95 wt%)	5	0.06	93	5.5	Wei *et al.* (1998)
PVA-PES (GA)	80	EG-water (82.5 wt%)	3	0.38	231	87.4	Chen and Chen (1996)
*PVA4 (TMC)	60	EG-water (90 wt%)	7	0.36	987	355.3	present work

Note: MA: maleic acid; GA: glutaraldehyde; PAN : poly(acrylo nitrile); PES: poly(ether sulfone); *PVA4 is a composite membrane with porous poly(sulfone) PSf support layer.

6.4.3 Effect of crosslinking agent concentrations and reaction times

Note that the PVA4 composite membrane shows the highest separation index of 355.3 kg/m^2/hr, as compared to other composite membranes. Figure 6.7 shows the total flux and selectivity against the TMC concentration (wt%) for the composite membranes with two feed mixtures. With an increases in crosslinking agent TMC concentration, the total flux decreases but the selectivity increases. The rate of the decrease in flux is more pronounced at low EG concentrations than at high EG concentrations in the feed mixtures. When the crosslinking

agent TMC has a low concentration, the degree of crosslinking is also low (higher crystallinity), which leaves a hydrophilic membrane to facilitate the permeation of water molecules. However, at a high TMC concentration (above 0.5 wt% TMC), the enhanced crosslinking renders low crystallinity and a less hydrophilic membrane, thereby decreasing the water and hence total flux. The selectivity increase with TMC concentration may also

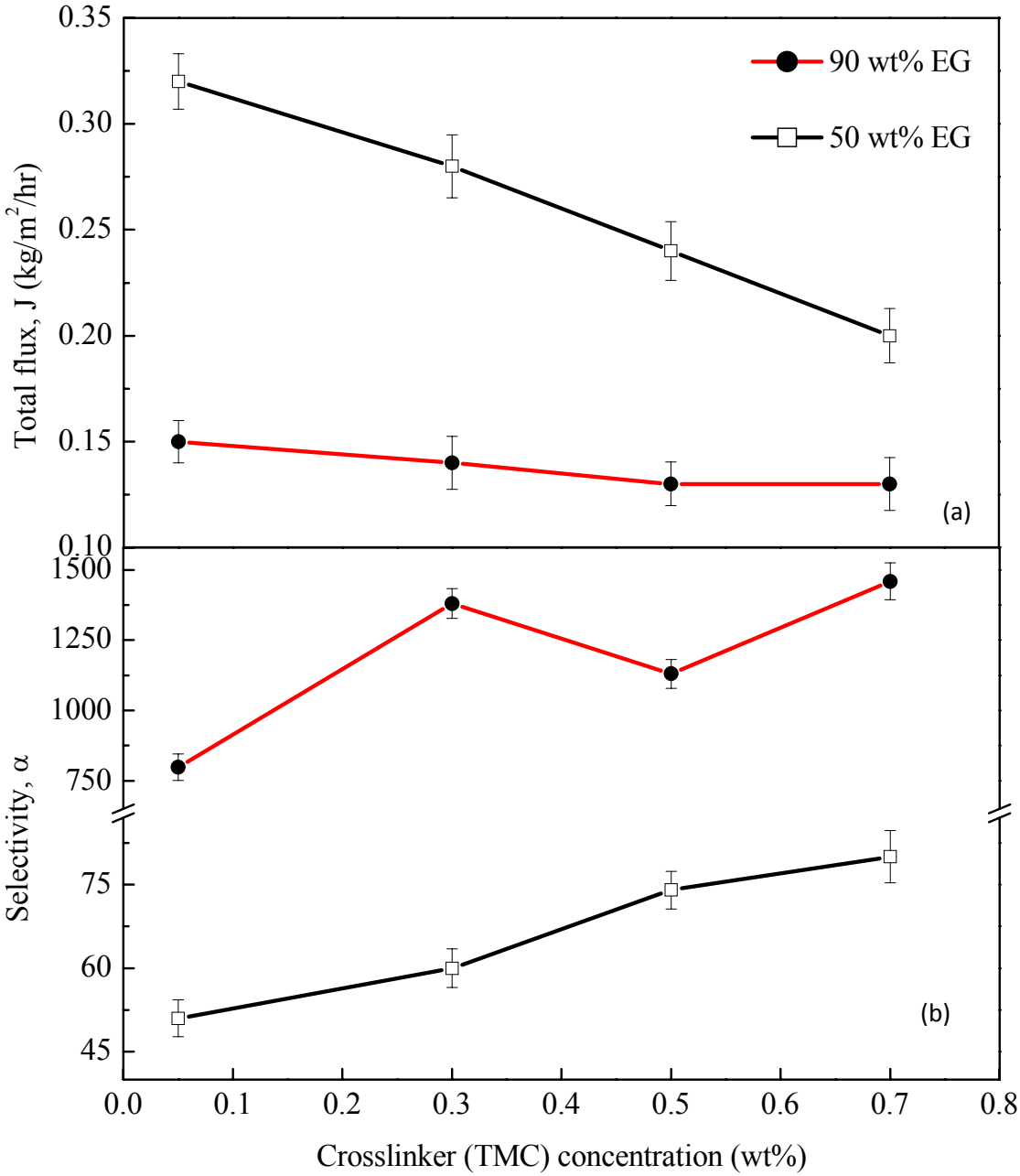

Figure 6.7: (a) Total flux and (b) selectivity against TMC concentration for 50 and 90 wt% feed EG in mixtures at 25^{O}C for PVA1 to PVA4 membranes. Crosslinking reaction time was 60 min for all membranes.

relate to the decrease in crystallinity, leading to preferential permeation of water molecules as compared to EG molecules. For all the crosslinked composite membranes, the total flux and selectivity are summarized in Table 6.4, for two different feed solutions (50 and 90wt% EG in feed mixtures). A longer crosslinking reaction time allows TMC molecules to penetrate

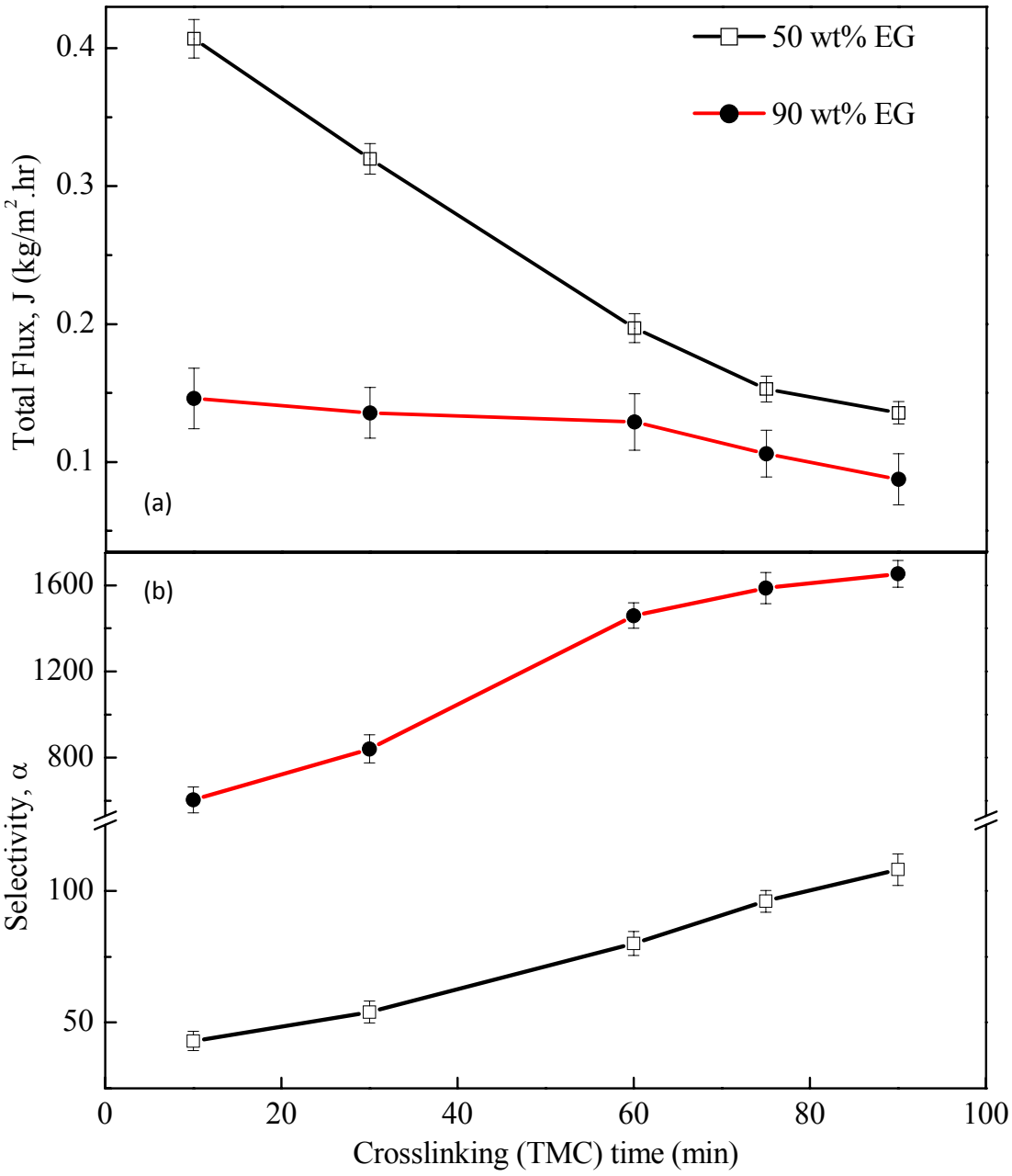

Figure 6.8: (a) Total flux and (b) selectivity against TMC reaction time for different feed EG in mixtures at 25^{O}C for PVA4 to PVA8 membranes. TMC concentration was 0.7 wt% for all membranes.

deeper into the PVA layer and the degree of crosslinking is hence increased. Figure 6.8 shows the total flux and selectivity against crosslinking reaction time (min) at two different EG-water mixtures. The total flux decreases, while the selectivity increases, with reaction time. For 50 wt% EG in the feed mixture, the total flux decreases with time almost linearly, but for 90 wt% EG, the decreasing rate of the flux is relatively low.

Table 6.4 Separation results at 50 and 90wt% EG in feed mixtures

Composite Membranes	(50wt% EG in feed mixture)		(90wt% EG in feed mixture)	
	Total flux, J ($kg/m^2/hr$)	Selectivity α_{WA}	Total flux, J ($kg/m^2/hr$)	Selectivity, α_{WA}
PVA1	0.32	51	0.15	798
PVA2	0.28	60	0.14	1380
PVA3	0.24	74	0.13	1130
PVA4	0.20	80	0.13	1459
PVA5	0.41	43	0.19	604
PVA6	0.32	54	0.16	841
PVA7	0.15	96	0.11	1587
PVA8	0.11	108	0.09	1653

Note: The separation experiments above were performed at $25^{O}C$ ($\pm 2^{O}C$). Average error for total flux is ± 3.8 % and for selectivity is ± 6.5%

6.4.4 Diffusion coefficients

In PV dehydration, the mass transports of mixture components are generally described by the solution-diffusion mechanism [Huang, 1991] and total flux and selectivity are greatly affected by the diffusion of components across the membrane. Therefore, it is important to estimate the diffusion coefficient from the experimental flux by applying the Fick's law of diffusion [Baker, 2004],

$$J_i = D_i \frac{dC_i}{dx} \tag{6.3}$$

where J_i is the flux of mixture component ($kg/m^2/s$), D_i is the diffusion coefficient (m^2/s), C_i is the concentration (kg/m^3) and x is the diffusion path distance (m). For a linear

concentration profile across the membrane, the diffusion coefficient in eq (6.3) can be written as [Kusumocahyo and Sudoh, 1999],

$$D_i = \frac{J_i}{\Delta C_i} L \tag{6.4}$$

where L is the membrane thickness (m). The diffusion coefficient in Eq. (6.4) is based on the assumption that the flux is not affected by component interactions.

On the other hand, the diffusion coefficient can be calculated using semi-empirical correlation based on the activity of the components. For polymeric systems, the flux can be expressed as [Mulder and Smolders, 1984; Chen and Chen, 1996]

$$J_i = -\rho_i D_{im} \frac{d \ln(a_i)}{dz} \tag{6.5}$$

where ϕ_i is the volume fraction and D_{im} is the diffusivity of components i for the polymer matrix. Some of the assumptions are (i) for each feed concentration, the diffusion coefficients of the feed components through the membrane are constant, (ii) the coupling effects between solvent components are negligible and (iii) the temperature across the membrane thickness is constant. For an n component system, if it assumed that the activity a_i of component i depend on the volume fractions of all the other components in the polymer, then Eq. (6.5) can be simplified to

$$J_i = -\rho_i D_{im} \left[\sum_{j=1}^{n} \frac{\partial \ln(a_i)}{\partial \phi_j} \frac{d\phi_j}{dz} \right] \tag{6.6}$$

For a binary solvent-polymer system, in Eq. (D.6) can be written as

$$D_{1m} = -\frac{J_1}{\rho_1} \left[\frac{\partial \ln(a_1)}{\partial \phi_1} \frac{d\phi_1}{dz} + \frac{\partial \ln(a_1)}{\partial \phi_2} \frac{d\phi_2}{dz} \right]^{-1} \tag{6.7}$$

$$D_{2m} = -\frac{J_2}{\rho_2} \left[\frac{\partial \ln(a_2)}{\partial \phi_1} \frac{d\phi_1}{dz} + \frac{\partial \ln(a_2)}{\partial \phi_2} \frac{d\phi_2}{dz} \right]^{-1} \tag{6.8}$$

where D_{1m} and D_{2m} are the diffusivities of binary component 1 and 2, respectively. It can be seen from Eq. (6.7) and (6.8), that the diffusivity of a component does not only depend on its

own concentration gradient but also on the concentration gradient of the other components in the membrane. Details of this semi-empirical approach are presented in Appendix D.

The diffusion coefficient were calculated for 50 and 90 wt% feed EG concentrations at 25^0C (Table 6.2) using Eqs. (6.4) and (6.7)-(6.8). The diffusion coefficients of water and EG decrease from PVA1 to PVA4 membranes, where the crosslinker TMC concentration is increased progressively. A decrease in diffusion coefficient of water could be due to a higher degree of crosslinking and hence a reduced degree of swelling in the membrane. From PVA5 to PVA8, the diffusion coefficients also decrease with increasing crosslinking reaction time. A longer reaction time leads to a higher degree of crosslinking, and the membrane becomes

Table 6.5 Diffusion coefficients of water-EG-PVA system at 25^OC

Composite Membranes	90 wt% EG in feed mixture				
	Activity of water	Diffusion coefficient (Eq. 6.4)		Diffusion coefficient (Eq. 6.7 and 6.8)	
		D_w x 10^{-8} [m^2/s]	D_{EG} x10^{-9} [m^2/s]	D_{wm} x 10^{-9} [m^2/s]	D_{EGm} x 10^{-10} [m^2/s]
PVA1	0.35	47.67	0.6	3.2	1.96
PVA4		32.53	0.19	1.7	1.19
PVA5		46.12	0.76	5.4	2.54
PVA8		21.93	0.13	0.9	1.04

less hydrophilic, resulting in a reduced water diffusion rate. It is interesting to note that for all composite membranes, the diffusion coefficient of water decreases with a decrease in feed EG concentration, even though the swelling degree is increased. For example, for the PVA1 membrane, the diffusion coefficient of water decreases from 47.67 to 20.13 (x 10^{-8}) m^2/s with a decrease in feed EG concentration from 90 to 50 wt%, while the swelling degree is increased from 102.3 to 159.6 %. However, an opposite trend is observed for the EG diffusion coefficient, which increases with a decrease in EG concentration in the feed mixture. With low EG fractions in the feed, the membrane swells more and EG molecules permeate across the membrane more easily. As a result of the opposite trends in diffusion coefficient change between water and EG, the membrane selectivity decreases with decreasing the EG concentration in the feed solution (Table 6.4). The diffusion coefficients

of Eq. (6.4) (without interaction of components) were compared to the results obtained from diffusivity correlation (with component interactions) presented in Table 6.5. It can be seen, water diffusivities (with interaction) are at least two orders of magnitude lower than the diffusivity calculated from simple S-D theory. For EG-water-PVA system, Chen and Chen (1998) calculated the diffusivity of water to be 0.6 to 2.9 (x 10^{-9}) m^2/s that falls within the range of our diffusivity calculation from Eqs. (6.7).

Table 6.6 Comparison of different crosslinker from literature

Membrane (crosslink agent)	Temp (^{O}C)	Type of mixture & concentration	Thickness (μm)	J ($kg/m^2.hr$)	α	PSI ($kg/m^2.hr$)	References
PVA (MA)	25	AA-water (87 wt%)	50	0.35	6.2	1.8	Huang and Rhim (1993)
PVA (GA)	35	AA-Water (90 wt%)	12-14	0.10	263	26.2	Yeom and Lee (1996)
PVA (SSA)	70	Et-Water (90 wt%)	20-30	0.29	171	49.3	Rhim *et al.* (1998)
PVA (TMC)	60	IPA-water (90 wt%)	50-60	0.11	562	61.7	Xiao *et al.* (2006)
PVA (GA)	70	EG-water (80 wt%)	15	0.21	933	195.7	Guo *et al*. (2007)
PVA4 (TMC)	60	EG-water (90 wt%)	7	0.36	987	355	present work

MA: Maleic acid; GA: glutaraldehyde; SSA: Sulfur-succinic acid; AA: Acetic Acid

In Table 6.6, results of the dehydration performance of different aqueous feed mixtures are presented, to compare among crosslinking agents for PVA membranes. The selectivity of the TMC crosslinked PVA composite membrane (PVA4) is significantly higher than other chemical crosslinked PVA membranes. The total flux of the TMC crosslinked is found to be high as well. When calculating the pervaporation separation index, the TMC crosslinked membrane has the highest value of all, indicating that it is most capable of achieving a high flux and a high selectivity simultaneously. Therefore, TMC should be

recommended for use of crosslinking hydrophilic membranes in the pervaporation dehydration.

6.5 Conclusions

Trimesoyl chloride crosslinked PVA composite membranes were prepared for the pervaporation dehydration of EG-water mixtures. The PVA layers were successfully crosslinked with TMC using varying concentration and reaction time, as demonstrated by ATR-FTIR measurements. Atomic force microscopy and contact angle measurements showed that crosslinking affected both surface roughness and hydrophobicity of the membrane. A change in TMC concentration affected hydrophobicity more than that in TMC reaction time. From X-ray diffraction and swelling studies, crystallinity and swelling degree of the crosslinked PVA layer were found to decrease with increasing TMC concentration and reaction time. The decrease in swelling could be due to the decrease in crystallinity and hydrophilicity. For EG-water solution dehydration, the total flux was found to decrease with an increase in TMC concentration and reaction time. At high water fractions in the feed mixtures, the decrease in flux is more prominent due to swelling of the membrane by water. The selectivity was found to increase with increasing TMC concentration and reaction time. Diffusion coefficient were found to be strongly affected by membrane-permeant interaction and are two orders of magnitude lower than diffusion coefficient calculated from simple S-D theory. The results show that TMC crosslinked PVA composite membranes could be an excellent candidate for the dehydration of EG-water mixtures.

CHAPTER 7

Pervaporation Dehydration of Alcohol-Water Mixtures: Optimization of Operating Conditions for Permeate Flux and Selectivity by Central Composite Rotatable Design

7.1 Introduction

Pervaporation (PV), an energy efficient membrane separation process, has gained considerable attention as an industrial process for the separation of organic-water mixtures, especially for azeotropic mixtures [Huang, 1991; Oasada and Nakagawa, 1992, Baker, 2005]. In pervaporation, the flux and selectivity could be affected by a number of factors such as the physicochemical nature of the membrane (such as crystallinity and hydrophobicity) and operating variables (such as temperature, feed concentration and flow-rate) [Binning *et al*., 1961; Huang and Rhim, 1993; Oasada and Nakagawa, 1992]. Therefore, it is important to determine the operating variables at which the flux and selectivity reach their optimum values [Smitha *et al*., 2004]. Researchers generally study the PV separation performance by using the "one-factor-at-a-time" approach [Kang *et al*., 1990; Pesek and Koros, 1993; Lee *et al*., 1995; Yeom and Lee, 1996; Guo *et al*., 2007], such as the feed concentration being varied while keeping the temperature and feed flow-rate constant [Huang and Rhim, 1993]. However, the effect of temperature, concentration and flow-rate may not be independent of each other and it is necessary to consider their interactions.

One possible solution is to use the response surface methodology (RSM) approach that is widely used to analyze the effects of multiple factors and their interactions [Lee *et al*., 1995; Feng and Huang, 1996]. The experimental designs commonly used for engineering process analysis and modeling include full or partial factorial analysis and the central composite rotatable design (CCRD) [Myers and Montgomery, 2002; Montgomery, 1991]. The CCRD has been applied to various engineering processes for data interpretation and optimization [Montgomery, 1991; Kiran *et al*., 2001; Mota *et al*., 2006; van der Ven *et al*., 2002]. It requires fewer experimental runs than factorial designs, providing savings on time and resources [Diniz and martin, 1996; Rodrigues *et al*., 2006]. In pervaporation, the CCRD could be an ideal tool for optimizing the flux and selectivity in terms of operating variables.

Ethanol forms an azeotropic mixture with water at 95.5wt%, which evaporates at 78.2^{O}C under the atmospheric pressure; it cannot be separated by distillation [Baker, 2004]. Likewise, isopropanol forms an azeotropic mixture at 87.5wt% with water, which evaporates at 82.5^{O}C. In the last two decades, PV dehydration of alcohol-water azeotropic mixtures had been studied extensively at different operating temperatures by keeping the flow-rate constant [Binning *et al*., 1961; Huang and Rhim, 1993; Yeom and Lee, 1996; Guo *et al*., 2007]. However, to date, no systematic study is available that optimizes the flux and selectivity as a function of all operating variables involved.

In this work, the objective was to use the CCRD for analyzing and optimizing the effects of temperature, feed alcohol concentration and flow-rate on the PV flux and selectivity of homogeneous crosslinked poly(vinyl alcohol) membranes. The results were fitted to a quadratic regression equation using the least-square algorithm. To determine the validity of the regression model, the predicted results from the regression equation were compared to the experimental data. The predicted flux and selectivity from the regression model were also presented in 3-D surface plots to identify the contributions of operating variables. From the regression model, sets of operating variables were determined for optimizing the laboratory dehydration of azeotropic alcohol-water mixtures.

7.2 Theory

Response surface methodology (RSM) is a collection of statistical and mathematical methods that involves experimental designs to achieve adequate and reliable measurement of the response of interest. The response surface can be expressed as

$$y = f(x_1, x_2, \ldots x_n) \tag{7.1}$$

where y is the response and x_i's are the operating variables of the process. An important assumption is that the operating variables are continuous and controllable by experiments with negligible errors.

Among different RSM experimental designs, the CCRD has been widely used because it requires fewer experimental runs and provides sufficient information as compared to a factorial design. The number of experiments required for the CCRD includes a standard 2^k factorial (k: the number of operating variables), with its origin at the center, $2k$ points fixed axially at a distance α from the center to generate the quadratic terms, and replicate tests at the center. Replicates of the test at the center are very important as they provide an

independent estimate of experimental errors. The axial points are chosen such that they allow rotatability [Kiran *et al*., 2001], which ensures that the variance of the model prediction is constant at all points equidistant from the center. For three variables, the recommended number of experiments at the center is six [Myers and Montgomery, 2002]. Hence, the total number of tests required for the three independent variables (temperature, feed concentration and flow-rate) is $2^3 + (2\times3) + 6 = 20$.

The correlation of the operating variables and the responses based on the CCRD design is fitted to a quadratic polynomial equation using the least-square method of the form

$$Y_k = b_0 + \sum_{i=1}^{3} b_i X_i + \sum_{i=1}^{3} b_{ii} X_i^2 + \sum_{i=1}^{2} \sum_{j>1}^{3} b_{ij} X_i X_j + \varepsilon \qquad (7.2)$$

where

Y_k = dehydration responses (Y_1 for flux and Y_2 for selectivity),

b_0 = constant,

ε = residual (error) term,

b_i = linear coefficients,

b_{ii} = quadratic coefficients,

b_{ij} = interaction coefficients, and

X_i = dimensionless coded variables (X_1 for temperature, X_2 for alcohol feed concentration and X_3 for flow-rate).

The operating variables are coded according to the following equation

$$X_i = \left(x_i - x_{i0}\right) / \Delta x_i \qquad (7.3)$$

From Eq. (7.2), the advantage of using the CCRD over that of a factorial design is obvious: the quadratic and interaction terms of the operating variables can relate to curvatures or warpings of the response surfaces.

In RSM, the desirability function (DF) is widely used to determine a combination of variables to optimize multiple responses [Harrington Jr., 1965; Kalil *et al*., 2000]. A DF method finds operating conditions that provide the "most desirable" responses. A desirability function method consists of the following three steps:

(1) Conduct experiments and fit response models (y_k) for all k responses;

(2) Define individual desirability functions for each response (d_k);

(3) Maximize the overall desirability with respect to the controllable factors.

For each response $y_k(x_i)$, a desirability function $d_k(y_k)$ assigns numbers between 0 and 1 to the possible values of y_k, with $d_k(y_k)$ =0 representing a completely undesirable value of y_k and $d_k(y_k)$ =1 representing a completely desirable or ideal response value. Depending on whether a particular response y_i is to be maximized, minimized, or assigned to a target value, different desirability functions $d_k(y_k)$ can be used. The individual desirability functions from the considered responses are then combined to obtain a total desirability function, D ($0 \leq D \leq 1$), defined by [Derringer and Suich, 1980]

$$D = f(d_1, d_2, \ldots d_n) \tag{7.4}$$

$$D = (d_1 \cdot d_2 \cdot \ldots \cdot d_n)^{(1/n)} \tag{7.5}$$

The optimum values of variables are determined from the values of individual desirability functions that maximize D. Note that if any response k is completely undesirable [$d_k(y_k) = 0$], then the overall desirability is zero. In practice, fitted response models y_k are used in the method. The rationale behind using the geometric mean [Eq. (7.5)] is that if any quantity characteristic has an undesirable value [i.e., $d_k(y_k(x)) = 0$] at some operating condition $x = x_o$, then the overall result, as a product, is wholly unacceptable, regardless of the values taken on by other responses.

7.3 Experimental

7.3.1 Materials

Poly(vinyl alcohol), PVA, (99.7% hydrolyzed, MW 108,000, PDI 1.3) was purchased from Fisher Scientific, Canada. All other chemicals, including acetic acid (glacial, 99.7%), acetone (99%), glutaraldehyde (25% aqueous) and sulfuric acid (98%), were obtained from BDH, Toronto, Canada. Deionized water (18.4 MΩ cm) used for all the experiments was produced by a Millipore system. The chemicals and solvents were used as received.

7.3.2 Membrane preparation

The poly(vinyl alcohol) solution was prepared by dissolving 5wt% of PVA in deionized water at 90^{O}C for 1 hour, stirring the solution until it was completely homogeneous. 10 ml of the PVA solution was then cast onto a glass plate and dried under ambient conditions (25^{O}C and 70% relative humidity) in fumehood for 24 hours. After that, the membrane film with the glass plate was dried in a vacuum oven (at 40^{O}C) for 3 h for the removal of traces of solvent. Later, the dried films were peeled off the glass plate for crosslinking reaction. The membrane

film was hydrophilic and absorbed water quickly, assuming a swollen film state. Swelling of the PVA membrane was not desirable since it would disrupt the membrane integrity and lower the separation efficiency. Thus, the membranes used were further crosslinked with chemical agents. The membrane was interfacially crosslinked by pouring a glutaraldehyde (GA) solution on top of the film [Yeom and Lee, 1996]. The chemical crosslinking solution consisted of 3wt% glutaraldehyde, 0.5wt% sulfuric acid (H_2SO_4), 47wt% acetone, and rest deionized water. Each dry PVA film was immersed in the prepared crosslinking solution for 30 minutes at room temperature (25^OC). After the reaction, the membrane was taken out and washed several times with pure water and finally immersed in pure water for 6 hours at 40^OC to eliminate residual H_2SO_4. The crosslinked membrane was then dried in a vacuum oven for 24 hours. The thickness of the crosslinked membrane was about 22 ± 3 μm.

7.3.3 Pervaporation experiments

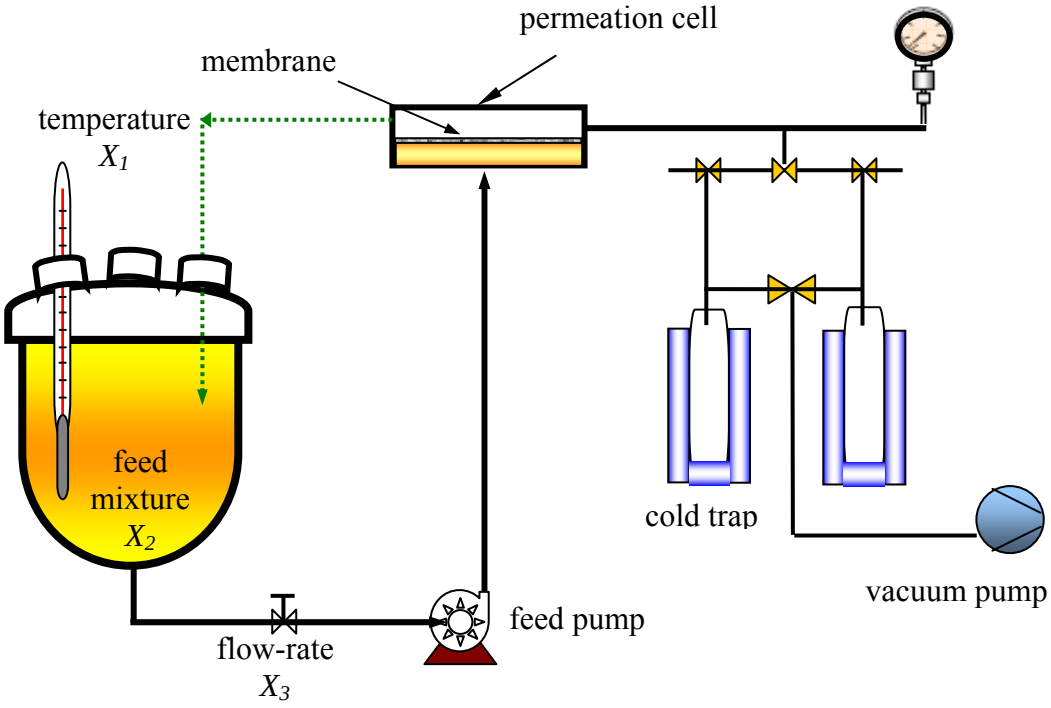

Figure 7.1: Schematic diagram of a pervaporation experimental setup.

The prepared membranes were tested for pervaporation dehydration on a setup shown in Fig. 7.1. Pervaporation experiments were conducted for the dehydration of two alcohol-water systems: isopropanol-water (IPA-water) and ethanol-water (Et-water) mixtures. Dehydration experiments were performed with flat sheet membranes (with an effective membrane area 20.2 cm^2). The feed solution was circulated with a pump (Magnetek Universal Electric, MI,

USA) through the membrane surface in the cell and returned back to the circulation. The feed flow-rate was varied with a control valve. Partial vacuum was applied to the permeate side as a driving force for diffused solvents to evaporate easily. The feed pressure was at atmospheric pressure while the pressure on the permeate side was kept below 3 mbar using a vacuum pump (Leeson Electric Co., WI, USA). To achieve a steady-state at a given temperature, the experiment was run for two hours prior to collection of permeates. To assess experimental errors, each experiment was repeated three times. The permeate vapor was condensed and collected in a cold trap (glass tube) immersed in liquid nitrogen for about 20 minutes. The permeate was then heated to room temperature and weighed to determine the mass. The separation temperature was varied with a temperature controller (accuracy ± 2^{O}C). The total flux (J) and selectivity were calculated based on Eq (2.3) and (2.4).

7.4 Experimental design

Based on the capability of the experimental setup and the preliminary single-variable tests, the ranges of operating variables were chosen as follows: temperature - 33 to 67^{O}C, feed flow-rate - 46-114 L/hr, and feed alcohol fraction - 83 to 92 wt% IPA for the IPA-water system and 93 to 98wt% Et for the Et-water system. The levels, codes and intervals of variation of the operating variables are given in Table 7.1. This design is composed of 2^3 factorial design (runs 1–8; cf. Table 7.2), six axial runs of star points (9–14) and 6 replicates runs of the central point (15–20).

Table 7.1: PV operating variables with actual and coded levels for CCRD experiments

Feed factors	Code x_i	Isopropanol-Water (IPA-Water)					Ethanol-Water (Et-water)				
		Variation levels					Variation levels				
		-1.68	–1	0	+1	+1.68	–1.68	–1	0	+1	+1.68
Temperature (^{O}C)	x_1	33	40	50	60	67	33	40	50	60	67
Concentration (wt%)	x_2	83	85	87.5	90	92	93	94	95.5	97	98
Flow rate (L/h)	x_3	46	60	80	100	114	46	60	80	100	114

Note: CCRD consisting of experiments for the study of 3 operating factors in coded and actual levels. The ranges of variables were chosen based on preliminary dehydration experiments.

Once the desired ranges of values of the variables are defined, they are coded to lie at ±1 for the factorial points, 0 for the center point and ± α for the axial points [Diniz *et al*., 1996]. The codes are calculated as functions of the ranges of each variable as shown in Table

Table 7.2 Coded operating variables of PV dehydration data for alcohol-water mixtures

Test no.	Coded level of variables			Experimental data of IPA-water		Experimental data of Et-water	
	X_1	X_2	X_3	Flux ($g/m^2/hr$)	Selectivity	Flux ($g/m^2/hr$)	Selectivity
1	-1	-1	-1	71.11	105.89	37.62	103.76
2	-1	-1	1	60.21	111.77	61.89	98.82
3	-1	1	-1	31.06	142.90	35.48	77.91
4	-1	1	1	41.86	137.44	43.99	57.29
5	1	-1	-1	91.62	88.81	110.03	52.64
6	1	-1	1	85.27	69.11	108.39	41.1
7	1	1	-1	68.30	92.11	52.17	90.23
8	1	1	1	97.72	87.81	67.76	105.93
9	-1.682	0	0	53.76	120.46	48.91	78.27
10	1.682	0	0	113.90	60.83	101.22	48.59
11	0	-1.682	0	76.41	103.30	84.59	88.26
12	0	1.682	0	35.65	148.27	32.78	115.15
13	0	0	-1.682	48.73	98.10	57.13	75.07
14	0	0	1.682	58.70	95.27	68.76	71.06
15	0	0	0	54.80	98.09	57.95	90.14
16	0	0	0	53.52	92.23	65.8	79.37
17	0	0	0	55.03	96.37	55.92	82.22
18	0	0	0	52.80	105.46	62.07	84.37
19	0	0	0	48.41	95.29	57.13	87.19
20	0	0	0	54.59	100.58	51.97	80.66

Note: Dehydration experiments were performed for the three operating variables with experimental data of the flux and selectivity for IPA-water and Et-water systems.

7.1. The experiments were performed according to the central composite rotatable design (CCRD) matrix given in Table 7.2, where the values of the independent variables x_i were coded as the variables, X_i, in the range of ±1.682 levels. The regression analysis was done by hand calculations and was later verified by commercial PC software, Statistica(R). The software was also used for generating all 3-D response surfaces, contour plots and for the optimization of responses. The optimization of the flux and selectivity of the dehydration process was aimed to establish the maximum levels within the operating variables. The system can be solved as an unconstrained problem via a penalty function approach and

numerical iteration to achieve convergence at an optimized value [Derringer and Suich, 1980].

7.5 Results and discussion

7.5.1 Modeling the responses for alcohol-water dehydration

Table 7.3 Analysis of variance for the regression models

Mixtures	Response	Source	Degrees of freedom	Sum of Squares	F-value	*p*-value
(IPA-water)	Flux, Y_1	Model	9	8420.91	66.90	<0.0001*
		Residual	10	139.85		
		Lack of fit	5	108.76	3.49	0.097
		Pure error	5	31.09		
		R^2	0.98			
	Selectivity, Y_3	Model	9	8842.97	49.04	<0.0001*
		Residual	10	200.34		
		Lack of fit	5	137.93	2.21	0.202
		Pure error	5	62.40		
		R^2	0.96			
(Et-water)	Flux, Y_2	Model	9	9181.90	29.61	<0.0001*
		Residual	10	344.55		
		Lack of fit	5	225.05	1.88	0.2520
		Pure error	5	119.50		
		R^2	0.97			
	Selectivity, Y_4	Model	9	6627.03	18.67	<0.0001*
		Residual	10	394.29		
		Lack of fit	5	309.02	3.62	0.089
		Pure error	5	85.27		
		R^2	0.94			

* Models are statistically significant ($p = 0.05$)

The effect of temperature, feed alcohol concentration and flow-rate, on the flux ($g/m^2/hr$) and selectivity for IPA-water and Et-water mixtures by PV dehydration were investigated using a CCRD response surface design model. The linear and quadratic effects of the operating variables and their interactions on the responses were obtained by analysis of variance (ANOVA). The significance of the lack-of-fit, regression and coefficient of determination (R^2) are summarized in Table 7.3 to judge the validity of the CCRD model. As shown in Table 7.3, for the IPA-water system, the value of R^2 of each quadratic polynomial regression was 0.98 and 0.96 for flux and selectivity, respectively, with no significant lack of fit at $p >$ 0.05. The results indicate that the CCRD regression model developed to predict the flux and selectivity is adequate. The regression coefficients for the flux and selectivity along with

their *p*-value are given in Table 7.4. The significance of each coefficient was determined by the *p*-value. The smaller the *p*-value is, the more significant the corresponding coefficient. In

Table 7.4 Estimated coefficients of the regression models of flux and selectivity

Effect	IPA-Water				Et-Water			
	Flux		Selectivity		Flux		Selectivity	
	Coef.	*p*- value	Coef.	*p*- value	Coef.	*p*- value	Coef.	*p*- value
Intercept	53.077	<0.0001*	99.194	<0.0001*	58.489	<0.0001*	84.029	<0.0001*
X_1	17.805	<0.0001*	-19.439	<0.0001*	18.111	<0.0001*	-7.176	0.0018*
X_2	-10.089	<0.0001*	11.737	<0.0001*	-15.056	<0.0001*	5.859	0.0062*
X_3	2.909	0.0165*	-2.076	0.1173	4.854	0.0121*	-2.052	0.2549
X_1^2	11.223	<0.0001*	-2.639	0.0491*	5.593	0.0047*	-7.362	0.0012*
X_2^2	1.748	0.1062	9.252	<0.0001*	-0.1942	0.9025	6.119	0.0041*
X_3^2	0.932	0.3663	-1.034	0.4008	1.311	0.416	-3.991	0.0365*
X_1X_2	5.941	0.0012*	-5.084	0.0093*	-9.809	0.0008*	21.166	<0.0001*
X_1X_3	2.895	0.0534	-3.054	0.0824	-2.354	0.283	3.696	0.1269
X_2X_3	7.185	0.0003*	0.509	0.7543	0.185	0.9309	1.509	0.5121

* Effects are statistically significant ($p = 0.05$)
Note: X_i represents the variables associated with coefficients in regression eq. (7.2)

In Fig. 7.2, the linear, quadratic and interaction coefficients of each operating variable are plotted in the form of Pareto charts for the flux and selectivity of the IPA-water system. The bar lengths are proportional to the absolute values of the estimated coefficient effects and are used for comparing their relative importance. The effect is significant if its corresponding bar crosses the vertical line at the $p = 0.05$ level. It can be seen in Fig. 7.2 that the linear coefficient of temperature (b_1) gives the most important effect on the flux, followed by the quadratic effect of temperature (b_{11}), and then the linear coefficient of IPA feed concentration (b_2). As for the selectivity, the linear coefficient of temperature (b_1) is the most significant, followed by the linear coefficient of IPA feed concentration (b_2), and then the quadratic coefficient of IPA concentration (b_{22}). Other significant estimated parameters in Fig. 2 can be identified easily. However, from Fig. 7.2, it can be seen that b_{13}, b_{22} *and* b_{33} are not significant (p<0.05) to the flux and b_{13}, b_3, b_{33} *and* b_{23} are not significant (p<0.05) to the selectivity. These coefficients will not be included in the regression model equations of the flux and selectivity, presented in the next section. Figures 7.2 (c) and (d) show the

comparison between the actual (from the experiments) and predicted (computed by the regression models) values of the flux and selectivity for the IPA-water system.

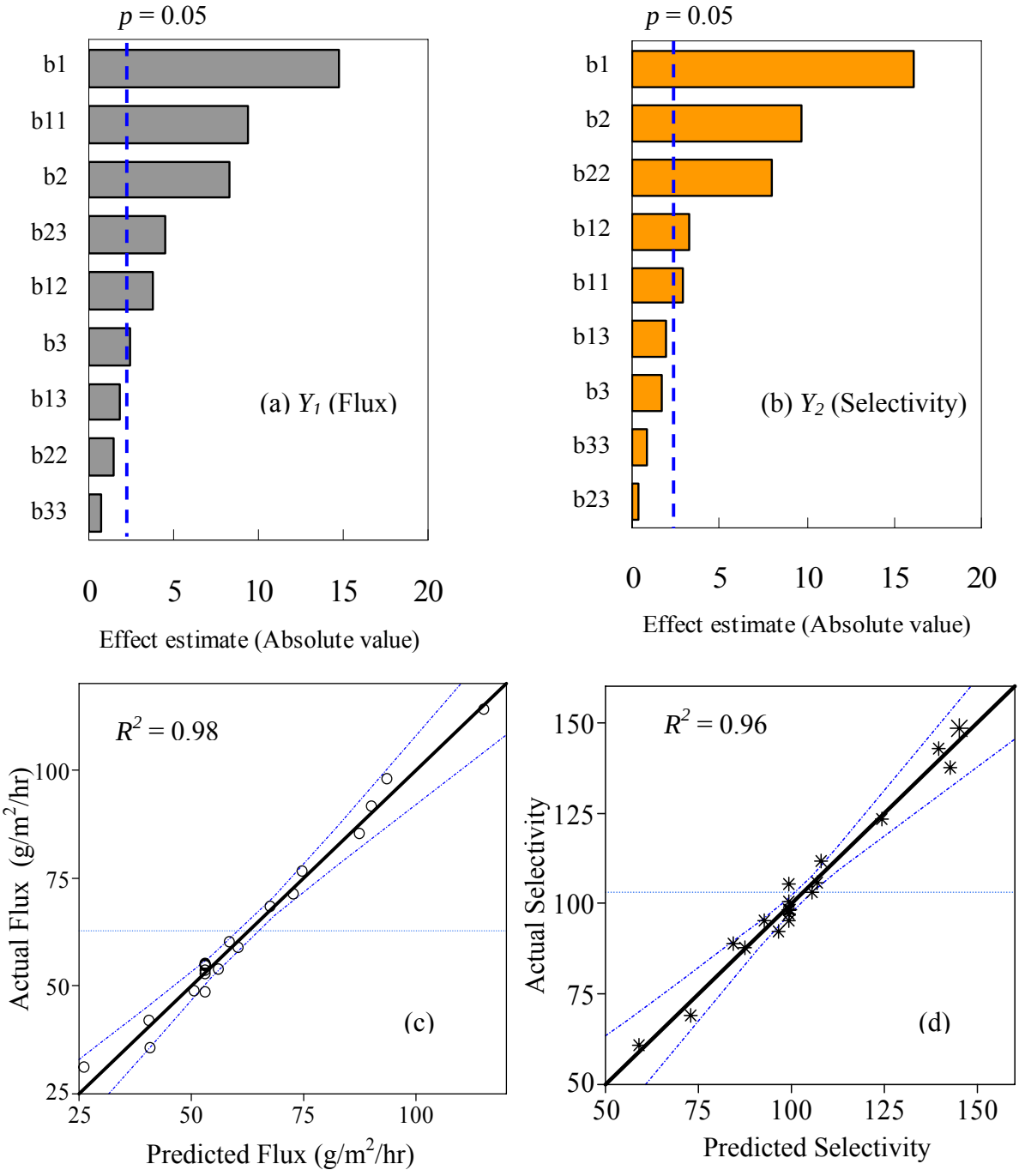

Figure 7.2: Significance of estimated coefficients *b*'s from Eq (7.2) on (a) flux and (b) selectivity of IPA-water system Actual response against predicted responses for (c) flux and (d) selectivity for IPA-water system.

The coefficients of determination (R^2) and the 95% confidence intervals (with the dotted line) are shown. Considering the R^2 values for the flux and selectivity of 0.98 and 0.96, the

regression models predict the experimental responses adequately. The residual (errors) flux and selectivity were plotted against predicted flux and selectivity in Fig 7.3. The random and

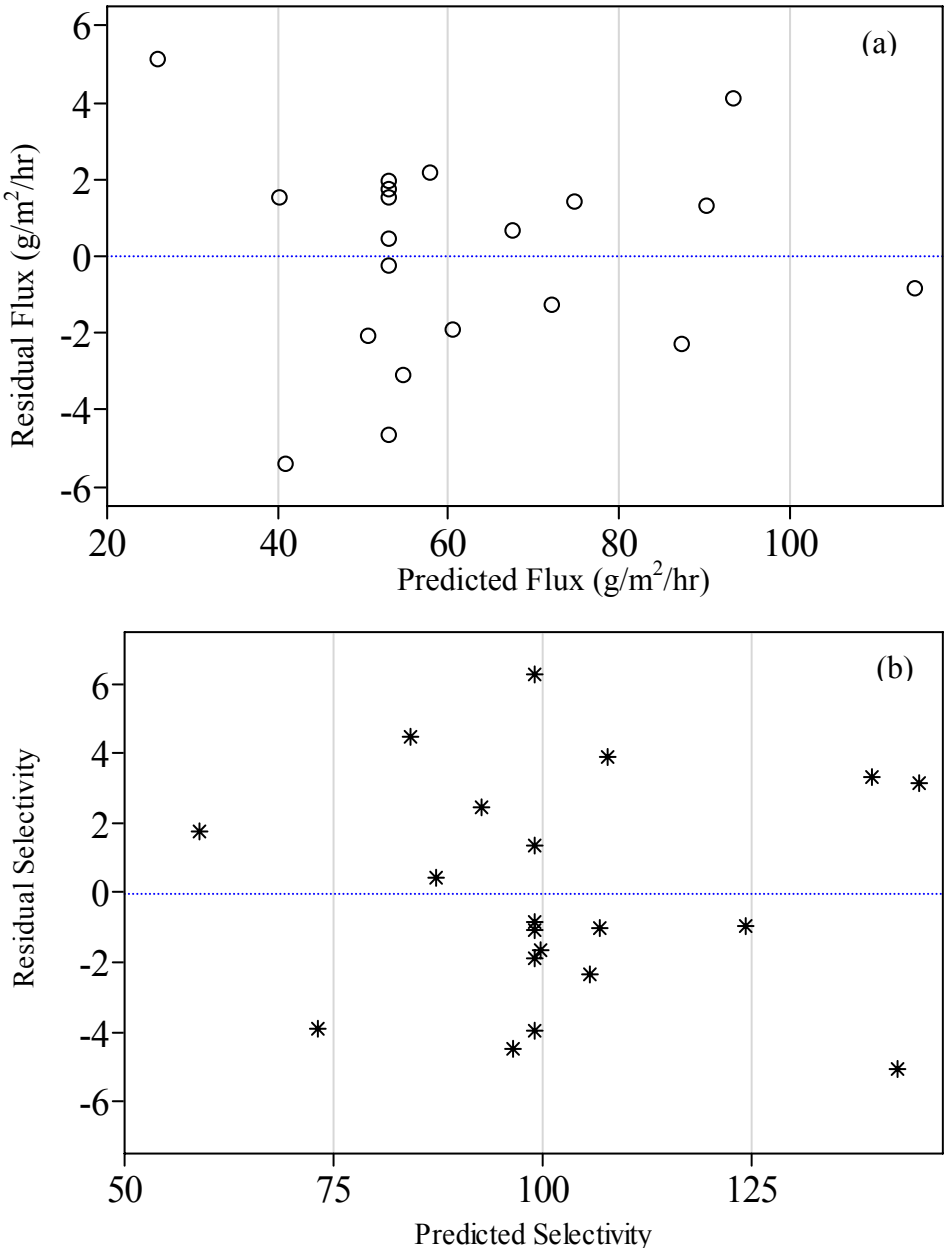

Figure 7.3: Plots of residuals against predicted responses for (a) flux and (b) selectivity of IPA-water system

even distribution of the residuals over and below the centerline suggests that the models for the flux and selectivity are statistically significant.

Similarly, the results of the Et-water system are shown in Fig.7.4. The estimated parameters effects are presented in Pareto plots in Figs. 7.4 (a) and (b). For the flux, the

linear coefficients of temperature (b_1) was found to be the most significant, followed by that of Et feed concentration (b_2). Interestingly, for the selectivity, the most significant effect was

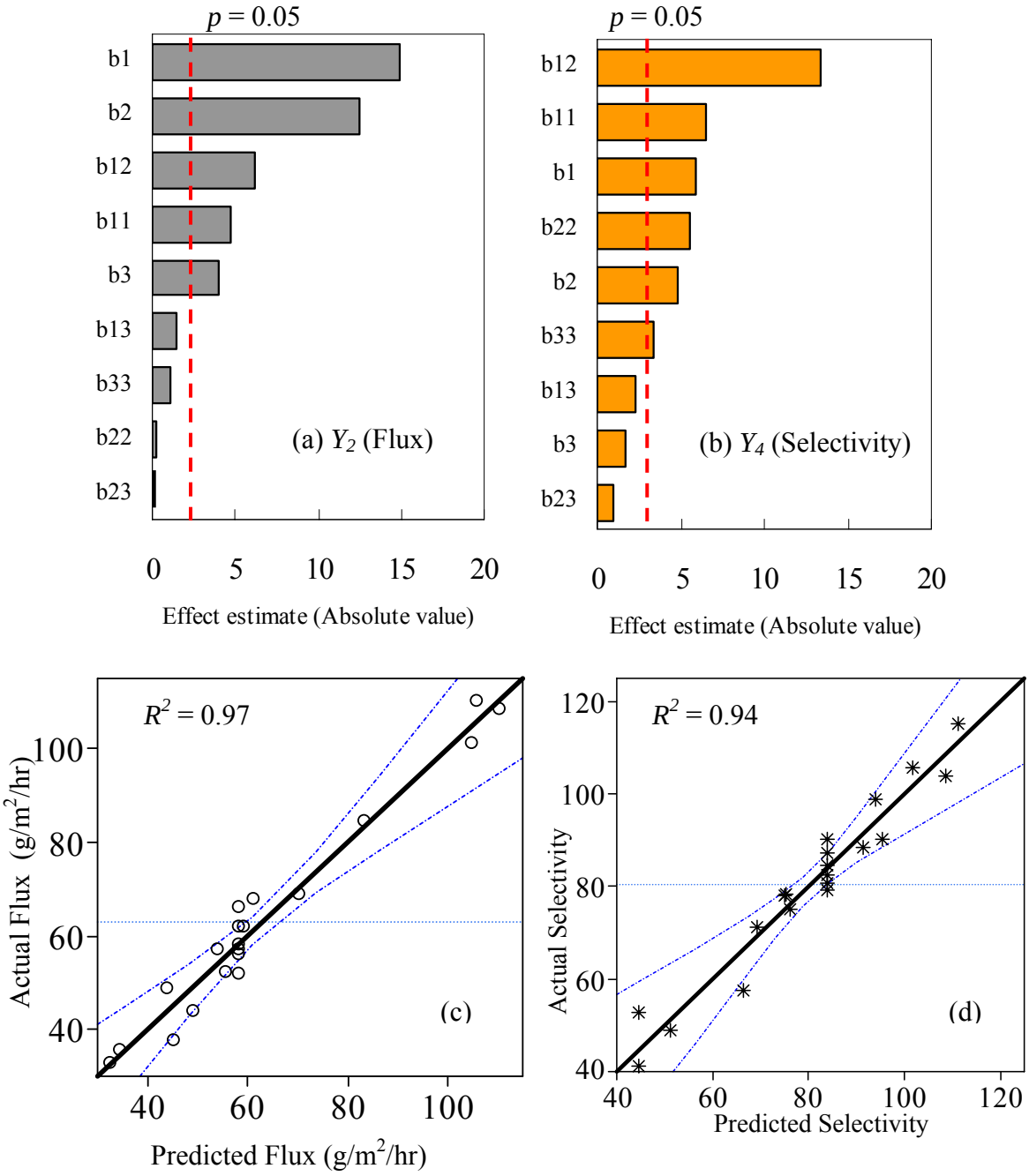

Figure 7.4: Significance of estimated parameters on (a) flux and (b) selectivity of Et-water system actual response against predicted responses for (c) flux and (d) selectivity for Et-water system

found to be the interaction coefficient of temperature and Et feed concentration (b_{12}), followed by the quadratic coefficient of temperature (b_{11}). The linear coefficient of temperature (b_1) was the third most significant parameter for the selectivity. These results

indicate that for the dehydration of the Et-water mixture it is necessary to consider the interaction of operating variables. In Figs. 7.4 (c) and (d), the actual and predicted responses

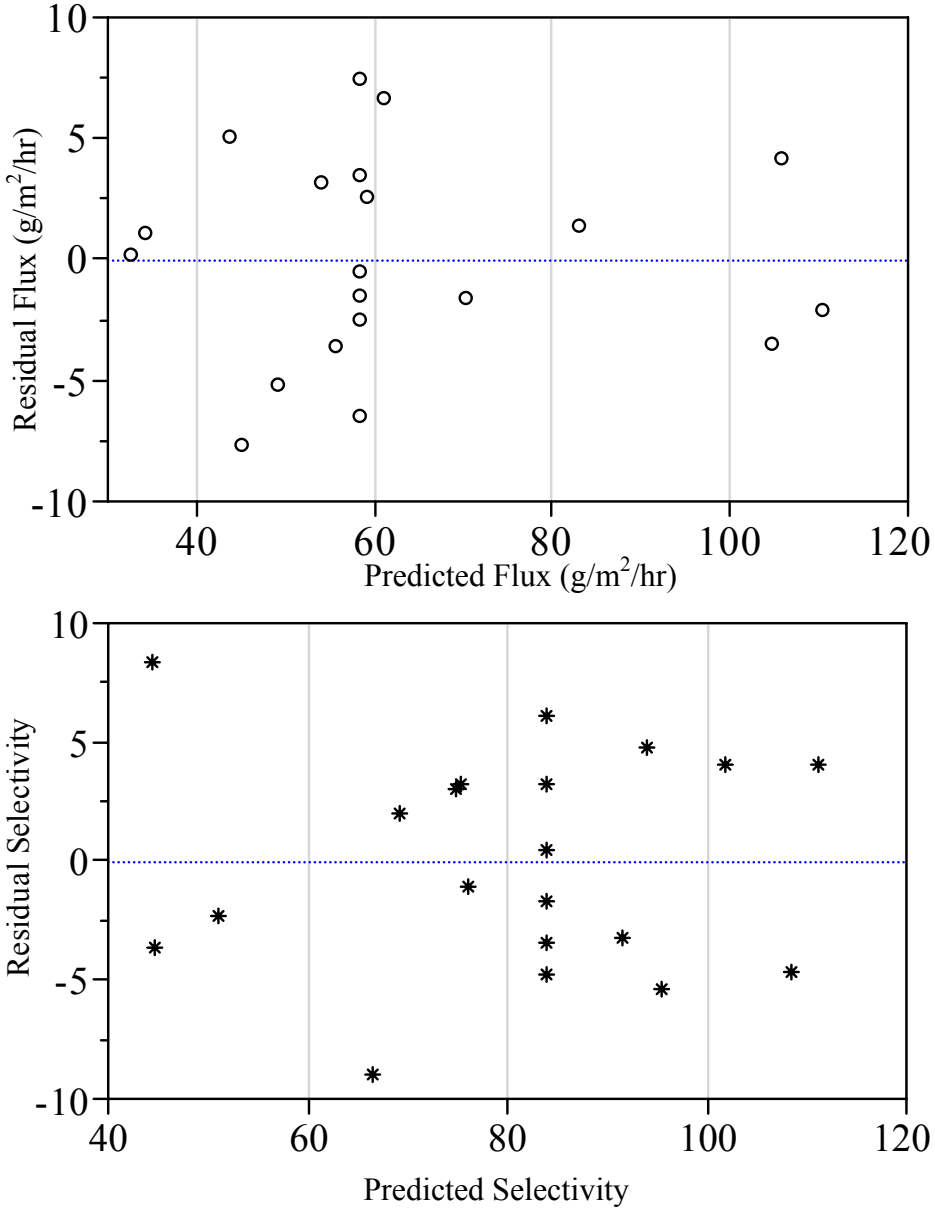

Figure 7.5: Plots of residuals against predicted responses for (a) flux and (b) selectivity of Et-water system

of the flux and selectivity are shown for Et-water dehydration (with R^2 and the 95% confidence intervals in dotted lines). As can be seen, the R^2 values for the flux and selectivity are 0.97 and 0.94 and the regression model predicts the experimental responses adequately. Also, the residual (errors) flux and selectivity are plotted against the predicted

flux and selectivity in Fig. 7.5, which are distributed evenly and randomly over and below the centerline.

7.5.2 Effect of operating variables on the flux

The experimental observations for the flux with different combinations of the operating variables are presented in Table 7.2. It varied from 31.06 to 113.89 g/m^2/hr within the ranges of variables studied. The quadratic regression equation describing the effect of the process variables on the flux in terms of coded levels of variables is given as (after neglecting non-significant coefficients)

$$\begin{aligned} Y_1 = 53.077 + 17.805X_1 - 10.089X_2 + 2.909X_3 \\ + 5.941X_1X_2 + 11.223X_1^2 + 7.185X_2X_3 \end{aligned} \tag{7.6}$$

where Y_1 is the predicted flux for the IPA–water system. The negative linear coefficient of the IPA concentration (b_2) indicates that the flux is decreased with increasing IPA concentration; while the positive coefficients of temperature (b_1) and flow-rate (b_3) indicate that the flux increases with increasing temperature and flow-rate. For the Et-water system, the quadratic regression equation of the flux is given as

$$\begin{aligned} Y_3 = 58.489 + 18.111X_1 - 15.056X_2 + 4.854X_3 \\ - 9.809X_1X_2 + 5.593X_1^2 \end{aligned} \tag{7.7}$$

where Y_3 is the predicted flux for the Et–water system. As can be seen, for the Et-water system, the flux is significantly affected by linear, quadratic and interaction coefficents of temperature.

7.5.3 Effect of operating variables on the selectivity

The experimental observations for the selectivity with different combinations of the operating variables are presented in Table 7.2. It varied from 48.82 to 147.89 within the ranges of variables studied. The quadratic regression equation describing the effect of the process variables on the selectivity in terms of coded levels of variables is given as

$$\begin{aligned} Y_2 = 99.194 - 19.439X_1 + 11.737X_2 - 5.084X_1X_2 + \\ - 2.6394X_1^2 + 9.252X_2^2 \end{aligned} \tag{7.8}$$

where Y_2 is the predicted selectivity for the IPA–water system. The positive coefficient of the IPA feed concentration (b_2) indicates that the selectivity is increased with increasing IPA feed concentration while negative coefficients of temperature (b_1) and flow-rate (b_3) indicate

that the selectivity decreases with increasing temperature and flow-rate. Similarly, for the Et-water system, the quadratic regression equation of the selectivity is given as

$$Y_4 = 84.029 - 7.176X_1 + 5.859X_2 + 21.166X_1X_2 + \\ -7.362X_1^2 + 6.119X_2^2 - 3.9916X_3^2 \tag{7.9}$$

where Y_4 is the predicted selectivity for the Et–water system. The selectivity is affected by linear and quadratic coefficients of temperature and Et feed concentration. However, only the linear coefficient of flow-rate affects the selectivity significantly.

7.5.4 3-D Response Surfaces

The surface plot helps to predict the response at any combination of operating variables. For the IPA-water system, the response surfaces are plotted with the contour lines using the regression Eqs. (7.6) and (7.8) for the flux and selectivity. In Figs. 7.6(a) - (c), the response surfaces of the flux are plotted against two operating variables while the third variable was kept constant (0 level). In Figs. 7.6(a) and (b), the flux was found to be strongly affected by temperature. The curvatures in the 3-D plots of the flux arise due to the quadratic dependency on temperature. Similar dependency of the flux was found for the IPA feed concentration as well from Figs 7.6(a) and (c). A strong interaction of temperature and IPA feed concentration was observed from the warping of the 3-D flux plot in Fig. 7.6(a). The flow-rate affects the flux only slightly at high temperatures (Figs. 7.6(b) and (c)). However, a strong interaction between feed flow-rate and IPA concentration is evident from the warping of the 3-D flux plot in Fig. 7.6(c). The 3-D selectivity plots in Figs. 7.6(d) and (f) show a strong effect of temperature and IPA feed concentration. The selectivity increases with

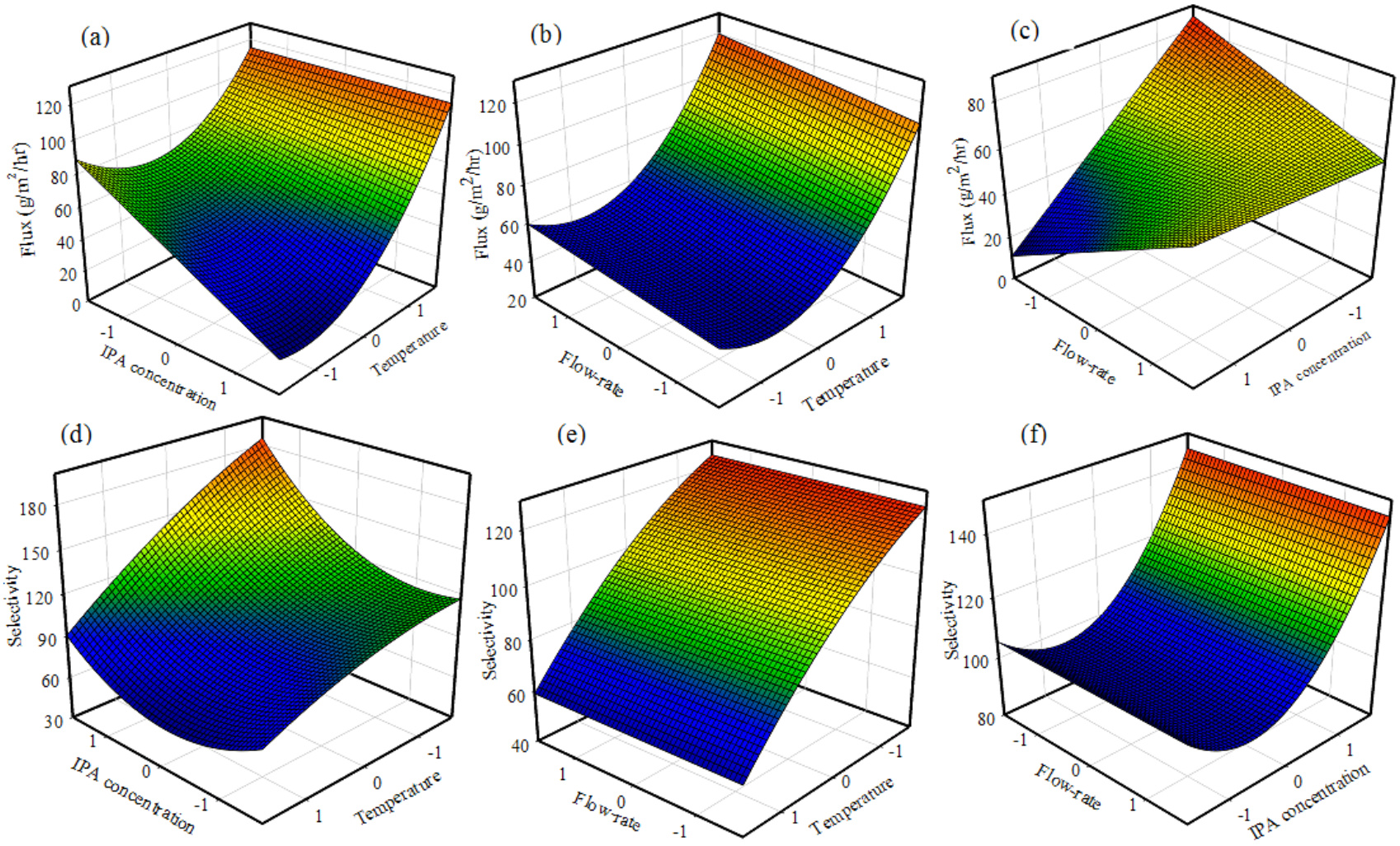

Figure 7.6: 3-D response surfaces of flux (a)-(c) and selectivity (d)-(f) against different operating variables for IPA-water system. Variables not shown in any plot was held constant at 0 levels.

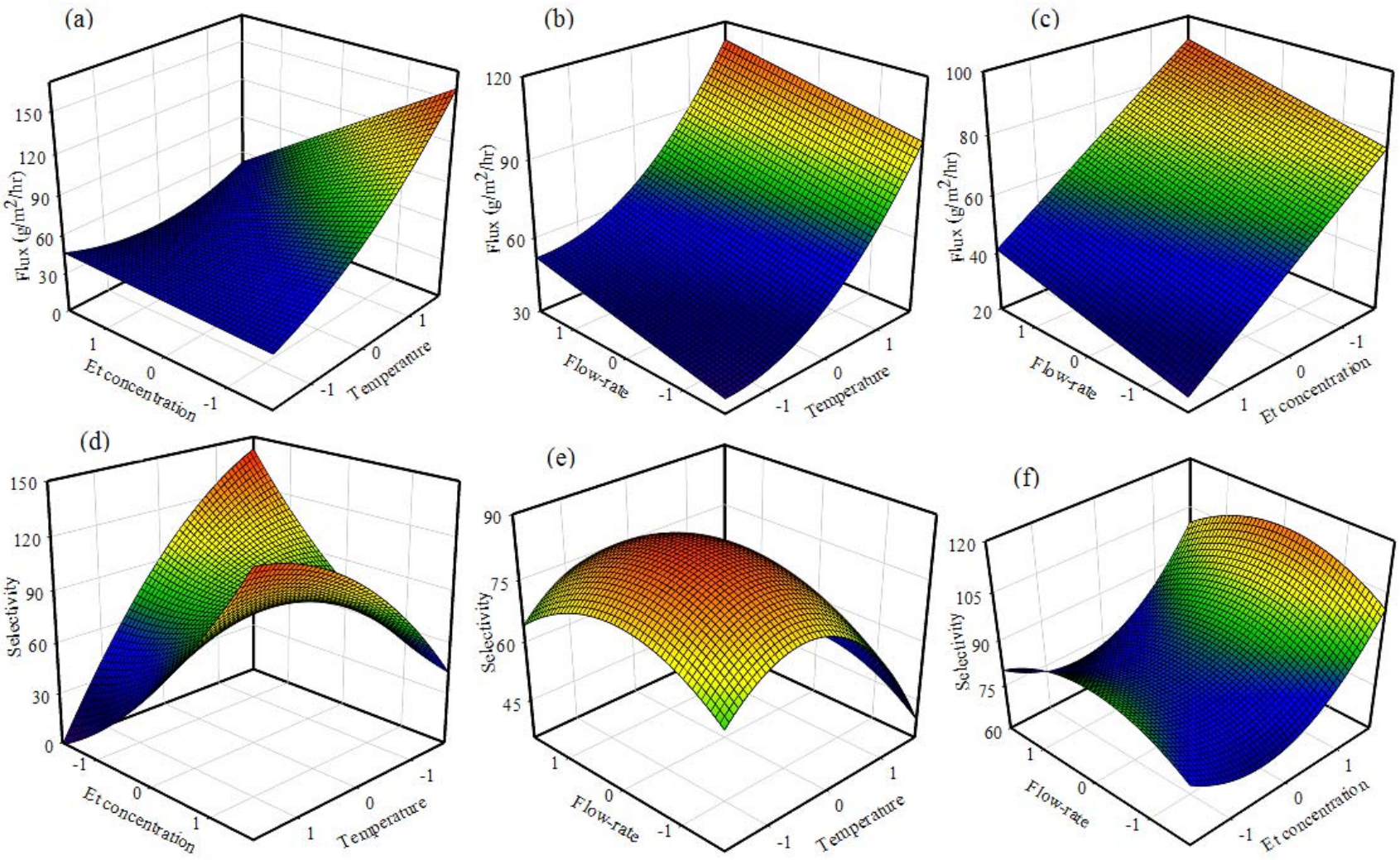

Figure 7.7: 3-D response surfaces of flux (a)-(c) and selectivity (d)-(f) against different operating variables for Et-water system. Variables not shown in any plot are held constant at 0 level.

increasing IPA feed concentration, but decreases with increasing temperature. From Figs. 7.6(e) and (f), the feed flow-rate affects the selectivity only slightly. Among the three operating variables studied, temperature is the most significant factor to affect the flux and selectivity, followed by the IPA concentration.

For the Et-water system, in Figs. 7.7(a) and (b), the 3-D plots of the flux show a strong effect of temperature. From Figs. 7.7(a) and (c), the Et feed concentration affects the flux on a linear scale, and curvatures are absent. An interaction effect on the flux can be seen in Fig 7.7(a) between temperature and Et feed concentration. From Figs. 7.7(b) and (c), the flux was affected by flow-rate only slightly. As for the selectivity, from Figs. 7.7(d) and (e), a strong effect of temperature and Et feed concentration is evident with curvatures and warping of 3-D selectivity plots. The strong interaction effect of temperature and Et feed concentration makes the 3-D selectivity surfaces warping, Fig. 7.7(d). The selectivity increases with increasing Et feed concentration at low temperatures, but decreases at high temperatures. From Figs. 7.7(e) and (f), the feed flow-rate affects the selectivity significantly. Any interaction effects of flow-rate with temperature or Et feed concentration are not visible in the 3-D selectivity plots [Figs. E.1 and E.2 in Appendix E].

The above findings revealed that temperature (X_1) was the major variable that affected the dehydration of alcohol-water mixtures. A rise in temperature helped in permeation of molecules by increasing the rate of diffusion and therefore a high flux and low selectivity was obtained. An increase in alcohol feed concentration (X_2) decreased the flux and increased the selectivity. Though the flow-rate (X_3) had lesser importance to the selectivity but it played an important role of increasing the flux. Thus, all three variables had an important role to play in the dehydration performance of alcohol-water mixtures. This finding was in accordance with the study reported by other researchers [Kang *et al.*, 1990; Huang and Feng, 1993; Yu *et al.*, 2002]. Even though these researchers used single factor experiments, their studies revealed temperature as the major factor, followed by alcohol concentration and flow-rate. However, interaction effects of temperature, alcohol concentration and flow-rate were not studied until now. As can be seen from 3-D plots for the IPA-water system, the interaction of temperature and IPA concentration (X_1X_2) was the most significant factor on the flux and selectivity, followed by the interaction of temperature

and flow-rate (X_1X_3). The interaction of IPA concentration and flow-rate (X_2X_3) affected the flux only.

7.6 Optimization

The objective of optimization was to find operating conditions that give the maximum dehydration flux and selectivity simultaneously. The desirability function approach was employed in this procedure.

7.6.1 Isopropanol-water system

For the IPA-water system optimization, the fluxes of 48 (d_k = 0) and 86 (d_k = 1) g/m^2/hr and the selectivities of 95 (d_k = 0) and 148 (d_k = 1) were selected as the minimum and maximum limits. Using these values, each individual desirability was calculated for the flux and selectivity with Eq. (7.4), then the individual desirabilities were combined to obtain the overall desirability D by using Eq. (7.5). Finally the maximum value of D was sorted out with a set of the operating variables. The set of operating variables along with the overall desirability were presented in Table 7.5. For the maximum overall desirability of 0.358, the coded levels of the operating variables are: X_1=0.589 for the temperature 56^{O}C, X_2=0.98 for the IPA concentration 90wt% IPA, and X_3=1 for the feed flow-rate 100 L/hr, with the predicted yield of 75.39 ± 5.57 g/m^2/hr for the flux, and 99.85 ± 6.32 for the selectivity.

Table 7.5 Optimization results for alcohol-water systems

Alcohol-water system	Optimized Coded level of variables			Predicted responses		Overall Desirability
	X_1	X_2	X_3	Flux (g/m^2/hr)	Selectivity	
IPA-water	0.589	0.98	1.001	75.39 ± 5.59	99.85 ± 6.32	0.36
Et-water	0.897	0.729	1.05	65.97 ± 8.37	91.35 ± 9.44	0.4
IPA-water (azeotrope)	0.056	0	0.673	56.59 ±3.34	96.12 ± 4.01	0.18
Et-water (azeotrope)	0.7	0	0.449	75.63 ± 5.41	74.82 ± 5.79	0.31

Note: For optimization of any alcohol-water systems, none of the three operating variables were held constant.

For azeotrope alcohol-water systems, the feed alcohol concentrations were held constant at 0 level, i.e., 87.5wt% IPA for IPA-water and 95.5wt% Et for Et-water system. Overall desirability was calculated using Eq. (7.5).

7.6.2 Ethanol-water system

For the Et-water system optimization, the fluxes of 52 ($d_k = 0$) and 105 ($d_k = 1$) g/m^2/hr, and the selectivities of 65 ($d_k = 0$) and 116 ($d_k = 1$) were selected as the minimum and maximum limits, respectively. Using the desirability approach described above, the overall desirability (D) was maximized for a set of operating variables. Results in Table 7.5 show that for the overall maximum desirability of 0.4, the coded levels of the operating variables are: X_1=0.897 for the temperature 59^{O}C, X_2= 0.729 for the Et feed concentration 96.6wt%, and X_3=1 for the feed flow-rate 102 L/hr, with the predicted yield of 65.97 ± 8.37 g/m^2/hr for the flux, and 91.35 ± 9.47 for the selectivity.

7.6.3 Azeotropic mixtures of alcohol-water

The overall desirability function was applied to find a set of operating temperatures and feed flow-rates that gave a maximum flux and selectivity for the dehydration of azeotropic alcohol-water mixtures (87.5wt% IPA in the IPA-water system and 95.5wt% Et in the Et-water system). Under this condition, the alcohol feed concentrations were held constant during optimization. For the IPA-water system, the temperature and flow rate were found to be 0.056 (50.5^{O}C) and 0.673 (93.5 L/h) with an optimized flux and selectivity of 56.59 ± 3.34 g/m^{2}hr and 96.12 ± 4.01, respectively, for an overall desirability of 0.18. On the other hand, for the azeotropic Et-water dehydration, the optimized temperature was 0.7 (57^{O}C) and flow-rate was 0.449 (89 L/hr) with a flux of 75.63 ± 5.41 and selectivity of 74.82 ± 5.79 for an overall desirability of 0.31. It is interesting to note that, the overall desirability was higher for the Et-water system as compared to the IPA-water system. This finding suggests that if experiments were performed for the azeotropic Et-water dehydration, the flux and selectivity data would match the predicted responses with greater confidence.

7.6.4 Verification

To ensure the predicted flux and selectivity are not biased, experimental rechecking was performed using the set of operating variables presented in Table 7.5. For example, for the IPA-water azeotropic mixture, the experimental flux and selectivity were 59.18 g/m^2/hr and 102.10 compared to the predicted flux and selectivity of 56.59 g/m^2/hr and 96.12. For the Et-water azeotropic mixture, the experimental flux and selectivity were 72.26 g/m^2/hr and 77.31, compared to the predicted flux and selectivity of 75.63 g/m^2/hr and 74.82. These experimental results were in agreement with the predicted responses within reasonable

accuracy (errors within 3-6%). The good correlations between these results confirmed that the regression model was adequate to describe the influence of the selected dehydration operating variables on PV flux and selectivity.

7.7 Conclusions

The effects of operating temperature, feed alcohol concentration and feed flow-rate were studied with the response surface methodology in PV dehydration of alcohol-water mixtures. A central composite rotatable design was used for regression modeling and optimizing the PV operating variables. Predicted values from the quadratic regression model equations were found to be in good agreement with observed values (R^2 value for flux and selectivity is 0.98 and 0.96 for the IPA-water system and 0.97 and 0.94 for the Et-water system, respectively). The CCRD regression model allows confident flux and selectivity predictions by interpolation over the range of data that was used to construct 3-D flux and selectivity surface plots. For both alcohol-water systems, the curvatures and warpings in the 3-D surface plots suggested strong interaction effects of the operating variables on flux and selectivity. The temperature has a significant effect on the flux and selectivity whilst the flow-rate has an insignificant effect. For the Et-water system, a strong interaction effect of feed ethanol concentration and temperature was observed on the selectivity. The interaction of temperature and alcohol feed concentration significantly affected the flux of the IPA-water system. For the dehydration of azeotropic alcohol-water mixtures, the predicted flux and selectivity agreed reasonably well with experiments with errors within 3-6 %. In addition to establishing optimal flux and selectivity, RMS also makes it possible to predict the responses if the composition of the variables is altered in some way, by using the quadratic model. This study demonstrates that CCRD can be successfully applied to modeling and optimizing the operation for PV dehydration that may save considerable time and resources to perform experiments.

CHAPTER 8

8.1 General Conclusions and Contributions to Original Research

Pervaporation membranes (non-porous) were studied in this work to understand the effect of crosslinking on the physicochemical properties and the dehydration behavior which is crucial for industrial applications. A combination of FTIR and X-ray spectroscopy, differential scanning calorimetry, atomic force microscopy and contact angle measurements is used to investigate the physiochemical properties of the poly(vinyl alcohol) based membranes. Permeation behaviour of the alcohol-water mixtures through the membranes were investigated by the solution-diffusion theory. An empirical regression model based on response surface methodology was also developed to study the effect of operating variables for the separation of azeotropic alcohol-water mixtures. The following conclusion can be drawn from this research:

1. Dense hydrophilic poly(vinyl alcohol) membranes were crosslinked thermally and chemically (with glutaraldehyde, trimesoyl chloride). The degree of crosslinking was characterized by ATR-FTIR and X-ray spectroscopy. Results showed that the degree of crosslinking increased with concentration and reaction time of crosslinking. PVA membranes showed an increase in the melting point and mechanical strength after crosslinking.

2. Atomic force microscopy (AFM) was employed to study the surface structures of the polymeric membranes. Topographic images from the AFM experiments showed that the uncrosslinked membrane surfaces possess nodular sized (nm) structures. However, the nodular structures were found to disappear after crosslinking and random rough surface structures was observed. The roughness of the membrane surface was calculated and found to be within 8-65 nm. Crosslinked membrane showed higher surface roughness than uncrosslinked membrane.

3. Poly(vinyl alcohol) based membranes studied in this research are hydrophilic in nature. Water contact angle results showed that the membrane surfaces hydrophilic decreases after crosslinking [with increasing crosslinking concentration as well as reaction time]. However, the apparent contact angles were within 45-65^{O}. Study of advancing and receding contact angle revealed that the contact angle hysteresis increased with degree of crosslinking.

4. For PVA–PSf composite membranes, the effect of selective PVA layer thickness were studied on the separation behavior of ethanol–water mixtures. An increase in selective layer thickness markedly decreased the total flux and the water mass transfer coefficient. The decrease in flux is more prominent at low ethanol concentrations in the feed than at higher ethanol concentrations. Results agreed with the S-D theory and the mass transfer resistance varies linearly with thickness. Analysis of the mass transfer resistance showed that the crosslinking resistance could be significant for thin membranes. Statistical analysis showed that the flux is significantly affected by the thickness of the PVA layer, but the selectivity is not. The selectivity was also shown to be affected by surface properties after membrane crosslinking, especially when the membrane is thin.

5. Effects of chitosan content on the separation performance of CS-PVA blend membranes were studied for ethylene glycol dehydration. Good blend compatibility was confirmed by DSC and XRD, whereas successful crosslinking was confirmed by ATR-FTIR. Pervaporation dehydration results show high flux and selectivity of the blend membranes, especially when the CS amount is between 70-80 wt%. With increasing temperature, the total flux increased markedly without a significant drop in selectivity. However, the selectivity was found to decrease markedly when the feed water concentration was above 20 wt%. The flux and selectivity was slightly affected by feed flow-rate and presence of concentration polarization was observed due to highly viscous EG-water mixture.

6. Trimesoyl chloride crosslinked thin PVA composite membranes were prepared for the pervaporation dehydration of ethylene glycol-water mixtures. PVA layers were successfully crosslinked with TMC using varying concentration and reaction time as suggested by ATR-FTIR measurements. For EG-water dehydration, the total flux was found to decrease with an increase in TMC concentration and reaction time. At high water fractions in the feed mixtures, the decrease in flux is more prominent due to low swelling. Selectivity was found to increase with increasing TMC concentration and reaction time. A diffusivity correlation was developed combining the thermodynamics of irreversible process and UNIQUAC theory in this study. The diffusion coefficient of water from the diffusivity correlation (with component interaction) was found to be lower by at least two orders of magnitude than simple S-D theory with no interaction.

7. The effects of separation temperature, feed alcohol concentration and feed flow-rate were studied with the response surface methodology in dehydration of alcohol-water mixtures. A central composite rotatable design (CCRD) was used for regression modeling and optimizing the PV operating variables. Predicted values from the quadratic regression model equations were found to be in good agreement with observed values (for IPA-water system, $R^2 = 0.98$ for flux and $R^2 = 0.96$ for selectivity). The CCRD regression model allows confident flux and selectivity prediction by interpolation over the range of data. The results show that the temperature has a significant effect on flux and selectivity whilst the flow-rate has an insignificant effect. For ethanol-water system, a strong interaction effect of feed ethanol concentration and temperature was observed on selectivity. The interaction effect of temperature and concentration was found to be significant as well compared to the interaction of flow-rate and temperature or flow-rate and concentration. For the dehydration of azeotrope alcohol-water mixtures, the predicted flux and selectivity agreed reasonably with experiment performed with the optimized process variables (temperature and flow-rate). This study demonstrates that CCRD can be successfully applied to modeling and optimizing process variables for PV dehydration that may save considerable time and experiments to perform.

8.2 Recommendations for Future Work

The effect of crosslinking on the physicochemical properties of hydrophilic poly(vinyl alcohol) based membranes were investigated and correlated to the pervaporation flux and selectivity of alcohol-water dehydration. It was found that membrane performances in pervaporation are affected by physicochemical properties as well operating conditions. While the physicochemical properties of membranes are measured parameters (strictly speaking, properties are not independent parameters), the operating conditions can be controlled independently within reasonable accuracy. For example, the physiochemical properties such as surface roughness and hydrophilicity were found to be dependent on each other. Therefore, recommended future work to study polymeric membranes for pervaporation can be divided into two major parts: (1) improvement of membrane materials and (2) separation of real life streams

8.2.1 Improvement of membrane materials

- **The effect surface roughness**

The study the effect of surface roughness independently, membrane films can be casted onto glass substrate of varying surface roughness. A simple way to prepare glass substrate of varying roughness is to use microgrit sandpaper (8 to 60 μm particle diameters). This will allow studying the effect of surface roughness on flux and selectivity without affecting other physiochemical properties, systematically.

- **The effect of crystallinity**

The crosslinked membranes showed a decrease in crystallinity. Permeation in polymeric membrane occurs through glassy regions and crystalline regions hinder permeation. Blending seems to be an effective approach to control the crystallinity for optimum flux and selectivity. A combination of glassy and rubbery polymer can be studied to achieve optimum crystallinity for better permeation.

- **The effect of free volume in dense membrane**

Diffusion in dense membrane depends on the free volume of the polymer. The effect of crosslinking, blending can alter the free volume and thereby the permeation behavior of a membrane. Therefore, direct measurement of the free volumes in polymers would be useful to predict the transport mechanism. The membrane performance can be improved by optimizing the structure to reduce the mass transfer resistance of permeation. Choosing a polymeric membrane with optimum free volume may achieve high flux and selectivity. A special physical technique, positron annihilation spectroscopy (PAS) can be used to measure free volumes at the atomic and molecular levels as a function of chemical changes and molecular modifications in an interfacial polymerized membrane system.

8.2.2 Separation in real-life streams

Most studies in this work were carried out at a relatively constant concentration along the feed side of the membrane. From an engineering standpoint, it is recommended that the separations of different feed mixtures (e.g., ternary mixtures) are investigated to evaluate the recovery and productivity of the separation process. A ternary mixture such as salt-alcohol-water mixture can be studied which is very common in separation industries.

APPENDIX A

A.1 Laboratory pervaporation apparatus

The prepared membranes were tested for pervaporation dehydration on a setup shown in Fig. A.1.

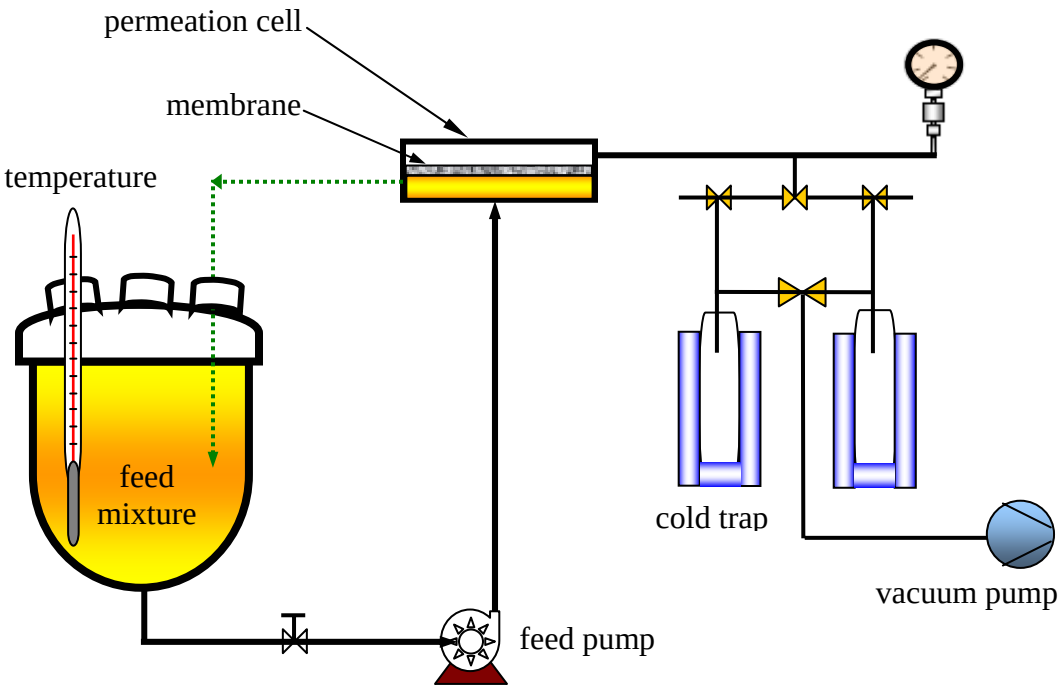

Figure A.1: Schematic representation of pervaporation equipment.

Pervaporation experiments were conducted for alcohol-water systems. Dehydration experiments were performed with flat sheet membranes (with an effective membrane area 20.2 cm^2). The feed solution was circulated with a pump (Magnetek Universal Electric, MI, USA) through the membrane surface in the cell and returned back to the circulation. The feed flow-rate was varied with a control valve. Partial vacuum was applied to the permeate side as a driving force for diffused solvents to evaporate easily. The feed pressure was at atmospheric pressure while the pressure on the permeate side was kept below 3 mbar using a vacuum pump (Leeson Electric Co., WI, USA). To achieve a steady-state at a given temperature, the experiment was run for two hours prior to collection of permeates. To assess experimental errors, each experiment was repeated three times. The permeate vapor was condensed and collected in a cold trap (glass tube) immersed in liquid nitrogen for

about 10-20 minutes. The permeate was then heated to room temperature and weighed to determine the mass. The separation temperature was varied with a temperature controller (accuracy ± 2^{O}C). Analysis of the mixture composition from the permeate side was conducted by a gas chromatograph with a thermal conductivity detector (TCD) (HP 5890 Series II, USA).

A.2 Membrane cell

The stainless steel membrane cell (diameter 210 mm, height 90 mm) was designed by Prof. Huang and built by the University of Waterloo workshop staff (Fig. A.2).

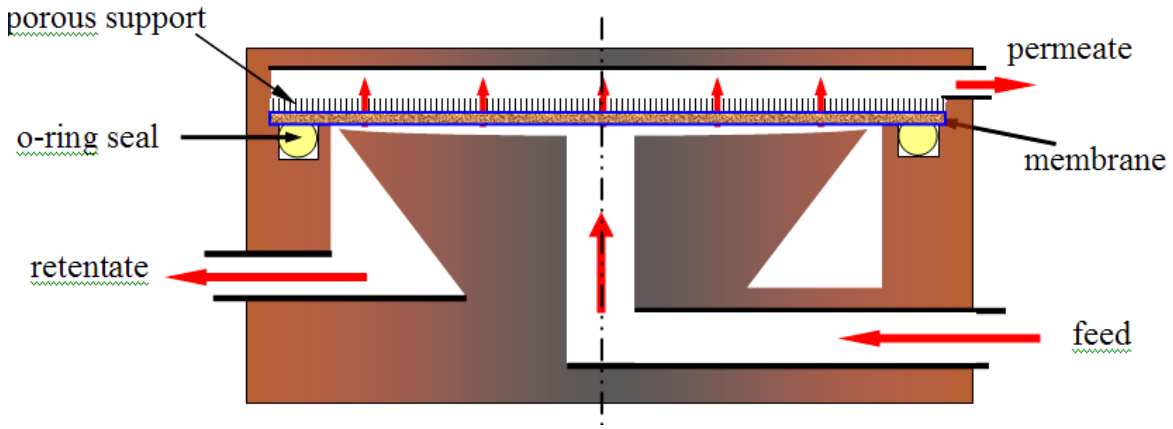

Figure A.2: Schematic of the permeation cell.

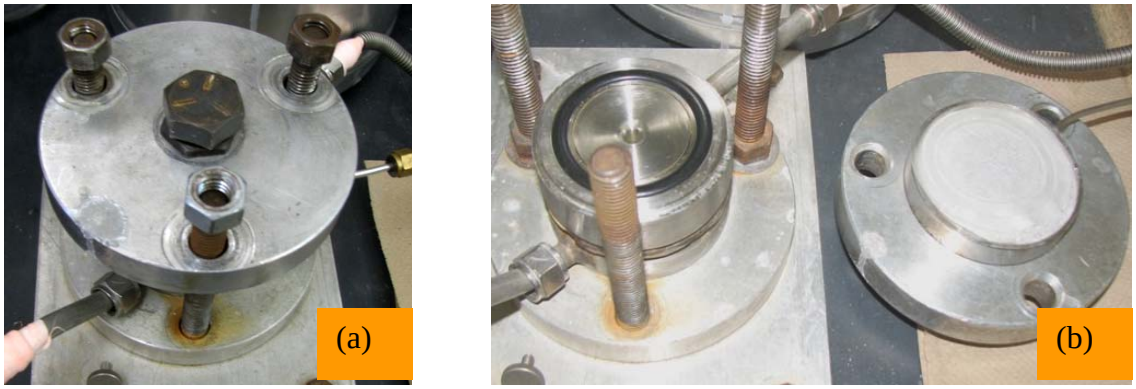

Figure A.3: Membrane permeation cell (a) permeate chamber and (b) open permeate chamber.

The upper section of the membrane cell had a filter cloth support (Fig. A.3). Thin film membranes need to be supported (to prevent perforation) without inhibiting vapor permeate removal on the downstream side. The inert filter cloth removed the possibility of organic molecules being attracted to the support, which would hinder permeation and evaporation into the permeate stream [Huang, 1991].

The lower section of the membrane unit contained O-ring seals (Fig. A.3, black o-ring). The rim of the perforated plate, and plate recesses were lubricated with Glisseal® before the unit was put together for each run.

A.3 Membrane

A circular template was used to cut each membrane to use in the permeation cell. The effective membrane area was 20.2 cm^2. Membranes were pre-soaked in feed solution for a minimum of 48 hours to minimize the time to reach steady-state. The dry and wet weight x6 microbalance measurements), thickness (x6 random digital micrometer screw-gauge measurements) and diameter across four quadrants (calipers) were measured for each membrane. The pre-soaked membranes were placed on the lower section of the permeation cell. The unit was then bolted together and the in/outlet lines connected. The entire membrane unit and feed lines were covered in insulation.

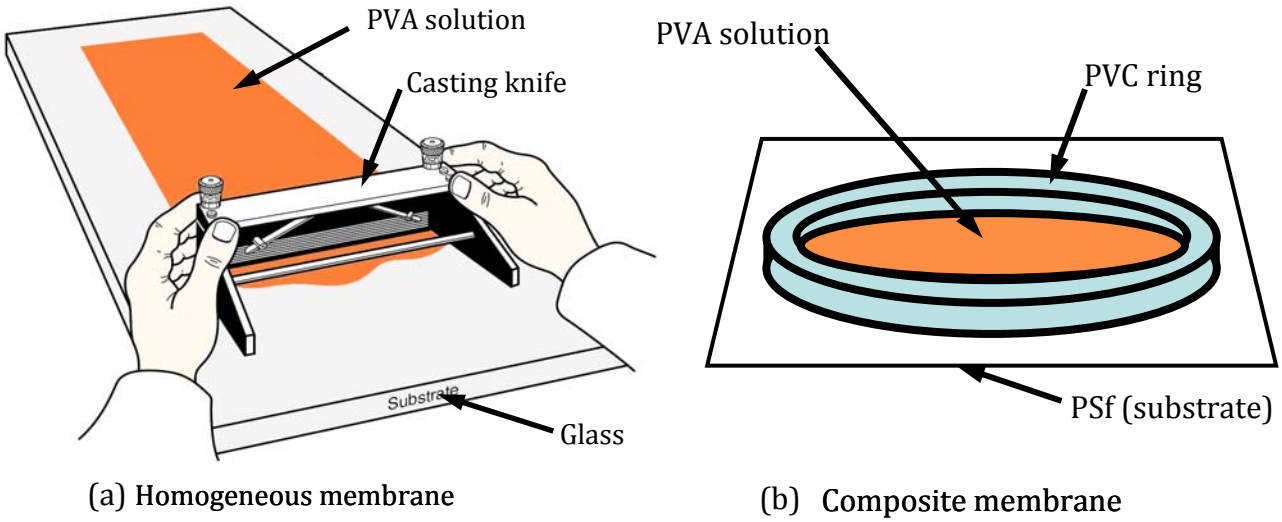

(a) Homogeneous membrane (b) Composite membrane

Figure A.4: Membrane preparation (a) film casting (b) composite film casting.

PVA film was casted on a glass substrate as shown in Fig. A.4(a) and the composite PVA-PSf membrane was prepared by pouring the PVA solution on top of PSf substrate as shown in Fig. A.4(b). Homogeneous PVA membrane appeared to be transparent whereas PVA-PSf composite membrane appeared to be opaque white due to the poly(sulfone) support layer. Blended CS-PVA membrane appeared to be slightly yellowish in color.

A.4 Atomic force microscopy

Atomic force microscopy (AFM) is becoming increasingly important in polymer characterization with regard to both surface topography and surface mechanical properties. A commercial AFM (PicoScan, Molecular Imaging, Tempe, AZ, USA) was employed in the surface microscopy study. The instrument is capable of both contact and non-contact modes of operation, including force modulation imaging and tapping mode imaging. Of particular interest in determining topography and phase morphology in polymer films is tapping mode AFM. In tapping mode, the silicon probe tip oscillates at its resonance frequency as it rasters across the sample surface, experiencing only intermittent contact with the surface. The scanning scales can be used ranging from 0.1 μm to 6.5 μm.

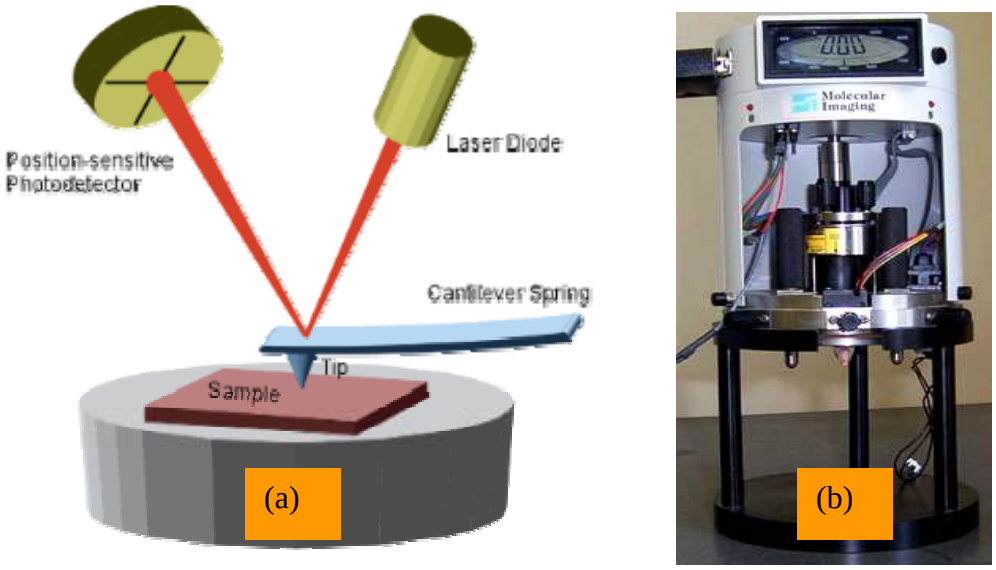

Figure A.5: (a) Schematic representation of AFM operation and (b) Picoscan® AFM

Tapping mode technique in AFM allows high resolution topographic imaging of sample surfaces that are easily damaged, loosely held to their substrate, or difficult to image by other AFM techniques. Tapping mode overcomes problems associated with friction, adhesion, electrostatic forces, and other difficulties that plague conventional AFM scanning methods by alternately placing the tip in contact with the surface to provide high resolution and then lifting the tip off the surface to avoid dragging the tip across the surface. As shown in Fig A.5, tapping mode imaging is implemented in ambient air by oscillating the cantilever assembly at or near the cantilever's resonant frequency using a piezoelectric

crystal. The piezo-drive causes the cantilever to oscillate with a high amplitude (typically greater than 20 nm) when the tip is not in contact with the surface.

The oscillating tip is then moved toward the surface until it begins to lightly touch, or tap the surface. During tapping mode operation, the cantilever oscillation amplitude is maintained constant by a feedback loop. Selection of the optimal oscillation frequency is software-assisted and the force on the sample is automatically set and maintained at the lowest possible level.

A.5 Contact angle experiment

Sessile drop contact angle measurements using ADSA-P could be performed as a function of time. A small drop of water was placed at the center of the membrane surface. The sample chamber was kept saturated during the measurement. The sample was mounted on a glass slide and the syringe was connected to a motor-driven programmable controller. An initial drop with a radius of around 2.5 mm was deposited onto the sample surface so as to ensure that the drop was axisymmetric. While using the motor-driven syringe to pump liquid steadily into the sessile drop from below the surface, a sequence of images of the growing drop were captured and the advancing contact angle was obtained. Subsequently, withdrawing the liquid from the drop, the receding contact angle was obtained. The advancing/receding rate used was 2 μl per second. All advancing and receding contact angle measurements were repeated three times and the results were averaged. For static contact angle, the initial drop volume was kept constant.

A schematic of the ADSA setup is shown in Fig. A.6. When using ADSA, it is important to acquire good quality images so that the accuracy of selecting coordinate points along the experimental drop profile can be guaranteed. In ADSA-P, a high-resolution camera is mounted on a microscope. The drops are illuminated from behind, using a white-light source. The illuminating light travels through a heavily frosted diffuser in order to minimize the heat absorption into the drop, and also to provide a uniformly lit background, which produces high contrast in the acquired images. The video signal of the sessile drop is transmitted to a digital video processor or an image processor (such as Parallax XVideo board or ITI image processor), which performs the task of frame grabbing and image digitization. The digitized image contains data in form of pixels. Usually, there are

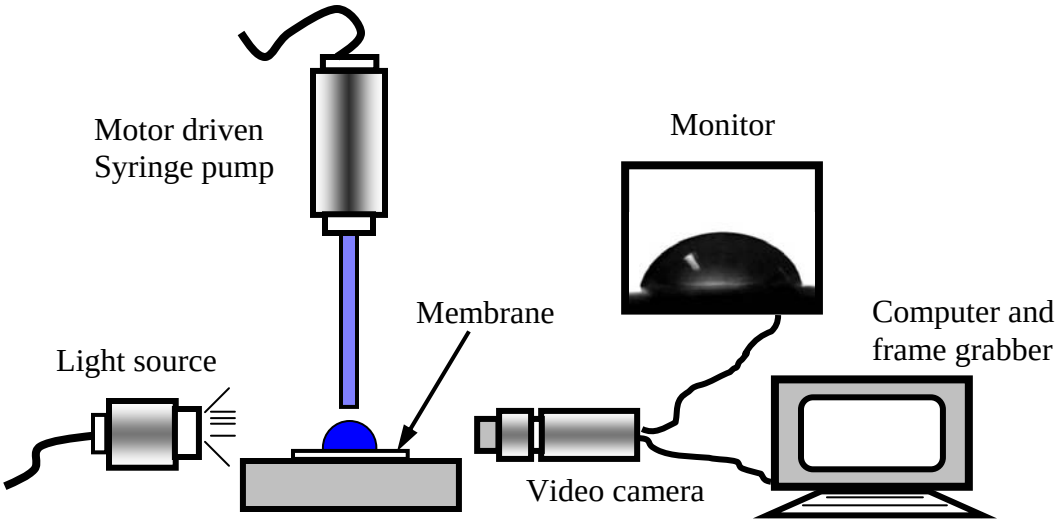

Figure A.6: Schematic of contact angle measurements

640 x 430 pixels in an image with each pixel having a value ranging from 0 (i.e., black) to 255 (i.e., white), which represents the intensity or gray level at the corresponding position. In other words, a digitized image is mathematically represented by an array of integer numbers from 0 to 255. In this fashion, a computer (such as a personal computer) can acquire images of a drop through the digital camera, and perform the image analysis and computation on the acquired images. It is important to note that the experiment is performed on a vibration-free table, in order to isolate the system from any possible external vibration.

In-house developed image analysis software, CAMADS, was used to measure contact angles of sessile drops and liquid lenses. Its basic principle is to employ an image analysis scheme, with edge detection in sub-pixel resolution, to extract edge profiles from a drop image with 256 gray levels. Then a geometric algorithm is adopted to locate intersection points and one of six curve-fit methods is used for calculating contact angles with high accuracy. CAMADS can be used to analyze any portions of regular and irregular drop shapes. Using a batch-processing function, the user can deal with a stack of images once initial drop shape profile has been detected.

For rough and heterogeneous polymer surfaces, it is commonly observed that for the sessile drop method, if one measures the contact angle of a liquid drop being advanced slowly over a surface and then makes the drop retreat along its previous path, the two contact angles observed are different. The former is called the advancing contact

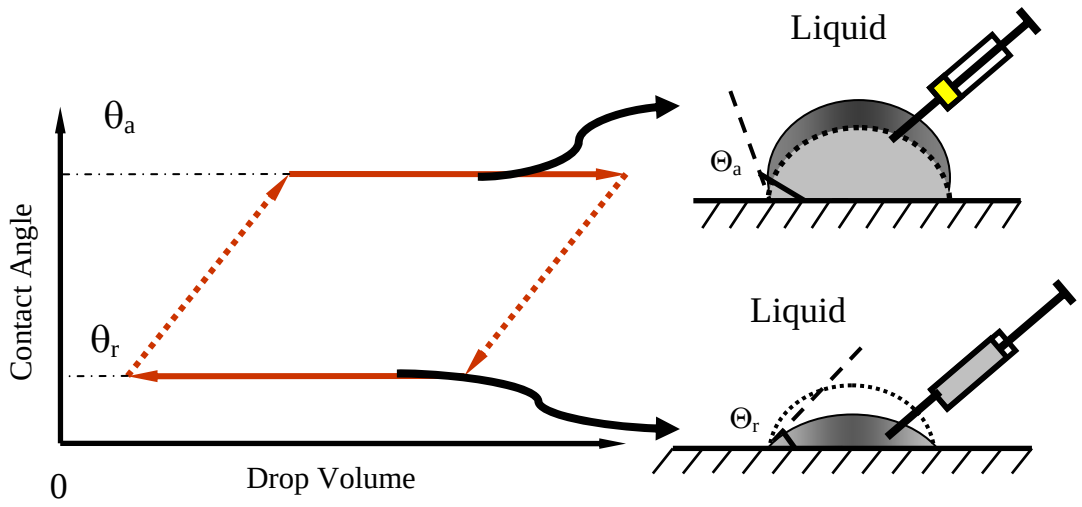

Figure A.7: Schematic representation of contact angle hysteresis.

angle, θ_a and the later the receding contact angle, θ_r. The difference in the advancing angle and the retreating angle is called contact angle hysteresis as shown in Fig A.7. Contact angles on polymer surfaces are not only influenced by the interfacial tensions according to Young's equation but also by many other phenomena, such as surface roughness, chemical heterogeneity, sorption layers, molecular orientation, swelling, and partial solution of the polymer or low-molecular constituents in the polymer material [Andrade, 1985; Franken *et al*, 1987].

E.6 AFM results

Some of the topographic images are shown in Fig A.8 and A.9 for the homogeneous, composite and blend membranes. As can be seen from the images, there is not any particular features visible on the surface such as symmetric nodular structure when the membranes were crosslinked. As a result, only the surface roughnesses were calculated from the AFM image analysis and were correlated to membrane separation performance.

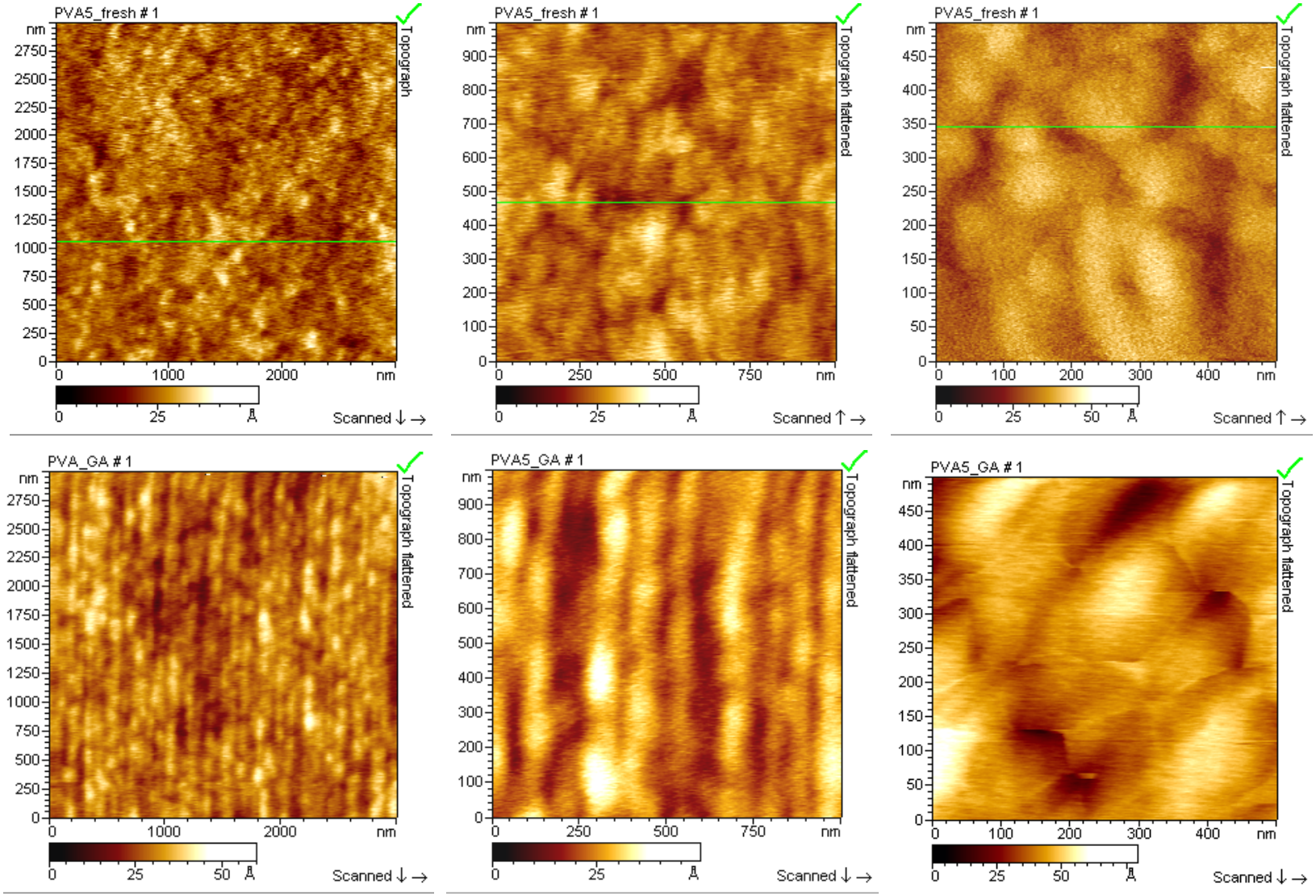

Figure A.8: AFM topographic (surface) images of PVA membranes.

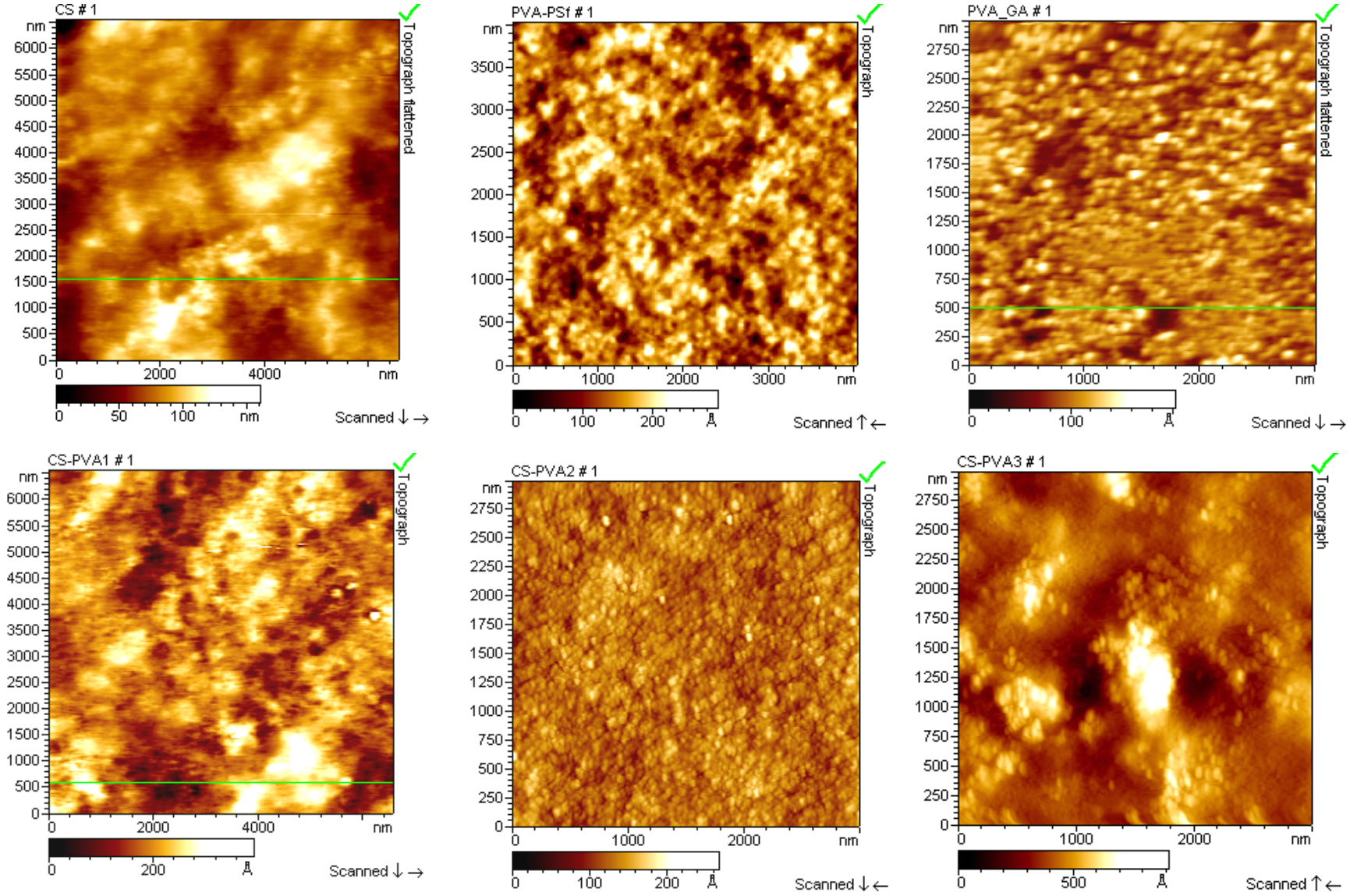

Figure A.9: AFM topographic (surface) images of polymeric membranes.

APPENDIX B

Solution properties of multicomponent polymer solutions

B.1 Introduction

The different physical properties of polymer solutions which will be used during this study will be discussed in this chapter. These include properties of pure components as well as of mixtures. Depending on process conditions, it is sometimes more appropriate to use mass fractions compared to volume fractions or vice versa. To transform these quantities into each other, the density must be known as a function of composition. Different experimental techniques are used in this thesis which requires a transformation of the measured signal to a physical quantity related to composition and total mass or volume. The viscosity of the pure solvents and binary mixtures were presented as well. Since in the studied system, diffusion plays a dominant role, diffusion coefficients have to be obtained from literature, experiments or predictive relationships.

B.2 Pure component properties

B.2.1 Polymers

In the study described in this thesis, three types of polymers will be used: polyvinyl alcohol (PVA), Chitosan (CS) and polysulfone (PSf). Polyvinyl alcohol was used throughout this work. Chitosan was used in the blended membrane studies in chapter 5 and polysulfone was used as the porous support for the PVA-PSf composite membranes in chapter 4 and 6. Properties of PVA, CS and PSf have been summarized in Table B-1.

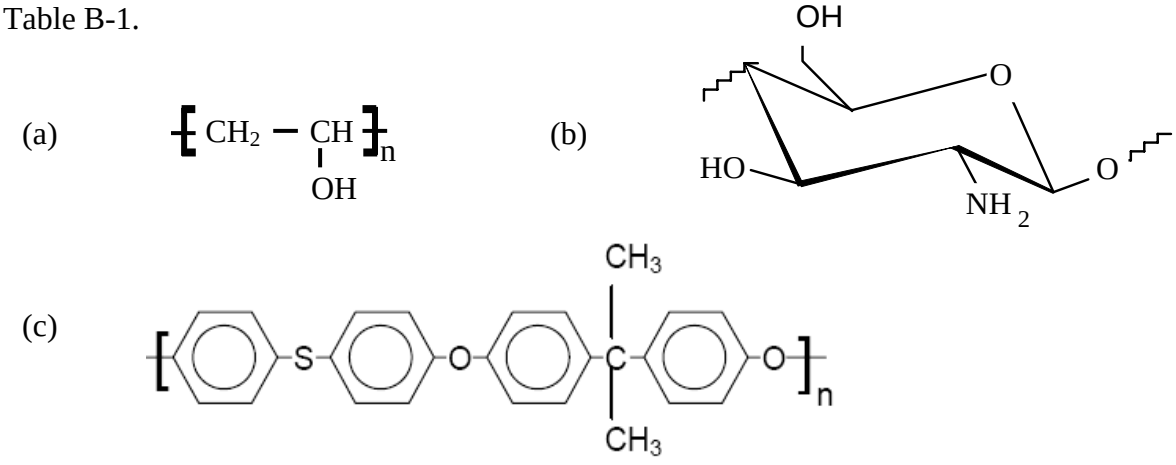

Figure B.1 Chemical structures of a) poly(vinyl alcohol), b) chitosan and c) poly(sulfone) (PSf)

Table B-1 Properties of polymers at room temperature used in membrane.

	Poly(vinyl alcohol)	**Chitosan**	**Poly(sulfone)**
CAS #	9002-89-5	9012-76-4	94336-28-4
Suuplier	Fisher Scientific	Kyowa Technos	Amoco Performance Products
Appearance	powder	flake	resin
Mw [$g.mol^{-1}$]	108,000	100,000	-
PDI	1.3	-	-
ρ [g/cc]	1.26	-	1.24
T_m [^OC]	196	287	343
Tg [^OC]	53	205*	179*
Purity [%]	99.7	-	-

M_w = molecular weight, ρ = density, T_m = melting point and Tg = glass transition temp
* Sakurai *et al.*, (2000)

B.2.2 Alcohols

Pervaporation dehydration experiments were conducted using aqueous solutions of the following alcohols: ethanol (Et), isopropanol (IPA) and ethylene glycol (EG). Chemical structures of the pure solvents [Hyperchem® 8] are given in Fig. B-2, and the properties are listed in Table B-2.

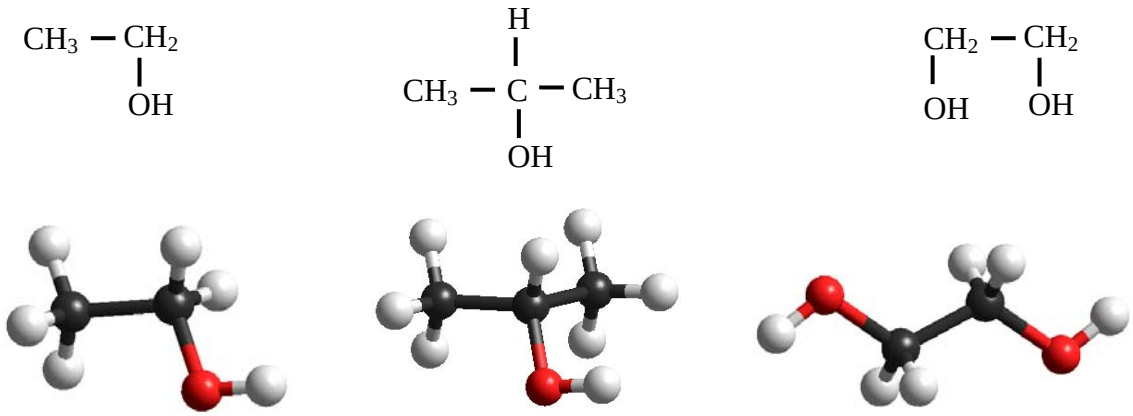

(a) Ethanol (Et) (b) Isopropanol (IPA) (c) Ethylene Glycol (EG)

Figure B.2 Chemical structures of different alcohols used in this work.

Table B-2 Properties of alcohols and water at 25^{O}C

	Ethanol	**Isopropanol**	**Ethylene Glycol**	**Water**
CAS #	64-17-5	67-63-0	107-21-1	7732-18-5
Supplier	Sigma-Aldrich	Sigma-Aldrich	Fisher Scientific	Millipore
M_w [g.mol^{-1}]	46.08	60.096	62.068	18.015
γ [mN.m^{-1}]	22.1	23.1	47.3	72.1
μ [mPa.s]	1.2	1.96	16.1	0.98
ρ [g.cc^{-1}]	0.79	0.78	1.11	0.99
B.P. [^{O}C]	78.4	82.3	197.3	100
P_v [mmHg]	59.07	42.74	0.07	23.74
Purity [%]	99.5	99.5	99.4	-

M_w = molecular weight, γ = surface tension, μ = viscosity, ρ = density, B.P. = boiling point and P_v = vapor pressure

The viscosity and surface tension measurements were done at university of Waterloo and the other properties were obtained from supplier's MSDS brochures.

Table B-3 Densities of alcohol-water mixtures at 25^{O}C

Alcohol (wt%)	**$\rho_{Et\text{-}water}$** [g.cc^{-1}]	**$\rho_{EG\text{-}water}$** [g.cc^{-1}]
0	0.997	0.997
20	0.968	-
30	0.951	1.033
50	0.917	1.058
70	0.868	1.079
90	0.815	1.091
100	0.788	1.11

B.3 Viscosity of alcohol-water mixtures

Knowledge of alcohol-water mixture viscosity helps understanding the feed hydrodynamics during pervaporation. The feed hydrodynamics can affect the sorption process and thereby flux and selectivity. Depending on the alcohol fractions in feed mixtures, the sorption can be affected by the flow-rate as well as fluid viscosity.

Therefore, it is important to determine how the viscosity of feed mixture changes with alcohol fractions.

The viscosities were determined for different feed mixtures using a viscometer (Fann 34A viscometer) at room temperature. Extrapolation of measured shear stresses as a function of shear rate to zero shear rate gives the viscosity at zero shear rate. This viscosity is reported here. From Fig. B-3, the mixture viscosities of Et-water and IPA-water were found to increase slightly around 0.2 wt% alcohols, then decreased linearly with increasing alcohol fractions. However, EG-water viscosities were found to increase with increasing EG fractions over the whole range of mixtures.

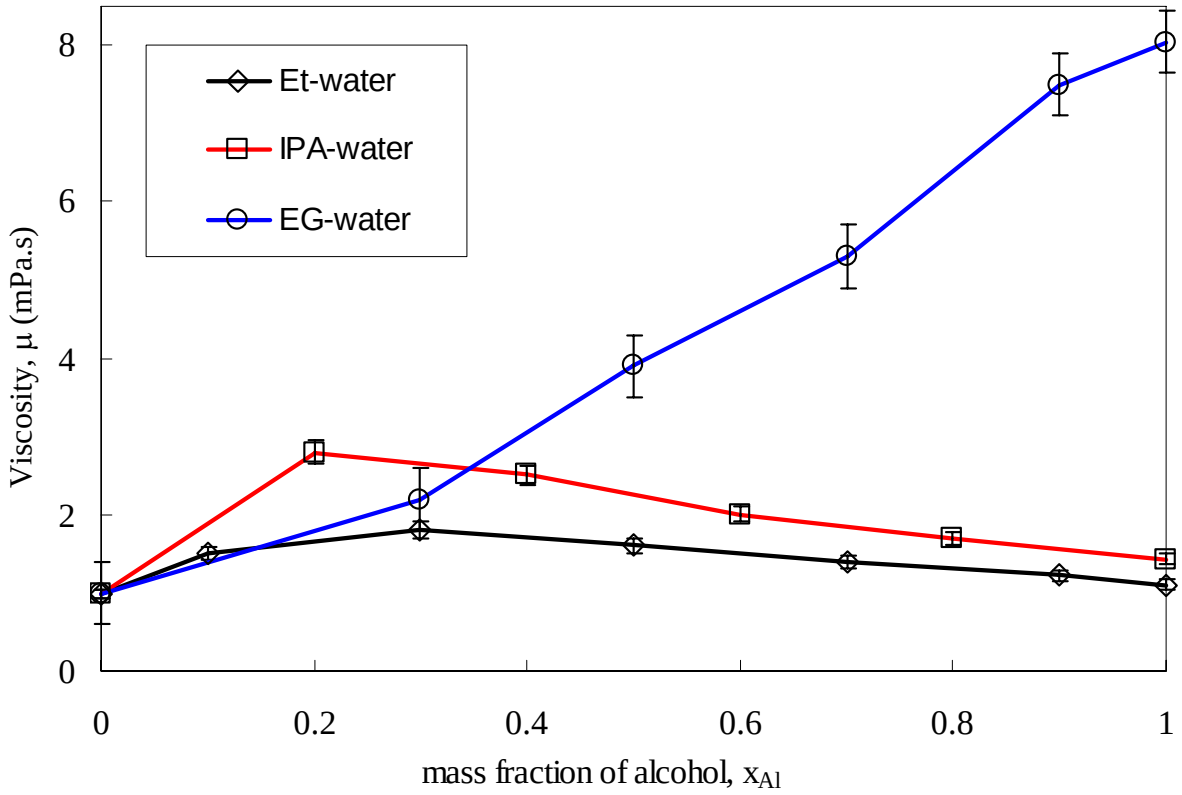

Figure B.3 Viscosities of feed alcohol-water mixtures.

APPENDIX C

Concentration polarization

During pervaporation, for binary mixture, one component permeates through the membrane preferentially. The other component, retained on the feed side may concentrate near the membrane surface. Therefore, a concentration gradient can be developed by a boundary layer on the membrane surface as shown in Fig. C.1. Concentration polarization causes components that are enriched in the permeate to be depleted in the boundary layer, and components that are depleted in the permeate to be enriched in the boundary layer. Thus, concentration polarization works against the separation achieved by the membrane, reducing flux and selectivity.

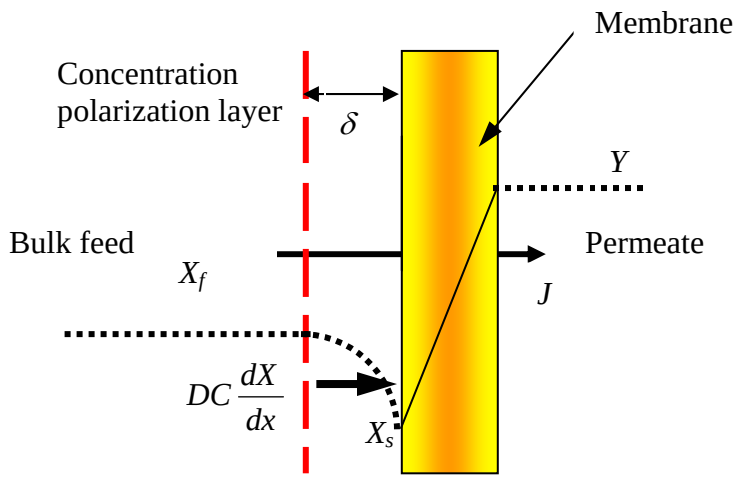

Figure C.1: Schematic representation of concentration polarization [Feng and Huang, 1994]

Within the boundary layer, the concentration of the permeating component decreases. This phenomenon is called concentration polarization. A simple model [Feng and Huang, 1994] based on "film theory" can be used to check the effect of concentration polarization. According to the model, if the mole fractions of water on the membrane surface and in the bulk feed are X_s and X_f respectively, then,

$$\frac{Y - X_s}{Y - X_f} = \exp(\nu / k) \qquad \text{(C.1)}$$

where, Y is the mole fractions of water on the permeate side; ν is the molar average velocity [m/s]; and k is the boundary layer mass transfer coefficient [m/s]. By expressing

Eq. (C.1) in terms of the intrinsic enrichment factor (β=Y/X_S), Feng and Huang (1994) defined the concentration polarization index (CPI) as

$$X_s / X_f = \left[\beta - (\beta - 1)\exp(-\nu / k)\right] \tag{C.2}$$

Generally the mole fraction on the membrane surface, X_s is unknown and the CPI is calculated simply by assuming negligible concentration polarization which allows to express $\beta = \beta_1$ = enrichment factor = Y/X_f [Guo *et al.*, 2007]. Please note that parameters on the right hand side of Eq. (C.2) can be calculated as follows: the molar average velocity, $\nu = J/C_L$, where, J and C_L are molar permeation flux and total molar feed concentration, respectively; k = boundary layer mass transfer coefficient = D/δ can be estimated from appropriates correlations of the Sherwood number (Sh) in terms of Reynolds number (Re) and Schmidt number (Sc) defined as [Bandini *et al.*, 1997]

$$Sh = \frac{kd}{D} = 0.026\ \mathrm{Re}^{0.8}\ Sc^{0.33}$$

$$\mathrm{Re} = \frac{\rho u d}{\mu} \tag{C.3}$$

$$Sc = \frac{\mu}{\rho D}$$

where d is the diameter (5 x 10^{-3} m) of the flow passage, D is the diffusion coefficient, u is the velocity on the membrane surface, ρ is the density and μ is the dynamic viscosity of the feed mixture.

Table C.1 Semi-empirical correlations for mass transfer coefficient

Configuration System	k_{bl}
Hollow fiber	$Sh = 1.80\ \mathrm{Re}^{0.47}\ Sc^{0.33}$ [1]
Spiral wound	$Sh = 0.065\ \mathrm{Re}^{0.875}\ Sc^{0.25}$ [1]
Circular cell with two parallel plates	$Sh = 0.3\ \mathrm{Re}^{0.5}\ Sc^{0.33}$ [1]
Rectangular membrane channel	$Sh = 1.82\ \mathrm{Re}^{0.33}\ Sc^{0.33}$ [2]
Radial flow between parallel plates	$Sh = 0.026\ \mathrm{Re}^{0.8}\ Sc^{0.33}$ [3]

[1] Lipski and Cote, (1990), [2] Mulder (1991) and [3] Bandini et al. (1997)

According to Eq. (C.2), when CPI approaches unity, the effect of concentration polarization becomes negligible. The CPI can be increased with

- a decrease of mass transfer coefficient (k)
- an increase in feed flow-rate thereby increasing molar average velocity, v
- a decrease of concentration of the preferentially permeating component in the feed mixture.

The mass transfer coefficient, k depends on the feed concentration, chemical nature of permeating components and feed hydrodynamics [Feng and Huang, 1994; Guo *et al.*, 2007]. Therefore, to reduce concentration polarization, high feed flow-rate can be applied to produce good mixing on the feed side and reduce the effect of boundary layer. Using the Eqs. (C-2), the calculated CPI results are presented in Table C.2 and C.3 for different flow-rates of various membranes.

For PVA4 membrane in Table C.2, CPI decreases with an increase in flow-rate.

Table C.2 X_s/X_f for CS-PVA1 blended membrane at different feed flow rate

Membrane	Alcohol in mixtures (wt%)	Flow-rate (L/hr)	Parameters		
			Re	v (x 10^{-7}) [m/s]	X_s/X_f
CS-PVA1	90 wt% ethylene glycol	40	379	2.62	0.898
		80	757	2.87	0.927
		120	1135	3.51	0.945
	90 wt% Ethanol	40	1542	2.51	0.961
		80	3085	2.84	0.976
		120	4628	2.96	0.987

Table C.3 X_s/X_f for CS-PVA3 blended membrane at different feed flow rate.

Membrane	Mixtures	Flow-rate (L/hr)	Parameters		
			Re	v (x 10^{-7}) [m/s]	X_s/X_f
CS-PVA3	90 wt% ethylene glycol	40	379	2.31	0.937
		80	757	2.79	0.954
		120	1135	2.94	0.963
	90 wt% Ethanol	40	1542	2.12	0.968
		80	3085	2.59	0.985
		120	4628	2.89	0.994

It can be seen from Table C.2 and C.3 that the CPI is always high for ethylene glycol mixtures. The high viscosity of ethylene glycol mixture (compared to ethanol-water mixture) in the feed develops a laminar type of flow that enhances the concentration polarization. With increasing flow-rate the CPI value of EG-water increases, however, it is always lower than Et-water mixture.

On the other hand, comparing two different membranes in Table C.2 and C.3, CS-PVA1 (with lower surface roughness ~35 nm) membrane showed lower CPI compared to CS-PVA3 membrane (surface roughness ~63 nm).

APPENDIX D

D.1 Diffusivity correlations

In order to calculate the diffusivities, it is necessary to represent Eq. (6.7) and (6.8) explicitly in terms of the concentration gradients as follows:

$$\frac{d\phi_1}{dz} = \frac{\rho_1 D_{1m} \dfrac{\partial \ln a_1}{\partial \phi_2} J_2 - \rho_2 D_{2m} \dfrac{\partial \ln a_2}{\partial \phi_2} J_1}{\rho_1 \rho_2 D_{1m} D_{2m} \left[\dfrac{d \ln(a_1)}{d\phi_1} \dfrac{\partial \ln a_2}{\partial \phi_2} - \dfrac{\partial \ln(a_2)}{\partial \phi_1} \dfrac{\partial \ln a_1}{\partial \phi_2} \right]} \tag{D.1}$$

$$\frac{d\phi_2}{dz} = \frac{\rho_2 D_{2m} \dfrac{\partial \ln a_2}{\partial \phi_1} J_1 - \rho_1 D_{1m} \dfrac{\partial \ln a_1}{\partial \phi_1} J_2}{\rho_1 \rho_2 D_{1m} D_{2m} \left[\dfrac{d \ln a_1}{d\phi_1} \dfrac{\partial \ln a_2}{\partial \phi_2} - \dfrac{\partial \ln a_2}{\partial \phi_1} \dfrac{\partial \ln a_1}{\partial \phi_2} \right]} \tag{D.2}$$

Eq. (D.1) and (D.2) represent a set of simultaneous ordinary differential Eq. (ODE) which need to be solved to find the diffusion coefficient of the components. In order to evaluate the partial differentials of the activities with respect to the volume fractions of the components, it is necessary to have a sorption model which describes the variation in activity of component *i* with volume fractions of the various component in the polymer. For a binary solvent-polymer system, Eq. (2.17) can be written as

$$\begin{aligned} \ln a_i(\phi_1, \phi_2, \phi_m) = {} & \ln \phi_i + \frac{Z}{2} q_i \ln\left(\frac{\theta_i}{\phi_i}\right) + l_i - \sum_{j=1}^{2} \phi_j \frac{r_i}{r_j} l_j \\ & - r_i \phi_m \left(\frac{Z}{2}\left(1 - \frac{q_m}{r_m}\right) - 1 \right) - q_i^* \ln \sum_{j=1}^{m} \theta_j^* \tau_{ji} + q_i^* - q_i^* \sum_{j=1}^{m} \frac{\theta_j^* \tau_{ij}}{\sum_{k=1}^{n} \theta_k^* \tau_{kj}} \end{aligned} \tag{D.3}$$

The partial derivative of the activity with respect to the volume fraction can be written as

$$\begin{aligned} \frac{\partial \ln a_i}{\partial \phi_i} = {} & \frac{1}{\phi_i} + \frac{Z}{2} q_i \frac{\phi_i}{\theta_i} \frac{\partial}{\partial \phi_i}\left(\frac{\theta_i}{\phi_i}\right) - l_i + r_i \left[\frac{Z}{2}\left(1 - \frac{q_m}{r_m}\right) - 1 \right] - \frac{q_i^*}{\sum_{j=1}^{n} \theta_j^* \tau_{ji}} \left[\sum_{j=1}^{m} \tau_{ji} \left(\frac{\partial \theta_j^*}{\partial \phi_i} \right) \right] \\ & - q_i^* \sum_{j=1}^{m} \frac{\left(\sum_{k=1}^{m} \theta_k^* \tau_{kj} \right) \left(\tau_{ij} \dfrac{\partial \theta_j^*}{\partial \phi_i} \right) - \theta_j^* \tau_{ij} \left[\sum_{k=1}^{m} \tau_{kj} \left(\dfrac{\partial \theta_k^*}{\partial \phi_i} \right) \right]}{\left(\sum_{k=1}^{m} \theta_k^* \tau_{kj} \right)^2} \end{aligned} \tag{D.4}$$

$$\frac{\partial \ln a_i}{\partial \phi_l} = \frac{Z}{2} q_i \frac{\phi_i}{\theta_i} \frac{\partial}{\partial \phi_l}\left(\frac{\theta_i}{\phi_i}\right) - \frac{r_i}{r_l} l_l + r_i\left[\frac{Z}{2}\left(1-\frac{q_m}{r_m}\right)-1\right] - \frac{q_i^*}{\sum_{j=1}^{n}\theta_j^*\tau_{ji}}\left[\sum_{j=1}^{m}\tau_{ji}\left(\frac{\partial\theta_j^*}{\partial\phi_l}\right)\right]$$

$$- q_i^* \sum_{j=1}^{m} \frac{\left(\sum_{k=1}^{m}\theta_k^*\tau_{kj}\right)\left(\tau_{ij}\frac{\partial\theta_j^*}{\partial\phi_l}\right) - \theta_j^*\tau_{ij}\left[\sum_{k=1}^{m}\tau_{kj}\left(\frac{\partial\theta_k^*}{\partial\phi_l}\right)\right]}{\left(\sum_{k=1}^{m}\theta_k^*\tau_{kj}\right)^2} \qquad \text{for } i \neq 1 \qquad \text{(D.5)}$$

The partial derivatives on the right hand side of Eq. (D.4) and (D.5) are defined as

$$\frac{\partial}{\partial\phi_k}\left(\frac{\theta_i}{\phi_i}\right) = \frac{-\left(\frac{q_i}{r_i}\right)\left[\sum_{j=1}^{m}\frac{\partial}{\partial\phi_k}\left(\frac{q_j}{r_j}\phi_j\right)\right]}{\left(\sum_{k=1}^{m}\phi_j\frac{q_j}{r_j}\right)^2} \qquad \text{for all } k \text{ and } i \qquad \text{(D.6)}$$

$$\frac{\partial\theta_i}{\partial\phi_k} = \frac{\sum_{j=1}^{m}\left(\phi_j\frac{q_j}{r_j}\right)\left(\frac{q_i}{r_i}\right)\frac{\partial\phi_i}{\partial\phi_k} - \left(\frac{q_i}{r_i}\phi_i\right)\left[\sum_{j=1}^{m}\frac{\partial}{\partial\phi_k}\left(\frac{q_j}{r_j}\phi_j\right)\right]}{\left(\sum_{k=1}^{m}\phi_j\frac{q_j}{r_j}\right)^2} \qquad \text{for all } k \text{ and } i \qquad \text{(D.7)}$$

$$\frac{\partial\theta_i^*}{\partial\phi_k} = \frac{\sum_{j=1}^{m}\left(\phi_j\frac{q_j^*}{r_j}\right)\left(\frac{q_i^*}{r_i}\right)\frac{\partial\phi_i}{\partial\phi_k} - \left(\frac{q_i^*}{r_i}\phi_i\right)\left[\sum_{j=1}^{m}\frac{\partial}{\partial\phi_k}\left(\frac{q_j^*}{r_j}\phi_j\right)\right]}{\left(\sum_{k=1}^{m}\phi_j\frac{q_j^*}{r_j}\right)^2} \qquad \text{for all } k \text{ and } i \qquad \text{(D.8)}$$

Eq. (D.7) to (D.12) can be simplified by using the constraint equation as

$$\phi_m = 1 - \phi_1 - \phi_2 \qquad \text{(D.9)}$$

The parameters r_i, q_i, q_i* and the ratio q_m/r_m can be estimated from the molecular structure or from data reported in literature [DECHEMA 2006]. For water-alcohol-PVA system, this data has been reported by Heintz and Stephan (1994). The binary parameter τ_{ij} for water-alcohol solvents can be estimated from VLE data in literature. The corresponding binary parameters for solvent-polymer material can be obtained by fitting Eq. (D.3) (for a single component in membrane) to the pure component vapor sorption data [Hauser *et al.*, 1989]. The coordination number, *Z*, is generally assumed to be 10. The binary solvent-polymer parameters can be further expressed as functions of temperature as shown in Eq. (D.10).

$$\tau_{ij} = \exp\left(-u_{ij}/RT\right) \qquad \text{(D.10)}$$

The binary components interaction parameters can be estimated as complex functions of temperature,

$$\tau_{ij} = \exp\left(a_{ij} + \frac{b_{ij}}{T}\right) \tag{D.11}$$

The parameters a_{ij} and b_{ij} in Eq. (D.11) were obtained from DECHEMA database. To evaluate the boundary conditions, one needs to assume that both the feed-membrane and permeate-membrane interfaces are in equilibrium. Mathematically, this can be expressed as

$$a_{i,f} = a_{im,f} \qquad for\ all\ i \tag{D.12}$$

$$a_{i,p} = a_{im,p} \qquad for\ all\ i \tag{D.13}$$

where, $a_{i,f}$ and $a_{i,p}$ refer to the activities of component i in the feed and permeate respectively. $a_{im,f}$ and $a_{im,p}$ refer to the activities of component i in the membrane on the feed and permeate side respectively. The L.H.S. of Eq. (D.12) can be computed by substituting the composition of the liquid feed in Eq. (D.3). The L.H.S. of Eq. (D.13) on the other hand, can be simply obtained by the ratio of the partial pressure of components i in the permeate to the vapor pressure at that temperature ($P_i/P_{i,sat}$). The R.H.S. of Eq. (D.12) and (D.13) can be substituted by the R.H.S. of Eq. (D.3). Both Eq. (D.12) and (D.13) thus represent a set on n simultaneous nonlinear algebraic equation. The solution of Eq. (6.7), (6.8), (D.1) to (D.9) yields the binary diffusivities (D_{im}) of components through the membrane.

Table D.1: Input UNIQUAC parameters for the diffusivity correlations

Solvent	a_{1s}	b_{1s} [K]	a_{s1}	b_{s1} [K]	u_{sm}/R [K]	u_{ms}/R [K]	r	q	q^*
Ethanol	-2.49	756.9	2	-728.9	632	230.9	2.11	1.97	0.92
Isopropanol	0	124.2	0	79.2	1072.4	318	2.78	2.51	0.89
Ethylene Glycol	0	444.8	0	-442.1	363.6	-305.2	2.41	2.25	0.47
Water	-	-	-	-	539.5	-366	0.92	1.47	1

solvent1: water; solvent2: alcohol; m: membrane

PVA polymer: q/r = 0.934 and q*/r*= 0.434

Table D.2 Diffusivities of water-EG-PVA system (Ch. 6) at 25^{O}C

Composite Membranes	50 wt% EG in feed mixture			90 wt% EG in feed mixture		
	Activity of water	Diffusivity		Activity of water	Diffusivity	
		D_{1m} x 10^{10} [m^2/s]	D_{EG} x10^{11} [m^2/s]		D_{1m} x 10^{10} [m^2/s]	D_{2m} x 10^{11} [m^2/s]
PVA1	0.84	15.35	1.11	0.35	3.2	1.96
PVA4	0.84	9.28	0.82	0.35	1.7	1.19
PVA5	0.84	18.13	1.68	0.35	5.4	2.54
PVA8	0.84	7.51	0.68	0.35	0.9	1.04

Comparing the diffusion coefficients from Table D.2 and Table 6.2 (using simple S-D model) great difference can be observed. The Fickian diffusivities from simple S-D theory are at least 2 orders of magnitude higher than the diffusivities obtained by the empirical correlations used here. In simple S-D theory, the interactions of the components are neglected as well as the sorption effect.

D.2 Sample MATLAB™ code for diffusion coefficient calculations

```
function diff_Phi=pervaporation_final(t,Phix)

Phi(1)=Phix(1);Phi(2)=Phix(2);
x(1)=0.8563;
x(2) = 1-x(1);
J1 =1.25e-07;
J2 = 0.406935e-8;
D1T = 4.91e-10;
D2T = 6.1e-11;
PPw=10;
PPe=0.33;
T=328.16;
Z=10;
q(2) = 1.97; q(1) = 1.47;
qs(1) = 1; qs(2) = .92;
u(2,3) = 632.044; u(3,2) = 230.93;
u(3,1) = 366.01; u(1,3) = 539.5;
Tau(1,1) = 1; Tau(2,2) = 1; Tau(3,3)= 1;
r(1)= .92; r(2)= 2.11;
L = 0.1e-4;
qr3 = .934; qrs3 = .434; q(3) = .934;
qs(3) = .434; r(3) = 1;
rho(1) = 1.0; rho(2) = .785;
a(1,2) = -2.4936; b(1,2) = 756.947;
a(2,1) = 2.0046; b(2,1) = -728.97;
Aw = 8.07131; Bw = 1730.63; Cw = 233.426-273.16; %Antoine's Constants for
Water
Ae = 8.1122; Be = 1592.864; Ce = 226.184-273.16; %Antoine's Constants for
Alcohol
VPw = 10^(Aw-Bw/(T+Cw));
VPe = 10^(Ae-Be/(T+Ce));
Tau(1,2) = exp(a(1,2)+b(1,2)/T);
Tau(2,1) = exp(a(2,1)+b(2,1)/T);
Tau(2,3) = exp(-u(2,3)/T);
Tau(3,2) = exp(-u(3,2)/T);
Tau(3,1) = exp(u(3,1)/T);
Tau(1,3) = exp(-u(1,3)/T);
 for i=1:2
    l(i)=Z/2*(r(i)-q(i))-(r(i)-1);
 end
 Phi(3)=1-Phi(1)-Phi(2);
 sumfk=Phi(1)*q(1)/r(1)+Phi(2)*q(2)/r(2)+Phi(3)*q(3)/r(3);
 sumsk=Phi(1)*qs(1)/r(1)+Phi(2)*qs(2)/r(2)+Phi(3)*qs(3)/r(3);
 for i=1:3
theta(i)= Phi(i)*q(i)/(r(i)*sumfk);
thetas(i)= Phi(i)*qs(i)/(r(i)*sumsk);
 end
 for i=1:3
     summ=0.0;
      for j=1:3
           summ=summ+thetas(j)*Tau(j,i);
      end
ThetasTau(i)=summ;
 end
```

```
 dthetasdphi=zeros(3,3);
  val_q(1)=q(1)/r(1)-q(3)/r(3);
  val_q(2)=q(2)/r(2)-q(3)/r(3);
  val_qs(1)=qs(1)/r(1)-qs(3)/r(3);
  val_qs(2)=qs(2)/r(2)-qs(3)/r(3);

 for i=1:2
       for j=1:2
         if(i==j)
    dthetadphi(i,j)=(sumfk*q(i)/r(i)-(Phi(i)*val_q(j)*q(i)/r(i)))/sumfk^2;
    dthetasdphi(i,j)=(sumsk*qs(i)/r(i)-
(Phi(i)*val_qs(j)*qs(i)/r(i)))/sumsk^2;
         else
      dthetadphi(i,j)=(-(Phi(i)*val_q(j)*q(i)/r(i)))/sumfk^2;
      dthetasdphi(i,j)=-(Phi(i)*val_qs(j)*(qs(i)/r(i)))/sumsk^2;
         end
      dthetaphidphi(i,j)=-val_q(j)*q(i)/r(i)/sumfk^2;
      end
  end
  dthetasdphi(3,1)= -dthetasdphi(1,1)-dthetasdphi(2,1);
  dthetasdphi(3,2)= -dthetasdphi(1,2)-dthetasdphi(2,2);
  dthetasdphi(3,3)= -dthetasdphi(1,3)-dthetasdphi(2,3);
   dlnadphi =zeros(2,2);
for i=1:2
    for j=1:2
        sumkk=0.0;
         for k=1:3
sumkk=sumkk+qs(i)*(dthetasdphi(k,j)*Tau(k,i))/ThetasTau(i)+qs(i)*(ThetasTau(
k)*Tau(i,k)*dthetasdphi(k,j)-
thetas(k)*Tau(i,k)*(Tau(1,k)*dthetasdphi(1,j)+Tau(2,k)*dthetasdphi(2,j)+Tau(
3,k)*(-dthetasdphi(1,j)-dthetasdphi(2,j))))/ThetasTau(k)^2;
         end

dlnadphi(i,j)=Z/2*q(i)*Phi(i)/theta(i)*dthetaphidphi(i,j)-
(r(i)*l(j)/r(j))+r(i)*(Z/2*(1-q(3)/r(3))-1)-sumkk;
                  if(i==j)dlnadphi(i,j)=1/Phi(i)+dlnadphi(i,j);
                  end
    end
end

diff_Phi = zeros(2,1);
diff_Phi(1)=(Phi(1)*D1T*dlnadphi(1,2)*J2-
Phi(2)*D2T*dlnadphi(2,2)*J1)*L/(Phi(1)*Phi(2)*D1T*D2T*(dlnadphi(1,1)*dlnadph
i(2,2)-dlnadphi(1,2)*dlnadphi(2,1)));
diff_Phi(2)=(Phi(2)*D2T*dlnadphi(2,1)*J1-
Phi(1)*D1T*dlnadphi(1,1)*J2)*L/(Phi(1)*Phi(2)*D1T*D2T*(dlnadphi(1,1)*dlnadph
i(2,2)-dlnadphi(1,2)*dlnadphi(2,1)));
```

APPENDIX E

Error Analysis

The objective of this analysis is to estimate the error in a calculated quantity which has propagated from the measured quantities due to their uncertainties. The desired quantity is expressed as a function of the measured variables. The uncertainties in each measured variable are expressed in terms of its standard deviation σ. If *y* is the desired quantity, then the uncertainty in y due to the measured variables $x_1, x_2,....x_n$, is given by:

$$\sigma_y^2 = \sum_{x=i}^{n} \left[(\partial y / \partial x_i) \sigma_{xi}^2 \right] \qquad \text{(E.1)}$$

where σ_{xi}^2 represents the uncertainties in the measured variables $x_1, x_2,....x_n$.

Error Propagation in Permeate Collection:

The permeate samples were collected in sampling bottles and the weight of each sample was calculated by the subtracting the weight of the empty bottle from the weight of the bottle containing the sample. If S is the weight of a sample, SB is the weight of the sample plus sampling bottle, and B is the weight of the bottle, then:

$$S = SB - S \qquad \text{(E.2)}$$

Since the uncertainty in SB is the same as the uncertainty in B, the uncertainty in the weight of a sample can, be represented by:

$$\sigma_S^2 = \sigma_{SB}^2 + \sigma_B^2 = 2\sigma_B^2 \qquad \text{(E.3)}$$

Using the weights of the samples collected at various times, the cumulative weight of the permeate collected (data point) is calculated by adding the weights of all the samples collected until that time. Hence, the n' data point involves n^{th} measurements of SB and n measurements of S. Therefore, the uncertainty in the n^{th} data point can be calculated by:

$$\sigma_{Wn}^2 = 2n^2\sigma_B^2 \qquad \text{(E.4)}$$

or

$$\sigma_{Wn} = \pm 1.44n\sigma_B \qquad \text{(E.5)}$$

In this study, the uncertainty in measuring weights (σ_{SB} and σ_B) is taken as 0. l g.

Error Propagation in Gas Chromatography:

The uncertainty in the weight percent calculated by gas chromatography (GC) is assumed to be only due to the uncertainties in sample preparation as discussed earlier in the previous section. Therefore, the uncertainty in the results of *GC* can be written as:

$$\sigma^2_{w_{GC}} = \left(\partial w_{GC} / \partial w_a\right)^2 \sigma^2_{wa} \qquad \text{(E6)}$$

where w_{GC}, is the weight percent of alcohol obtained by the GC. The weight percent of alcohol in the mixture can be related to the weights of the individual components as:

$$w_a = \frac{W_a}{W_a + W_b} x\,100 \qquad \text{(E.7)}$$

where W_a is the weight of alcohol and W_b is the weight of water used in making the mixture. Therefore, uncertainty in w_a can be written as:

$$\sigma^2_{w_a} = \left(\partial w_a / \partial W_a\right)^2 \sigma^2_{Wa} + \left(\partial w_a / \partial W_b\right)^2 \sigma^2_{Wb} \qquad \text{(E.8)}$$

where σ^2_{Wa} and σ^2_{Wb}, are the uncertainties in the weights of alcohol and water respectively and can be quantified as the weight of a drop of these components (taken as l g in this study) plus the uncertainty in each weight measurement as given by equation (A3) in the previous section.

Using equations (A6), (A7) and (A8), the final form of the equation for the uncertainty in GC results is:

$$\sigma^2_{w_{GC}} = 10^4 \left(\partial w_{GC} / \partial w_a\right)^2 \left[\frac{W_b^2}{\left(W_a + W_b\right)^4}\sigma^2_{Wa} + \frac{W_a^2}{\left(W_a + W_b\right)^4}\sigma^2_{Wb}\right] \qquad \text{(E.9)}$$

The partial derivative $\partial w_{GC} / \partial w_a$ can be calculated from a straight line fit relating weight percent alcohol obtained by GC and the weight percent alcohol as prepared in the sampling bottles. Since the samples are prepared independently, the error bars are not influenced by the number of data points.

Error Propagation in Permeate Flux:

The permeate flux is calculated by dividing the amount of permeate collected in a unit time by the area of the membrane used by pervaporation:

$$J_i = \frac{W_i}{A t_b} = \frac{4 W_i}{\pi\, t\, D^2} \qquad \text{(E.10)}$$

The uncertainty in flux can be written as:

$$\sigma_{J_i}^2 = \left(\frac{4}{\pi t\, D^2}\right)^2 \sigma_{Wi}^2 + \left(\frac{4W_i}{\pi t^2\, D^2}\right)^2 \sigma_t^2 + \left(\frac{8W_i}{\pi t^2\, D^3}\right)^2 \sigma_D^2 \qquad \text{(E.11)}$$

Error Propagation in Selectivity:

Selectivity of the membrane for component *i* is defined as:

$$\alpha_{ij} = \frac{y_i / y_j}{x_i / x_j} \qquad \text{(E12)}$$

where y_i, y_j are the weight fractions of components *i* and *j*, respectively, in the permeate and x_i, x_j are their weight fractions in the feed. The uncertainty in selectivity propagates due to the uncertainties in y_i, y_j, x_i, and x_j and therefore, be represented by:

$$\sigma_\alpha^2 = \left(\frac{x_j}{x_i y_j}\right)^2 \sigma_{y_i}^2 + \left(\frac{y_i x_j}{x_i y_j^2}\right)^2 \sigma_{j_j}^2 + \left(\frac{y_i x_j}{y_j x_i^2}\right)^2 \sigma_{x_i}^2 + \left(\frac{y_i}{x_i y_j}\right)^2 \sigma_{y_j}^2 \qquad \text{(E.13)}$$

Error Propagation in Component Flux:

The component flux can be calculated by:

$$J_i = \frac{w_i}{100} J \qquad \text{(E14)}$$

where J is the total flux and w_i is the weight percent of the component *i*. The uncertainty in the component flux can, therefore, be estimated by:

$$\sigma_{J_i}^2 = 10^{-4}\left[w_i \sigma_{Ji}^2 + J_2 \sigma_{Wi}^2\right] \qquad \text{(E.15)}$$

Sample Calculation of Flux:

This section shows a sample of how an error in a measurable quantity, *x*, is propagated as an error in the dependent quantity, *y*. For instance, the case of the cumulative weight of permeate collected (*y*) as a function of the weight of the sample collected (*x*) at a particular time, *t* during pervaporation of 20 wt% aqueous ethanol through PVA is presented below:

t	x	y	σ_y	σ_y/y
6	7.32	7.61	± 0.1422	± 0.0187
18	7.12	22.34	± 0.4183	± 0.0188
24	7.11	29.25	± 0.5741	± 0.0196

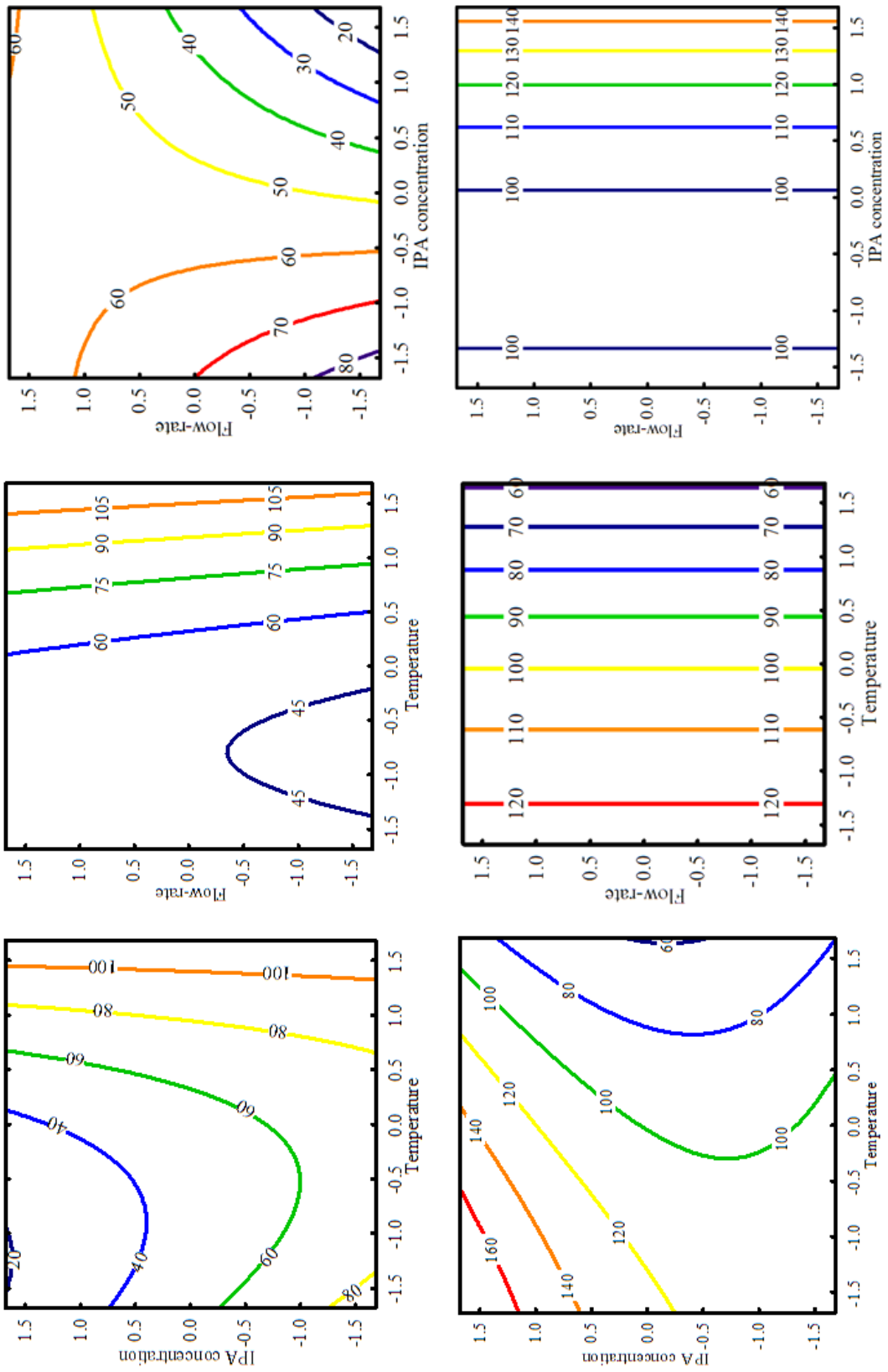

Figure E.1: Contour plots of flux (top row) and selectivity (bottom row) against different operating variables for IPA-water system. Variables not shown in any plot was held constant at 0 levels.

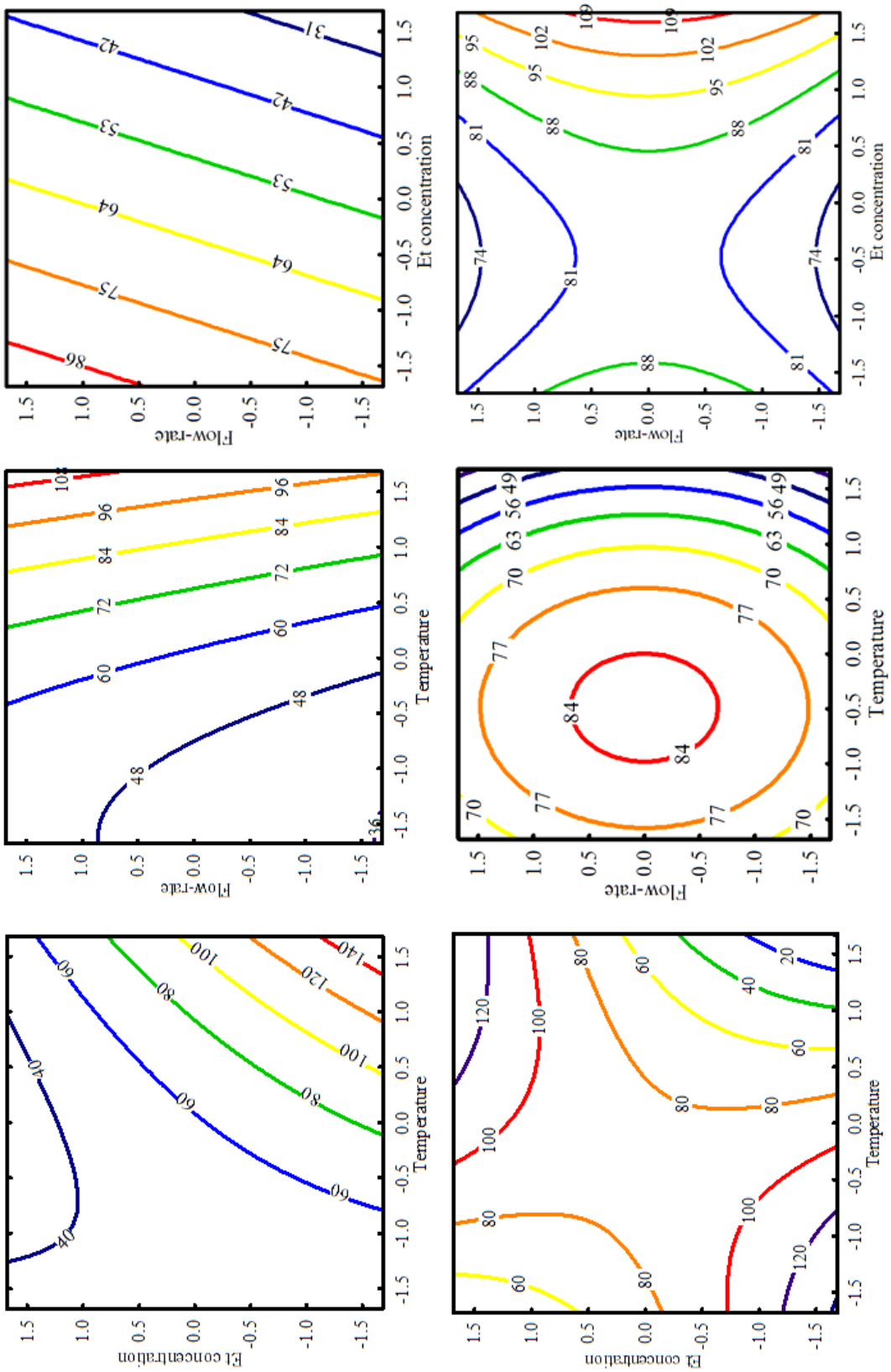

Figure E.2: Contour plots of flux (top row) and selectivity (bottom row) against different operating variables for Et-water system. Variables not shown in any plot was held constant at 0 levels.

Interactions of variables (IPA-water)

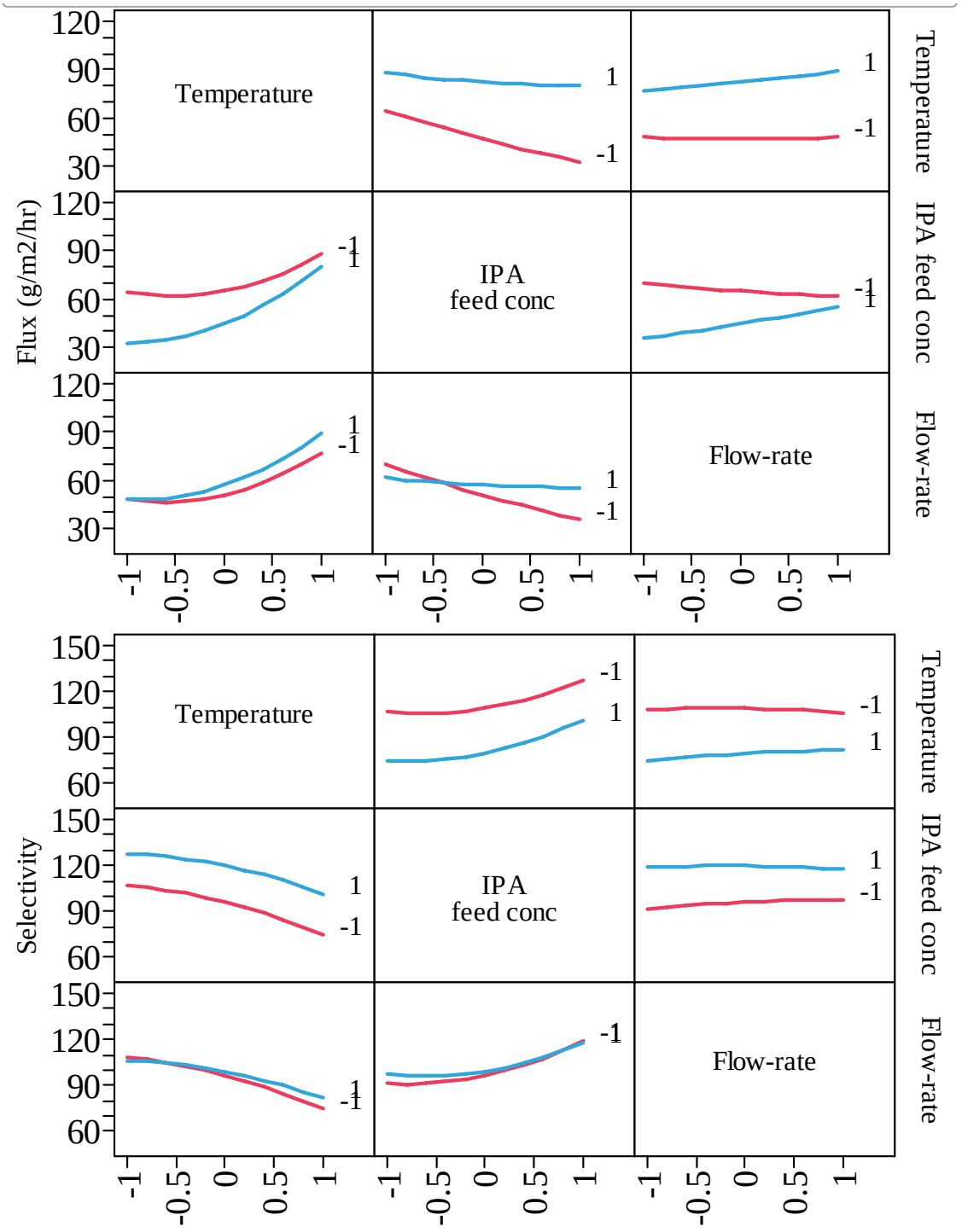

Figure E.3: Interaction plots of operating variables for IPA-water modeling.

The interaction plots shows a matrix of plots when there are interaction effects in the model. In Fig E.1, evidence of interaction shows as nonparallel lines such as for flux, interaction exists between temperature and flow-rate, IPA concentration and flow-rate.

Interactions of variables (Et-water)

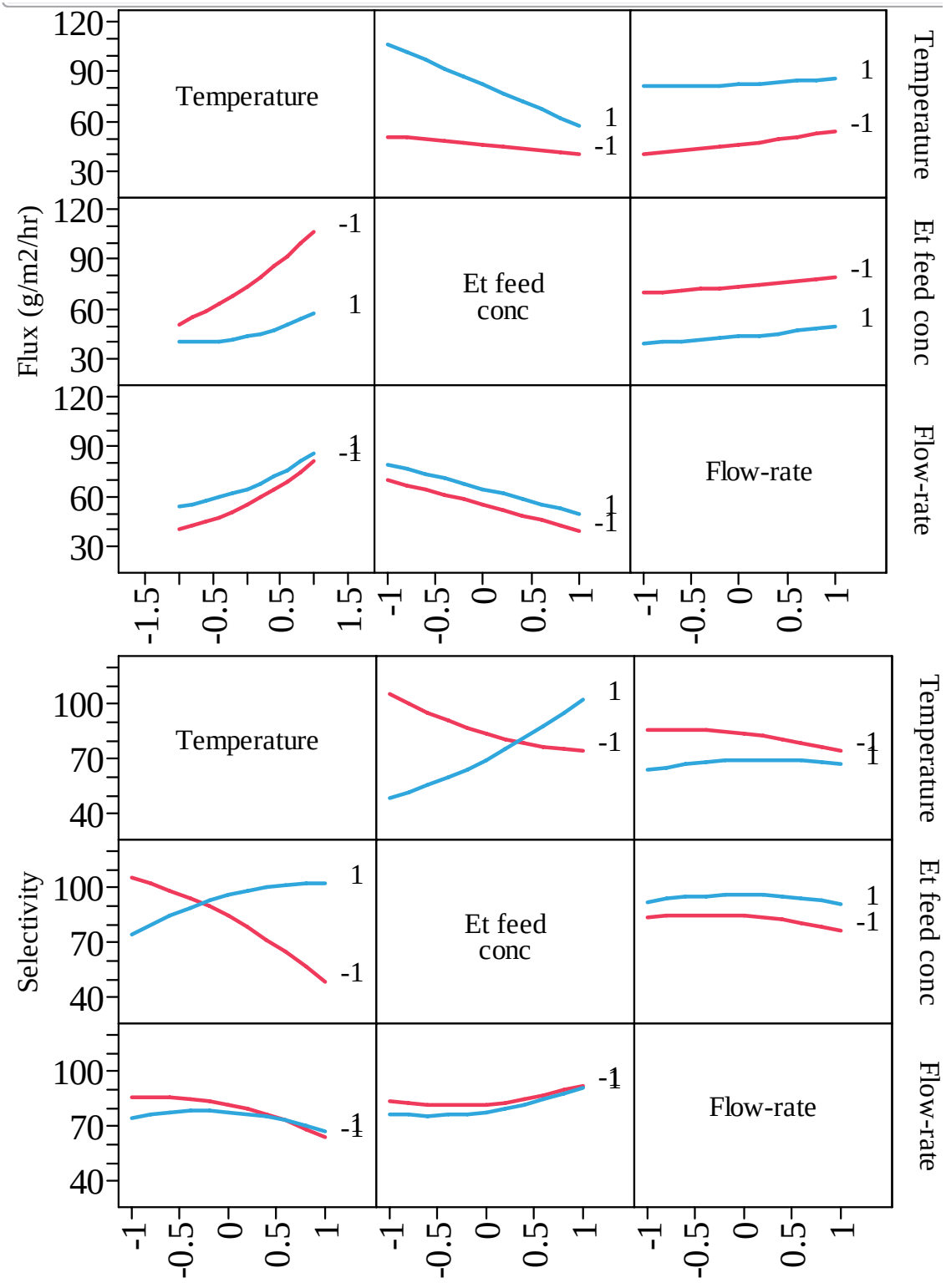

Figure E.4: Interaction plots of operating variables for Et-water modeling.

BIBLIOGRAPHY

Abrams, D. S., Prausnitz, J. M., Statistical Thermodynamics of the Liquid Mixtures: A New Expression for the Excess Gibbs Energy of Partly or Completely Miscible Systems, AIChE, 21, 116 (1975).

Acharya, H. R., Stern, S. R., Liu, Z. Z. Cabasso, I., Separation of Liquid Benzene/Cyclohexane Mixture by Perstraction and Pervaporation, J. Membr. Sci., 37, 205 (1988).

Ahmad, A.L., Ooi, B.S., Properties–performance of thin film composites membrane: study on trimesoyl chloride content and polymerization time, J. Membr. Sci. 255, 67–77 (2005).

Almeida, E., Balmayore, M., Santos, T., Some relevant aspects of the use of FTIR associated techniques in the study of surfaces and coatings, Prog. Org. Coat. 44, 233–242 (2002).

Anderson, T. F. and Prausnitz, J. M., Application to the UNIQUAC Equation to Calculation of Multicomponent Equilibria. I. Vapor-Liquid Equilibria, Ind. Eng. Chem. Process Des. Dev., 17, 552 (1978).

Andrade J.D., Smith, L.M and Gregonis, D.E., Protein Adsorption, Surface and Interfacial Aspects of Biomedical Polymers, Vol. 1 - Surface Chemistry and Physics, Vol. 2 , J. D. Andrade, (ed)., Plenum Press, New York, 249 (1985).

Aptel, P., Cuny, J., Jozefonvicz, J., Morel, G., Neel, J., Liquid transport through membranes prepared by grafting of polar monomers onto poly(tetrafluoroethylene) films. II. Some factors determining pervaporation rate and selectivity, J. Appl. Polym. Sci. 18, 351-364 (1974).

Ariyaskul, A.S., Huang, R.Y.M., Douglas, P.L., Pal, R., Feng, X., Chen, P., Liu, L., Blended chitosan and polyvinyl alcohol membranes for the pervaporation dehydration of isopropanol, J. Membr. Sci. 280, 815–823 (2006).

Baker, R.W. Membrane technology and applications, 2nd ed., John Wiley & Sons Ltd, New York, (2004)

Bandini, S., Saavedra A., Sarti G.C., Vacuum Membrane Distillation: Experiments and Modeling, AIChE J., 43(2), 398-408 (1997).

Belfer, S, Purinson,Y, Kedem, O, Surface modification of commercial polyamide reverse osmosis membranes by radical grafting: an ATR-FT-IR study, Acta Polym., 4, 574 (1998).

Bessières, A., Meireles, M., Coratger, R., Beauvillain, J., Sanchez, V, Investigations of surface properties of polymeric membranes by near field microscopy, J. Membr. Sci., 109, 271 (1996).

Bhattacharya, S. Hwang, S.T., "Concentration Polarization, separation factor, and Peclet number in membrane processes," J. Membr. Sci., 132, 73-90 (1997).

Biesheuvel, P.M., Verweij, H., Design of ceramic membrane supports: permeability, tensile strength and stress, J. Membr. Sci. 156, 141-152 (1999).

Binning, R.C., Lee, R.J., Jennings, J.F., Martin, E.C., Separation of Liquid Mixtures by Permeation, Ind. Eng. Chem. 53, 45 (1961).

Bird, R.B., Stewart, W.E., Lightfoot, E.N., Transport Phenomena, 2nd edition, John Wiley & Sons, New York (2002).

Bitter, J. G. A., Effect of Crystallinity and Swelling on the Permeability and Selectivity of Polymer Membranes, Desalination, 51, 19 (1984).

Bitter, J. G. A., Transport Mechanisms in Membrane Separation Processes, Plenum Press, New York, (1991).

Blume, I., Wijmans, J. G., Baker, R. W., "The Separation of Dissolved Organics from Water by Pervaporation", J. Membr. Sci., 49(3), 253 (1990).

Bowen, W. R., Doneva, T. A., Atomic force microscopy studies of nanofiltration membranes: surface morphology, pore size distribution and adhesion, Desalination, 129, 147-162 (2000).

Brown, C.G., Trumbull, D., Klein-Schwartz, W., Walker, J.D., Ethylene glycol poisoning, Ann Emerg Med. 12, 501-506 (1983).

Brun, J.P., G. Bulvestre, A. Kergreis, M. Guillou, Hydrocarbons separation with polymer membranes. I. Butadiene-isobutene separation with nitrile rubber membranes, J. Appl. Polym. Sci. 18, 1663-1683 (1974).

Brun, J. P., Larchet, C., Melet, R., Bulvestre, G., "Modeling of the Pervaporation of Binary Mixtures through Moderately Swelling, Non-interacting Membranes", J. Membr. Sci., 23, 257 (1985).

Bruschke, H. E. A., State of Art of Pervaporation, Proceedings of 5th Conference on Pervaporation Processes in the Chemical Industry, ed. R. A. Bakish, 2 (1991).

Bueche, A. M., Interaction of polydimethylsiloxanes with swelling agents, J. Polym. Sci., 15, 97 (1955).

Cabasso, I., Ultrastructure of asymmetric and composite membranes, in: A.F. Turbak (Ed.), Synthetic Membranes, Vol. 1, Desalination, ACS Symp. Ser., No. 153, American Chemical Society, Washington, DC, 267 (1981).

Casassa, E. F. and Berry, G. C., in Comprehensive Polymer Science, (Ed.) Allen, S. G. and Bevington, J. C., Pergamon Press, Oxford, 2, 77 (1989).

Chan W.-H., Ng, C.-F., Lam-Leung, S.-Y., X. He, Water–alcohol separation by pervaporation through chemically modified poly(amidesulfonamide)s, J. Membr. Sci.160, 77–86 (1999).

Chen, F.R., Chen, H.F., Pervaporation mixtures using crosslinked PVA–PES composite membranes. Part I. Effect of membrane preparation conditions, J. Membr. Sci. 109, 247–256 (1996).

Chen, F.R., Chen, H.F., A diffusion model of the pervaporation separation of ethylene glycol-water mixtures through crosslinked poly(vinyl alcohol) membrane, J. Membr. Sci. 139, 201–209 (1998).

Chiang, W.-Y., Lin, Y.-H., Properties of modified poly(vinyl alcohol) membranes prepared by the grafting of new polyelectrolyte copolymers for water–ethanol mixture separation, J. Appl. Polym. Sci. 86, 2854–2859 (2002).

Cowan, G., Statistical Data Analysis, Clarendon Press, Oxford, United Kingdom (1998)

Cussler E.L., Diffusion: Mass transfer in fluid systems, 2nd edition, Cambridge university press, New York (1997).

Del Castillo, E., Montgomery, D.C., McCarville, D. R., Modified desirability function for multiple response optimization, J. Quality Tech., 28, 337-345 (1996).

Derringer, G., Suich, R., Simultaneous Optimization of Several Response Variables, J. Quality Tech., 12, 214-219 (1980).

Dietz, P., Hansma, P.K., Inaker, O., H.D. Lehmann, K.H. Hermann, Surface pore structures of micro- and ultrafiltration membranes imaged with the atomic force microscope, J. Membr. Sci. 65, 101-111 (1992).

Diniz, F.M., Martin, A.M., Use of response surface methodology to describe the combined effects of p^H, temperature and E/S ratio on the hydrolysis of dogfish (*Squalus acanthias*) muscle, Int. J. Food Sci. Technol. 31, 419–426 (1996).

Du, R., X. Feng, A. Chakma, Poly(N,N-dimethylaminoethyl methacrylate) /polysulfone composite membranes for gas separations, J. Membr. Sci. 279, 76-85(2006).

Dutta, B. K., Sikdar, S. K., "Separation of Azeotropic Organic Liquid Mixtures by Pervaporation", AIChE J., 37(4), 581(1991).

Enneking, L., Stephan, W. Heintz, A., "Sorption and Diffusivity Measurements of Cyclohexane /Benzene and Cyclohexane/Toluene Mixtures in Polyurethane Membranes and Modeling the Pervaporation Process", Ber. Bunsenges. Phys. Chem., 97, 912 (1993).

Extrand, C. W., A Thermodynamic Model for Contact Angle Hysteresis, J. Colloid Interface Sci., 207, 11 (1998)

Extrand, C. W., A Thermodynamic Model for Wetting Free Energies from Contact Angles, Langmuir, 19, 646(2003).

Fan, S.-C., Wang, Y.-C., Li, C.-L., Lee, K.-R., Liaw, D.-J., Huang, H.-P., Lai, J.-Y., Effect of coagulation media on membrane formation and vapor permeation performance of novel aromatic polyamide membrane, J. Membr. Sci. 204, 67-79 (2002).

Fang, S. M., Stern, S. A., Frisch H. L., A Free Volume Model of Permeation of Gas and Liquid Mixtures through Polymeric Membranes, Chem. Eng. Sci., 30, 773 (1975).

Favre, E., Clement, R., Nguyen, Q. T., Schaetzel, P., Neel, J., Sorption of Organic Solvents into Dense Silicone Membranes. Part 2. Development of a New Approach Based on a Clustering Hypothesis, J. Chem. Soc. Faraday Trans., 89, 4339 (1993).

Feng, X., Huang, R.Y.M., Pervaporation with chitosan membranes I. Separation of water from ethylene glycol by a chitosan/polysulfone composite membrane, J. Membr. Sci. 116, 67-76 (1996).

Feng, X., Huang, R.Y.M., Liquid separation by membrane pervaporation: a review, Ind. Eng. Chem. Res., 36, 1048-1066 (1997).

Finch, C.A., Polyvinyl Alcohol, Properties and Applications, Wiley–Interscience, New York (1973).

Fleming, H.L., Slater, C.S., Part III pervaporation. In: W.S.W. Ho and K.K. Sirkar, Editors, Membrane Handbook, Van Nostrand Reinhold, New York 103–159 (1992).

Flory, P. J., "Principles of Polymer Chemistry", Cornell University Press, Ithaca, NY (1953).

Franken, A.C.M, Nolten, J.A.M., Bargeman, D., Smolders, C.A., Wetting criteria for the applicability of membrane distillation, J. Membr. Sci., **33**, 315 (1987).

Fredenslund, A., Jones, R. L., Prausnitz, J. M., Group Contribution Estimation of Activity Coefficients in Nonideal Liquid Mixtures, AIChE, 21, 1086 (1975).

Freger, V, Gilron, J., Belfer, S., TFC polyamide membranes modified by grafting of hydrophilic polymers: an FT-IR/AFM/TEM study, J. Membr. Sci., 209, 283 (2002).

Frenesson, I., Tragardh, G., Hagerdahl, B. H., Pervaporation and Ethanol Upgrading -A Literature Review, Chem. Eng. Comm., 45, 277 (1986).

Fujita, H., Kishimoto, A., Matsumoto, K., Concentration and Temperature Dependence of Diffusion Coefficients for Systems – PolymethylAcrylate and N-Alkyl acetates, Trans. Faraday Soc., 56, 424 (1960).

Fujita, H., Diffusion in Polymer-Diluent Systems, Adv. Polym. Sci., 3, 1 (1961).

Ghai, R. K., Ertl, H., Dullien, F. A. L., Liquid Diffusion of Nonelectrolytes: Part 1, AIChE J., 19, 881 (1987).

Gierke T.D., Munn G.E., Wilson F.C., The morphology in Nafion perfluorinated membrane products, as determined by wide-angle and small-angle X-ray studies, J. Polym. Sci., Polym. Phys. Ed., 19, 1687 (1981).

Gilman, J.W., VanderHart, D.L., Kashiwagi, T., Thermal decomposition chemistry of poly(vinyl alcohol), Fire and Polymers. II. Materials and Test for Hazard Prevention, ACS Symposium Series 599 Washington, DC, August 21–26 (1994) (Chapter 11).

Gmehling, J., Group Contribution Methods for the Estimation of activity coefficients, 10, 119 (1986).

Goncalves, M.P., Trypsin hydrolysis of whey protein concentrates: characterization using multivariate data analysis, Food Chem. 94, 278–286 (2006).

Goydan, R., Reid, R. C., Tseng, H. S., Estimation of the Solubilities of Organic Compounds in Polymers by Group Contribution Methods, Ind. Eng. Chem. Res., 28, 445 (1989).

Graham T., *Philos. Mag.*, 32, 401, (1866).

Grant, D. W., Takeru, H., Solubility Behavior of Organic Compounds, Techniques of Chemistry, Volume XXI, John Wiley & Sons, New York, USA, (1989).

Greenlaw, F. W., Shelden, R. A., Thompson, E. V., Dependence of Diffusive Permeation Rates on Upstream and Downstream Pressures. II. Two Component Permeation, J. Membr. Sci., 36, 331 (1988).

Gref R., Nguyen, Q. T., Schaetzel, P., J. Neel, Transport Properties of Poly (vinyl alcohol) Membranes of Different Degrees of Crystallinity. I. Pervaporation Results, J. Appl. Polym. Sci. 49, 209-218 (1993).

Guo, R., Hu, C., Li, B., Jiang, Z., Pervaporation separation of ethylene glycol/water mixtures through surface crosslinked PVA membranes: Coupling effect and separation performance analysis, J. Membr. Sci. 289,191–198 (2007).

Hansen, C. M., The universality of the solubility parameter." Industrial & Engineering Chemistry Product Research and Development 8(1), 2-11(1969).

Harrington Jr., E. C., The Desirability Function. Ind. Quality Control, 21, 494-498 (2002).

Heintz, A., Stephan, W., A Generalized Solution-Diffusion Model of the Pervaporation Process through Composite Membranes. Part I. Prediction of Mixture Solubilities in the Dense Active Layer using the UNIQUAC MODEL, J. Membr. Sci., 89, 14 (1994).

Heintz, A., Stephan, W., Separation of Aliphatic/Aromatic Mixtures by Pervaporation using Polyurethane Membranes. Model Calculations and Comparison with Experimental Results, in Proceedings of Sixth International Conference on Pervaporation Processes in the Chemical Industry, Ottawa, Canada, September 27-30, 292 (1992).

Hickey, P., Gooding, C. H., "The Economic Optimization of Spiral Wound Membrane Modules for the Pervaporative Removal of VOCs from Water", J. Membr. Sci., 97, 53 (1994).

Higuchi A., Iijima T., DSC investigation of the states of water in poly(viny1 alcohol- coitaconic acid) membranes, Polymer, 26, 1833 (1985).

Hind, A.R., Bhargava, S.K., McKinnon, A., At the solid/liquid interface: FTIR/ATR—the tool of choice, Adv. Colloid Interface Sci. 93, 91–114 (2001).

Hollis, J. M., Lovas, F. J., Jewell, P. R., Coudert, L. H., Interstellar Antifreeze: Ethylene Glycol, AstroPhysical J. 571, 59-62 (2002).

Hsieh, H. P., Inorganic Membranes for Separation and Reaction. Membrane Science and Technology Series, Elsevier, Amsterdam (1996)

Huang, R. Y. M., Pervaporation Membrane Separation Processes, Elsevier, Amsterdam, (1991)

Huang R.Y.M., Feng, X., Dehydration of isopropanol by pervaporation using aromatic polyetherimide membranes, Sep. Sci. Tech., 28, 2035-2048 (1993).

Huang,R.Y.M., Rhim, J.W., Separation characteristics of pervaporation membrane separation processes using modified poly(vinyl alcohol) membranes, Polym. Int. 30,123–128 (1993).

Huang, R.Y.M., Lin, V.J.C., Separation of mixtures by using polymer membranes. I. Permeation of binary organic liquid mixtures through polyethylene, J. Appl. Polym. Sci. 12, 2615-2631 (1968).

Hyder, M.N., Huang, R.Y.M., Chen, P., Correlation of physicochemical characteristics with pervaporation performance of poly(vinyl alcohol) membranes, J. Membr. Sci. 283, 281-290 (2006).

Hyder, M.N., Huang, R.Y.M., Chen, P., Effect of Selective Layer Thickness on Pervaporation of Composite Poly(vinyl alcohol)-Poly(sulfone) Membranes, J. Membr. Sci. 318, 387-396 (2008).

Immelman, E., Sanderson, R.D., Jacobs, E.P., Van Reenen, A.J., Poly(vinyl alcohol) gel sublayers for reverse osmosis membranes. I. Insolubilization by acid-catalyzed dehydration, J. Appl. Polym. Sci., 50, 1013 (1993).

Jeon, E. J., Kim, S. C., Computer Simulation for the Pervaporation Process of Water/Ethanol Mixture through interpenetrating polymer network (IPN) membranes, J. Membr. Sci., 70, 193 (1992).

Ji, W., Hilaly, A., Sikdar, S. K., Hwang, S. T., Optimization of Multicomponent Pervaporation for Removal of Volatile Organic Compounds from Water, J. Membr.Sci., 97, 109 (1994).

Johnson, T., Sabu Thomas, Effect of epoxidation of natural rubber on the pervaporation separation of acetone–chlorinated hydrocarbon mixtures, J. Membr. Sci., 155, 133-145 (1999).

Jonquières, A., D. Roizard, J. Cuny, P. Lochon. Solubility and polarity parameters for assessing pervaporation and sorption properties. A critical comparison for ternary systems alcohol /ether/polyurethaneimide. J. Membr. Sci. 121(1), 117-133 (1996).

Jonquieres, A., Perrin, L., Arnold, S., Clement, R., Lochon, P., From Binary to Ternary Systems: General Behavior and Modeling of Membrane Sorption in Purely Organic Systems Strongly Deviating from Ideality by UNIQUAC and Related Models, J. Membr. Sci., 174, 255 (2000).

Kalil, S.J., Maugeri, F., Rodrigues, M.I., Response surface analysis and simulation as a tool for bioprocess design and optimization, Process Biochem. 35, 539–550 (2000).

Kang, Y.S., Lee, S.W., Kim, U.Y., Shim, Y.S., Pervaporation of water–ethanol mixtures through crosslinked and surface-modified poly(vinyl alcohol) membrane, J. Membr. Sci. 51, 215–226 (1990).

Karlsson, H., Tragarth, G., "Pervaporation of Dilute Organic-Water Mixtures. A Literature Review on Modeling Studies and Applications to Aroma Compound Recovery", J. Membr. Sci., 76, 121 (1993).

Kataoka, T., Tsuru, T., Nakao, S., Kimura, S., Permeation Equations Developed for prediction of Membrane Performance in Pervaporation, Vapor Permeation and Reverse Osmosis Based on the Solution-Diffusion Model, J. Chem. Eng. Japan, 24, 326 (1991).

Kim, J.H., Kim, J.Y., Lee, Y.M., Kim, K.Y., Properties, swelling characteristics of cross- linked poly (vinyl alcohol)/chitosan blend membrane, J. Appl. Polym. Sci., 45, 1711-1717 (1992).

Kiran, K.R., Manohar, B., Divakar, S., A central composite rotatable design analysis of lipase catalyzed synthesis of lauroyl lactic acid at bench-scale level, Enzyme and Microbial Tch. 29, 122–128 (2001).

Kober, P. A., Pervaporation, Perstillation and Percrystallization, J. Am. Chem. Soc., 39 (1917).

Koo, J.Y., Petersen, R.J., Cadotte, J.E., ESCA characterization of chlorine-damaged polyamide reverse osmosis membrane, Polym. Prepr., Amer. Chem. Sot., Div. Polym. Chem., 27, 91 (1986).

Koops, G.H., Smolders, C.A., In pervaporation Membrane Separation Process, Huang, R.Y.M., Ed.; Elsevier Science, Ch.5, 253-278 (1991).

Koops, G.H., Nolten, J.A.M., Mulder, M.H.V., Smolders, C.A., selectivity as a function of membrane thickness: Gas separation and pervaporation, J. Appl. Polym. Sci. 53, 1639-1651 (1994).

Kreituss, A., Frisch, H. L., Free-Volume Estimates in Heterogeneous Polymer Systems. I. Diffusion in Crystalline Ethylene-Propylene Copolymers, J. Polym. Sci. Phys. Ed., 19, 889 (1981).

Krumova, M., Lopez, D., Benavente, R., Mijangos, C., Perena, J.M., Effect of crosslinking on the mechanical and thermal properties of poly(vinyl alcohol), Polymer 41, 9265–9272 (2000).

Kusumocahyo, S.P., Sudoh, M., Dehydration of acetic acid by pervaporation with charged membranes, J. Membr. Sci. 161, 77-83 (1999).

Lang, K., Sourirajan, S., Matsuura, T., Chowdhury, G., A study on the preparation of polyvinyl alcohol thin-film composite membranes and reverse osmosis testing, Desalination 104, 185-196 (1996).

Lee, C. H., “Theory of Reverse Osmosis and Some Other Membrane Permeation Operations”, J. Appl. Polym. Sci., 19, 83 (1975).

Lee, K-R., Yu, S-J., Huang, S-L., Wang, D-M., Lai, J.Y., Pervaporation of water- ethanol mixtures through plasma graft polymerization of polar monomer onto crosslinked polyurethane membrane, J. Appl. Polym. Sci., 67, 1789 (1998).

Lee, C.J., Wang, S.S., Lin, G.C., Hu, W., Chert, L.T., Pilot production of polysulfone hollow fiber for ultrafiltration using ortbogonal array experimentation, Ind. Eng. Chem. Res., 34, 813-819 (1995).

Lee, Y. M., Nam, S. Y., Kim, J. H., Pervaporation of water-ethanol through poly(vinyl alcohol) /chitosan blend membrane, Polymer Bulletin 29, 423-429 (1992).

Lee, Y.M., Modified chitosan membranes for pervaporation, Desalination 90, 277 (1993).

Lee, Y.M., Nam, S.Y., Woo, D.J., Pervaporation of ionically surface crosslinked chitosan composite membranes for water-alcohol mixtures, J. Membr. Sci. 133,103 (1997).

Lelkes, Z., Szitkai, Z., Rev E., Fonyo, Z., Rigorous MINLP model for ethanol dehydration system**,** Computers & Chemical Engineering, 24(2-7), 1331 (2000).

Li, D. Q., Neumann, A. W., Thermodynamic status of contact angles, In Applied Surface Thermodynamics (A. W. Neumann and J. K. Spelt, Eds), Chapter 3, Marcel Dekker, Inc.: New York, (1996).

Li, G., Zhang, W., Yang, J., Wang, X., Time-dependence of pervaporation performance for the separation of ethanol/water mixtures through poly(vinyl alcohol) membrane, J. Colloid Interface Sci. 306, 337–344 (2007).

Lipski, C., Côté, P. The Use of Pervaporation for the Removal of Organic Contaminants from Water, Env. Prog., 9, 254-261(1990).

Lloyd, D. R., Meluch, T. B.. Selection and evaluation of membrane materials for liquid separations, American Chemical Society symposium series. Materials Science of Synthetic Membr. 269 , 49-79 (1985).

Long, J. Tzoganakis, C., Chen,P., Surface Characteristics of Hydrosilylated Polypropylene, J. of Appl. Polym. Sci., 88, 3117 (2003).

Lu, L., F. Peng, Jiang, Z., Wang, J., Poly (vinyl alcohol)/Chitosan Blend Membranes for Pervaporation of Benzene/Cyclohexane Mixtures, J. App. Polym. Sci., 101, 167–173 (2006).

Mandal, S., Pangarkar, V. G.. Effect of membrane morphology in Pervaporative separation of isopropyl alcohol-aromatic mixtures - a thermodynamic approach to membrane selection. J. Appl. Polym. Sci. 90(14), 3912-3921 (2003).

Masuda, T., Takatsuka, M., Tang, B. Z., Higashimura, T., Pervaporation of Organic Liquid-Water Mixtures through Substituted Polyacetylene Membranes, J. Membr. Sci., 49, 69 (1990).

Merz, E., Danziger, R. S., A New Industrial Pervaporation module Design Combining a High Permeate Flux and Good Servicability, Proceedings of Seventh International Conference on Pervaporation Processes in the Chemical Industry, Reno, Nevada, 94 (1995).

McNeill, I.C., Thermal degradation mechanisms of some addition polymers and copolymers, J. Anal. Appl. Pyrolysis 40-41,21–41(1997).

Meuleman, E.E.B., Bosch, B., Mulder, M.H.V., Strathman, H., Modeling of liquid/liquid separation by Pervaporation: Toluene from Water, AIChE Journal 45,2153-2160 (1999).

Miranda J. M., Campos, J. B. L. M., Impinging jets confined by a conical wall: Laminar flow predictions, AIChE J., 45, 2273-2285 (2004).

Montgomery, D.C., Design and Analysis of Experiments, 3rd Ed. John Wiley and Sons Inc., New York (1991).

M.P. Goncalves, Trypsin hydrolysis of whey protein concentrates: characterization using multivariate data analysis, Food Chem. 94, 278–286 (2006).

Mulder, M. H. V., Kruitz, F., Smolders, C. A., Separation of isomeric xylenes by pervaporation through cellulose ester membranes, J. Membr. Sci. 11,349-363 (1982).

Mulder, M. H. V., Smolders, C. A., On the Mechanism of Separation of Ethanol/Water Mixtures by Pervaporation 1. Calculation of Concentration Profiles, J. Membr. Sci., 17, 289 (1984).

Mulder, M. H. V., Smolders, C. A., Pervaporation, Solubility Aspects of the Solution-Diffusion Model, Sep. and Purif. Methods, 15, 1 (1986).

Mulder, M. H. V., Franken, T. amd Smolders, C. A., On the Mechanism of Separation of Ethanol-Water Mixtures by Pervaporation 2. Experimental Concentration Profiles, J. Membr. Sci., 23, 41 (1985).

Mulder, M., Basic Principles of Membrane Technology, Kluwer Academic Publishers, Dordrecht, Netherlands, 286 (1991).

Myers, R.H., Montgomery, D.C., Response Surface Methodology: Process and Product Optimization Using Designed Experiments, 2nd ed., John Wiley and Sons Inc., New York (2002).

Nam, S.Y., Lee, Y.M., Pervaporation of ethylene glycol-water mixtures I. Pervaporation performance of surface crosslinked chitosan membranes, J. Membr. Sci. 153, 155-162 (1999).

Nguyen, Q. T., Nobe, K., Extraction of organic contaminants in Aqueous Solutions by pervaporation, J. Membr. Sci., 30, 11 (1987).

Nguyen, Q. T., Modeling of the Influence of Downstream Pressure for highly selective pervaporation, J. Membr. Sci., 27, 217 (1987).

Nijhuis, H.H., Mulder, M.H.V., Smolders, C.A., Removal of trace organics from aqueous solutions: Effect of membrane thickness, J. Membr. Sci, 61, 99-111 (1991).

Nugay, T., Akcora, P., Hortacsu, O., Surface modified polyvinyl alcohol membranes for water /ethanol separation via pervaporation, Polym. Mat. Sci. and Eng., 83,42 (2002).

Oasada, Y., Nakagawa, T., Membrane Science and Technology, 1st Ed., Marcel Dekker Inc., New York (1992)

Okada, T., Yoshikawa, M. and Matsuura, T., A Study on the Pervaporation of Ethanol/Water Mixtures on the Basis of Pore Flow Model, J. Membr. Sci., 59, 151 (1991).

Ohya, H., Matsumoto, K., Negishi, Y., Hino, T., Choi, H. S., The separation of water and ethanol by pervaporation with PVA-PAN composite membranes, J. Membr. Sci. 68, 141-148 (1992).

Oishi, T., Prausnitz, J. M., “Estimation of Solvent Activities in Polymer Solutions using a Group Contribution Method, Ind. Eng. Chem. Proc. Des. Dev., 17, 333 (1978).

Olsson, J., Tragardh, G., Lipnizki, F., The influence of permeant and membrane properties on mass transfer in pervaporation of volatile organic compounds from dilute aqueous solutions, Sep. Sci. Tech. 187,119–1223 (2002).

Pal, S. M., Pangarkar, V. G., Acrylonitrile-based copolymer membranes for the separation of methanol from a methanol-toluene mixture through pervaporation, J. Appl. Polym. Sci. 96, 243-252 (2005).

Park, J.Y., Paul, D.R., Correlation and Prediction of Gas Permeability in Glassy Polymer Membrane Materials via a Modified Free Volume Based Group Contribution Method, J. Membr. Sci. 125, 29 (1997).

Peng, L. Lu, F., Jiang, Z., Wang, J., Poly (vinyl alcohol)/Chitosan Blend Membranes for Pervaporation of Benzene/Cyclohexane Mixtures, J. App. Polym. Sci., 101, 167–173 (2006).

Pesek, S.C., Koros, W.J., Aqueous quenched asymmetric polysulfone hollow fibers prepared by dry/wet phase separation, J. Membr. Sci., 88,71-88 (1993).

Plate, N.A., Yampol'skii Y.P., Relationship between Structure and Transport Properties for High Free Volume Polymeric Materials, in Polymeric Gas Separation Membranes, D.R. Paul and Y.P. Yampol'skii (eds), CRC Press, Boca Raton, FL, 155–208 (1994).

Pusch, W., Walch, A., Membrane structure and its correlation with membrane permeability, J.Membr. Sci. 10,325-360 (2002).

Qunhui, G., Ohya, H., Negishi, Y., Investigation of the permselectivity of chitosan membrane used in pervaporation separation II. Influences of temperature and membrane thickness, J. Membr. Sci. 98, 223-232 (1995).

Rao, K. S. V. K., Subha, M. C. S., Sairam, M., N. N. Mallikarjuna, T. M. Aminabhavi, Blend Membranes of Chitosan and Poly(vinyl alcohol) in Pervaporation Dehydration of Isopropanol and Tetrahydrofuran, J. Appl. Polym. Sci. 103, 1918–1926 (2007).

Rautenbach, R. Herion, C., Franke, M., "Dehydration of Multicomponent Organic Systems by a Reverse Osmosis Pervaporation-Hybrid Process Module – Process Design and Economics", Desalination, 70, 445 (1988).

Ray, S. K., Sawant, S. B., Joshi, J. B., Pangarkar, V. G., Dehydration of acetic acid by pervaporation, J. Membr. Sci. 138, 1-17 (1998).

Ren, J., Jiang, C., Transport phenomena of chitosan membrane in pervaporation of water–ethanol mixture, Sep. Sci. Technol. 33, 517 (1998).

Rhim, J., Lee, S., Kim, Y., Pervaporation separation of water-ethanol mixtures using metal-ion-exchanged polyvinyl alcohol (PVA)/ sulfosuccinic acid (SSA) membranes, J. Appl. Polym. Sci., 85, 1867 (2002).

Rhim, J.-W., Yeom, C.-K., Kim, S.-W., Modification of poly(vinyl alcohol) membranes using sulfur-succinic acid and its application to pervaporation separation of water-alcohol mixtures, J. Appl. Polym. Sci. 68,1717–1723 (1998).

Rodrigues, L., Teixeira, J., Oliveira, R., van der Mei, H.C., Response surface optimization of the medium components for the production of biosurfactants by probiotic bacteria, Process Biochem. 41,1–10 (1998).

Rosa, M.J., de Pinho, M.N., Membrane surface characterization by contact angle measurements using the immersed method, J. Membr. Sci. 131,167-180 (1998).

Ruckenstein, E., Sun, F., Hydrophobic-hydrophilic Composite Membranes for the Pervaporation of Benzene-Ethanol Mixtures, J. Membr. Sci., 103, 271 (1995).

Sakurai K., Maegawa T., Takahashi T., Glass transition temperature of chitosan and miscibility of chitosan/poly(*N*-vinyl pyrrolidone) blends Polymer, 41, 7051-7056 (2000)

Sanders, U., Soukup, P., Design and Operation of a Pervaporation Plant for Ethanol Dehydration, J. Membr. Sci., 36, 463 (1988).

Schellekens, R., Bastiansen, C. J., A drawing behaviour of polyvinyl alcohol fibers, J Appl Polym Sci 43, 2311-2315 (1998).

Scherer, J.R., Bailey, G.F., Water in polymer membranes. Part I. Water sorption and refractive index of cellulose acetate, J. Membr. Sci., 13, 29 (1983).

Semenova, S. I, Ohya, H., Soontarapa, K., Hydrophilic Membranes for Pervaporation: An Analytical Review, Desalination, 110, 251 (1997).

Schwarz, H.H., Jaromír, L., Richau, K., Surface and permeability properties of membranes from polyelectrolyte complexes and polyelectrolyte surfactant complexes, J. Membr. Sci. 218, 1-9 (1998).

Sharma, A., Thampi, S.P., Suggala,S.V., Bhattacharya, P.K., Pervaporation from a dense membrane: Roles of Permeant-Membrane Interactions, Kelvin Effect, and Membrane swelling, Langmuir, 20(11), 4708 (2004).

Shieh, J.-J., Huang, R.Y. M., Pervaporation with chitosan membranes II. Blend membranes of chitosan and polyacrylic acid and comparison of homogeneous and composite membrane based on polyelectrolyte complexes of chitosan and polyacrylic acid for the separation of ethanol-water mixtures, J. Membr. Sci. 127,185-202 (1998).

Smirnov, L.V., Kulikova, N.P., Platonova, N.V, Infrared spectra of polyvinylalcohol, Polym. Sci. U.S.S.R. 9, 2849–2856 (1998).

Smitha, B., Suhanya, D., Sridhar, S., Ramakrishna, M, Separation of organic-organic mixtures by pervaporation-a review, J. Membr. Sci. 241,1-21 (1998).

Sourirajan, S., Matsuura, T., Reverse Osmosis/Ultrafiltration Process Principles, National Research Council of Canada, Ottawa, (1985).

Sourirajan, S., Bao, S., Matsuura, T., An Approach to Membrane Separation by Pervaporation, in Proceedings of Second International Conference on Pervaporation, 251 Processes in the Chemical Industry, ed. R. A. Bakish, Bakish Materials Corp., Englewood, NJ, 209 (1987).

Spitzen, J.W.F., Koops, G.H., Mulder, M.H.V., Smolders, C.A., The Influence of Membrane Thickness on Pervaporation Performance, R. Bakish (Ed.), in Proceedings of third International Conference on Pervaporation Processes in Chemical Industry, Nancy, France, Bakish Materials Corp., Englewood, NJ,252 (1998).

Stern, S.A., Polymers for gas separations: The next decade, J. Membr. Sci., 94, 1-65 (1994).

Stuart B., Infrared Spectroscopy: Fundamentals and Applications, John Wiley and Sons Ltd, Kent, UK (2004).

Suzuki, F., Onozato, K., Pervaporation of Benzene-Cyclohexane Mixtures by Polymethyl-glutamate Membrane and Synergistic Effect of their Mixture on Diffusion Rate, J. Appl. Polym. Sci., 27, 4229 (1982).

Tsai, H.A., Chen, H.C., Chou, W.L., Lee, K.R., Lai, J.Y., Pervaporation of water/alcohol mixtures through chitosan/cellulose acetate composite hollow-fiber membranes, J. Appl. Polym. Sci. 94,156 (1998).

Uemura T., Inoue, T., Electron microscopic study of ultrathin solute barrier layer of composite membranes and their solute transport phenomena by the addition of alkali metal salts, in: Drioli and Nakagaki (Eds.), Membranes and Membrane Processes, Plenum, New York, NY, 379 (1984).

Uragami T., Takigawa, K., Permeation and separation characteristics of ethanol-water mixtures through chitosan derivative membrane by pervaporation and evaporation, Polymer 31,668 (1998).

Uragami, T., Matsuda, T., Okuno, H., T. Miyata, Structure of chemically modified chitosan membranes and their characteristics of permeation and separation of aqueous ethanol solutions, J. Membr. Sci. 88,243-251 (1998).

van der Ven, C., Gruppen, H., de Bont, D.B.A., Voragen, A.G.J., Optimization of the angiotensin converting enzyme inhibition by whey protein hydrolysates using response surface methodology, Int. Dairy J. 12, 813–820 (1998).

Vane, L. M., Hitchens, L., Alvarez, F. R., Giroux, E. L., Field demonstration of pervaporation for the separation of volatile organic compounds from a surfactant-based soil remediation fluid**,** J. of Hazardous Materials, 81(1-2), 141 (2001).

Villaluenga, J.P.G., Khayet, M., Godino, P., Seoane, B., Mengual, J.I., Analysis of the membrane thickness effect on the pervaporation separation of methanol/methyl tertiary butyl ether mixtures, Sep. Purif. Technol. 47, 80-87 (2005).

Villaluenga, J. P. G., A. Tabe-Mohammadi, A review on the separation of benzene/cyclohexane mixtures by pervaporation processes, J. Membr. Sci., 169, 159 -174 (2000).

Website, Surface Roughness, http://www.predev.com/smg/intro.htm

Wenzel, R.N., Resistance of Solid surfaces to wetting by water, Ind. Eng. Chem., 28, 988 (1936).

Wijmans, J. G., Baker, R. W., A Simple Predictive Treatment of the Permeation Process in Pervaporation, J. Membr. Sci., 79, 101 (1993).

Wijmans, J. G., Athayde, A. L., Daniels, R., L., J. H., Kamaruddin, H. D., Pinnau, I., The Role of Boundary Layers in the Removal of Volatile Organic Compounds from Water by Pervaporation, J. Membr. Sci., 109, 135 (1996).

Wei, Y., Huang, R. Y. M., Pervaporation with Latex Membranes: A Study on Membrane and Pervaporation Effects, Sep. Sci. Tech., 30, 697 (1995).

Wei, Y-M., Xu, Z-L., Qusay, F. A., Wu, K., Polyvinyl Alcohol/Polysulfone (PVA/PSF) hollow fiber composite membranes for pervaporation separation of Ethanol/Water solution, J. Appl. Polym. Sci. 98,247–254 (1998).

Wu, L-G., Chang-Luo, Z., Liu,M., Study of a new pervaporation membrane Part 1. Preparation and characteristics of the new membrane, J. Membr. Sci. 90, 199–205 (2002).

Wynn, N., Pervaporation Comes of Age, Chem. Eng. Progress 97, 66-72 (2001).

Xia, F.; Chen, P., An image analysis program for measuring contact angles of arbitrary drop shape, J. Imaging Sci. and Tech. 47(1), 44 (2003).

Xiao, S., Huang, R.Y.M., Feng, X., Preparation and properties of trimesoyl chloride crosslinked poly(vinyl alcohol) membranes for pervaporation dehydration of isopropanol, J. Membr. Sci. 286, 245–254 (1998).

Xie, H. A., Nguyen, Q. T., Schaetzel, P., Neel, J., Dehydration of Amines and Diamines by Pervaporation with Ionomer and PVA-based Membranes, J. Membr. Sci., 81, 97 (1993).

Yalkowsky, S. H., Banerjee, S., Aqueous Solubility - Methods of Estimation for Organic compounds, Marcel Dekker Inc., New York, USA, (1992).

Yamaguchi, T., Nakao, S., Kimura, S.. Solubility and pervaporation properties of the filling polymerised membrane prepared by plasma-graft polymerisation for pervaporation of organic -liquid mixtures." Ind. Eng. Chem. Res. 31,1914-1919 (1998).

Yang, J. M., Sua, W.Y., Leub, T. L., Yang, M.C., Evaluation of chitosan/PVA blended hydrogel membranes, J. Membr. Sci. 236, 39–51 (1998).

Yeom, C.-K., Lee, K.-H., Pervaporation separation of water-acetic acid mixtures through poly(vinyl alcohol) membranes crosslinked with glutaraldehyde J, Membr. Sci. 109, 257–265 (1996).

Yeom, C. K., Huang, R. Y. M., A New Method for Determining the Diffusion Coefficients of Penetrants through Polymeric Films from Steady State Pervaporation Experiments, J. Membr. Sci., 68, 11 (1992a).

Yeom, C. K., Huang, R. Y. M., Modeling of the Pervaporation Separation of Ethanol-Water mixtures through Crosslinked Poly(vinylalcohol) Membrane, J. Membr. Sci., 67, 39 (1992b).

Yong, S.K., Sang, W.L., Un, Y.K., Jyong, S.S., Pervaporation of water-ethanol mixtures through crosslinked and surface-modified poly(vinyl alcohol) membrane, J. Membr. Sci. 51,215-226 (1996).

Yoshida, W., Cohen, Y., Ceramic-Supported Polymer Membranes for Pervaporation of Binary Organic/Organic Mixtures, J. Membr. Sci., 213, 145 -157 (2003).

Yu, J., Lee, C.H., Hong, W.H., Performances of crosslinked asymmetric poly(vinyl alcohol) membranes for isopropanol dehydration by pervaporation, Chem. Eng. Process. 41, 693(2002).

Zeng, Z., Xiao, X., Gui, Z., Li, L., AFM study on surface morphology of $Al2O_3$-SiO_2-TiO_2 composite ceramic membranes, J. Membr. Sci., 136, 156 (1997).

Zhang, W, Hallstrom, B, Membrane characterization using contact angle technique I Methodology of the captive bubble technique, Desalination 79, 1 (1990).

Zhou Y., Yang, D., Chen, X., Xu, Q., Lu, F., Nie, J., Electrospun Water-Soluble Carboxyethyl Chitosan/Poly(vinyl alcohol) Nanofibrous Membrane as Potential Wound Dressing for Skin Regeneration, Biomacromolecules, 9,349–354 (2002).